N-Butyryl arginine and 3-Hydroxybutyrate arginine, for the treatment of DMD through oral administration

Sara Vianello

UNIVERSITÉ PARIS SUD

Comprendre le monde, construire l'avenir®

UNIVERSITE PARIS-SUD

ÉCOLE DOCTORALE : Biosigne- 419

DISCIPLINE *Biochimie, Biologie Cellulaire et Moléculaire*

THÈSE DE DOCTORAT SUR TRAVAUX

Soutenue le 04/09/2013

par

Sara Vianello

N-Butyryl arginine and *3-Hydroxybutyrate arginate*, for the treatment of DMD through oral administration

Directeur de thèse Dr. Sabine De La Porte, *Chargée de Recherche INSERM*

Composition du jury :

Président du jury : Dr. Philippe Vernier, *Directeur de Recherche CNRS*

Rapporteurs : Dr. Gillian Butler-Browne, *Directeur de Recherche INSERM*
Pr. Bernard Jasmin, *Vice-Doyen Université d'Ottawa*

Examinateurs : Dr. Luis Garcia, *Directeur de Recherche CNRS*
Dr. Yves Fromes, *Directeur de Recherche Institut de Myologie*

Laboratoire de Neurobiologie et Développement
Institut de Neurobiologie A. Fessard - CNRS UPR 3294 - Gif sur Yvette, France

Remerciements

Pendant le temps passé en France beaucoup des gens ont croisé mon chemin.
Je veux remercier d'abord l'équipe (Evelyne, Romulo, Jordi Aurelie, Bao, Patricia et Emanuelle), mais aussi Adil et Sandrine pour m'avoir soutenue et avec qui j'ai partagé des moments très joyeux. Un grand merci en particulier a Sabine qui m'a appris à aimer l'être chercheuse dans le moment de réussite mais sur tout dans les moments désespérés.

Un grand merci a Alessandro, Aurélie, Emilie, JB, Gaelle, Ludo, Tibi, Yanik, Simone et Simonetta qui m'ont super soutenu, aidé, hébergé, partagé les voyage en rer et avec qui j'ai bu pas mal d'aperò !!

Un grand merci a Marta (m'a super colocataire !!), Marco, Stefania, Lara, Sara, Richy, Marco jr, Natalie, Silvia, Valmo, Davide, Marta DF, Erwan, Alberto, Laura et Paolo Silvano, Lorenzo, avec qui j'ai grandi pendant ces dernière quatre ans. Andrea, Laura, Anna, Giobbe, la petite Benedetta, Agnese, Cuppo pour votre compagnie et soutien d'Italie.

Un grand merci a ma famille (Mara et Vincenzo) pour m'avoir toujours encouragé a poursuivre mes désires. Un SUPER MERCI à Antonio qui m'a attendu, soutenu et encouragé.

Je veux remercier particulièrement Dr. Gillian Butler-Browne, Pr. Bernard Jasmin, Dr. Luis Garcia, Dr. Yves Fromes et Dr. Philippe Vernier pour avoir accepté de faire partie de mon jury de thèse.
Je veux remercier encore plus particulièrement Dr. Alvaro Rendon, mon tuteur de thèse, pour m'avoir suivi pendant ces trois ans.

TABLE OF CONTENTS

TABLE OF CONTENTS 1

Abstract 4

Abbreviations 6

Introduction 8

1.1 DMD and DYSTROPHIN 9

1.2 DYSTROPHIN: from GENE to PROTEIN 9

1.2.1 The gene *9*

1.2.2 The protein *11*

1.3 DYSTROPHIN ASSOCIATED PROTEIN COMPLEX (DAPC) 14

1.4 THE MUTATIONS 17

1.5 UTROPHIN: from GENE to PROTEIN 18

1.5.1 The gene *18*

1.5.2 The protein *20*

1.6 THE ANIMAL MODELS 22

1.6.1 The mdx mouse *22*

1.6.2 The CXMD dog *22*

1.6.3 The HFMD cat *23*

1.7 CLINICAL AND MOLECULAR FEATURES 24

1.7.1 Clinical features and natural history of Duchenne Dystrophy *24*

1.7.2 Physiopathology of DMD *25*

1.7.2.1 Membrane permeability 26

1.7.2.2 Calcium Homeostasis 26

1.7.2.2.1 Role of calcium in muscle 26

1.7.2.2.2 Calcium homeostasis in dystrophy 27

1.7.2.3 Muscular strength 29

1.7.2.3.1 Muscular ability before exercise 29

1.7.2.3.2 Muscular ability after exercise 30

1.7.2.4 Apoptosis 30

1.7.2.5 Fibrosis 31

1.7.2.6 Satellite cells and muscle repair 32

1.7.2.7 Regeneration 34

1.8 CARDIOMYOPATHY 36

1.8.1 Description 36

1.8.2 Underlying mecanisms 37
1.8.3 Treatments 40
1.9 NO & NOS IN SKELETAL MUSCLE 41
1.10 HISTONE DEACETYLASE (HDAC) ENZYME 44
1.11 THERAPIES 46
1.11.1 INDEPENDENT STRATEGIES *46*
1.11.2 CELL THERAPY *47*
1.11.3 THERAPIES TARGETING DYSTROPHIN: *49*
1.11.3.1 PHARMACOLOGICAL APPROACHES 49
1.11.3.2 GENE THERAPY 52
1.11.4 THERAPIES TARGETING UTROPHIN *54*
1.11.5 ASSOCIATED THERAPIES *58*
THESIS PROJECT 60
PUBLICATIONS AND MANUSCRIPTS 65
3.1 Publication 1. “Arginine butyrate: a therapeutic candidate for Duchenne muscular dystrophy” 68
3.2 Manuscript 2. “*Per os* administration of arginine butyrate preserve *mdx* mice from cardiomyopathy, kyphosis and axonal excitability defaults.” 69
3.3 Manuscript 3. “Low doses of arginine butyrate derivatives alleviate dystrophic phenotype and restore the membrane integrity in *DMD* murine model.” 70
SUPPLEMENTARY RESULTS 71
DISCUSSION 75
Conclusion 88
BIBLIOGRAPHY 90
Appendix 117

Abstract

Duchenne muscular dystrophy is an X-linked progressive neuromuscular disease affecting 1:3500 boys at birth. It is caused by the absence of dystrophin, a subsarcolemmal protein that confers membrane stability linking cytoskeletal actin to the extracellular matrix. It is part of a multi-protein complex called dystrophin associated protein complex (DAPC), which contains, among the other components, b-dystroglycan and nitric oxide synthase (NOS).

The consequences of the absence of dystrophin are: deregulation of calcium homeostasis, tissue necrosis, progressive accumulation of fat and fibrosis, muscle weakness, cardiac and respiratory failure leading to patient's death, around the age of 20-30 years.

The objective of my PhD is to improve different aspects of the dystrophic phenotype. In particular I have tested two different ways of administering arginine butyrate (AB), the reference drug, through feeding-force and intraperitoneal injection. In addition I have studied two new pharmacological molecules, AB derived, which could be administered orally to DMD patients. These compounds are: 3-Hydroxybutyrate arginate (refer as ABE) and N-butyryl arginine (refer as ABA). All of these molecules partially restore dystrophic phenotype activating two independent pathways (both the nitric oxide pathway and the inhibition of the histone deacetylase), which are known to be beneficial for *mdx* mice.

AB, ABE and ABA have been tested *in vitro* on human DMD myotubes and *in vivo* on the *mdx* mice.

The first goal of my project is the observation that the positive effects obtained after intraperitoneal injections of AB can also be detected after oral administration, promoting the idea that the oral administration has to be developed for future clinical trials. I have focused my attention on modifications in cardiax function; in particular, starting from the 8^{th} month, a monthly study on cardiac activity based on echocardiography has been performed on *mdx* mice treated with AB. We have analysed the potential benefit of the oral administration of arginine butyrate on deformation of the spine and electromyogram abnormalities, with a non-invasive automatized method developed in the clinic and then applied to animals. The results obtained from these experiments show that AB preserves heart activity, reverses kyphosis of the vertebral column and all of the axonal excitability parameters that were modified in saline-treated *mdx* mice.

Finally, I tested different concentrations of ABE and ABA *in vivo*. The positive effects on many structural and functional dystrophic parameters, previously obtained with high dose of AB

administered *per os* (800 mg/kg/d), has been observed with doses 10 times lower with both new compounds.

In parallel, both products were tested *in vitro* on human muscle cell cultures to investigate their capacity to increase the level of utrophin. Moreover, the potential ability of histone deacetylase inhibitors (butyrate, valproic acid, trichostatin A and isobutyramide) to increase the expression of utrophin and related proteins (β-dystroglycan and embryonic myosin) has been studied.

Finally, the alteration of calcium homeostasis, largely implicated in the cascades resulting in muscle necrosis/degeneration, was investigated. The spontaneous Ca^{2+} activity recorded in patient myotubes, *i.e.* without sarcolemmal integrity was strongly reduced after treatment acting on the NO-pathway activation and/or with HDAC inhibitors.

All together, these data constitute a proof of principle of the beneficial effects of arginine butyrate and its derivates on muscular dystrophy, by enhancing NO pathway and inhibiting HDAC.

Abbreviations

2OMP: 2’-O-methylphosphorothioate

AAV: adeno-associated

AB: arginine butyrate

ABA: N-butyryl arginine

ABE: 3-Hydroxybutyrate arginate

ABD: Actine Binding Domain

ABS: actin-binding sequences

AONs: antisense oligonucleotides

B: butyrate

βDG: β-dystroglycan

CH: calponin-homology

cGMP: cyclic guanosine monophosphate

CATs: cationic amino acid transporters

CK: creatine kinase

CTGF: connective tissue growth factor

DAPC: dystrophin associated protein complex

DMD: Duchenne muscular dystrophy

DHPR: dihydropyridine receptors

EC: excitation-contraction

ECG: echocardiogram

EDL: Extensor Digitorum Longus

EF: ejection fraction

ER: endoplasmic reticulum

FS: fractional shortening

HDAC: histone deacetylases

HGF: hepatocytes growth factor

ISO: isobutyramide

KI: kyphosis index

LV: left ventricular

LVID: left ventricular inner diameter

LVOD: left ventricular outer diameter

mdx : X-linked muscular dystrophy

mDYS: mini-dystrophin

μDys: micro-dystrophin

NF: nuclear factor

NO: nitric oxide

NOS: nitric oxide synthase

PMOs: phosphorodiamidate morpholino oligomers

PNAs: peptide nucleic acids

PKA: protein kinase A

PTP: permeability transition pore

RyR: ryanodine receptors

ROS: reactive oxygen species

SOC: store-operated channels

SR: sarcoplasmic reticulum

TRPC: transient receptor potential channel

TGF: transforming growth factor

TSA: trichostatin A

VPA: valproic acid

Introduction

1.1 DMD and DYSTROPHIN

Duchenne muscular dystrophy (DMD) is a progressive neuromuscular disease affecting 1/3500 male at birth and it is caused by a mutation of a gene located at the Xp21 locus (Fig.1A) coding for dystrophin, a sub-sarcolemma protein. Dystrophin, a 427 kDa protein, is the central component of the dystrophin-glycoprotein complex that links actin cytoskeleton to the extracellular matrix, thus maintaining muscle fibre membrane integrity. The lack of this protein induces a weakness of skeletal, smooth and cardiac myofibres, due to mechanical muscle contraction and leading to dramatic muscle deterioration. In addition to this principal cause, Ca^{2+} leakage, oxidative stress, inflammatory response and fat infiltration are observed in human dystrophic muscle (Blake et al., 2002). Although the primary genetic defect is known, the dystrophy process has not been definitively identified.

1.2 DYSTROPHIN: from GENE to PROTEIN

1.2.1 The gene

The *DMD* gene is the largest described, spanning ~ 2.5 Mb of genomic sequence and it is composed of 79 exons. The full-length 14 kb mRNA transcribed from the DMD locus was found to be predominantly expressed in skeletal and cardiac muscle with smaller amounts in brain. The protein product encoded by this transcript was named dystrophin since the lack of it causes dystrophy (Hoffman et al., 1987).

The expression of the full-length transcript is controlled by three independently regulated promoters situated within a large genomic interval of ~ 400 kb. The brain (B), muscle (M) and Purkinje (P) promoters consist of unique first exons spliced to a common set of 78 exons.
The *DMD* gene also has at least four internal promoters that give rise to shorter dystrophin proteins lacking the actin-binding domain but retaining the cystein rich and carboxy-terminus domains that contain the necessary binding sites for a number of dystrophin-associated proteins.
Each of these promoters utilizes a unique first exon that splices into exons 30, 45, and 46, respectively, to generate protein products of 260 kDa, highly expressed in the retina, 140 kDa, expressed in brain, retina and kidney tissues, 116 kDa, only expressed in adult peripheral nerves,

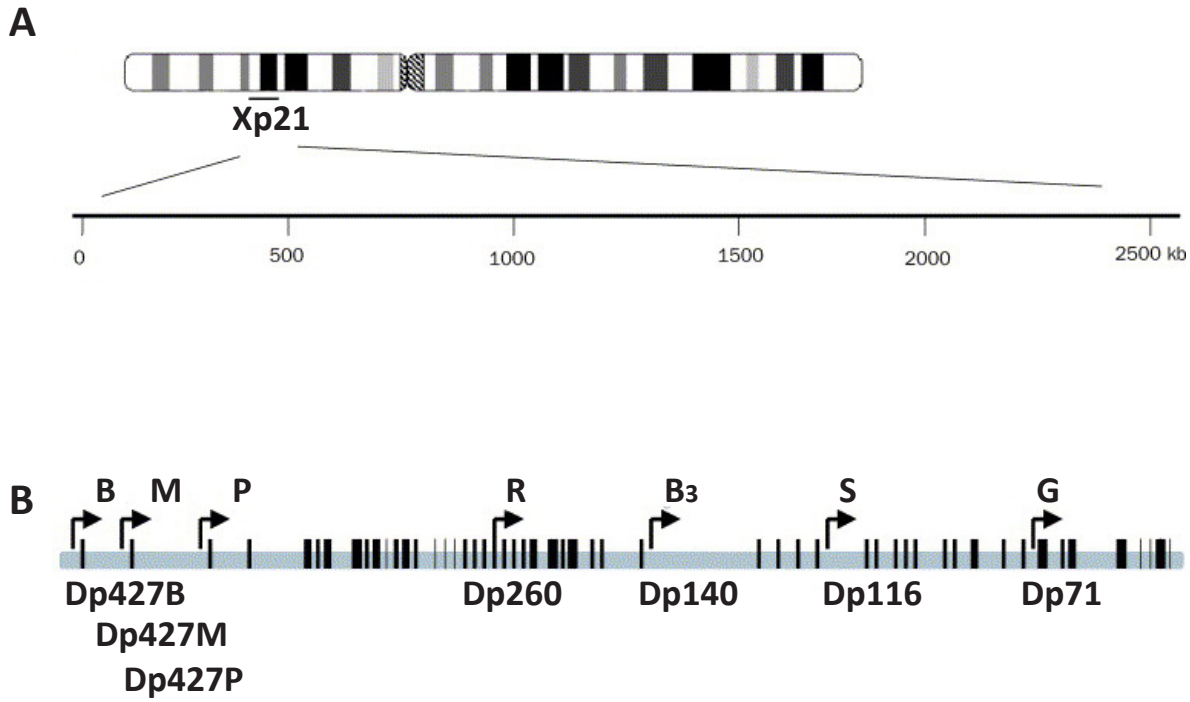

Figure 1: (A) Schematic representation of the X chromosome. The DMD gene is located on Xp21.2, it spans for 2.5 Mb and is composed of 79 exons. (B) Different promoters are contained inside the DMD gene. In a large genomic interval of 400 kb are situated three promoters that control the expression of the full-length form (Dp427) of the protein located in different tissues: B for brain, M for muscle and P for Purkinje. Inside the gene there are also four internal promoters that give rise to the retina (Dp260), brain (Dp140), peripheral nerves (Dp116) and general ubiquitously expressed (Dp71) isoforms of the protein. Adapted from (Muntoni et al. 2003).

and 71 kDa, expressed in most non-muscle tissues and is present in cardiac muscle (Muntoni et al., 2003) (Fig. 1B and 2).

Alternative splicing at the 3'end of the dystrophin gene generates an even greater number of isoforms (Feener et al., 1989). This differential splicing may regulate the binding of dystrophin to dystrophin-associated proteins at the membrane.

The M promoter:

The promoter is active in skeletal, smooth and cardiac tissues (Gilgenkrantz et al., 1992). The promoter is expecially active during cellular differentiation and with a transcrit level 10-times more in adult myotubes. After direct injection of the promoter in differentiated myotubes, its activity was 30-times lower than in immatures cells. One possible explanation of the discrepancy between the transcript level and the promoter activity, could be related to the presence of an enhancer into the intron 1 of the gene (Klamut et al. 1996).

The link between the dystrophin promoter binding factor (DPBF) with the CCArGG-box (position -91) favorise the activation of the promoter. At the CCArGG-box could also link YY1, a nuclear zinc finger factor that is able to inhibit dystrophin expression in C2C12 cells. The expression level of the negative regulator factor in non-differentiated cells, interferes with spacial conformation of the promoter and blocks the binding site for dystrophin promoter binding factor (Galvagni, Cartocci, and Oliviero 1998)

The B promoter

The brain promoter is active only at neuronal level, in particular it has been observed an increased of mRNA level during maturation *in vitro* (Chelly et al. 1990). In this type of promoter there are not TATA-box or regulatory sequences that promote the transcription, but the process starts 266 pb upsteam form the first ATG codon in phase with the reading frame of dystrophin (Makover et al. 1991).

The P promoter

The last promoter that control the full length protein has been identify in the Purkinje cells (Górecki et al., 1992). The level of expression of the Purkinje promoter is different between skeletal muscle, heart and brain, and its activation depends on tissular type and development states (Holder et al., 1996).

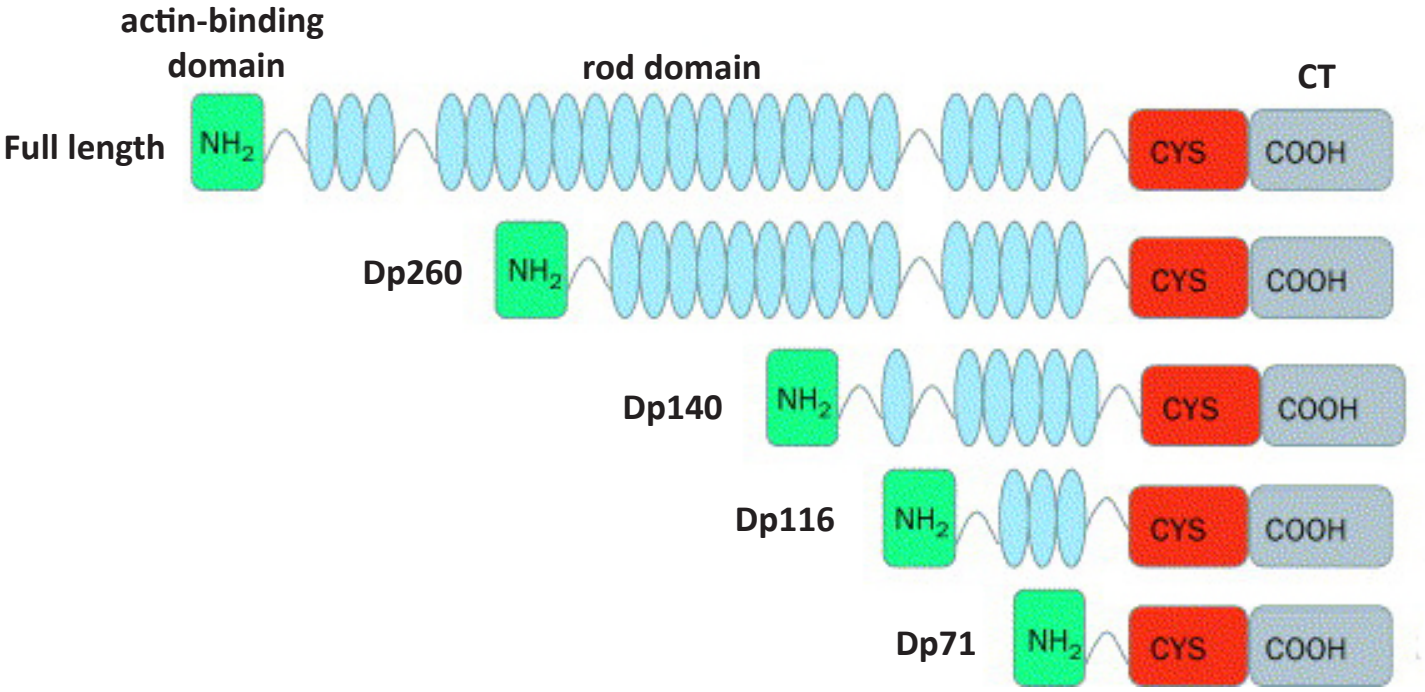

Figure 2: Schematic representation of dystrophin protein and its isoforms. The full-length protein is organized into four separate regions: the actin-binding domain at the NH2 terminus, the central rod domain, the cysteine-rich domain and the COOH-terminal domain.

Each of the isoforms maintained the N- and C- terminus domains and the CYS domain, while the rod domain change. Adapted from (Muntoni et al. 2003).

A TATA-box can be found in the human promoter but not in the mouse one. In the P promoter there are also binding site for transcription factors such as the E-box and a sequence for the AMPc (cyclic adenosine monophosphate) (Abdulrazzak et al., 2001).

1.2.2 The protein

Molecular weight of dystrophin is 427 kDa and it derives from a 14 kb mRNA sequences (Hoffman et al., 1987). It is composed of 3685 AA. Dystrophin molecules are not uniformly spread over the surface of mammalian muscle fibers. Confocal microscopy reveals aligned fluorescent points or intermittent lines along the sarcolemma, most points corresponding to the I bands. These molecules form a network of dense transverse rings or costamers, and fine longitudinal interconnections. The network at the surface of the muscle fibres is organized in relation with the contractile apparatus. Likewise, vinculin, γ-actin, talin and spectrin constitute a submembrane cytoskeletal network with a costameric distribution. Dystrophin binds strongly to talin and this binding is inhibited by vinculin, because of steric hindrance. Dystrophin is abundant at the membrane surface of the intrafusal fibers and at the neuromuscular junction, where dystrophin is localised in the depths of junctional folds. Dystrophin is discontinuously distributed in the submembrane region of human muscle cells in culture. In contracting conditions, it occurs continuously along the inner face of the sarcolemma and in periodic dense aggregates. The contractile activity of the muscle therefore plays an important role in the continuous distribution of dystrophin along the sarcolemma during development.

Dystrophin is linked to the sarcolemma of normal muscle by a protein complex composed of at least 10 different proteins: the dystrophin-associated protein complex (DAPC). This complex spans the membrane and links the actin-based cytoskeleton to the muscle basal lamina. Thus the DAPC can be thought as a scaffold connecting the inside of a muscle fibre to the outside. The DAPC can be divided into several separate subcomplexes based on their location within the cell and their physical association with each other, the dystroglycan complex, the sarcolycan:sarcospan complex and the cytoplasmic dystrophin-containing complex (Hoffman et al., 1987).

It is organized into four separate regions: the actin-binding domain at the NH_2 terminus, the central rod domain, the cysteine-rich domain and the COOH-terminal domain (Fig. 2).

-The NH_2 terminus domain contains the binding site for the F-actin. In this region there is an actin binding domain (ABD1) that is composed of two tandem calponin-homology (CH) domains, in which three actin-binding sequences (ABS1-3) have been identified (Banks et al., 2007; Hemmings et al., 1992; Jarrett and Foster, 1995; Levine et al., 1992).

The link between dystrophin and actin could be modulated by the phosphorylation pattern of dystrophin. When dystrophin is phosphorylated by PKC, the interaction is inhibited, when dystrophin is phosphorylated by PKA, the interaction is favoured (Senter et al., 1995).
Moreover, in the N-terminal domain there are calmodulin-binding sites (CBS1 and 2, 18-42 and 104-125 respectively). The bound with calmodulin is Ca^{2+} dependent and could regulate the interaction with actin (Jarrett and Foster, 1995).

Recently is has been shown that in *mdx* mice the expression of a mini-dystrophin lacking only a portion of ABD1 are not able to restore the normal muscular morphology and develop the specific force compared to wild-type mice. Instead, *mdx* mice expressing a minidystrophin with a complete N-terminal domain displayed normal morphology and specific force generation and were partially protected from contraction-induced injury when evaluated at 4 months of age. The authors suggest also a clustering role of the domain because of the presence of abnormal accumulation near the nuclei of fibres expressing the truncated sequence (Banks et al., 2007).

-The rod domain is composed of 24 repeating units of variable length (about 100 amino acids) that are similar to the triple helical repeats of spectrin. This repeating unit accounts for the majority of the dystrophin protein and is thought to give the molecule a flexible rodlike structure and, because of the presence of four proline-rich hinge within α-helical coiled-coil repeats, it is able to combine in order to form filaments (Cross et al., 1990). Deletions truncating this region reduce the extensibility of the molecule without affecting acting binding that characterized Becker muscular dystrophy (BMD), the milder form of dystrophinopathy. Dystrophin can interact with actin not only by the ABD1 but also by ABD2 that is located in this region. They interact *via* electrostatic attraction (Amann et al., 1998).
Recently Ervasti's group have shown that a fragment of dystrophin spanning from the N-terminal domain through ABD 2 bound actin molecules with high affinity compared to segment lacking ABD

1 or 2. Moreover, the affinity evaluated is lower than full-length dystrophin and they suggest that C-terminal domain could influenced the bound with actin even if they do not interact with the molecule (Henderson et al., 2012). The fourth proline-rich region is immediately followed by the WW domain, that binds to proline-rich substrates. This region, with the following one, mediates the interaction between β-dystroglycan and dystrophin, since the cytoplasmic domain of β-dystroglycan is proline rich (Jung et al., 1995).

-The cysteine-rich domain (142 amino acids) contains two EF-hand motifs that could bind intracellular Ca^{2+}. The ZZ domain is also part of the cysteine-rich domain and contains a number of conserved cysteine residues that are predicted to form the coordination sites for divalent metal cations such as Zn^{2+}. This region binds to calmodulin in a Ca^{2+}-dependent manner (Blake et al., 2002).

-The COOH terminus of dystrophin (422 amino acids) contains two polypeptide stretches that are predicted to form α-helical coiled-coil similar to those in the rod domain (Blake et al., 1995). These regions of dystrophin forms the binding site for dystrobrevin and may modulate the interaction between syntrophin and other dystrophin-associated proteins (Sadoulet-Puccio et al., 1997). The C terminal domain could be phosphorylated at different site by MAP kinases and CaM kinases or casein kinase; instead dephosphorylation occurs by calcineurin (Michalak et al., 1996; Milner et al., 1993).

The monomers of dystrophin combine spontaneously in antiparallel homodimers by matching of central repetitive domains, forming a hexagonal network. The N- and C- terminal regions are therefore juxtaposed and associate with one another or with other dimers of dystrophin.

The full-length sequence of dystrophin protein is localized under the sarcolemma of all muscle fibres and interacts with DAPC. During human gestation, its expression and localisation become around week 8 in smooth and cardiac muscle, whereas in skeletal muscles dystrophin is first found in the cytoplasm and around week 10, founds at the membrane. In adults there more dystrophin in skeletal and cardiac muscle than in smooth one (review: (Voisin and de la Porte, 2004)).

1.3 DYSTROPHIN ASSOCIATED PROTEIN COMPLEX (DAPC)

DAPC a protein complex composed of at least of 10 different proteins, linking dystrophin to the sarcolemma of normal muscle (Fig 3). This complex spans the membrane and links the actin-based cytoskeleton to the muscle basal lamina. Thus the DAPC can be thought as a scaffold connecting the inside of a muscle fibre to the outside.

The DAPC can be divided into several separate subcomplexes based on their location within the cell and their physical association with each other. DAPC could be dissociated into three distinct complexes: the dystroglycan complex, the sarcoglycan:sarcospan complex and the cytoplasmic, dystrophin-containing complex (Yoshida et al., 1994). The description of the different complex could be applied to utrophin, the foetal homologous to dystrophin (Matsumura et al., 1992).

Dystroglycan complex:

The single dystroglycan gene (3p21) produces a precursor protein (97kDa) that is processed to produce α- and β-dystroglycan (156 and 43 kDa respectivelly). The dystroglycan gene is composed of only two exons and there is no evidence of alternative splicing. The dystroglycan proteins are expressed all along the development in an ubiquitous way in all muscles types (skeletal and others) (Schofield et al., 1995).

- **β-dystroglycan** has a single transmembrane domain and is inserted into the muscle plasma membrane with the COOH terminus on the cytoplasmic side. The extreme COOH terminus of β-dystroglycan contains several proline residues that are required for dystroglycan binding to dystrophin (Blake et al., 1998). In particular, the WW domain and the EF-hand region of dystrophin interact with the C-terminal domain of β-dystroglycan (Einbond and Sudol, 1996; Jung et al., 1995; Rentschler et al., 1999; Suzuki et al., 1992, 1994). The last 15 amino acids of β-dystroglycan appear to bind directly to the cysteine-rich region of dystrophin. The structure of this region of dystrophin shows that dystroglycan forms contacts with both the WW domain and EF hands. The COOH terminus of β-dystroglycan also binds to the adaptor protein Grb2; these interactions are mediated by the SH3 domain of Grb2 that binds to proline-rich sequences of β-dystroglycan (Russo et al., 2000). Another molecule have been described to interact with the C-terminal domain of the β-dystroglycan, Caveolin-3 (Sotgia et al., 2000), that competes with dystrophin for the same binding site, the tetrapeptide PPPY. In addition, rapsyn, a protein essential for neuromuscular

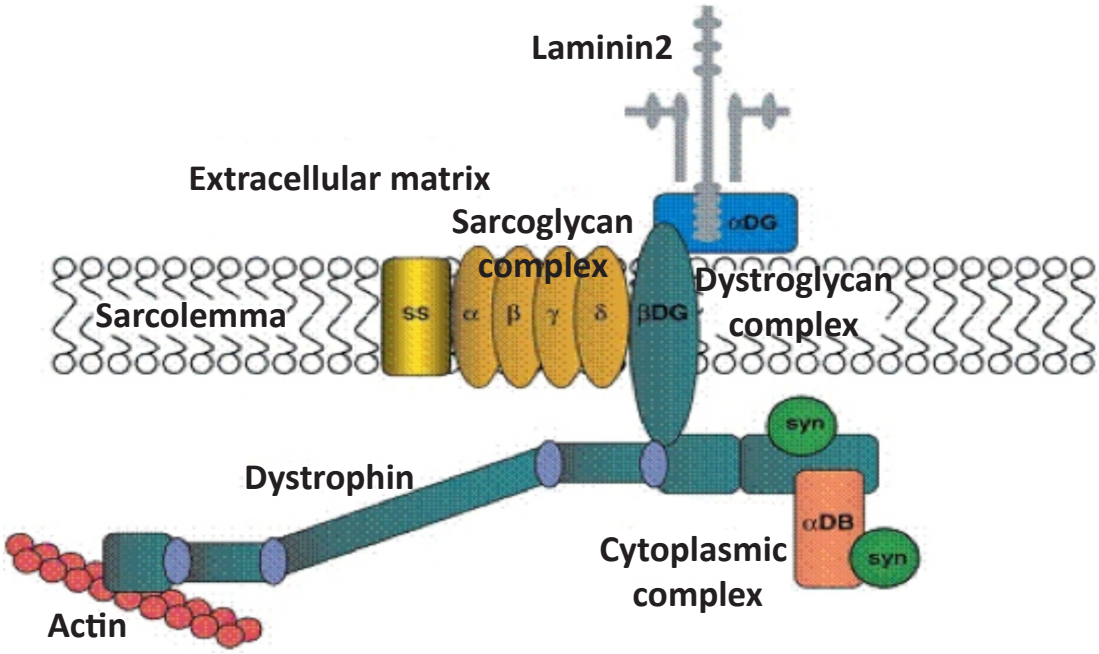

Figure 3: The dystrophin-associated protein complex (DPC) in skeletal muscle. Dystrophin binds to cytoskeletal actin at its NH2 terminus. At its COOH terminus, dystrophin is associated with a number of integral and peripheral membrane proteins that can be classified as the dystroglycan subcomplex, the sarcoglycan-sarcospan subcomplex, and the cytoplasmic subcomplex. The cytoplasmic subcomplex includes the syntrophins (syn) and α-dystrobrevin (αDB). The sarcoglycan-sarcospan subcomplex comprises the sarcoglycans (α, β, δ, γ) and sarcospan. The extracellular component of the dystroglycan complex, α-dystroglycan (αDG), binds to laminin-2 in the extracellular matrix and β-dystroglycan (βDG) in the sarcolemma. In turn, β-dystroglycan binds to the dystrophin, thus completing the link between the actin-based cytoskeleton and the extracellular matrix. Adapted from (Blake et al. 2002).

junction formation, binds β-dystroglycan (Cartaud et al., 1998). This interaction has important implications for the role of both α- and β-dystroglycan in neuromuscular junction formation.

- In contrast, **α-dystroglycan** is located in the extracellular matrix where it is thought to be directly associated with β-dystroglycan through multiple covalent interactions. α-dystroglycan is a dumbbell-shaped protein that has a central mucin-like region flanked by globular domains. α-Dystroglycan binds extracellular protein, in particular laminin G (LG) domains in laminins 1 and 2 (c_1-chain and α_2-chain) in a calcium dependent manner, and perlecan with varying affinities (Ervasti and Campbell, 1993; Yamada et al., 1994). The interaction between the α-dystroglycan and the extracellular protein is essential for the link of the cytoskeleton with the extracellular matrix and the glycosylation of the dystroglycan seems to be essential for this process (Ibraghimov-Beskrovnaya et al., 1992; Martin, 2003). At the neuro-muscular junction α-dystroglycan links also agrin that is implicated in the correct clustering of the acetylcholine receptors (Apel and Merlie, 1995; Campanelli et al., 1996).

Sarcoglycan complex:

In skeletal and cardiac muscle, the sarcoglycan complex is composed of four transmembrane glycoproteins α-, β-, δ-, γ-sarcoglycan and sarcospan, a member of the tetraspan family. The molecular associations of the sarcoglycan-sarcospan components and the associations with the other components of the DAPC are currently unclear (Blake et al., 2002). α-Sarcoglycan (387 AA) has a signal sequence that allow the positioning of the C-terminal domain of the protein to the interior of the muscular fibres (Roberds et al., 1993). This type of sarcoglycan is totally absent in smooth muscles but there is another sarcoglycan that shared 44% of homology with α-sarcoglycan: the ε-sarcoglycan (Barresi et al., 2000; Ettinger et al., 1997; Straub et al., 1999).

Syntrophin:

The syntrophin family of proteins is composed of five members (α1, β1, β2, γ1 and γ2). The last two are specific of the neuronal cells (Piluso et al., 2000). The classification is based on the physical chemical properties and on their localisation (Ahn et al., 1996; Peters et al., 1994, 1997). Even if they are coded by different genes, they shared a similar structure consisting of a split PH

domain and intact PH domain, a PDZ domain, and the syntrophin unique region at the COOH terminus. Through the PDZ domain it is associated with nitric oxide synthase (NOS) and voltage-dependent sodium channels (Brenman et al., 1996; Ort et al., 2000; Schultz et al., 1998). Thanks to the distal region and the PH domain of syntrophins, these proteins are able to interact directly with dystrophin.

Dystrobrevin:

Dystrobrevin protein was discovered as a dystrophin-related protein that had significant protein sequence homology to the COOH terminus of dystrophin (Wagner et al., 1993). The dystrobrevin family of proteins is encoded by two different genes, but the promoters drive the expression of each dystrobrevin isoform in different tissues. The α-dystrobrevin gene is located on human chromosome 18 (mouse chromosome 18) and encodes at least five different protein isoforms (Sadoulet-Puccio et al., 1996). The β-dystrobrevin is encoded by a gene on human chromosome 2 (mouse chromosome 12) that produces a number of COOH-terminal alternatively spliced variants (Blake et al., 1998). This family of proteins are able to bind directly to dystrophin, syntrophin and dystroglycan. Though its COOH domain the dystrobrevins link syntrophin forming two tandem α helics and the stoichiometry of the interaction is controlled by the alternative splicing of the dystrobrevin itself (Newey et al., 2000). The interaction with dystrophin is made the coild coil regions of the two proteins (Sadoulet-Puccio et al., 1997); instead the interaction with dystroglycans is made by the EF-hand of dystrobrevin (Chung and Campanelli, 1999). More recent experiments suggest that the α-dystrobrevins are associated with the sarcoglycan complex. This association is thought to be mediated by the NH2-terminal region of α -dystrobrevin common to all isoforms, anchoring all three dystrobrevin (α-dystrobrevin-1, -2 and -3) isoforms to the DAPC.

The localisation of the different isoforms of dystrobrevin has been studied. The isoform α –dystrobrevin -1 and -2 has been found more abundant at neuromuscular junction and at the sarcolemma where the isoform 2 is predominant. In the absence of dystrophin this sarcolemmal localisation is largely lost Instead of α –dystrobrevin -3 that is more aboundant at heart level (Blake et al., 2002). At the neuromuscular junction α –dystrobrevin may be associated with utrophin and it could be implicated in the recrutement of the acetylcholine receptors (Newey et al., 2001).

DAPC in DMD patients and *mdx* mice

In 1990 Campbell et al. showed for the first time a 90% reduction of α-dystroglycan in DMD muscles compared with healthy one (Ervasti et al., 1990). Then it has been shown that all the protein complex was reduced by about 80-90% (Ohlendieck et al., 1993) but the mRNA level was not systematically reduced for all the proteins of the complex (Ibraghimov-Beskrovnaya et al., 1992). Mutations at the C-terminus of dystrophin promote the most severe form of dystrophy and are accompanied with the reduction of the proteins belonging to the DAPC (Matsumura et al., 1993).

On the other hand, in BMD patients, the decrease of DAPC is less important than in DMD form: the expression of truncated dystrophin allows the binding of the complex (Matsumura et al., 1994). At neuromuscular junction level but also at sarcolemmal level can be found the DAPC anchored at the membrane through utrophin, thanks of the natural overexpression of utrophin in dystrophic muscles (Matsumura et al., 1992; Mizuno et al., 1994).

In the *mdx* mouse all dystrophin-associated proteins are greatly reduced (80-90%) in the muscle due to the absence of dystrophin and not to secondary effects of the degradation of muscle fibers. There is a reduction in α- and β-dystroglycan in these dystrophic mice. Similarly, α-sarcoglycan mRNA is present in *mdx* muscles, but the protein is greatly reduced. The regulation of these proteins is therefore post-translational in these muscles, so the fact that they are not traceable in the membrane is due to the disruption of the sarcolemmal structure (Ervasti and Campbell, 1993).

DACP can be found at the neuromuscular junction lbut also at the sarcolemma anchored at the membrane through utrophin, thanks to the natural overexpression of utrophin in dystrophic muscles (Matsumura et al., 1992; Mizuno et al., 1994).

1.4 THE MUTATIONS

In patients, the open reading frame of the dystrophin gene is altered by deletions, duplications, point mutations, or other rearrangements (Kalman et al., 2011). A significant number (around 30%) of all DMD cases are the result of random spontaneous genetic abnormalities of the dystrophin gene that can occur during pregnancy regardless of family history (Bennett et al., 2001). The majority of large deletions cluster are around two mutation hot spots, probably due to

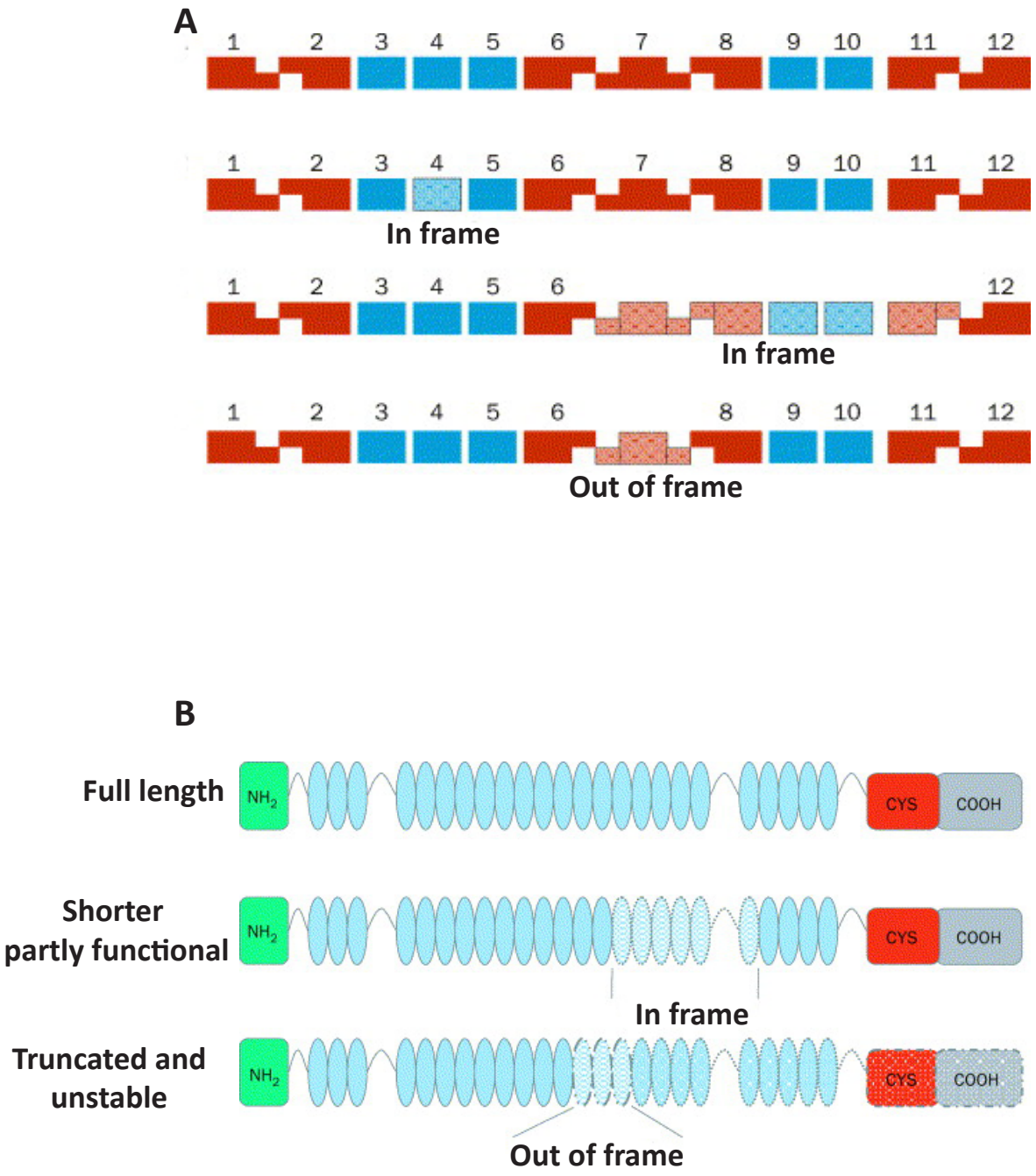

Figure 4: Schematic representation of in frame and out of frame deletions. (A) The open reading Sframe (ORF) is maintained after the deletion of the exon 4 or of the exons 7-11. On the other hand the ORF is lost when the exon 7 is depleted. (B) The effects of these types of deletions are a shorter but partially functional protein in case of in frame deletions or a truncated and unstable product in case of out of frame deletions. Adapted from (Muntoni et al. 2003).

the chromatin structure in the Xp21. Region I spans exons 45-53 and removes part of the road domain, while region II spans exons 2-20 and removes some or all of the actin-binding sites together with part of the rod domain (Blake et al., 2002). Thanks to Monaco a model of correlation between a mutation and the gravity of the pathology has been established (Monaco et al., 1988). Mutations that maintain the reading frame of the gene, resulting in partially functional protein, are associated to BMD phenotype. On the other hand, mutations that alter the reading frame of the gene, resulting in unstable RNA that eventually lead to the production of nearly undetectable concentrations of truncated proteins, are associated to DMD phenotype (Fig. 4). This theory operates in 90% of the cases but some exceptions have been described (Koenig et al., 1989; Malhotra et al., 1988; Winnard et al., 1993).

In the rest of the cases of DMD patients point mutations have been described. For this type of alterations there are not hot spot site but they can be found all along the gene. They introduce premature stop codons but usually very little or no protein is detected (despite the hypothesis of the production of normal amount of truncated protein) (Blake et al., 2002).
In the case of BMD point mutations are very rare and they promote missense mutations (Roberts et al., 1992, 1994; Sitnik et al., 1997). The importance of the actin-binding domain at the NH_2 terminus of dystrophin was demonstrated by the identification of a point mutation that resulted in a missense mutation (Arg for Leu-54) (Prior et al., 1993).

1.5 UTROPHIN: from GENE to PROTEIN

1.5.1 The gene

Utrophin has been identified by three different groups in the world. Fardeau's group discovered the presence of a protein at the neuromuscular junction of dystrophic fibres with antibody against dystrophin. Davies' group discovered utrophin studying similar sequences to dystrophin through cDNA toward the C-terminal domain; and thanks to Khurana's work it is now possible to know the protein structure of utrophin (Fardeau et al., 1990; Khurana et al., 1990; Love et al., 1989). Thanks to Davies' study it has been possible to localize *UTRN* gene on human chromosome 6 (q24) (chromosome 10 for mouse) and to observe the 65% of homology with dystrophin gene and 80% between the two proteins. *UTRN* gene consists in 74 exons and it is one-third the size of the DMD gene. The genomic organisation of the genes is similar for the 3' and 5'extremities, on the other

hand the homology for the sequences that codify for the central domain of the proteins is under 45% (Pearce et al., 1993).

As described for dystrophin, utrophin expression is under the control of different promoters. In particular for the expression of the full length protein there are two promoters (A and B), but also some others promoters that control the expression of truncated isoforms as dystrophin (Up71, Up113and Up140). The amount of mRNA of utrophin, determined by RT-PRC and *in situ* hybridation, in healthy and dystrophic skeletal muscles do not change. In both cases its localisation is preferentially within the postsynaptic sarcoplasm of adult muscle fibres, but it could be found at extrasynaptic level (Vater et al., 1998). The 3'UTR region is essential for control of stabilisation and localisation of utrophin mRNA in skeletal muscles (Jasmin et al., 2002). The AU rich-region between 332 and 969 nucleotides of the 3'UTR region is responsible for the correct localisation. The 3'UTR region between the nucleotides 161 and 332 control the half-life of utrophin mRNA (Gramolini and Jasmin, 1999; Gramolini et al., 2001a).

The A promoter:

The A promoter, the first to be described (Dennis et al., 1996), is the most active in skeletal muscles. The promoter sequence is located in 5' of the first exon and it is composed of 155 bp. It contains different binding site for transcription and regulator factors. The A promoter is rich in CpG island; it contains a binding site for Sp1 and 3, a N-box and a E-box binding site for MyoD family members. The expression of the promoter is increased during the myogenesis through the interaction between the myogenic factors and the E-box (Gramolini et al., 1999a). This promoter is also controlled by a sequence called DUE (Downstream Utrophin Enhancer) that contains a binding site for AP-1 (Activator Protein-1) particularly important during muscular regeneration (Galvagni et al., 2002).

The N-box is the protagonist for the activation of this promoter because of is the interaction with the "ets-related GABPα/β transcription factors" under the control of heregulin (Gramolini et al., 1999a; Khurana et al., 1999). It has been shown that the inhibition of ERK decrease the utrophin expression, even if in presence of heregulin. It is possible because ERK is implicated in the phosphorylation of GABPα that is essential for the formation of the complex GABPα/β to interact with the N-box (Basu et al., 2007) (Fig.5). On the other hand the activation of the A promoter is

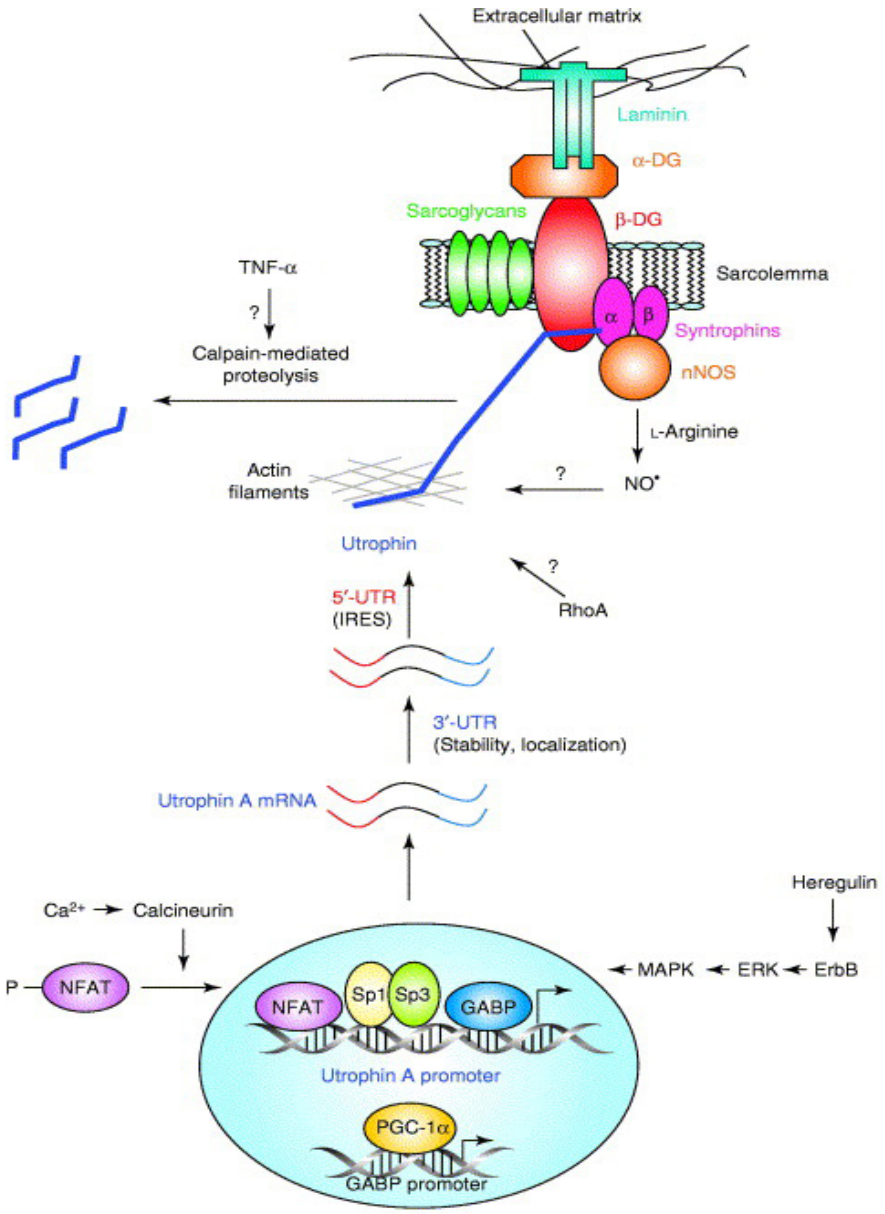

Figure 5: Schematic representation of utrophin localisation at the post synaptic sarcoplasm (top) and expression (bottom). At the sarcolemma it links the components of the dystrophin associated protein complex linking the extracellular matrix to the cytoskeletal actin. In the synaptic region, the heregulin enhance a cascade of events that allow the expression of utrophin GABA-dependent. Meanwhile the transcription factors Sp1 and 3 bind specific regions in the promoter. At extra-synaptic regions the expression of utrophin gene is enhanced by calcineurin that dephosphorylates NFAT allowing its translocation in the myonucleus where it activates the gene expression. Adapted from (Miura and Jasmin 2006).

repressed by ERF that links N-box/Ets-site (Perkins et al., 2007). The activity of ERF depends on ERK activity and nuclear localisation (Le Gallic et al., 2004).

The B promoter:

The second promoter described is located into the second intron. Whereas the first exon differs between promoter A and B, after alternative splicing, the mRNAs are the same. The B promoter do not contain binding site for synaptic regulation element, like the N-box (Burton et al., 1999), it means that it is responsible for the vascular endothelial and ubiquitary expression of utrophin (Weir et al., 2002). The activation of this promoter seems to be directed by different factors as Est, Ap-1 or GATA-2 (Briguet et al., 2003; Perkins and Davies, 2003).

1.5.2 The protein

Utrophin shares 80% amino acid identity with dystrophin. It is a 395 kDa protein encoded by a 13kb transcript that is expressed ubiquitously but at widely differing levels in tissues and cell lines, more over the transcript is particularly abundant in several human foetal tissues (heart, placenta, intestine,...) (Tinsley et al., 1992). The comparison between the two amino acids (AA) sequences allowed to highlight the same domains of dystrophin (Fig. 6) (Blake et al., 2002).

- The NH_2 terminus of this protein is composed by 250 AA and it shares 80% of identity with the same domain in dystrophin (Tinsley et al., 1992). Utrophin is able to link F-actin through its N-terminal domain, but the affinity of the interaction is less important (Kd=19 μM) than dystrophin one (Kd=44 μM) despite the presence of ABS 1, 2 and 3 as described for dystrophin (Winder et al., 1995). Moreover, the binding is calcium dependent (Winder and Kendrick-Jones, 1995). The ABSs are part of two large domains CH that are implicated in the interaction with actin. In particular, ABS1 and 3 correspond to the helix α1 in the first and second domain respectively, while ABS2 correspond to α5 and α6 of CH1 (Keep et al., 1999). It has been shown that CH1 is more implicated in the interaction with actin and that CH2 has a secondary role in the bound (Moores et al., 2000).

- The central domain of utrophin is composed by the repetition of 110 AA sequence as dystrophin, but is shorter (Tinsley et al., 1992). The coild-coil C-terminal extremity of the domain is common with dystrophin and is conserved with different species (Blake et al., 1995).
- The C-terminal region is conserved between utrophin and dystrophin with more than 80% of identity (Tinsley et al., 1992). The binding site of the DAPC are present also in this protein (Tommasi di Vignano et al., 2000). At this level can be found the α hI and α hII helixs separated by a sequence rich in proline that favorised dimerisation and the bound with other proteins (Blake et al., 1995).

A different between utrophin and dystrophin is their localisations: dystrophin is confined at muscular and brain level, instead utrophin is widely expressed. The protein can be found in skeletal, cardiac and smooth muscle but also in vascular endothelial, retinal glial cells, platels, Schwann cells of the peripheral nerves and satellite cells. In adult healthy muscle the gene of utrophin remains intact but quiescent and the protein is confined at neuromuscular junctions and myotendinous junctions (Blake et al., 2002). At neuromuscular junction level utrophin is found at the crests of the junctional folds in close proximity to the acetylcholine receptors (Bewick et al., 1992), whereas dystrophin occurs mainly in the troughs (Fig. 7).
In dystrophic muscles the protein can be found not only at the neuromuscular junction but also at extrasynaptic level and there is an increase of protein expression (Karpati et al., 1993) at about 10 times compared to healthy muscle. This could be explained as a protective role of the protein against dystrophic phenotype.
Also in regenerating muscles there is an increase of the quantity of protein at about 4 to 7 times without a change in the amount of mRNA sign of post-traductional events (Gramolini et al., 1999b). In this case, utrophin is rapidly replaced by dystrophin.
The expression of utrophin has been studied during human development in healthy and dystrophic conditions. Utrophin is present in the muscles before the 9th week of gestation with a non-homogeneous pattern; then the protein expression become uniform and the maximal expression can be observed at 17-18 weeks. At 26 weeks the expression decreases and the localisation is the same of adult fibres (Clerk et al., 1993).

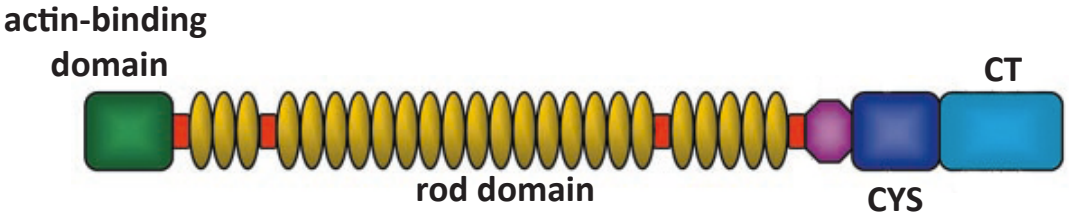

Figure 6: Schematic representation of the organization of the utrophin protein. Similar to dystrophin at the N-terminus domain the actin-binding domain is located, followed by the road domain, the CYS one and the C-terminus domain at which it links NOS. Adapted from (Blake, Weir et al. 2002).

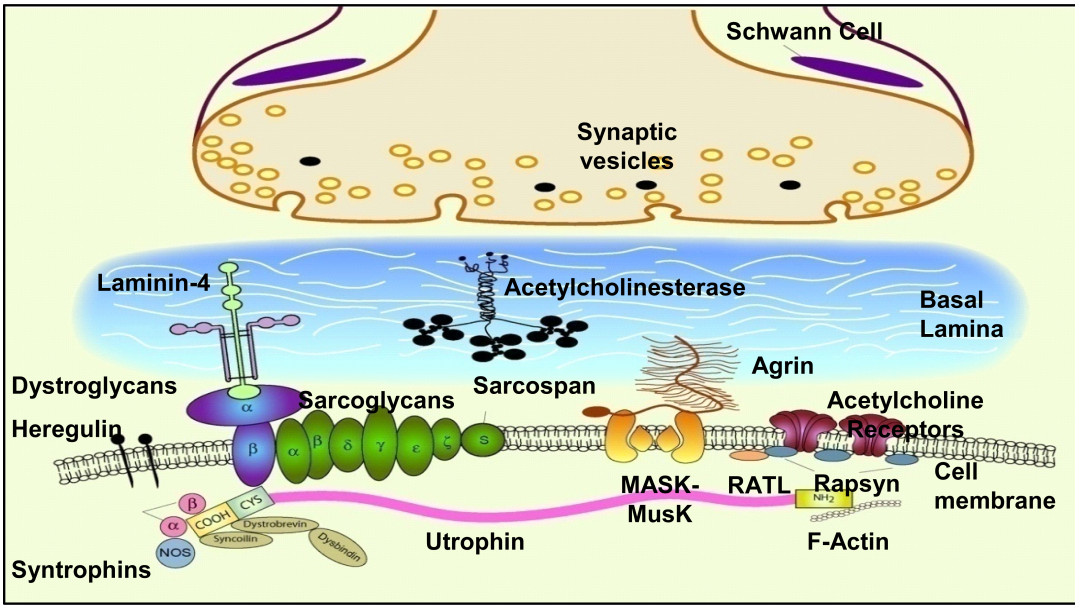

Figure 7: Schematic representation of localization of utrophin at the neuromuscular junction. It links the dystrophin associated protein complex with the CYS rich- domain, while it is linked to the NOS with the C-terminal domain. On the other side, it is linked to actin with the N-terminal domain.

1.6 THE ANIMAL MODELS

In this section the three main animal models utilised to study DMD are described: the *mdx* mouse, the CXMD dog and the HFMD cat.

1.6.1 The *mdx* mouse

In 1984 studying the creatine kinase (CK) level in the serum C57BL/10 animals were found with very high levels of CK similar to those observed in DMD patients. In the same study it has been identified that the anomalie was related to X chromosome and was accompanied by muscle lesions. The animals were named *X-linked Muscular Dystrophy* (*mdx*) (Bulfield et al., 1984). Later with the discovery of dystrophin it was demonstrated that in those animals dystrophin was absent because of a point mutation introducing a stop codon (C→U) (Hoffman et al., 1987; Sicinski et al., 1989).

In spite of the absence of the protein, *mdx* mice do not show severe clinical features as DMD patients. The fibre degeneration existing in humans is also visible in the animal but is compensated by an intense regeneration process characterized by central nuclei (Coulton et al., 1988; Tanabe et al., 1986). This process decreases with age (65-104 weeks) in favour of necrosis and animals display a muscle phenotype close to the human condition (Lefaucheur et al., 1995; Pastoret and Sebille, 1993, 1995).

The development of the disease in *mdx* mice can be divided into four phases: (i) different steps of necrosis, (ii) reduction of muscle weight and (iii) force, and the (iv) increased of time of relaxation (Tanabe et al., 1986). The decrease of muscular force of mdx mice is about 28% with age and about 20% compared to wild type animals (Lynch et al., 2001). Only diaphragm displays clinical features, fibrosis and degeneration, comparable to DMD patients (Stedman et al., 1991). From mechanical analysis a decrease of force about 50-60% compared to wild type mice has been recorded (Lynch et al., 1997; Tinsley et al., 1998).

1.6.2 The CXMD dog

The canine model develops Duchenne muscular dystrophy very close to the human form (Cooper et al., 1988). Called Canine-X-linked muscular dystrophy (CXMD) presents necrosis and

regeneration process in muscle, with fibrotic and fatty tissues and abnormal diameter of the fibres, all lifelong with more predominance in young animals (Valentine et al., 1988).

The Golden Retriever Muscular Dystrophy (GRMD) is the most described in literature. The mutation that produces the absence of dystrophin is a single base change in the 3' consensus splice of intron 6. The seventh exon is skipped which predicts a termination of the dystrophin reading frame within its N-terminal domain in exon 8 (Sharp et al., 1992).

As observed in humans and in the *mdx* mice there is an increase in utrophin expression compared to healthy dogs especially in the extra-synaptic areas and an increase of CK level after physical exercises (McCully et al., 1991; Wilson et al., 1994).

1.6.3 The HFMD cat

In 1989 the first dystrophic cat was described in literature. It shares with humans the same development and histopathological features of the disease, even if it has two important differences: the lack of fat infiltration and the presence of prominent hypertrophy (Carpenter et al., 1989). In the feline model, hypertrophy is the principal characteristic of the disease especially in the diaphragm, giving the name to the animal: Hypertrophic Feline Muscular Dystrophy (HFMD) (Gaschen et al., 1992). This animal model is also characterized by the calcification of the muscles, especially the tongue.

The mutation that leads to the absence of dystrophin in the HFMD cat has been identified as a deletion in the promoter of muscle and Purkinje cells.

1.7 CLINICAL AND MOLECULAR FEATURES

1.7.1 Clinical features and natural history of Duchenne Dystrophy

John Little and Edward Meryon reported and described the disease in 1853. They described two brothers, 12 and 14 years old, who had shown “abnormal increases of bulk of muscle combined with contraction and adipose degeneration”. The older brother barely walked alone at the age of 19 month, never crawled, was unwilling to exercise, had difficulty rising from ground and “was sluggish in physical and moral temperament”. By the age 6 he could walk 3 to 4 miles on a level surface, but walked with the head and body inclined backward and then he sat. After the age of 6 he began gradually to decline and between ages 9 and 11 he lost his ability to stand. Contractures of the heel cords began at the age of 6 and marked enlargement of the calf muscles was present at the age of 11 (Emery and Emery, 1993). The younger brother was similarly affected but was able to walk until the age of 11.

Disease activity, evidenced by high serum CK and muscle fibres necrosis, is present in the neonatal period, but the illness is seldom manifested during infancy. Although height and weight are normal at birth, subsequent growth is slow and the growth curve falls below the normal centiles in the first years of life. At the preclinical stage short stature is a common finding.
Early symptoms are developmental delay, difficulty in running or climbing stairs, frequent falls and enlargement of the calf muscles that is stil present at 5-6 years. Between 3 and 6 years of age the gait becomes lordotic and waddling and the Gowers sign appears.

Between 6 and 11 years of age the strength of limb and torso muscles decreases steadily and essentially linearly. When DMD patient are evaluated by the Vignos scale (1-normal function; 9-unable to ambulate), most spend a long time in functional grade 2 and then traverse the remaining stages rapidly, over the course of 2 or 3 years. During the second decade of life, and especially after ambulation is lost, all limb and torso muscles decrease in size. Due to increasing weakness of the upper extremities, the patients can eventually perform only limited activities involving the forearm and hand muscles.

The natural course of the deformity in DMD patients has been classified into three types depending on unremitting progression with kyphosis (thoracolumbar deviation in a dorsal plane),

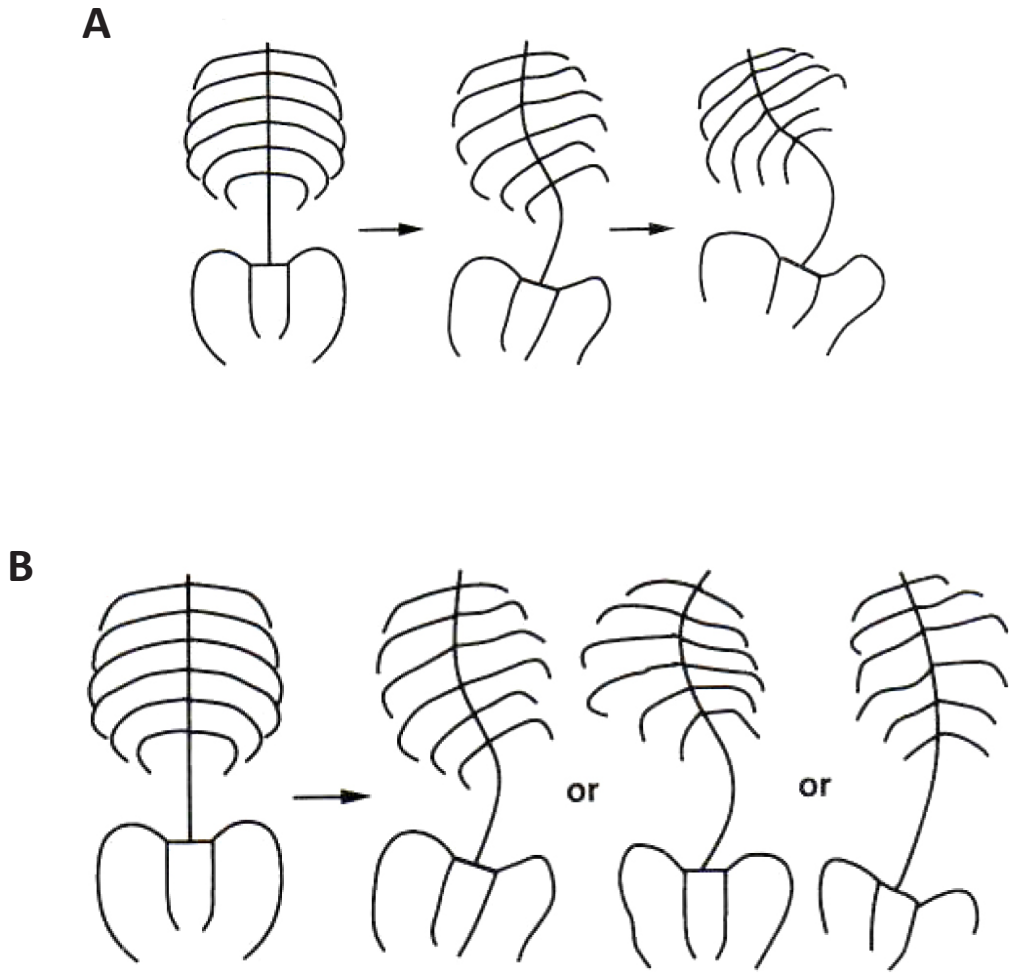

Figure 8: Schematic representation of dorsal deformity in DMD patients. (A) Example of unremitting progression with kyphosis and (B) transition from kyphosis to lordosis. Adapted from (Oda et al. 1993).

the transition from kyphosis to lordosis (deviation in the ventral plane, Fig. 8A) and less deformity (Fig. 8B) (Oda et al., 1993). As well as exacerbating respiratory dysfunction in affected boys, kyphosis negatively impacts their quality of life in their wheel-chair dependent years, leading to surgery or chronic pain.

Significant weakness of respiratory muscles, indicated by abnormally low maximal inspiratory and expiratory pressures and by decreased vital and total lung capacities, begins at the age of 8 or 9 and increases consistently with age and decreasing functional ability. Respiratory failure, with carbon dioxide retention and anoxemia, occur terminally with respiratory infections. Pure respiratory failure without infections can also occur and signals an irreversible, terminal event.
Cardiac alterations (see section "*Cardiomyopathy"*) are also common features of DMD patients.

Electromyography and nerve conduction studies have been performed in DMD patients. Needle electromyography findings are myopathic, with short duration, low amplitude polyphasic motor unit potentials, particularly in proximal muscles. Abnormal spontaneous activity in the form of fibrillation potentials, positive sharp waves and complex repetitive discharges may be detected due to denervation and some re-innervations in necrotic muscles. This may also result in the presence of satellite motor unit potentials. Over time the motor units become very small and some areas become electrically silent. Nerve conduction studies are normal in early DMD. As the disease progresses, compound muscle action potentials decrease in amplitude (Yiu and Kornberg, 2008).

1.7.2 Physiopathology of DMD

Lack of dystrophin has numerous functional and structural consequences in muscles: alterations of membrane permeability, intra-cellular calcium homeostasis, muscle strength, and muscle regeneration capacity, as well as numerous histopathological changes (Blake et al., 2002).

1.7.2.1 Membrane permeability

The first sign of a malfunction of the membrane permeability is the presence of muscle enzymes found in the serum of dystrophic patients. In 1959 Ebashi et al. showed for the first time a systematic increase of CK activity in patients with progressive muscular dystrophy. Later, Okinaka and Schapira determined that the higher dose was observed in DMD patients and that 2/3 of the patients' mothers displayed an increase of the enzyme in the serum (OKINAKA et al., 1961). The molecules of CK are able to pass through the plasmic membrane because of a deficit in the lipid bilayer in dystrophic muscles (Ozawa et al., 1999).

Concerning DMD patients the CK level is not stable all lifelong: between 1 and 6 years it is maximal then it declines (Zatz et al., 1991). Instead in the *mdx* mice the amount of CK is normal until the 3rd week of age then it increase and it remains elevate for a lot of months (McArdle et al., 1995). Some other muscular enzymes can be detected in dystrophic condition, as for example pyruvate kinase, parvalbumin or myoglobin (Jockusch et al., 1990; Kagen et al., 1980; Zatz et al., 1978).

Others extra-muscular molecules can be detected in muscles, as for example albumin, different IgGs and IgMs (Straub et al., 1997). The membrane permeability is studied through coloured vital markers that are able to pass the plasma membrane, such as Evans Bleu links albumin, to detect necrotic fibres. The permeability differs between different muscles, and there is a certain variability between the fibres of the same muscular type according to the necrotic status (Straub et al., 1997).

1.7.2.2 Calcium Homeostasis

1.7.2.2.1 Role of calcium in muscle

The coupling between the stimulation of skeletal muscle by its motoneuron and the contractile response occurs through a unique mechanism, called excitation-contraction (EC) coupling. The muscle contraction results when a motoneuron triggers in each of its muscle fibres a depolarization of the postsynaptic membrane that penetrates in the muscle fibres *via* the transverse tubule system and subsequently leads to the activation of the voltage-sensing dihydropyridine receptors (DHPRs). The direct physical interaction between DHPRs and Ryanodine Receptors (RyR) triggers the release of Ca^{2+} from the sarcoplasmic reticulum (SR) (Al-Shanti and

Stewart, 2009). Ca^{2+} binds to troponin C and removes the steric inhibition of actin-myosin ATPase by troponin and tropomyosin promoting the actin-myosin binding, the sarcomeric/myofibrillar shortening, and fibre force production.

In skeletal muscle, an increase in intracellular Ca^{2+} levels not only results in contractile activity but it is also responsible for muscle-specific gene expression through activation of downstream transcriptional pathways that leads to muscle growth, hypertrophy and adaptation (Mozzetta et al., 2009; Al-Shanti and Stewart, 2009) (Fig. 9). Ca^{2+}/calmodulin-dependent transcriptional pathway and calcineurin should also be considered as potential mediators of muscle growth in post-natal development and hypertrophy.

1.7.2.2.2 Calcium homeostasis in dystrophy

DMD: The total Ca^{2+} measured in muscle biopsies from DMD patients was greater than that from normal muscle. Ca^{2+} mishandling in DMD suggested that dystrophin may regulate Ca^{2+}-signalling cascades such as Ca^{2+} entries. Instead, several experiments have supported the idea that a small and persistent inward Ca^{2+} leak in dystrophin-deficient muscle cells could be the consequence of the alteration of the control normally supported by dystrophin on trans-membrane channels especially during contractions. Indeed, while human DMD myotubes in primary culture did not develop a significant increase in Ca^{2+} $concentration_i$, well-differentiated and contracting human DMD myotubes displayed elevated steady-state Ca^{2+} levels dependent on muscle spontaneous activity.

A recent work has suggested that increases in Ca^{2+} $concentration_i$ was related to the degree of mechanical stress and that Ca^{2+} elevations and muscle damage were prevented by stretch-activated channel blockers. The studies conducted by Constantin's group on human myotubes confirmed that SACs were more active in the plasma membrane of DMD myotubes (Vandebrouck et al., 2001).

Another type of channel that could be involved in Ca^{2+} homeostasis is the L-type. This type of channel is not directly implicated in the aberrant homeostasis of Ca^{2+} but the absence of dystrophin is able to alter its properties (Imbert et al., 2001) and the expression of a mini-dystrophin restore normal properties profile (experiment performed on transgenic *mdx* mice) (Friedrich et al., 2004).

Mdx: A similar situation could be found in *mdx* mice. Studies performed on dystrophic muscle cells from *mdx* mice have suggested that a persistent intake of Ca^{2+} activates Ca-sensitive proteolytic

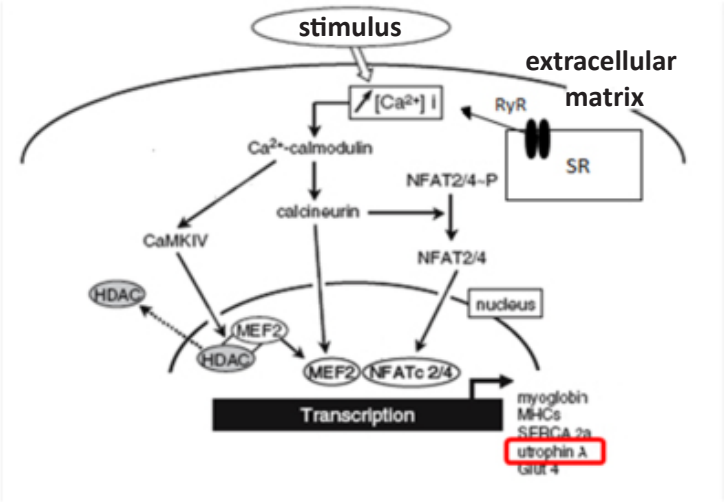

Figure 9: Role of Ca2+/Calmodulin pathway in mucle gene expression. Ca2+/Calmodulin activates CaMKIV wich translocates into the nucleus where it phosphorylates and deactivates HDAC4/5 and HDAC1/2 complex enhancing MEF2. MEF2 acts in combination with NFAT that after Ca2+/Calmodulin dependent dephosphorilation, translocates into the nucleus. Adapted from (Al-Shanti and Stewart, 2009).

and phospholipolytic activities resulting in the degradation of dystrophic muscle fibres (Constantin et al., 2006). Forced expression of mini-dystrophin in these myotubes, reactivates appropriate sarcolemmal expression of dystrophin-associated proteins and restores normal Ca^{2+} handling in the cytosol. Furthermore, the recombinant mini-dystrophin reduces the store-operated Ca^{2+} influx across the sarcolemme, the mitochondrial Ca^{2+} uptake during this influx, the L-typeCa^{2+} channels *via* a direct or indirect linkage and the Ca^{2+} release from sarcoplasmatic reticulum, sign that dystrophin may influence excitation-Ca^{2+}-release coupling (Constantin et al., 2006).

Further studies were conducted to determine whether mini-dystrophin could control Ca^{2+} influx through specific plasma-membrane channels and Kurebayashi et al. showed that store-operated calcium entries, also named capacitative calcium entries (CCEs), can be activated in muscle fibres even by a partial depletion of the cellular stores (Kurebayashi and Ogawa, 2001). Moreover, the slow cumulative Ca^{2+} entry through store-operated channels (SOC) is crucial for long-term Ca^{2+} homeostasis, because they control capacitative entry of extracellular calcium after depletion of intracellular calcium stores in the endoplasmic or sarcoplasmic reticulum (ER/SR), and that reduced SOC activity exaggerates muscle fatigue (Pan et al., 2002). More importantly, the activity of SOCs was increased in dystrophic fibres (Sabourin et al., 2009), and it was therefore hypothesized that these SOCs could belong to the transient receptor potential channel (TRPC) family. In a recent study it has been hypothesized a role of TRPC1 in the progression of the disease in axial muscles of *mdx* mice (diaphragm, *sternomastoid*, *biceps brachii* and *tibialis anterior*). Matsumura et al. observed, only in the diaphragm, an increase in TRPC1 associated with a Ca^{2+} level four times higher than in the other muscles. Ca^{2+} level could be restored by the treatment with streptomycin, a stretch-activated channel blocker, to reach level of control mice (Matsumura et al., 2011).

In addition to the theory that ions could accumulate in dystrophic fibres through a loss of regulation of membrane ion channels, a second theory is that ions could accumulate through membrane tears due to the lack of dystrophin (Whitehead et al., 2006). A theory supported by the fact that the profile of the phospholipids in sarcolemma is different in the areas of necrosis/regeneration in *mdx* (Touboul et al., 2004) and DMD patients (Tahallah et al., 2008) muscle, and restored in *mdx* mice treated with molsidomine (a nitric oxide (NO) donor) (Benabdellah et al., 2009).

Recently the interaction between reactive oxygen species (ROS) and Ca^{2+} homeostasis in the case of DMD has been confirmed (Khairallah et al., 2012). They have described a process yet known in the heart named X-ROS. In the X-ROS process the microtubule-dependent activation of NADPH oxidase is driven by a brief physiologic stretch: in particular, the microtubule network transmits the mechanotrasduction signals through the protein NADPH oxidase-2 (NOX2) to generate ROS (Prosser et al., 2011). The direct correlation between X-ROS and Ca^{2+} homeostasis in skeletal muscle has been demonstrated by the observation of a decrease in the ion concentration after the depolymerisation of the microtubule network and the inhibition of NOX2 with colchicine and gp91dsTAT respectively, in old *mdx* mice fibers under mechanical stretch. They also demonstrated that the increase of intracellular Ca^{2+} after mechanical stretch is due to SACs and not to SR release.

Moreover, it has been described that resting intracellular Ca^{2+} is indirectly implicated in NO production through the modulation of NF-*k*B pathway in *mdx* mice (Altamirano et al., 2012). These authors demonstrated that the increase in Ca^{2+} resting is a multifactorial *scenario* involving both calcium entry and Ca^{2+} SR leak (through RyRs and IP_3Rs) and that the increase of the ion found in the case of DMD, causes altered function of the transcription factor NF-*k*B leading to iNOS expression and NO production. In accordance with this hypothesis, L-arginine decreases inflammation and modulates the NF-*k*B pathway, directly or indirectly *via* utrophin up-regulation (Hnia et al., 2008).

1.7.2.3 Muscular strength

Different studies have been done in order to investigate functional properties of dystrophic muscles compared to healthy muscles before or after activity.

1.7.2.3.1 Muscular ability before exercise

The studies have been performed principally on *soleus*, *EDL* and diaphragm in *mdx* mice: *soleus* and *EDL* are examples of slow and rapid muscles respectively, and diaphragm displays similar disease progression to human (Stedman et al., 1991). In order to determine if dystrophic muscles undergo easier to membrane damage when submitted to high stress level, Moens et al. submitted *soleus* and *EDL* to a series of isometric contraction followed by a series of contraction with stretches, and observed that the most important difference between the two strains was for the fast muscle after contractions with stretches. In fact, after isometric contractions only a small force drop was observed, sign of no membrane damage in *soleus* and *EDL*. After contraction with

stretches a force drop of 10% was observed in *soleus* of both strains and in the *EDL* of wild type mice. Moreover, the *EDL* of the *mdx* mice displayed an irreversible force drop of 40-60%. Histological analysis confirmed that the decrease of force was associated to membrane damage (Moens et al., 1993).

In the case of diaphragm muscle, the mechanic parameters are very altered if compared to healthy animals, such as isometric contraction, tetanic contraction or twitch force (Stevens and Faulkner, 2000). Differences have been observed between young and adult *mdx* mice concerning diaphragm properties. In young animals the maximal isometric force decrease about 50% compared to wild type animals and in adult *mdx* mice the decrease was further 25%, compared to wild type mice at the same age (Petrof et al., 1993).

1.7.2.3.2 Muscular ability after exercise

The distance performed in a wheel by *mdx* and wild type mice have been recorded. In young *mdx* mice the distance performed was lower than in wild type mice at the same age, while older *mdx* mice ran 31-48% of adult control values. After exercise, *soleus* of young and adult *mdx* mice displayed hypertrophy with no changes in strength or fatigability. Only the *EDL* of older *mdx* mice exhibited slight hypertrophy with a loss of strength (Carter et al., 1995). A strong difference in force recovery can be detected between healthy and dystrophic mice. Within three days after repetitive contractions, dystrophic muscles showed a complete recovery of force, whereas for healthy animals the recovery was about 80%, suggesting a enhanced rate of recovery in *mdx* mice (Brooks, 1998).

1.7.2.4 Apoptosis

The *mdx* fibres stained with Evans Blue present DNA fragmentation at about 180 bp and their nuclei are positive to TUNEL (terminal deoxynucleotidyl transferase-mediated dUTP nick end labelling), both are sign of apoptotic program (Matsuda et al., 1995). After histological analysis it has been shown that apoptotic process in *mdx* fibers precedes necrosis and coexist with it (Tidball et al., 1995). Moreover, dystrophic mice submitted to physical activity display apoptosis two days after (Podhorska-Okolow et al., 1998; Sandri et al., 1995, 1997) . In parallel in DMD patients Sandri et al. observed an increase of apoptotic myonuclei, bax and bcl-2-positive myofibres and an increase of the activity of caspase 3 (Sandri et al., 2001).

On the contrary, other studies suggest that apoptosis is not the mechanism of cell death. Olivé et al. studying nuclear DNA fragmentation with *in situ* labelling in muscle biopsis of DMD patients, observed that nuclei of dying muscle cells were not stained (Olivé et al., 1997) Moreover, two recent works have shown that apoptosis does not contribute to muscle loss in dystrophic fibres because neither the overexpression of ARC (apoptosis repressor with caspase recruitment domain) (Abmayr et al., 2004) nor BCL-2 in skeletal muscle neither the inactivation of BAX could stop cells loss (Dominov et al., 2005). This could be explain by the fact that excessive apoptosis through pathways that are regulated by ARC or the BCL-2 family does not seems to contribute to pathogenesis in dystrophin-deficient mice and suggests that muscle loss in *mdx* mice and human patients occurs by necrosis rather than by apoptosis (Miller and Girgenrath, 2006)

1.7.2.5 Fibrosis

Replacement of muscle tissue by collagen and fatty deposits is a common feature in DMD patients and *mdx* mice and is accentuated with age (Goldspink et al., 1994). This fact could be related with the loss of proliferative capacity of muscle cells (Pastoret and Sebille, 1993, 1995). The accumulation of collagen (especially type III) probably causes membrane damage contractile activity and it has been suggested that a vicious cycle is established in which contractile activity results in membrane damage that leads to further collagen accumulation and yet more membrane damage in skeletal muscles but it is mainly found in *mdx* diaphragm, a muscle constantly requested (Goldspink et al., 1994). Further more a progression of collagen deposition is observed all life long: at 9 month of age *mdx* mice present 4 times more collagen than wild type mice at the same age and, at 12 months, 7 times more (Itagaki et al., 1995).

In patients with Duchenne muscular dystrophy, transforming growth factor (TGF)- β l, which is the best-characterized fibrogenic mediator, is over expressed and the increase of its mRNA level is associated with the initial stage of tissue fibrosis. Subsequently connective tissue growth factor (CTGF), the downstream autocrine mediator of TGF- β l, is overexpressed (Igarashi et al., 1993). CTGF is an extracellular matrix-associated protein expressed at high levels in fibroblasts that modulates many cellular functions, including proliferation, migration, adhesion and extracellular matrix production. In addition, being a potent fibroblast mitogen and chemoattractant, CTGF stimulates the production of procollagen and fibronectin in fibroblasts (Sun et al., 2008).

Recently, Mezzano et al. evidenced a particular role of TGF-β1 and CTGF in fibroblasts isolated from the diaphragm of adult *mdx* mice. In particular, TGF-β1 and CTGF are able to control the production level of fibronectin (FN), an extracellular matrix protein. Moreover they speculate that dystrophic fibroblast are "reprogrammed" during the development of the disease because they did not find the same pattern of expression for FN in fibroblast isolated from the diaphragm of young *mdx* mice compared with old mice. Furthermore, when wild type fibroblasts are incubated with medium of *mdx* fibroblasts, they produce more FN protein that in normal conditions. This allow to think that dystrophic fibroblasts secrete some factor that can stimulate extracellular matrix synthesis into their culture medium maintaining fibrotic phenotype (Mezzano et al., 2007).

1.7.2.6 Satellite cells and muscle repair

Human muscular dystrophies are characterized by repeated cycle of muscle fibre necrosis and regeneration. These cycles usually involve scattered myofibres or small fibre bundles, and lead with time to alterations in muscle structure with variation in myofibres size, due to incomplete fusion of regenerative myotubes, progressive exhaustion of the regenerative capacity of satellite cells and substitution of muscle tissue with fibrous and adipose tissue.

The healthy mammalian skeletal muscle has the ability to complete a rapid and extensive regeneration in response to severe damage (Fig. 10). It is characterized by three phases (Ciciliot and Schiaffino, 2010):

1. Inflammatory phase

The initial event of muscle regeneration is the necrosis of the muscle fibres that leads to dissolution of the plasma membrane with calcium influx and activation of calcium-dependent proteases, such as calpains, that produce rapid disintegration of myofibres. The complement cascade is activated and it induces chemotactic recruitment of leukocytes, initially neutrophils, and then macrophages, mainly derived from blood monocytes. They infiltrate the injured site to phagocytose cellular debris and may affect other aspects of muscle regeneration by activating myogenic cells.

Two distinct subpopulations of macrophages sequentially invade injured muscle tissue. The early macrophages (M1), characterized by the expression of the CD68 marker, secrete pro-inflammatory

cytokines such as TNFα and IL-1β. They are responsible for the phagocytosis of necrotic tissue. Within days of injury the number of CD68 macrophages and neutrophils decline and the number of second population of "anti-inflammatory" macrophages increase. They are characterized by the expression of the CD163 marker and are important for muscular growth, repair and regeneration (Tidball and Wehling-Henricks, 2007). The macrophage switch is driven by interleukin (IL)-10 and, in absence of this cytokine, not only macrophage transition is abolished but muscular repair is slowed down (Deng et al., 2012; Villalta et al., 2011a).

Interferon-γ (IFNγ) plays an important role in this phase in dystrophic scenario. It is not only implicated in the indirect activation of M1 macrophages, but also in the inhibition of M2 macrophages. Recently it has been shown that the disruption of IFNγ mediated signalling in dystrophic muscles of 12 weeks-old *mdx* mice could decrease the pathophysiology of muscular dystrophy. In particular the ablation of IFNγ promote a doubling of treadmill running time and a significant reduction in muscle fibre injury, promoting M2 macrophages activity and muscular regeneration (Villalta et al., 2011b). Interestingly, in a recent study a shift to M2 macrophage phenotype and a decrease of the total immune cell infiltration has been obtained treating mdx mice with 100 mg/kg of resveratrol (Gordon et al., 2013).

2. Satellite cells activation and differentiation

Satellite cells have a distinct location within the basal lamina of all skeletal muscle, surrounding individual myofibres, juxtaposed between the plasma membrane of the muscle fibre and the basement membrane. The morphological characteristics of these cells are signs of mitotic quiescence and transcriptional silence. Increased density of satellite cells have been observed at the neuromuscular junctions and adjacent to capillaries, suggesting that some factors emanating from these structures may play a role in homing satellite cells to specific muscle locations or in regulating the satellite cell pool by other means. The satellite cell population varies also with age: during postnatal muscle growth, there is a dramatic decrease in the portion of satellite cell nuclei and this is due to the dramatic increase in myonuclei number following satellite cell fusion.

Following injury, satellite cells undergo rapid proliferation, starting during the second day after injury. Multiple signals appear to trigger satellite cells activation. For example, the generation of sphingosine-1-phosphate in the inner side of the plasma membrane; the NO production by increased NOS activity is also important for satellite cells activation, possibly through activation of

matrix metalloproteinases, which induce the release of hepatocytes growth factor (HGF) from the extra-cellular matrix. By binding to its receptor, c-Met, which is expressed by satellite cells, HGF is able to stimulate satellite cells activation. Once activated, satellite cells rapidly expressed *Myf5* and *MyoD,* members of the MRFs family, and start to proliferate (Chargé and Rudnicki, 2004). After the proliferation phase, these cells fuse; expressing *Myogenin* and MRF4, and newly formed multinucleated myotubes express developmental markers, such as embryonic MyHC. Once fusion is completed, newly formed myofibres increase in size and myonuclei move to the periphery of the muscle fibre (Fig. 10).

3. Maturation of newly myofibres

The subsequent growth of regenerated muscle may vary according to various factors, including the type of muscle injury, the involvement of blood vessels, etc. A crucial factor for successful muscle regeneration is the maintenance of the basal lamina of muscle fibres. Within the intact basal lamina satellite cells and myotubes can proliferate and fuse to form almost normal muscle fibres in a short time period.

1.7.2.7 Regeneration

In postnatal life, growth and repair of skeletal muscle fibres are mediated by satellite cells, which are located between the sarcolemma and the basal lamina of the muscle fibre. In response to muscle injury, or degenerative myopathies such as DMD, these cells divide and fuse to repair or replace the damaged fibres. However, the self-renewal potential of adult satellite cells is limited, decreases with age, and can be exhausted in case of DMD, in which most muscle tissue is lost and replaced by connective tissue. As the number of resident satellite cells in adult muscle is much smaller than the number of committed myogenic precursors that populate the muscle tissue soon after injury, so a recruitment of cells could occur from other districts, for example from bone marrow (Ferrari et al., 1998) .

Human dystrophic muscle exhibit a persistent necrosis which is not balanced by muscle fibre regeneration, and the muscle are soon invaded by fibrous and fatty tissue resulting in increasing weakness and death (Pastoret and Sebille, 1995). This can be explained by the fact that the self-renewal of satellite cells, responsible for the regenerative process, is limited especially in adults. In contrast, in *mdx* mice skeletal muscle appears normal until about 2 weeks after birth when there is

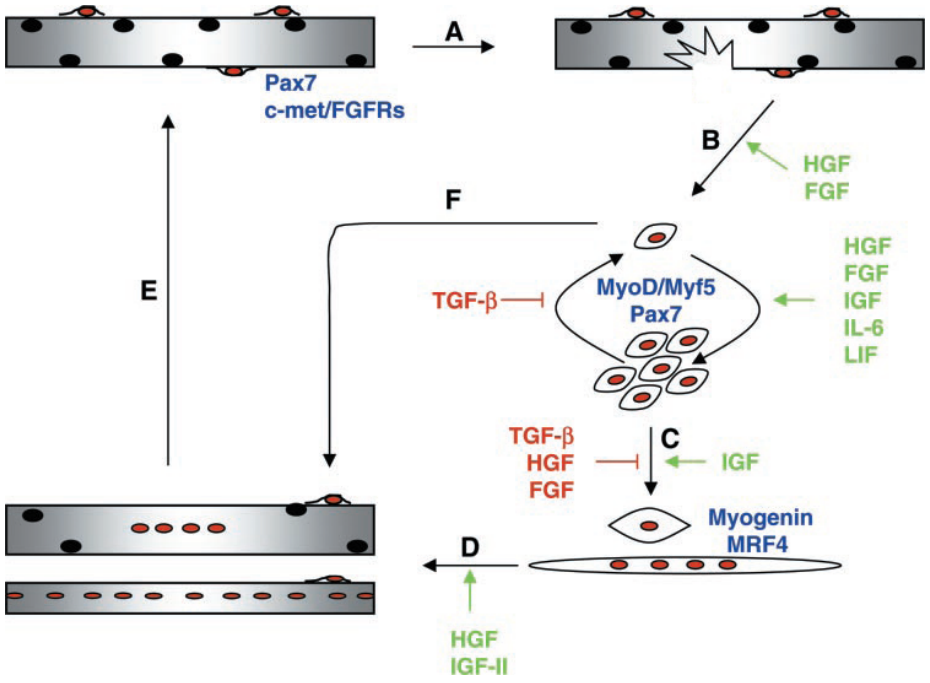

Figure 10: Schematic representation of muscle repair after injury. (A) Quiescent satellite cells after muscular injury are activated and start to (B) proliferate expressing MyoD and Myf5. (C-D) The proliferation phase is followed by the fusion of satellite cells to form new myofiber and by the final differentiation. Myoblast terminal differentiation is characterized by the expression of myogenin and MRF4. (E) Repaired myofibers are now formed. (F) Not all the activated satellite cells are implicated in muscular repair, but little pool is required for quiescent satellite cells maintenance. Adapted from (Chargé and Rudnicki 2004).

massive degeneration of virtually all fibres. There follows an immediate regeneration of new fibres and by week 10 the muscle appears fairly normal but with over 95% of nuclei centrally located, sign of a regenerative process (Schmalbruch, 1986) . In this regenerative process the role of the growth factor in proliferation, fusion and differentiation of myogenic cells has been shown, for example the bFGF (basic Fibroblasts Growth Factor) (Crisona, Allen et al. 1998). The injection of bFGF *in vivo* increased four times proliferation rate in a dose-dependent manner (Lefaucheur and Sebille, 1994). This could be explained by the fact that primary satellite cells have a high number of HSPG (heparin sulphate proteoglycans) receptors, the bFGF receptors (Crisona et al., 1998) .

1.8 CARDIOMYOPATHY

1.8.1 Description

Cardiomyopathy is a frequent cause of mortality in DMD patients. Preclinical abnormalities are detectable by electrocardiogram in 59% of patients between 6 and 10 years of age and 90% of patients, in the second decade of life, present a dilated cardiomiopathy, characterised by progressive decline in cardiac contractility, ventricular dilatation and cardiac arrhythmias (Ferlini et al., 1999). Electrical and functional cardiac abnormalities in DMD patients have been attributed to cardiac fibrosis, which suggests that fibrosis is an important component of cardiomyopathy in diseases. In accordance with this hypothesis, post-mortem examination of cardiac tissue shows that extreme fibrosis is the most histological feature of the pathology (Moriuchi et al., 1993).

Hearts of *mdx* mice share many features of the DMD cardiomyopathy. Similar to DMD patients, the animal model experiences a progressive development of cardiac defects, echocardiographic abnormalities, autonomic dysfunctions, impaired conduction, arrhythmias and dilated cardiomyopathy, although the pathology is less severe. In some studies any signs of cardiomyopathy have been observed in young animals (6 weeks old) compared to age-matched wild-type mice and only slight difference were present in *mdx* mice at the age of 29 weeks old. At the age of 42/43 weeks could be detected an established cardiomyopathy (Au et al., 2011; Quinlan et al., 2004; Spurney et al., 2008). On the contrary, Stuckey et al. observed by magnetic resonance imaging that left ventricular filling and ejection fraction rates were lower at 3 months and 6 months of age. These abnormalities were lost at 12 months old and they suppose that progressive remodelling and hypertrophy may compensate for dysfunction and mask the original abnormalities. More over at 3 months they observed right ventricular end systolic volume and ejection fraction abnormalities in *mdx* mice (Stuckey et al., 2012). Echocardyographic abnormalities have been detected in young *mdx* mice by Koenig et al. They studied voltage-gated channels dysfunction in young and old *mdx* mice and discovered that significant sodium channels impairments and considerably reduced calcium channel inactivations are already present in neonatal animals. All of this triggers to the shortening of PR interval in neonatal animals and to considerably prolonged QRS intervals in adult animals (Koenig et al., 2011). *Mdx* hears develop a severe, progressive accumulation of connective tissue, suggesting that, also in the animal, fibrosis may be responsible for some features of the cardiomyopathy. In particular, in older mice there is

an increase in the mRNA of protocollagen I and II and, the increase of fibrotic tissue in the heart is followed by the increase of connective tissue growth factor (CTGF) (Au et al., 2011).

1.8.2 Underlying mecanisms

Dystrophin-deficient skeletal muscles and hearts experience inflammation and inflammatory cells are known to promote fibrosis in numerous pathologies (Strutz and Neilson, 2003). In a dystrophic *scenario* inflammatory cells may induce fibrosis by secreting cytokines such as transforming growth factor-β (TGF-β), which stimulate connective tissue production by fibroblasts (Gosselin et al., 2004). Moreover, previews studies (Wehling et al., 2001) showed that inflammation in dystrophic skeletal muscles is exacerbated by the loss of nNOS from muscle. So, the expression of nNOS transgene in *mdx* skeletal muscles can normalize NO production and cause a reduction of the inflammation. In particular the increasing of nNOS expression in dystrophin deficient hearts has significant beneficial effects: heart sections appear histologically normal with the absence of large, fibrotic lesions that are associated with improvement in physiological indices of echocardiography (Wehling-Henricks et al., 2005). Different studies have observed a decrease of NO production in *mdx* heart mice at about 75-80%, which is similar to the loss of NOS activity that occurs in skeletal muscle (Bia et al., 1999; Ramachandran et al., 2012a). It is also important to note that while in skeletal muscles nNOS is located at the sarcolemma, in heart tissue the enzyme can be found also in the sarcoplasmic reticulum and mitochondria (Kanai et al., 2001; Wehling-Henricks et al., 2005; Xu et al., 1999). Thus deficiency in nNOS activity in this organ may primarily reflects defects in its regulation rather than loss of binding to the dystrophin complex (Wehling-Henricks et al., 2005).

cGMP is produced by soluble guanylyl cyclase activity under the stimulation of NO. Khairallah et al. tested the hypothesis that enhancing cGMP improves the contractile function, energy metabolism and sarcolemmal integrity of the *mdx* heart. This hypothesis was tested by two different approaches: transgenic (generation of *mdx* mice overexpressing guanylyl cyclase, in a cardiomyocyte specific manner), and pharmacological (*mdx* mice treated with Sildenafil, a phosphodiesterase 5 inhibitor (PDE5)). In both cases they demonstrated that enhancing cGMP signalling in dystrophin-deficient hearts, protects against sarcolemmal damage caused by mechanical workload and prevent the deterioration of myocardial contractile performance usually observed with advancing age in *mdx* mice (Khairallah et al., 2008). Two years later Adamo et al. planed three different protocols in which *mdx* mice were treated orally with long protocol of

Sildenafil at different start points: starting at 1 month after birth and at 12 months, both until 15 months, and starting at 12 months but only for 2 weeks. All along the treatment ECG exams were performed. Similarly to the previous work they observed that the drug could reverse cardiac dysfunction in case of established cardiomyopathy. Moreover, when the animals start the protocol at 1 month after birth any sighs of important cardiomyopathy could be visible, so they suppose that Sildenafil has a protecting/preventing role in the disease (Adamo et al., 2010).
Regarding a more specific action of Sildenafil in the progression of cardiomyopathy another group treated *mdx* mice with a single dose of the drug and cardiac mitochondria were studied. In particular, they investigate the role of Ca^{2+} and oxidative stress as major factors promoting permeability transition pore (PTP) opening in mitochondria (Zoratti and Szabò, 1995) that are deregulated in case of muscular dystrophy (Wallace and McNally, 2009). They observed a decrease of ion level in hearts treated with Sildenafil and a reduction of Ca^{2+} uptake in mitochondria. All of this increases the PTP opening similar to healthy hearts. On the other hands aconitase activity, a specific marker of mitochondrial oxidative stress, particularly in tissues with high mitochondrial content, was measured. In untreated animals the heart displays reduced activity of the enzyme following ischemia-reperfusion, suggesting the presence of greater oxidative stress. In hearts of treated mice, the activity was restored (Ascah et al., 2011).

More recently it has been observed a deregulation of L-arginine transporters at the membrane of dystrophic cardiomyocyte in *mdx* mice. Ramachandran et al. observed an increase of cationic amino acid transporters (CATs) (cationic amino acid transporters) expression in *mdx* mice and *mdx:utro* mice in order to improve the transport inside the cell and produce NO. In particular, they shown that the lower-affinity CAT (CAT-2A) is more expressed and they conclude that it could be a compensatory mechanism of the set in place, by DMD cardiac muscle cells, to oppose the effects of nNOS reduction (Ramachandran et al., 2012a).

Another aspect has been studied in dystrophic heart: increasing evidence suggests that ROS may play a critical role in the pathogenesis of dilated cardiomyopathies. An imbalance exists between ROS production and myocardial antioxidative stress defence mechanism, leading to increased ROS-induced myocardial injury with disease progression. Raised ROS levels lead to oxidation of various proteins, resulting in myocardial dysfunction. Myocardial proteins affected by these molecules include sarcolemmal, excitation-contraction (EC) coupling, contractile and stress-

sensitive signalling proteins. Increased ROS can also lead to inflammation and fibrosis *via* ROS-induced activation of proinflammatory pathways. Various enzymatic sources within the myocardium are capable of producing excess ROS, for example NOS, XO (xanthine oxidase) and NADPH. In particular NADPH oxidase activity is increased 1.4-folds in *mdx* mice (Williams and Allen, 2007a).

Calcium plays a particular role in cardiomyopathy. Resting intracellular Ca^{2+} concentration is high in old *mdx* compared with age-matched wild type mice. In the same work, Williams et al. recorded Ca^{2+} transient production by electrical stimulation of isolated ventricular myocytes and observed that the first Ca^{2+} transient in a series had the largest amplitude, with subsequent transient becoming smaller until a steady state, in both young and old animals. Moreover, the time to peak was shorter and the time to decay longer in dystrophic animals. They further explored the protein expression level of RyR2 in order to explain the shortening of time to peak and they discovered an increase of two times for young and of three times for adult animal compared with age-matched wild type animals that allow for a more rapid release of the ion from the sarcoplasmic reticulum store. On the other hand they suppose that the longer time to decay could be due, at least in part, to an increased inhibition of SERCA (sarco/endoplasmic reticulum Ca^{2+}-ATPase)-2. They also investigated the role of a particular calcium channel: the stretch-activated channel, in particular TRPC1, which is expressed three-fold more in old *mdx* mice than age-match wild type mice. The inhibition of stretch-activated channels by streptomycin or by the spider venom toxin GsMTx-4, reduced resting Ca^{2+} in old *mdx* mice and reveals a possible role of this type of channels in the pathogenesis of the cardiomyopathy (Williams and Allen, 2007b).

Similarly, Sarma et al. observed a diastolic sarcoplasmic reticulum Ca^{2+} release *via* ryanodine receptor type 2 (RyR2) enhancement in dystrophic cardiomyocytes. They suggest that increased phosphorylation of the serine 2808 (S2008) on RyR2 by protein kinase A (PKA) also contributes to enhanced sensitivity of RyR2 and sarcoplasmic reticulum Ca^{2+} leak and that the pharmacological/genetic inhibition of the phosphatase could prevents dystrophic cardiomyopathy (Sarma et al., 2010).

Concerning the effect of β-blockers, the common drugs delivered to treat dystrophic cardiomyopathy in patients, surprisingly, metroprolol did not modify the intracellular calcium influx in treated *mdx* mice (Blain et al., 2013).

1.8.3 Treatments

Nowadays corticosteroids are the common therapy for cardiomyopathy. They improve cardiac muscle function, stabilizing the shortening fraction (SF) in patients up to 10 years old, when treated with prednisone or deflazacon for a long period (McNally, 2007). In another clinical study, DMD patients with cardiomyopathy have been treated with ACE (angiotensin-converting-enzyme) inhibitor and/or β-adrenergic blockade, and the majority of the patients showed improvement or normalization of left ventricular function and size, consistent with cardiac remodeling (Jefferies et al., 2005; McNally, 2007).

1.9 NO & NOS IN SKELETAL MUSCLE

NO is a very small molecule, produced by different type of cells, that diffuse through cell membrane and regulates a wide variety of cellular functions such as vasodilatation (Moncada, 1999) and neuro-modulation (Baranano and Snyder, 2001). Moreover, recently it has been shown that NO is implicated in the global chromatin changes associated to gene expression (Colussi et al., 2009; Filippin et al., 2009).

During the three phases healing of muscle injury, (destruction, repair and remodelling, and remodelling (Filippin et al., 2009)), NO plays different roles. Vascularisation is an essential process for regeneration and angiogenesis is a prerequisite for the subsequent morphological and functional healing of muscles. NO can act both as an actor of angiogenesis and as a director of the process. In particular it contributes to the prosurvival/proangiogenic program of capillary endothelium by triggering and transducing cell growth and differentiation *via* endothelial-constitutive NO synthase (ec-NOS or eNOS) activation, cyclic GMP (cGMP) elevation, mitogen activated kinase (MAPK) activation and fibroblast growth factor-2 (FGF-2) expression (Ziche and Morbidelli, 2000). During the second step of healing (repair and remodelling (Filippin et al., 2009)) NO plays a role in the activation of satellite cells in a direct (Anderson, 2000) and indirect ways, promoting the release of hepatocyte growth factor (HGF) from the extracellular matrix in a pH-dependent manner. Hepatocyte growth factor has the ability to activate early division of adult satellite cells (Tatsumi et al., 2002). In the remodelling phase, transforming growth factor-β (TGF-β) and NO play antagonist role in muscle injury repair. Darmani et al. demonstrated that inhibition of NO production by L-NAME, at the time of injury, leads to a chronic expression of transforming growth factor-β *in vitro* that provokes the increasing deposition of collagen by stimulated fibroblasts (Darmani et al., 2004).

Moreover, NO molecules produced by nNOS (neuronal isoform of NOS enzyme) modulate vasoconstriction by acting directly on adrenergic system. In DMD patients and in *mdx* mice the low level of NO favorises ischemic process due to misregulation of vasoconstriction (Thomas et al., 1998). The contribution of NO to physiopathology in *mdx* has been studied in arteries of wild-type and *mdx* mice under different intensities of blood flows. The authors concluded that arteries belonging to *mdx* mice are not able to adapt properly to flow changes probably in relation with the decrease of NO quantity produced in the absence of dystrophin (Loufrani et al., 2002).

NOS enzyme: three different isoforms

NO is generated by NOSs, a group of conserved cytosolic or membrane-bound isoenzymes. NOSs are members of a dual-flavin reductase family, which transfer electrons from NADPH to a variety of heme protein acceptors in a linear manner from NADPH to FAD to FMN. These enzymes catalyze the NAPD- and O_2– dependent conversion of L-arginine (Arg) to citrulline and NO (Fig. 11).

The three mammalian NOS enzymes are coded by three different genes with a similar genomic structure: neuronal (nNOS, type I), endothelial (eNOS, type III) and inducible (iNOS, type II). The first two are reversibly activated by the Ca^{2+}- binding protein calmodulin to enable their participation in biological signalling cascades. By contrast, iNOS binds calmodulin regardless of the Ca^{2+} concentration and can remain continuously active (Stuehr et al., 2009). NOSs have a bidomain structure: an N-terminal oxygenase domain containing the binding site for heme, BH_4 and L-arginine, and a C-terminal reductase domain homologue to P450 reductase, wich contains the binding domain for different cofactors (FAD, FMN and NADPH) (Alderton et al., 2001). Types II and III are located mainly in central and peripheral nerves and vascular endothelial cells. nNOS is also located in selective non-adrenergic, non-cholinergic nerves at the periphery, where NO acts as a neurotransmitter to relax smooth muscle in the gastrointestinal and urogenital tracts. The activation of eNOS isoform at vascular level most probably represent an important mechanism for the regulation of blood pressure and tissues perfusion (Bogdan, 2001).

muNOS: in healthy and dystrophic muscles

In healthy adult mammals, the muscle isoform muNOS is localise under the sarcolemma. This alternative spliced isoform, with catalytic activity equivalent to the neuronal isoform, has an insertion of 102 base pairs between exons 16 and 17, corresponding to 34 AA more than nNOS (Silvagno et al., 1996). This isoform is also called nNOS-μ and links α-syntrophin, a member of the DAPC, with the PDZ protein domain located in the N-terminus. *In vitro* it has been shown that its expression is increased during myogenesis (Lee et al., 1994). *In vivo*, during the development, the nNOS is located in the cytoplasm and then translocated at sarcolemmal level at adult stage. It is particularly abundant at the neuromuscular junction, myotendinous junction and at costamer (Grozdanovic and Gossrau, 1998; Lee et al., 1994).

In DMD patients and in *mdx* mice the muNOS is not anchored at the sarcolemma because of the absence of dystrophin, but it is localized at cytoplasm level with an expression level inferior to

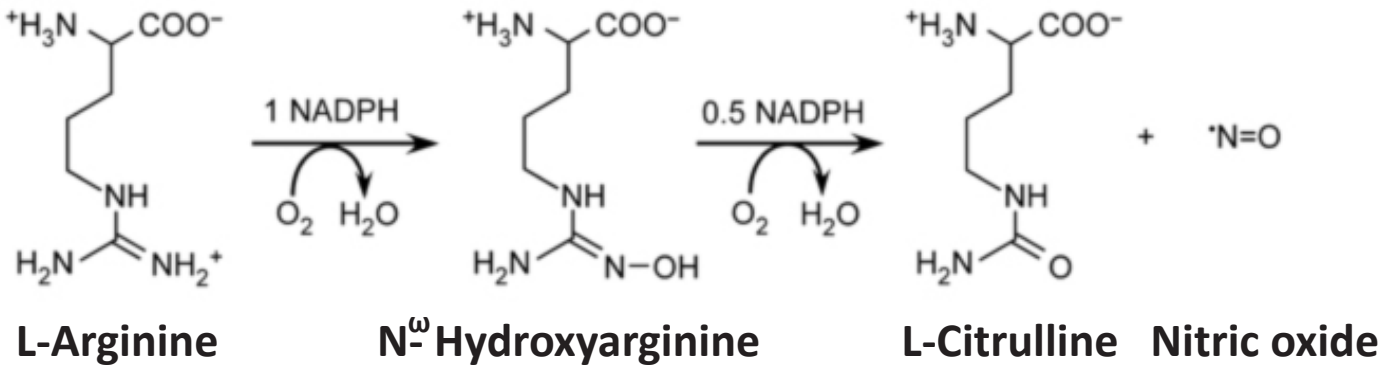

Figure 11: Schematic representation of NOS reaction. NOS enzymes catalyze the NADPH- and O2-dependent conversion of L-arginine to citrulline and nitric oxide via the intermediate N-hydroxyarginine. From:http://www.biocompare.com/Product-Reviews/125278-NOS-Activity-Assay-Kit-from-Cayman-Chemical/.

control samples (Brenman et al., 1995; Chang et al., 1996). At the end of the 90s it has been shown, by two independent studies, that the mislocation or the total absence of nNOS in the muscles of *mdx* mice did not increase or favorise a dystrophic phenotype (Chao et al., 1998; Crosbie et al., 1998). They observed that the typical features of membrane damage, necrosis and degeneration/regeneration cycles observed in *mdx* mice, can be found in *mdx:nNOS*$^{-/-}$ mice. These results allow us to think that the mNOS is not implicated in the development of the dystrophic phenotype.

In contrast, an improvement of dystrophin phenotype has been observed after the expression of a NOS transgene in *mdx* mice. In particular, Wehling et al. confrim that non mechanical factors contribute to the dystrophic scenario and that the correct NO production reduced the occurence of many of the key indices of pathology, such as central nucleation, inflammation and fibre membrane damage. Moreover, their results support the conclusion that the protective effect of NO is attributable to its anti-inflammatory action, because of the decrease in macrophages and macrophages-mediated damage (Wehling et al., 2001). Recently it has been shown that dystrophin and utrophin do not display the same affinity for anchoring muNOS at the sarcolemma: the over expression of utrophin did not restore the localisation of muNOS at the sarcolemma (Li et al., 2010).

1.10 HISTONE DEACETYLASE (HDAC) ENZYME

HDAC and the switch utrophin/dystrophin during development (Israël, 2003) (Fig. 12)

After fertilization, the genetic clock of the ovocyte seems to be set at zero and this is operated by a general demethylation of the DNA. In the course of development the methylation process will be progressively re-established, switching off the early genes. Initially, the metabolism of the foetus is glycolytic, kemogenic and ammonotellic and a first set of metabolic sensors have a high concentration (lactate, butyrate, NH_4, NO and CO_2). Some of these compounds, in particular butyrate, which inhibits HDAC, promotes the expression of genes adapted to foetal life, such as foetal hemoglobin, and does not regulate utrophin, which is more mechanically adapted than dystrophin to embryonic muscle. The metabolic sensor butyrate is known to inhibit HDAC and maintains the histone unbound, preventing the silencing of these genes.

With the change in O_2 supply and the respiration, the Krebs-urea cycle become predominant, and the previous set of metabolic sensors start to be replaced by others: urea, ATP, O_2^{o-}, CO_3H^-, related to a metabolism that becomes oxidative, ureollic and lipidytic. The lower level of butyrate facilitates the action of HDAC. The essential phenomenon is the expression of nuclear methylases that methylate CpG-rich regions, which will recruit a methyl binding protein (MBP) and HDAC that is no longer inhibited. Histones will lose their acetylated tail, bind more firmly to DNA and silence the foetal genes in favour of respective adult copies. This takes place because cytosolic methylases takes over, giving new compounds such as creatine. Many other methylations take place in the cytosol, and a third set of compounds are formed. The consequence is that nuclear methylases are starved because they do not receive enough S-adenosylmethionine (SAM), the common methyl donor, now captured by the cytosolic methylation. The genes adapted for postnatal develoment are poorly methylated and will be expressed to replace the previous ones, which are turned down when nuclear methylases are at work at an early stage.

Adult haemoglobin, dystrophin and other genes are now expressed and their proteins are regulated, responding to environmental changes, for example, adult hemoglobin is regulated by 2,3-DPG, its allosteric ligand that decreases its O_2 affinity.

HDAC inhibitors ameliorate dystrophy phenotype

Different studies have demonstrated that the administration of HADC inhibitors, such as trichostatin and valproic acid in *mdx* mice, can ameliorate dystrophic phenotype in term of muscular architecture and skeletal muscul activity (Gurpur et al., 2009; Minetti et al., 2006), *via* an

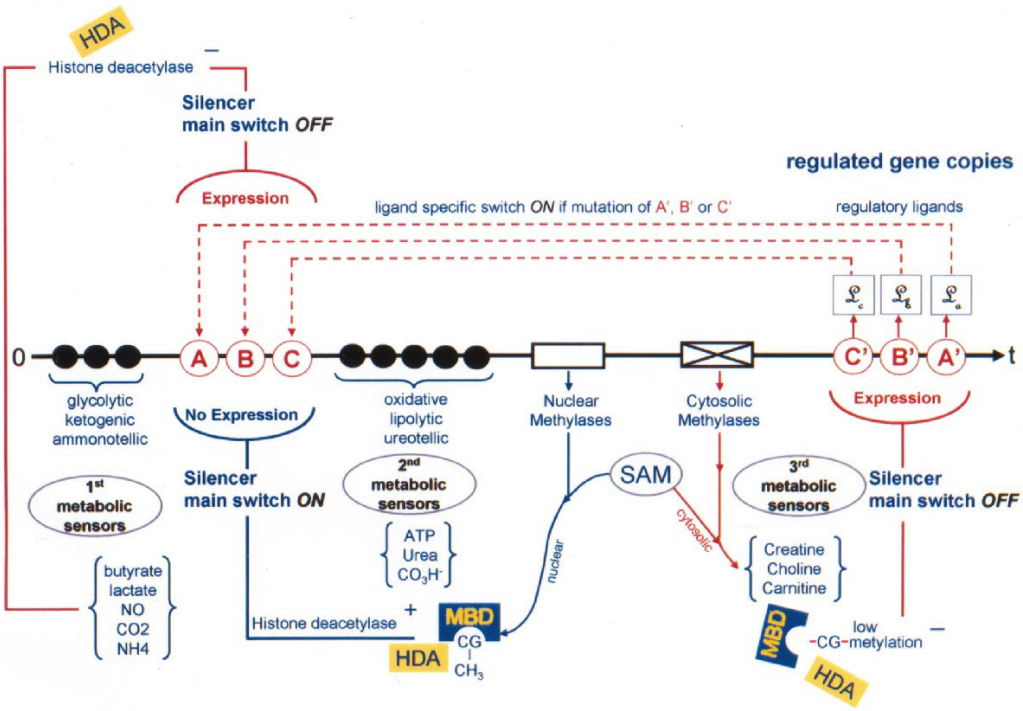

Figure 12: Schematic representation of genetic regulation and adaptation. The model explains how a set of genes A, B and C will be switched off and replaced by their copies A', B' and C' more adapted to the new situation of an organism and how a gene may be re-expressed if its adapted copy is mutated. Adapted from (Israel 2003).

increase in follistatin, which has been shown in part to inhibit the activity of myostatin, and by activating the Akt/mTOR/p70S6K pathway, respectively.

Recently other HDAC inhibitors have been described as a possible treatment for DMD patients: givinostat and suberoylanilide hydroxamic acid (SAHA) (Colussi et al., 2010a; Consalvi et al., 2013) In particular, givinostat is currently tested in a phase I safety study in children affected by systemic onset juvenile arthritis. Consalvi et al. observed *in vitro*, an increase of the size of the human myotubes and, *in vivo*, an increase of muscular weight accompanied by an increase of cross sectional area correlated with the maintenance of muscular architecture after givinistat treatment. They also observed a drastic reduction of fibrosis, of fatty infiltration and of MPO activity (a marker of inflammation); an increase of functional parameters of skeletal muscles activity and a reduction of Evan's blue dye uptake. Colussi et al. treated *mdx* mice with SAHA and described the recovery in muscular strength and histological amelioration, accompanied by the rescue of plasma protein profile. In particular they observed an increase of running time and cross sectional area, and a decrease of inflammation and fibrosis.

1.11 THERAPIES

Therapeutics approaches to treat DMD can be separated into two different categories: palliative treatment, such as pharmacological therapy, and curative ones, such as cell and gene therapies. These strategies could also be classified according to their objective: independent from dystrophin/utrophin, targeting dystrophin and targeting utrophin.

In the following sections we describe independent strategies, cell therapy, curative approaches targeting dystrophin and utrophin, and, finally, associated curative approaches.

1.11.1 INDEPENDENT STRATEGIES

The aim of these strategies is to improve dystrophic phenotype to slow disease progression, prolonging ambulation and improve quality of life and survival. Nowadays glucocorticoid treatment is the most utilized, in particular prednisone and prednisolone (the active form of the drug). These molecules are able to induce myogenesis (Sklar et al., 1991) and to prevent the increase of calcium in hypo-osmotic conditions *in vitro* (Metzinger et al., 1995). Glucocorticoid are typically used to suppress inflammation thanks to the bind with glucocorticoid receptor that enhance the transcription of anti-inflammatory genes, and to its capacity to bind and inhibit pro-inflammatory factors (Baltgalvis et al., 2009). In addiction, part of the benefits observed after glucocorticoid treatment could be attributed to its capacity to enhance utrophin expression (Miura et al., 2008).

The most common posology for prednisolone is the daily treatment at the dose 0.75 mg/kg/day. At this concentration, an increase on strength occurs 10 days–1 month after the beginning of the treatment. The improvement carry on for 2 to 3 months but strength gains plateau after 3-6 months of treatment (Escolar et al., 2011; Manzur et al., 2008). Recently, a 14-year follow-up study has just ended, 5 patients were treated with corticosteroid (prednisone at the beginning and deflazacort at the end to decrease the risk of weight gain) and 3 patients as controls. The aim of the study was to determine whether corticosteroids produce a beneficial effect when given earlier than usual and to better assess the side- effects of long- term corticosteroid treatment in DMD boys. They concluded that long- term treatment is effective in prolonging function but not in recovering lost function, and that an early use seems appropriate (Merlini et al., 2012).

On the other hand, in two recent studies on *mdx* mice treated for a long period (6 months and

over 3 years) with prednisone, an amelioration of dystrophin phenotype was observed early but these beneficial effects were lost with continued treatment. In particular, they show the decrease of heart function and an increase of fibrotic tissue in heart, accompanied by a deficit skeletal muscle, suggesting that glucocorticoid treatment could be detrimental in mice, in case of long term treatment (Guerron et al., 2010; Sali et al., 2012).

Nowadays other molecules are currently studied with the aim to target different aspects of the disease; among them muscular growth, fibrosis prevention, damages caused by oxidative stress and necrosis inhibition. The recombinant human antibody Myo-029, that inhibits myostatin action, and ACE-031, a soluble activin type IIB receptor both belong to this first category. Both control the increase of muscle size and strength, through the inhibition of myostatin. Follistatin and insulin growth factor 1 (IGF1) are two other targets for the modulation of muscle growth in DMD *scenario*.

The prevention of fibrosis can be done through the inhibition of TGFb pathway and different drugs are currently being tested: losartan, halofunginone, pirfenidone and two antineoplastic drugs (suramin and imatinib mesylate).

The great damage caused by ROS stimulated the study of antioxidant molecules, such as N-acetylcysteine that, prevent increased membrane permeability, promote force generation following stretch-induced muscle damage in *mdx* mice and utrophin expression; green tea, which regulates NF-kB signaling activity in regenerating fibres; melatonin and idebenone.

Finally the non-specific action of glucocorticoids helps the reduction necrosis thanks to the inhibition of the activation and/or action of the NF-kB signalling pathway (for review see (Malik et al., 2012)).

1.11.2 CELL THERAPY

This therapy is based on the ability of cells to generate new muscle in place of injured areas. This can be performed by muscle precursor cells (myoblasts and satellite cells) or stem cells, both are able to differentiate into muscle cells. The major obstacles of cell therapy are the immune response of the host and the cell migration from the injected areas.

Myoblasts and satellite cells

Numerous studies have been done with this type of cells in *mdx* mice but also in DMD patients. In particular, myoblast transplantation is a procedure that involves injection or transplantion of donor muscle precursor cells (myoblasts) into a dystrophic host. The goal of this technique is to allow fusion of donor, dystrophin-positive myoblasts with host, dystrophin-deficient muscle fibers (Chakkalakal et al., 2005).

However, there is an absence of positive effects and of the transcript 3 months after the injection of modified cells (review: (Voisin and de la Porte, 2004)), in a second time, an immune response appeared, probably due to the synthesis of the dystrophin protein (Morandi et al., 1995), requiring to associate the transplantation with a correct immunosuppessive treatment (Hong et al., 2002). A recent work shown that *mdx* mice pre-treated with Losartan, an inhibitor of the transforming growth factor (TGF) pathway, the transplantation of human myoblasts revealed more human dystrophin-positive fibres, 1 month post-transplantation, than non-treated mice. The benefit of losartan is probably due to an increase of myoblasts proliferation and fusion, a decrease of macrophage activation and the change of expression pattern of myogenic regulator factor (Fakhfakh et al., 2012). Furthermore, two main difficulties were described, to rise the number of cells transplanted do not increase the efficiency (Pellegrini and Beilharz, 2011) and only a small number of satellite cells are able to repopulate injured skeletal muscle (Hall et al., 2010).

For this type of therapeutic approach it is essential to isolate satellite cells with a high proliferative capacity. At the end of 90s, G. Butler-Brown group has demonstrated that the proliferative capacity of these cells decreased with age and was related to the telomere length, that could be considered as a marker of proliferative capacity (Decary et al., 1996, 1997). Moreover, the telomere length decrease after each cellular division and for a dystrophic child the decrease is 14 times more than that of healthy child (Decary et al., 2000). In order to avoid this decrease, satellite could be transfected with the gene of the telomerase. The transfected cells form multinucleated myotubes and do not develop tumor *in vivo* (Di Donna et al., 2003).

A major limitation of this approach is the inability of intravenous and intraperitoneal injections of myoblasts. The disadvantage of intramuscular injection is that myoblasts fuse mainly with the myofibres near the site of delivery, resulting in restricted zones of muscle zones and recovery (Fairclough et al., 2011).

Stem cells

Satellite cells were at first the only ones implied in the growth and maintenance of skeletal muscle. Nowadays, it is know that other types of cells could play role in these processes (Fairclough et al., 2011), the muscle-derived stem cells, the muscle side-population cells and the muscle-derived CD133+ progenitors. There is also a population of non-muscle derived cells that are able to participate in myogenesis and differentiate into mesodermal cells including myoblasts: the bone marrow-derived mesenchymal stem cells (Bhagavati and Xu, 2004). This type of cells is able to fuse with dystrophic cells and produce factors that enhance the activity of endogenous repair cells. Moreover, they possess anti-inflammatory properties (Ichim et al., 2010). It has been shown that another class of cells could be used in cellular therapy, the mesoangioblasts cells. In particular, intra-arterial delivery of wild-type canine mesoangioblasts results in an extensive recovery of dystrophin expression, normal muscle morphology and function in the canine animal model (Sampaolesi et al., 2006). Further analyses are required to design a clinical study.

1.11.3 THERAPIES TARGETING DYSTROPHIN:

1.11.3.1 PHARMACOLOGICAL APPROACHES

About 15% of the mutations at the *DMD* gene are point mutations that converse an amino acid into a premature stop codon, allowing the production of a non-active protein. The strategies currently studied in order to promote the re-expression of dystrophin gene can be divided into "stop codon read-through" and "exon skipping" (Pichavant et al., 2011).

Stop codon read-through

This approach is based on the evidence that some drugs have been shown to enable stop codon read-through by introducing an amino acid at the premature stop codon to continue the mRNA translation. These molecules are the aminoglycoside antibiotics, in particular gentamicin. The antibiotics interfere with the translational machinery at the 40s ribosomal subunit, when it recognizes a stop-codon (Palmer et al., 1979). Twenty years later this discovery, *mdx* mice have been treated with gentamicin and interesting this drug induced up to 20% dystrophin-positive

fibres (Barton-Davis et al., 1999) but were not applied in long clinical trials because of its side effects, such as renal complications.

Nowadays other molecules that induce ribosomal read-through of non-sense mutation in mRNA allowing the production of the full-length functional protein have been tested. For example, ataluren (PTC124) that promotes between 20 and 25% of dystrophin positive fibres in *mdx* mice (Welch et al., 2007), tested in human patients, but no clear quantitative analyses have been presented (Finkel, 2010). Moreover, preclinical studies have been performed recently with RTC13 and RTC14. RTC13 gave better results in term of dystrophin expression that gentamicin, PTC124 and RTC14 (Kayali et al., 2012).

Exon Skipping

The aim of this approach is to convert the severe form of the disease into a milder form by modulating pre-mRNA splicing and achieving reading frame restoration (Aartsma-Rus, 2012; Fairclough et al., 2012). Antisense oligonucleotides (AONs) bind to specific intronic or exonic sites of pre-mRNA and mask the targeted exon to the splicing machinery, promoting specific exon exclusion from the mature mRNA. Different types of AONs restore the open reading frames of dystrophin gene (Aartsma-Rus, 2012), but two categories are mainly used (Pichavant et al., 2011): 2'-O-methylphosphorothioate (2OMP) and the phosphorodiamidate morpholino oligomers (PMOs).

At the first category belong two recurrent modifications:

1. Replacement of the non-bridging oxygen with a sulfur atom in the phosphate backbone. This type of AON is called PS- AON.
2. Addition of a methyl (2OMe) or methoxyethyl (2OMOE) group at the 2'O atom of the ribose sugar.

These modifications make the AONs more resistant to nucleases, improve their affinity to RNA, provide favourable pharmacokinetic properties and prevent RNase H to induce cleavage of RNA:RNA hybrids (Aartsma-Rus, 2012; Goyenvalle and Davies, 2011).

The second category is obtained by replacing the ribose of the AON with a morpholine ring and the oxygen present in the phosphodiester link, replaced by a nitrogen atom. These modifications allow PMOs to be biologically stable and have antisense properties (Hudziak et al., 1996; Partridge et al., 1996).

The third-generation of AONs are all resistant to exo- and endo-nucleases and RNase H cleavage. They consist of peptide nucleic acids (PNAs) with a 2-aminoethyl glycine backbone linked to nucleobases.

Initial experiments in *mdx* mice involved local intramuscular injections of 2OMePS. When delivered with a copolymer than acted as an AON depot, high and sustained exon 23 skipping was induced and dystrophin was detectable for at least 3 months with a local muscular increase (Lu et al., 2003). Later experiments used PMO or PNA. The results obtained with PMO shown a more efficient exon skipping and high level of dystrophin after local injection (Aartsma-Rus, 2012). In order to verify if these compounds could be efficient in human, they have been tested in the transgenic hDMD mice model (Heemskerk et al., 2009), having a complete copy of the human dystrophin gene integrated into his genome ('t Hoen et al., 2008). Because of the presence of muscular tissues in all the body, systemic treatment is required.
Different studies have been performed (Aartsma-Rus, 2012). After sub-cutaneus injections (the most friendly mode of administration for patient) of 2OMePS AONs there is a dose dependent increase in exon skipping and dystrophin levels. Moreover, the protein accumulates for at least 12 weeks after the treatment, CK level decreased and muscle function improved significantly. On the other hand studies with PMOs use the intravenous route of administration. Weekly treatment for 7 weeks resulted in significant levels of exon skipping and dystrophin in skeletal muscle and diaphragm, accompanied by reduced CK level and improved muscle function (Alter et al., 2006).

The obstacles of this technique are: the poor cellular uptake and the rapid clearance from the circulation, which require repeated administration to achieve some therapeutic efficacy; the high variability of the efficiency of the exon skipping after systemic administration and; the very little efficacy in the cardiac muscle. To solve this difficulty, recent studies have been investigate using cell penetrating peptides (CPP)-conjugated PMO (PPMO) (Goyenvalle and Davies, 2011; Wu et al., 2008).

To conclude, antisense-mediated exon-skipping strategies for DMD aim to remove the mutated exon alone or together with additional exons to restore the reading frame and consequently induce the expression of "BMD-like" forms of dystrophin retaining crucial functions. The use of

this approach is limited by the genetic heterogeneity of DMD patients that makes it mutation-specific such an example of personalized medicine (Goyenvalle and Davies, 2011).

1.11.3.2 GENE THERAPY

The second category of curative therapies is gene therapy. It is based on the replacement of dystrophic gene by a functional one. An advantage of this technique is that it is not dependent on any particular mutation in the genome of a DMD patient. The major difficulties of this technique are: penetrating cellular and nuclear membranes, cellular targeting and the chromosomal insertion without developing tumours. Moreover, in this particular case we have to consider also the size of dystrophin gene (14kb) and the mass of the muscles in the body to be treated (Voisin and de la Porte, 2004). Gene therapy could be done *in vivo,* through direct injection of vector or virus into the host, or *ex vivo* through the dissection of cells, the transfection and the re-injection into the organism.

To avoid the problem of size of dystrophin gene it has been design mini-dystrophin (mDYS, 6kb) and micro-dystophin (μDys, 4kb) cDNAs private of a portion of the central rod-domain. The construction of these mini or micro-dystrophins comes from the observation that some milder form of BMD patients could ambulate while carrying large genomic deletions of dystrophin in the rod-domain (Goyenvalle et al., 2011).

Gene therapy is divided in two distinct categories: those using viral vector to transfer the transgene, viral gene therapy, and those employing naked gene, nonviral gene therapy. Nonviral gene therapy allows the production of a transgene directly into a tissue in order to avoid any immune response due to viral capsids or other viral proteins. There are also no limits about transgene size but the transfection efficiency of this therapy is progressively reduced with the increasing plasmid size (Pichavant et al., 2011). On the other hand for viral gene therapy different viral vector could be used for DMD patients, but the use of adenoviral vector is complicated since half of the human population already has neutralizing antibodies against the adenoviral capsid and also tends to be far more immunogenic than adeno-associated (AAV) viral vectors and retroviral vectors (Pichavant et al., 2011). Moreover, AVV vectors can pass the cellular membrane easily than other viral vectors; they are little and allow a stable expression of the gene.

The first evidence for a possible role of AVVs in DMD therapy was observed at the beginning of two thousand by Wang et al. They treated *mdx* mice with an AVV vector that brings a mini-dystrophin gene under the control of the cytomegalovirus (CMV) promoter. In particular they

observed after the expression of the gene, the restoration of the DAPC, a decrease of centro-nucleated fibres and the protection of tissue integrity also after exercises (Wang et al., 2000). In 2004 Gregorevic et al. showed that after 6 weeks of the systemic administration of the recombinant adeno-associated virus pseudotype 6 (rAVV6) (this type of virus does not require an helper virus to reproduce and infect both dividing and non-dividing cells) to *mdx* mice, the expression of the mini-dystrophin is still present in the legs muscles and in the torso. Moreover, there is a decrease of 50% in CK level in the serum. Mini-dystophin gene was under the control of a regulatory sequence that allows the expression of the gene only at muscular level, avoiding immune response (Gregorevic et al., 2004).

In a recent clinical trial 6 DMD patients were treated with two different concentration of rAVV2 modified with a mDYS ($2x10^{10}$ and $1x10^{11}$ vector genomes per kilogram body weight). Only one patient belonging to the first group had robust T-cell activity 15^{th} days after the treatment. Two patients belonging to the second group (the high dose) develop a T-cell response only at day 60. A T-cell response was unexpectedly detected before the treatment in one patient belonging to the high-dose group. After the rAVV administration the T-cell response did not elicit the rapid increase in dystrophin-specific T-cell activity that was observed for the first patient. One possible explanation of the pre-existing cellular immunity is the expression of dystrophin in the revertant muscle fibres (Mendell et al., 2010). Different strategies have been proposed to avoid immune response against rAVV in a host. In particular: the use of a muscle-specific promoter, the purification of the viral vector from contamination such as products of residual viral genes in vectors or serum products, the reduction of the vector genome dosage (Goyenvalle et al., 2011).
For the viral approach it is also possible to use lentivirus instead of AVVs. They belong to the retrovirus family and they are able to stably integrate transgene into the genomes of quiescent and non-quiescent cells. A drawback of the integration into the genome of a host is the possibility to active proto-oncogenes (Goyenvalle et al., 2011).
Recently, it has been shown that there is a stable expression of a micro dystrophin (μDys), coupled with green fluorescent protein (eGFP) and intramuscularly injected into neonatal *mdx* mice, two years after the treatment. The choice to treat neonatal animals permits to escape a reduced or completely absence of immune response of the host against the vector and might allow for wider dissemination into a variety of myofibres and muscle progenitor cells.
To force the expression only in the muscle the vector utilizes a skeletal muscle-specific promoter

enhancer element, derived from the human *α-skeletal actin* gene (HSA). The protein was correctly expressed along the sarcolemma of numerous myofibres in injected muscles at all time point examined (4 weeks, 4 months, 1 year and 2 years after the treatment) with a general amelioration of muscle pathophysiology, as for example, a decrease of the percentage of centronucleated fibres, but with incomplete rescue of muscle specific force-generating level and the inability to confer significant protection from eccentric contraction-induced injury (Kimura et al., 2010).

All the limits described and the complete absence of an immune response after the expression of utrophin in the host make this approach easier to use and the vectors normally utilised to transfer dystrophin gene can also be used for this protein.

1.11.4 THERAPIES TARGETING UTROPHIN

In parallel to the therapies that contemplate dystrophin as playing a central role in the treatment of DMD patients, there are therapies that target its foetal homolog, utrophin. This protein is essential for structural and functional development of muscles during prenatal life but is rapidly substitute by dystrophin, after birth. In the adult, utrophin persists mainly at neuromuscular junctions and myotendinous junctions. The first evidence of the importance of utrophin to treat Duchenne muscular dystrophy belongs to the 90s. It has shown that the expression of utrophin transgene in the *mdx* mice, markedly reduce the dystrophic pathology. Davies's group observed the reduction of the CK level in the blood serum, a decrease of the percentage of centronucleated fibres and the correct localization of the DAPC at the sarcolemma after the expression of utrophin. Moreover, they have ascertained an improvement at diaphragm level, in particular the correct localisation of utrophin and DAPC at the sarcolemma, and this muscle looks as normal with no necrosis, regular myofibre size and virtually no centralized nuclei (Tinsley et al., 1996).

The over-expression of utrophin allows the answer to two key questions: "*Could it be expressed in all tissues?"* and "*Is there a temporal window to improve its expression?*. The absence of signs of toxicity in *mdx* mice treated with a transgene of utrophin expressed in muscle and non muscle tissue, provides a positive answer to the first question. It is not essential to drive utrophin expression only to muscles with a promoter muscle-specific (e.g. HSA) (Fisher et al., 2001). A year later the same team demonstrated that an earlier expression of utrophin improve dystrophic

phenotype better than in old mice, by using an inducible promoter that controlled utrophin gene (Squire et al., 2002).

Different strategies can increase utrophin (Fairclough et al., 2012):

Transcriptional regulation

- SMTC1100, the product of an exhaustive chemical screening developed to target molecules, transcriptionally upregulate the utrophin gene, and consequently improve dystrophic phenotype in sedentary and forced exercise *mdx* mice. An overall two-fold increase of utrophin expression (mRNA and protein) that alleviate dystrophic symptoms and increase muscle function was observed in *mdx* mice daily treated with SMTC1100 (Tinsley et al., 2011).

An alternative strategy to improve utrophin expression is based on the use of artificial zinc finger transcription factors (ZF ATFs) to target sequences internal to utrophin protein A promoter (Corbi et al., 2000; Onori et al., 2007). An example of ZF ATF is "Jazz" gene which encodes for a three-zinc finger peptide that binds nine-base pair DNA sequence, located in the promoter of both human and mouse utrophin gene (Corbi et al., 2000). *Mdx* mice encoding for Jazz show an increase of utrophin expression that is accompanied by a general improvement of dystrophic symptoms (Di Certo et al., 2010).

- A molecule that belongs to Jazz is Bagly, a four zinc-finger protein that binds human utrophin promoter A at the chromosomal site and activated endogenous gene transcription. An increase of utrophin transcript about 1.7-fold in treated HeLa cell line, compared to control clone (not-Bagly HeLa cells), correlates with an increased level of utrophin protein (Onori et al., 2007).

Post-transcriptional degradation

More recently it has been shown an active role of p38 in utrophin expression. In C2C12 cells transfected with a constitutive active MKK6-EE, an upsteam kinase of the p38 pathway, the level of utrophin protein and of its mRNA is increased. p38 controls post-transcriptional events, in particular it has an indirect role on mRNA stability with an extension of half life of utrophin transcripts by preventing the link between utrophin mRNA and KSRP, molecules implicated in transcripts degradation. The same results have been obtained *in vitro* and *in vivo* with heparin, an activator of p38, suggesting that this pathway could be investigated to treat DMD patients (Amirouche et al., 2013).

Translational repression

Recently it has been described a translational repression role of miRNA in regulating utrophin level, by suppression of utrophin at the translational level. In particular at least six miRNAs targets the utrophin 3'UTR controlling its translation, with particular interest for let-7c. The inhibition of let-7c using a 2OMePO could upregulate endogenous utrophin protein by over 2 fold in C2C12 cells, suggesting a possible new way to treat DMD patients (Basu et al., 2011).

Recruitment at the membrane

Instead of regulating utrophin expression, another strategy to improve dystrophic phenotype is through the use of biglycan, an extracellular matrix protein that plays an important role in developing muscles. It is a component of the DAPC, essential for the membrane localisation of the other component of the DAPC and nNOS (Mercado et al., 2006). Biglycan has been shown to play a role in skeletal muscle development and regeneration: it becomes up-regulated during muscle fibres regeneration and mice deficient in biglycan display delayed regeneration after injury (Casar et al., 2004). In the case of dystrophy, biglycan has an active utrophin dependent role, in the improvement of dystrophic phenotype when recombinant human biglycan (rhBGN) is delivered to *mdx* mice. Biglycan does not play a role in utrophin transcription and expression, as shown by RT-PCR, but recruits the protein at the membrane (Amenta et al., 2011).

Cell-penetrating facilitation

A example of an alternative therapy strategy is the TAT-utrophin, a full-length utrophin (Utr) or ΔR4-21 "micro" utrophin (μUtr) protein modified with the cell-penetrating TAT protein transduction domain. The systemic administration of TAT-μUtr to *mdx* mice promote the protein expression in all tissues of the body and restore dystrophic phenotype (Sonnemann et al., 2009).

Muscle plasticity

Slower, more oxidative muscle fibres in DMD patients are more resistant to the dystrophic pathology than faster, glycolytic fibres (Webster et al., 1988) In addition, in comparison to their fast, glycolytic homologous, slower and more oxidative muscles express significantly more utrophin (Gramolini et al., 2001b). A strategy to improve utrophin is targeting its expression pattern involved in the control of slow oxidative pathway (Fairclough et al., 2012). In particular the key regulators of muscle oxidative metabolism, PGC-1alpha and PPAR ß/∂, that seem to be

involved in the expression of utrophin A (Angus et al., 2005). It has been described that pharmacological activation of PPAR ß/∂ through its antagonist GW501516 promote an increase of utrophin A expression that are accompanied by an improvement of sarcolemmal integrity and the protection against eccentric contraction-induced damage of *mdx* skeletal muscles (Miura et al., 2009).

NO pathway

An efficient way to upregulate utrophin expression is through stimulation of the nitric oxide (NO) pathway. Previous studies showed that an effective activator of the NO pathway, L-arginine, increases utrophin levels in muscles and targets utrophin to the sarcolemma *in vivo* and *in vitro* (Anderson, 2000; Chaubourt et al., 2002). In culture of wild type and *mdx* myotubes, L-arginine and NO increase utrophin levels and enhance its correct membrane localization. The involvement of NO synthase in this process is renforced by the evidence that utrophin expression does not occur with D-arginine, L-NAME (an inhibitor of NO synthase) or ODQ (oxadiazolo-quinoxalin-1-one, an inhibitor of a soluble guanylate cyclase involved in the effects of NO) (Chaubourt et al., 2002). Improvement of dystrophic phenotypes via the NO pathway has been demonstrated by many studies in dystrophin-deficient *mdx* mice. Isometric force and resistance to eccentric contractions can thus be improved, serum creatine kinase levels reduced, muscle structure restored, muscle regeneration increased (Anderson and Vargas, 2003; Archer et al., 2006; Barton et al., 2005; Brunelli et al., 2007; Chazalette et al., 2005; Marques et al., 2005; Ségalat et al., 2005; Voisin et al., 2005), inflammation reduced (decreases in nuclear factor (NF)-κ B level and activity) (Hnia et al., 2008), and finally, a normal phosphatidylcholine ion peak intensity ratio of the membrane of skeletal muscle can be restored (Benabdellah et al., 2009).

NO inducers may have another beneficial effect. NO modulates the α adrenergic vasoconstriction in response to muscular metabolic changes during exercises (Lau et al., 1998; Thomas et al., 1998). In 2000 Sanders and colleagues performed a clinical assay to DMD and healthy boys, in order to study how this protective mechanism could be defective in case of absence in dystrophin, looking at the change of the oxygenated part of blood (HbO_2 + MbO_2) before and after low body negative pressure (LBNP) stimulation. They microvascular perfusion changes were investigated with near-infrared (NIR) light. In healthy boys the robust low body negative pressure-induced decrease in muscle oxygenation in resting forearm was diminished during forearm exercise. In contrast, in DMD boys, low body negative pressure produced similar decrease in muscle oxygenation in resting

and exercising forearm. In this case the defective modulation of reflex sympathetic vasoconstriction promote functional muscle ischemia (Sander et al., 2000). Basing on this evidence, another clinical study with BMD patients has been recently performed. Patients were treated with a single dose of Tadalafil, an inhibitor of phosphodiesterase 5A (PDE5A), which prolong the half-life of cGMP, instead of be degraded by phosphodiesterase 5A and permitted the correct modulation of vasoconstriction by NO. They observed that Tadalafin could alleviate microvascular ischemia and fully restore blood flow regulation in most of the patients treated (Martin et al., 2012). The hypothesis on the benefit of NO donor on muscle ischemia was recently confirmed by *in vitro* experiments with HCT 1026 (see below) in *mdx* mice (Thomas et al., 2012).

1.11.5 ASSOCIATED THERAPIES

Preclinical studies investigate the benefit of the association of NO with a drug with anti-inflammatory activity:

HCT 1026 and NCX 320

Mdx mice were treated with HCT 1026 that combines the beneficial effects of NO with nonsteroidal anti-inflammatory activity, avoiding the side effects of corticosteroids. The animals treated with the drug displayed the inhibition of inflammation phenomena, such as the generation of pro-inflammatory cytokines and infiltration of pro-inflammatory cells; the preservation of satellite cells number and function by protecting them from the pro-apoptotic environment. Moreover, HCT 1026 significantly enhanced the engrafting to muscle of intra-arterially delivered mesoangioblasts, so the drug could be associated to cellular therapy (Brunelli et al., 2007).

The same group have tested another molecule that, similar to HCT 1026, targets two mechanisms, NO and anti-inflammatory action, through cyclooxygenase inhibition. NCX 320 induces persistent and significant reduction of both fibre damage and inflammation, thus preserving muscle integrity. Moreover, it significantly increased the myoblast precursor number and differentiation capacity, maintaining the long-term regeneration capacity of muscle (Sciorati et al., 2011). More recently, another positive effect of HCT 1026 on muscle ischemia in the *mdx* mice was observed. The functional ischemia in *mdx* mice is reversed; and normal blood flow regulation is restored, by treatment with NO donating molecule. This effect was achieved within the first month of

treatment and was completely sustained for at least three month without any noticeable adverse systemic effect (Thomas et al., 2012).

Prednisolone and NO donors

Other studies tried to improve prednisolone effects and avoid side effects by coupling it with two NO donors drugs (MyoNovin and Isosorbide dinitrate). They studied in particular the effect on diaphragm of *mdx* in term of reduction of the disease progression and of the increase of muscle function by regulating satellite cells activation. Membrane permeability was decreased in animals treated with NO donors and prednisolone compared to animals treated with prednisolone alone and to untreated animals. Moreover, isosorbine treated animals display also the reduction of calcification probably due to improved wound healing, angiogenesis and vascular perfusion. Histopathology from animals treated with isosorbine reveals the improvement of regeneration resulting in increased central nucleation index (CNI) and regenerating areas, while MyoNovin reduced proliferation reducing c-met-expressing cells. This suggests that the donor reduces the need for satellite cell activation as part of the repair response to dystrophy while it promotes precursor fusion into regenerating fibres (Mizunoya et al., 2011).

THESIS PROJECT

As previously described DMD is a complex pathology. The total absence of dystrophin at the membrane results in numerous cellular damages (alteration of calcium homeostasis, inflammation, fibrosis and necrosis, etc…) that progressively induce cellular death. DMD patients are usually loose ambulation by 12 years of age and death occurs for respiratory and cardiac failures (Blake et al., 2002). Unfortunately, nowadays there are no curative for the disease, but only palliative treatments that allow a temporary improvement in the quality of life(Fairclough et al., 2011).

The objective of my thesis was to test a pharmacological approach to improve different aspects of the dystrophic phenotype. The compounds I used combined two independent pathways that have been confirmed to be beneficent for *mdx* mice, the NO pathway and the inhibition of HDAC, enzyme normally implicated in the silencing of genes (Anderson and Vargas, 2003; Archer et al., 2006; Brunelli et al., 2007; Chaubourt et al., 1999; Chazalette et al., 2005; Gurpur et al., 2009; Hnia et al., 2008; Marques et al., 2005; Sciorati et al., 2011; Ségalat et al., 2005; Thomas et al., 2012; Voisin et al., 2005). I focussed on the association of L-arginine, substrate of NOS, with butyrate, an inhibitor of HDAC enzymes.

This strategy is commonly used for the treatment of children with haemoglobinopathies in USA (Perrine, 2008). The drug, arginine butyrate (AB), is administered intravenously through a permanent catheter, with risks of local infections.

Recently I participated to a study that demonstrated that the same compound, AB, administered through intraperitoneal injections at the optimal dose of 800 mg/kg/d, could be used in the case of muscular dystrophy therapy. AB improves dystrophic phenotype *in vitro*, in human myotubes and *in vivo*, in *mdx* mice, through the re-expression of utrophin gene (Vianello et al., 2013).

In the case of DMD patients, the aim of the treatment is to be performed in paediatric patients and because of the way of administration and the optimal dose identify for AB, it is essential to evaluate compounds that allow an amelioration of these two parameters. I tested two different ways of administration for AB, the reference drug: force-feeding and intraperitoneal injection. In addition I studied two new pharmacological formulations that could be administered orally to DMD patients. These compounds, N-butyryl arginine (ABA) and 3-Hydroxybutyrate arginate (ABE), were divised with L-arginine and butyrate bound by a covalent link, amine link for ABA and ester link for ABE. The presence of covalent links confers stability to these prodrugs (for example a lesser influence to environmental conditions such as pH and temperature, or slower metabolism in

the gastric compartment). Two qualities supposed to reduce the concentrations to apply and to allow a switch to oral administration.

Main objectives

In particular, I want to confirm that the improvement of dystrophic phenotype is correlated with the up regulation of utrophin expression after the treatment, *in vitro* of human muscle cells and, *in vivo* of *mdx* mice.

The objectives of the *in vivo* studies are:

- Compare the effects of the AB administrated by intraperitoneal injections compared to oral administration.
- Compare the effects of the two new drugs synthesized to the effect of AB,
- Determine the optimal dose of ABA and/or ABE to use in *mdx* mice in comparison with the optimal dose of AB (800 mg/kg/d).

Means

To answer these questions the following parameters were evaluated:

1) The **weight** of mice: a loss of weight can be interpreted as a sign of toxicity of the drugs, while an increase or a stability of weight can be considered as a signs of a good tolerance of the drugs.

2) **Functional improvement** (force and fatique resistance): a drug developed with the objective to be used in a clinical trial in DMD patients must bring a functional improvement to the patients.

3) Decrease of the level of **CK** in the serum of treated and untreated mice, as an investigation of membrane permeability.

4) The **level of utrophin** protein in heart and *gastrocnemius* muscle in treated and untreated animals.

5) In collaboration with E. Benoit (Institut de Neurobiologie Alfred Fessard – FRC2118, Neurobiologie & Développement, CNRS, UPR 3294, Gif sur Yvette, France), I have assessed if the drugs could reverse or attenuate the **neuromuscular excitability** impairments that we observed in *mdx* mice (**Vianello** *et al.*, in preparation). Neuromuscular excitability has been analysed with QTRAC, a software especially finalized by Pr. Bostock (Institute of Neurology,

London) for non-invasive recording of excitability properties *in vivo.* With this technique about 40 neuromuscular parameters are recorded in succession.

6) A particular focus on the heart has been performed in collaboration with Y Fromes and S. Bouyon (Thérapie des maladies du muscle strié, Institut de Myologie, Plateau de physiologie expérimentale et évaluation in vivo des biothérapies. UMRS 974 - UPMC Univ. Paris 6 / U974 - Inserm / UMR7215 - CNRS/AIM, Hôpital Pitié-Salpétrière, Paris), and Allain Brunelle (Laboratoire de Spectrométrie de Masse, Institut de Chimie des Substances Naturelles, CNRS, Gif sur Yvette). I investigated the heart because cardiomyopathy, the second cause of death in DMD, occurs in more than 96% of DMD patients (Moriuchi et al., 1993) and causes cardiac dysfunction that leads to heart failure. First, heart was utilized as a model of non-regenerating organ in order to study the **lipid composition at the membrane in heart** samples of treated and untreated mice, and to compared with the results obtained in a regenerative tissue, the skeletal muscle (Tahallah et al., 2008). Secondly, we performed an **echocardiography layout** in a 7 months' time window (started in 8-month old animals), in *mdx* mice treated from 6 weeks of age until 15 months. Echocardiography has been performed every month in order to follow structural and functional cardiac improvement during the treatment. Animals were treated orally with AB at 800 mg/kg/d and ABE at the dose 80 mg/kg/d. At the end of the treatment, histological analyses were performed.

7) Moreover, in collaboration with the M. Herbin and Thierry Deschamps (Muséum National d'Histoire Naturelle, CNRS - UMR7179, Pavillon d'Anatomie Comparée, Paris) and C. Sébrié (CNRS, IR4M – UMR8081, Orsay) kyphosis index has been calculated because **spinal deformity** is one of the features of DMD patients. As well as exacerbating respiratory dysfunction in affected boys, kyphosis negatively impacts their quality of life in their wheel-chair dependent years, leading to surgery or chronic pain. Kyphosis also occurs in *mdx* mice. (Laws and Hoey, 2004).

The objectives of the *in vitro* studies were:

- Quantify the effects of ABE, ABA on the expression of 3 proteins of interest in the case of muscular dystrophies: utrophin, β-dystroglycan and embryonic myosin, in two model of human myotubes (primary cells and cell lines).
- Compare the effects of the new prodrugs (ABA and ABE) to the effects of the salt formulation (AB)

- Moreover, in collaboration with José Cancela (Centre de Neurosciences Paris-Sud, Orsay) I recorded the basal Ca^{2+} activity (spontaneous calcium spikes) in healthy, and dystrophic myotubes in culture without treatment or after 48h of treatment with ABE, ABA, B (butyrate), A (L-arginine) and TSA (trichostatin, an HDAC inhibitor efficient at low doses). In particular basal activity and calcium spike parameters (amplitude and frequence) have been monitored to study the drugs effect on calcium homeostasis in dystrophic myotubes.

PUBLICATIONS AND MANUSCRIPTS

In the following section the results obtained during my PhD will be presented and most of them are part of four publications (1 published, 2 submitted, 1 *in preparation*).

Part of my *in vitro* results was integrated in the first publication *"Arginine butyrate: therapeutic candidate for Duchenne muscular dystrophy"*. FASEB J. 2013 Jun; 27(6):2256-69. In this work I demonstrate that AB (the salt formulation), induces about a 2-fold increase in the level of utrophin in human dystrophic primary myotubes. Continuous and intermittent intraperitoneal injections have been studied. Continuous intraperitoneal administration to *mdx* mice also resulted in a 2-fold increase in utrophin (protein homologous to dystrophin) in skeletal muscle, heart, and brain, accompanied by an improvement of the dystrophic phenotype in both adult and new born mice (45 and 70% decrease in creatine kinase levels, respectively; 14% increase in tidal volume, 30% decrease in necrotic area in limbs and 23% increase in isometric force). Intermittent administration, as performed in clinical trials, was then used to reduce the frequency of injections and to improve safety. This also enhanced utrophin level about 2-fold and alleviated the dystrophic phenotype (inverted grid and grip test performance near to wild-type values, creatine kinase level decreased by 50%). Skin biopsies were used to monitor treatment efficacy, instead of invasive muscle biopsies, and this could be done a few days after the start of treatment. Furthermore, *in vivo* and *in vitro* experiments demonstrated that the drug combination acts synergistically.

The second manuscript *"Per os administration of arginine butyrate preserve mdx mice from cardiomyopathy, kyphosis and axonal excitability defaults" (submitted)* is mainly based on a long-term protocol. In particular animals have been treated with AB from the 6th week of age until 14 months of age. Starting from the 8th month a monthly study on heart activity based on echocardiography was performed. The monthly echocardiography evidenced that the treatment with AB preserves *mdx* mice from the drastic reduction of ejection fraction and factional shortening, and also from the ventricular dilatation and hypertrophy observed in saline-treated *mdx* mice. At the age of 14 months, before sacrifice, we looked at the potential benefits of the oral administration of AB on vertebral column deformation and electromyogram defaults, measured with a non-invasive automatized method, develop in the clinic and than appied to animals to study nerve excitability parameters. AB treatment protected from the progressive spinal deformity called kyphosis observed in *mdx* mice, another similarity with DMD patients. Finally most, if not all, of axonal excitability parameters that were modified in saline-treated *mdx* mice, did not show

any significant difference, compared with wild type animals, in AB-treated *mdx* mice whatever the mode of administration, oral or intraperitoneal.

While the protocol followed in the second manuscript was a long-term protocol, the third manuscript *"Low doses of arginine butyrate derivatives alleviate dystrophic phenotype and restore the membrane integrity in DMD murine model."* (submitted), in based on a short-term protocol in which AB (the salt formulation) and its two derivates, ABE and ABA, based on covalent links, were tested *in vivo* in *mdx* mice and *in vitro* in human DMD myotubes.

Excitability parameters *in vivo* and the functional improvements of skeletal muscle were monitored by the evaluation of muscle force (grip test) and fatigue (inverted grid test). We addressed also the benefit on cardiac necrosis. Furthermore, the restoration of sarcolemmal integrity was addressed by dosing the CK level in the serum, measuring the Evans blue incorporation in myofibres of limb, checking the increase of utrophin expression, and completed by an analysis of the lipid composition of the heart membrane through two mass spectrometry techniques. The abnormalities detected in saline-treated *mdx* mice were corrected, in a dose-dependent manner, when the treatment was initiated on young adult animals. The beneficial effect on many structural and functional dystrophic parameters, previously obtained with high dose of AB administered *per os*, were observed with doses 10 times lower with both new compounds.

In parallel, both products were tested *in vitro* on human muscle cell cultures to investigate (i) their capacity to increase utrophin levels, (ii) the potential ability of histone deacetylase inhibitors (byturate, valproic acid, trichostatin A and isobutyramide) alone to increase the expression of utrophin and related proteins (b-dystroglycan and embryonic myosin) (F. Consolaro, M2, Erasmus Padoue-Université Orsay, 2011). Finally, the alteration of calcium homeostasis, largely implicated in the cascades resulting in muscle necrosis/degeneration, was investigated: in particular, the spontaneous Ca^{2+} activity recorded in DMD patient myotubes was strongly reduced after treatment acting on the NO-pathway activation, and/or with HDAC inhibitors.

All together, these data constitute a proof of principle of the beneficial effects of AB and its derivatives on muscular dystrophy, *via* the association of NOS substrate and of an HDAC inhibitor.

3.1 Publication 1. “Arginine butyrate: a therapeutic candidate for Duchenne muscular dystrophy”

The FASEB Journal article fj.12-215723. Published online February 21, 2013.

Arginine butyrate: a therapeutic candidate for Duchenne muscular dystrophy

Sara Vianello,[*,1] Hua Yu,[*,1] Vincent Voisin,[*] Hafedh Haddad,[*] Xun He,[*] Arthur S. Foutz,[†] Catherine Sebrié,[‡,2] Brigitte Gillet,[‡,2] Morgane Roulot,[*] Françoise Fougerousse,[§] Caroline Perronnet,[‖,¶,3] Cyrille Vaillend,[‖,¶] Stefan Matecki,[#] Diana Escolar,[**] Laura Bossi,[††] Maurice Israël,[*] and Sabine de la Porte[*,4]

[*]Neurobiologie & Développement–Unité Propres de Recherche (UPR) 3294 and [†]Neurobiologie Génétique et Intégrative–UPR 2216, Centre National de la Recherche Scientifique (CNRS), Institut de Neurobiologie Alfred Fessard–FRC2118, Gif sur Yvette, France; [‡]CNRS, Institut de Chimie des Substances Naturelles, Résonance Magnétique Nucléaire(RMN) Biologique, Gif sur Yvette, France; [§]Généthon, Evry, France; [‖]Université Paris-Sud, Centre de Neurosciences Paris-Sud, and [¶]CNRS, Unité Mixte de Recherche (UMR) 8195, Orsay, France; [#]Institut National de la Santé et de la Recherche Médicale (INSERM), Equipe Région INSERM (ERI), Muscle et Pathologies, Centre Hospitalier Universitaire (CHU) A. de Villeneuve, Université de Montpellier, Montpellier, France; [**]Johns Hopkins School of Medicine, Baltimore, Maryland, USA; and [††]Domain Therapeutics, BioParc, Illkirch, France

ABSTRACT **As a strategy to treat Duchenne muscular dystrophy, we used arginine butyrate, which combines two pharmacological activities: nitric oxide pathway activation, and histone deacetylase inhibition. Continuous intraperitoneal administration to dystrophin-deficient *mdx* mice resulted in a near 2-fold increase in utrophin (protein homologous to dystrophin) in skeletal muscle, heart, and brain, accompanied by an improvement of the dystrophic phenotype in both adult and newborn mice (45 and 70% decrease in creatine kinase level, respectively; 14% increase in tidal volume, 30% decrease in necrotic area in limb and 23% increase in isometric force). Intermittent administration, as performed in clinical trials, was then used to reduce the frequency of injections and to improve safety. This also enhanced utrophin level around 2-fold (EC_{50}=284 mg/ml) and alleviated the dystrophic phenotype (inverted grid and grip test performance near to wild-type values, creatine kinase level decreased by 50%). Skin biopsies were used to monitor treatment efficacy, instead of invasive muscle biopsies, and this could be done a few days after the start of treatment. A 2-fold increase in utrophin expression was also shown in cultured human myotubes. *In vivo* and *in vitro* experiments demonstrated that the drug combination acts synergistically. Together, these data constitute a proof of principle of the beneficial effects of arginine butyrate on muscular dystrophy.—Vianello, S., Yu, H., Voisin, V., Haddad, H., He, X., Foutz, A. S., Sebrié, C., Gillet, B., Roulot, M., Fougerousse, F., Perronnet, C., Vaillend, C., Matecki, S., Escolar, D., Bossi, L., Israël, M., de la Porte, S. Arginine butyrate: a therapeutic candidate for Duchenne muscular dystrophy. *FASEB J.* 27, 000–000 (2013). www.fasebj.org**

Key Words: DMD · mdx · pharmacology · treatment · NO · histone deacetylase

Duchenne muscular dystrophy (DMD), a lethal X-linked recessive disorder, is characterized by progressive muscle degeneration due to the lack of expression of dystrophin, a cytoskeletal protein essential to muscle structure and function. Loss of muscle strength is typically observed at the age of 4–5 yr, and the disease leads to death due to cardiac or respiratory failure by the age of 25–30. Although various curative therapeutic approaches, such as cell, gene, and pharmacological therapies, are currently being investigated, they still show some limitations (1) and at present, only corticosteroids have a palliative effect on the disease, albeit with severe side effects. Thus, new approaches to com-

Abbreviations: 3D, 3-dimensional; AB, arginine butyrate; AB_{cf}, arginine butyrate clinical formulation; CK, creatine kinase; DAG, dystrophin-associated glycoprotein; DAP, dystrophin-associated protein; DMD, Duchenne muscular dystrophy; f_R, respiratory frequency; MRI, magnetic resonance imaging; NO, nitric oxide; qPCR, quantitative polymerase chain reaction; TA, tibialis anterior; V_E, minute ventilation; V_T, tidal volume; WT, wild type

[1] These authors contributed equally to this work.

[2] Current address: CNRS, U2R2M-UMR8081, Orsay, F-91405, France.

[3] Current address: Department of Cellular and Physiological Sciences, University of British Columbia, Vancouver, BC, Canada.

[4] Correspondence: CNRS, Ave. de la Terrasse, Bat. 32/33, Institut de Neurobiologie Alfred Fessard, Neurobiologie & Développement-UPR 3294 CNRS, Gif sur Yvette, F-91198, France. E-mail: sabine.delaporte@inaf.cnrs-gif.fr

doi: 10.1096/fj.12-215723

This article includes supplemental data. Please visit *http://www.fasebj.org* to obtain this information.

pensate for the lack of dystrophin are warranted. Whatever the pharmacological strategy envisaged to reverse the dystrophic phenotype in patients with DMD, it cannot be effective without restoration of dystrophin expression or overexpression of utrophin, to compensate for the absence of dystrophin. A treatment must restore sarcolemmal integrity (2).

Utrophin is a cytoskeletal protein that shares >80% sequence homology with dystrophin and has similar cellular functions (3). Under some conditions, the utrophin gene is naturally induced to resume function, as seen in DMD (4), in which the gene is up-regulated and low-level utrophin expression expands to the entire cytoskeletal membrane, in an inadequate attempt to compensate for the lack of dystrophin. Further reactivation and renewed expression of utrophin can be exogenously induced by gene (5, 6) or pharmacological therapies (2). A 2-fold up-regulation of utrophin is sufficient to alleviate dystrophic muscle pathology (7). The main advantage of up-regulating utrophin by pharmacological therapies is that there is no need for dystrophin gene replacement or repair. Moreover, targeting the muscles of the whole body appears to be easy with standard modes of administration.

One way to up-regulate utrophin expression is through stimulation of the nitric oxide (NO) pathway. Our previous studies showed that an effective activator of the NO pathway, L-arginine, increases utrophin levels in muscles and targets utrophin to the sarcolemma *in vivo* and *in vitro* (8, 9). In normal and *mdx* myotubes in culture, L-arginine and NO increase utrophin levels and enhance its membrane localization. The NO-induced increase in utrophin expression does not occur with D-arginine, L-NAME (an inhibitor of NO synthase), or oxadiazolo-quinoxalin-1-one (ODQ; an inhibitor of a soluble guanylate cyclase involved in the effects of NO), thus showing the involvement of NO synthase in this process (8). Improvement of dystrophic phenotypes *via* the NO pathway has been demonstrated by many studies in dystrophin-deficient *mdx* mice. Isometric force and resistance to eccentric contractions can thus be improved, serum creatine kinase (CK) levels reduced, muscle structure restored, muscle regeneration increased (10–18), inflammation reduced [decreases in nuclear factor (NF)-κB level and activity; ref, 19], and finally, a normal phosphatidylcholine ion peak intensity ratio of the muscular membrane can be restored (20). NO inducers may have other beneficial effects. First, NO may induce the vasodilatation required for effective supply of metabolites and oxygen to the working muscle, probably by counterbalancing the vasoconstrictor effect of the sympathetic adrenergic system (21, 22). Secondly, the expression of utrophin in vessels, *via* the NO produced by endothelial NOS, could compensate for the lost dystrophin.

Interestingly, the group of Perrine and Faller (23) has shown that administration of butyrate to treat β-globin disorders (sickle-cell disease and β-thalassemia) renewed expression of a fetal form of hemoglobin in erythroid progenitors of patients. Butyrate's effect is hypothesized to occur *via* the inhibition of histone deacetylases, leading to hyperacetylation of histone cores and activation of previously silenced genes. More recent clinical trials to treat β-globin disorders have used arginine butyrate (AB) in place of sodium butyrate to avoid toxicity due to sodium excess, and have demonstrated its safety for pediatric patients (24). Data from safety pharmacology studies (single-dose studies, repeated-dose toxicology, genotoxicity/mutagenicity, pharmacokinetics, and products of metabolism) demonstrate a favorable benefit/risk ratio, suggesting that AB could be used in patients with DMD. These data prompted us to evaluate whether the capacity of AB to renew fetal gene expression could be exploited in treatment of DMD, as utrophin can be considered as a fetal homologue of dystrophin. This hypothesis was further supported by recent studies showing alleviation of the dystrophic phenotype in *mdx* mice after treatment with trichostatin (25) and valproic acid (26), two distinct histone deacetylase inhibitors.

In the present study, our main goal was the preclinical evaluation of the effects of AB on the myopathy displayed in the *mdx* mouse model of DMD. As described above, we consider that AB combines two pharmacological activities that have been shown to be beneficial to the dystrophic phenotype, *i.e.*, NO pathway activation by arginine, and histone deacetylase inhibition by butyrate. Previous work initiated in the framework of a partnership with the pharmaceutical company Domain Therapeutics was performed using a high dose of AB (250 instead of 100 mg/kg/d, the optimal dose selected in chronic administration in the current study) for a long period (6 mo). This resulted in only modest beneficial effects in *mdx* mice, yet safety was good compared with prednisone (1 mg/kg/d), a corticosteroid with toxic effects (27). In the first part of the present study, we used the chronic protocol with lower doses of AB and a range of technical approaches with the aim of providing a proof of principle that AB can increase utrophin expression in muscle tissues and alleviate the dystrophic phenotype in *mdx* mice. The possible synergistic action of arginine and butyrate was addressed by assaying serum CK as a biomarker of muscle necrosis. We further detailed the phenotypic impact of this treatment at various levels, including utrophin and dystroglycan expression in distinct muscle types, effects of administration in newborn *vs.* adult mice, impact on muscle degeneration, respiratory function, body and muscle weights, and on isometric muscle force. Continuous perfusions cannot be easily considered in such a population, hence the importance of evaluating the effectiveness of intermittent administration. Toxicity studies indicate that in rat and dog, toxic effects are localized at the injection site (catheter) and are considered to be sequelae of the inflammation associated with continuous i.v. infusion (28). Because intermittent injections seem more appropriate for potential application to the human condition, the second part of our study was based on a protocol of intermittent injections that mimics protocols previously used to

treat thalassemic children (24). Future clinical trials will address ambulatory patients with DMD (9–11 yr old) with a comparable administration procedure. The goal was then to determine if this specific protocol would recapitulate the basic effects of AB: increased utrophin and dystroglycan expression, body weight increase, reduced CK levels and increased muscle strength, which constitute a restricted but relevant set of biomarkers of reduced myopathy. We also used very short injection schedules and specific biochemical markers to assess the possibility of a rapid evaluation of treatment effects in both animal and human biopsy material. Application to the human condition is supported by the observation of utrophin protein upregulation in human myotubes treated with AB. The comparison of chromatin acetylation states in human myotubes treated with L-arginine, butyrate, and AB confirmed that the combined formula of AB acts synergistically.

MATERIALS AND METHODS

AB preparation

L-arginine was prepared in MilliQ water (Millipore, Billerica, MA, USA) and *n*-butyric acid (Sigma-Aldrich, Lyon, France) was added to make 2 distinct stock solutions: a 26% solution (1 M arginine/1 M butyrate, pH 7) was used for continuous-chronic injections, as described previously (29), whereas a 12.5% solution (0.76 M arginine/1 M butyrate, pH 5.5) was used for intermittent injections (see below). The latter was adapted from U.S. Food and Drug Administration recommendations (personal communication) and corresponds exactly to the AB clinical formulation (AB_{cf}) currently used for administration to patients with β hemoglobinopathies. The stock solutions were diluted before use in 0.9% NaCl to obtain both injectable AB solutions.

Mouse experimental procedures

Since DMD is an X-linked genetic disorder, studies were performed using male mice. All experiments were performed in accordance with the guidelines established by the European Communities Council Directive (Guide for the Care and Use of Laboratory Animals: EEC86/609 Council Directive-Decree 2001-131).

Adult *mdx* and wild-type (WT) mice of the C57BL/10 strain were aged 8 wk at the start of experiments. The newborn mice were injected from postnatal d 2 or 3. Treatment was administered by intraperitoneal injection (1 ml/100 g body weight). Two main protocols of administration were used: continuous-chronic and intermittent. In the continuous-chronic treatment protocol, the mice received 1 daily injection, 5 d/wk for 6 wk. Adult animals were assigned to the saline group injected with 0.9% NaCl or to the treated group injected with either AB at 5, 25, 50, 100, 200, and 300 mg/kg/d or with butyrate alone (Sigma-Aldrich) at 5, 45, 50, 55, 60, and 80 mg/kg/d or L-arginine (Sigma-Aldrich) alone at 100, 200, 500, 800, and 1000 mg/kg/d. For the treatment of newborn mice, preliminary experiments were necessary to adjust the doses, which were 5, 10, 25, 50, 60, and 80 mg/kg/d. In the intermittent treatment protocol, adult mice were injected with saline (0.9% NaCl) or AB_{cf} doses (100, 200, 500, 600, 800, and 1000 mg/kg/d) as a series of 4 consecutive daily injections every 2 or 3 wk for 6 wk. One single series of 4 consecutive daily injections was also used to assess the early effects of this treatment, and the mice were then euthanized the day after (d 5) or 1 wk later (d 12).

Animals were weighed before each injection. *In vivo* functional evaluations were performed in a blinded fashion and carried out 24 h after the end of the treatment. Then, the mice were anesthetized with 10% pentobarbital sodium, blood samples were taken from the heart for measurement of serum CK levels, and mice were sacrificed by cervical dislocation; the muscles and brain were dissected out and frozen for molecular and biochemical analyses.

Immunofluorescence

After fixation in cold methanol (+4°C for 10 min), cryostat sections (7 μm) of muscles or culture dishes of human myotubes were incubated for 5 h at room temperature with a polyclonal antiutrophin antibody (mouse tissue: C19, 1:150 dilution; human tissue: N19, 1:100 dilution; Santa Cruz Biotechnology, Santa Cruz, CA, USA) and/or with a monoclonal anti-β-dystroglycan antibody (NCL-β-DG, 1:10 dilution: Novocastra, Newcastle-on-Tyne, UK), and/or with a monoclonal anti-embryonic myosin antibody (NCL-MHCd, 1:100 dilution; Novocastra) then for 1 h with fluorescent secondary antibody (polyclonal anti-goat Cy2 antibody diluted 1:1000 and monoclonal anti-mouse Cy3 antibody diluted 1:5000; Jackson Immunoresearch, Bar Harbor, ME, USA). Tissue sections were observed using a Leica DM RXA2 fluorescent-imaging microscope (Leica Microsystems, Wetzlar, Germany). Image capture was performed with a CoolSNAP camera (Roper Scientific, Trenton, NJ, USA) and Openlab software (Improvision, Coventry, UK).

Immunoblot analyses

The proteins were extracted from muscle, brain, and skin samples, as well as from cultured myotubes, in a buffer containing 10 mM Tris-HCl, 1 mM EDTA, and 10% SDS (pH 6.8). The total protein content was determined according to DC Protein Assay protocol (Bio-Rad, Hercules, CA, USA). Proteins were separated by SDS-PAGE on a 6–12% multiplex gel (12% for the histone H3 acetylation antibody; X-Cell II Mini Cell; Invitrogen, Saint Aubin, France) with a molecular weight marker (Rainbow; Amersham Pharmacia Biotech, Piscataway, NJ, USA) and then electroblotted onto an Immobilon-P polyvinyl membrane. We applied Coomassie G250 stain to verify the equal loading of gels.

The membrane was incubated with monoclonal antibodies against utrophin (NCL-DRP 2, 1:250 dilution; Novocastra), β-dystroglycan (NCL-β-DG, 1:50 dilution; Novocastra) embryonic myosin (anti-embryonic myosin (2B6), 1:50 dilution, a gift from Gillian Butler-Browne, Institut de Myologie, Paris, France) and/or the acetylated part of histone H3 (Lys 9; AcH3K9, 1:1000 dilution; Upstate-Millipore), and then with a secondary sheep anti-mouse antibody linked to horseradish peroxidase (1:4000 dilution; Jackson Immunoresearch). Immunostaining was revealed by a chemiluminescent reaction (ECL; Amersham Pharmacia Biotech). Desmin (53 kDa) and actin (43 kDa) were used as loading controls for muscle and brain extracts, respectively (desmin is not expressed in brain). Band intensity was quantified using Claravision analyzer software (Claravision, Paris, France). Experiments were repeated ≥3 times. For each experiment, the results in treated mice were normalized to the values obtained in saline-injected mice (treated/saline ratio). Quantification was performed on films obtained after different exposure times for distinct proteins (~30 s for β-dystroglycan, 2 min for desmin and

utrophin), but within quantifications of a given target protein, the same exposure times were used for the different doses shown on the histograms.

Quantitative polymerase chain reaction (qPCR) analysis

RNA was extracted using a standard protocol with TRIzol reagent (Invitrogen) and purified with the RNeasy Plus kit (Qiagen, Valencia, CA, USA). The quality and concentration of RNA were determined by spectrophotometry (OD at 260 nm) with a Nanodrop. Total RNA (200 ng) was reverse-transcribed in a 20-μl final reaction volume using the high-capacity cDNA reverse transcription kit with RNase inhibitor (Applied Biosystems, Paris, France, USA) following the manufacturer's instructions. qPCR reactions were then performed using the 7900HT real-time PCR system (Applied Biosystems). The forward and reverse primer sequences were as described previously (30): Utrophin-A forward, 5′-ACGAATTCAGTGACATCATTAAGTCC; Utrophin-B forward, 5′-CAGGCTTGCAGGAGATCCC; Utrophin-A and -B reverse, 5′-ATCCATTTGGTAAAGGTTTTCTTCTG. Each primer pair was tested, and melt curves were constructed and analyzed to ensure that only a single amplicon was generated. PCR was performed in plates in a final volume of 10 μl, containing Fast SYBR Green Master Mix, 0.5 μM of each primer, and cDNA corresponding to 0.6 ng of mRNA. Standard PCR conditions were used for the Applied Biosystems assays: 95°C for 20 s and 40 cycles at 95°C for 1 s alternating with 60°C for 25 s. All samples were assayed in duplicate for each target or 6 housekeeping genes, and the averaged values were used as cycle threshold. The most stable housekeeping genes were selected by analyzing results with GeNorm and Normfinder functions in Genex 4.3.8 (MultiD, Göteborg, Sweden). The geometric mean of the 5 best housekeeping genes (GAPDH, HPRT, L32, ACTB, and TUBB) was used to normalize utrophin-A and -B expression levels. Changes in the relative expression of genes of interest were calculated.

Serum CK determination

Blood samples were taken from hearts of anesthetized mice immediately before euthanasia. Serum CK activity was determined using a BioMérieux kit (enzyline CK NAC optimized 10; BioMérieux, Marcy-l'Étoile, France).

Magnetic resonance imaging (MRI)

MRI was performed as described previously in Voisin *et al.* (18). The percentage of normal muscle and necrotic muscle areas was calculated. AMIRA software permitted 3-dimensional (3D) hind-limb reconstruction and 3D visualization of muscle damage.

Masson's trichrome stain

Cryostat muscle sections (7 μm) were stained with Masson's trichrome stain to visualize connective tissue and muscle fibers in pink and collagen in blue (Sigma kit HT15; Sigma-Aldrich) and then observed using a Leica DM RXA2 microscope (Leica Microsystems). The sections were photographed using a CoolSNAP camera (Roper Scientific) and Openlab acquisition software (Improvision).

Evans blue dye

Evan's blue dye (10 mg/ml) in PBS was prepared extemporaneously and filtered through paper (31). A volume of 100 μl/10 g body weight was injected 9 h prior to euthanasia. Diaphragms were excised and digitally photographed for macroscopic evaluation with a binocular magnifying glass equipped with a Canon PowerShot S45 camera (Canon, Tokyo, Japan).

Measurement of ventilation

Breathing activity in adult mice was monitored using the barometric method. The mouse was placed in a plethysmograph chamber (700 ml) and was partially restrained by the tail, with a thin temperature rectal probe. Within the chamber, the animal was positioned in a small rectangular box (4×4×9 cm) opened at both ends, which allowed the animal to reposition itself during the experiment. The chamber was maintained at 27 ± 1°C and was hermetically sealed for 90 s during data collection sessions. Between sessions, the chamber was constantly flushed with fresh humidified air (1 L/min) or with two hypercapnic gas mixtures (6 and 8% CO_2, 21% O_2, balance N_2) administered sequentially for 10 min each. The mice were habituated to the chamber over the previous 2 d. During data collection, tidal volume (V_T) and respiratory frequency (f_R) were continuously recorded. Minute ventilation was then calculated ($V_E = V_T \times f_R$).

Mechanics of isolated muscles

Animals were anesthetized by intraperitoneal injection of a mix of 10 ml/kg of ketamine (10 mg/ml) and xylazine (1 mg/ml), in order to preserve muscle perfusion during dissection of the soleus muscles. The muscle was dissected free from adherent connective tissue and soaked in an oxygenated Krebs solution (95% O_2 and 5% CO_2) containing NaCl (118 mM), $NaHCO_3$ (25 mM), KCl (5 mM), KH_2PO_4 (1 mM), $CaCl_2$ (2.5 mM), $MgSO_4$ (1 mM), and glucose (5 mM) maintained at a temperature of 20°C.

Muscle strips were connected at one end to an electromagnetic puller and at the other end to a force transducer. Stimulation was delivered through electrodes running parallel to the muscle. Tetanic (100 Hz, 500 ms) isometric contractions were studied at L_0 (the optimal length at which maximal tetanic isometric force is observed).

For comparative purposes, normalized isometric force instead of force was assessed. Isometric force was calculated by dividing the force by the estimated cross-sectional area of the muscle. Assuming muscles have a cylindrical shape and a density of 1.06 mg/mm^3, cross-sectional area corresponds to the wet weight of the muscle divided by its fiber length.

Combined forelimb and hind-limb grip strength measurement

Grip strength was measured using a grip strength meter (Bioseb, Vitrolles, France). The apparatus consisted of a grid connected to a digital dynamometer. The animals were gently lowered over the top of the grid so that both sets of front paws and hind paws could grip the grid. While the torso of the animal was kept parallel to the grid, the mouse was gently pulled back by the tail until it released its grip. This procedure was repeated 3 times, and the values were averaged and normalized to mouse body weight.

Inverted grid test

Mice were placed individually on a cage wire grid ~35 cm above a table. After slowly turning the grid through 180°, the length of time the mice continued to grip the grid was

monitored (grip latency), a maximum score of 180 s being given if the animal did not fall. This procedure was repeated 3 times. The values were averaged and normalized to mouse body weight.

In vitro human myotube preparation

Satellite cell populations were isolated as described previously (32) from surgical samples obtained from 4 patients with DMD aged 14 to 25 yr (Banque de Tissus pour la Recherche, Paris, France). After 5 d, when the first mononucleated cells migrated out of the explants, the explants were removed, and the cells were trypsinized (trypsin-EDTA; Invitrogen), collected by centrifugation, and counted. The cell cultures were incubated at 37°C at an initial concentration of 30,000 cells/35-mm-diameter dish, in a humid atmosphere containing 5.5% CO_2. Cultures were grown in a medium consisting of Ham's F-10 supplemented with 20% FCS. After 5 d, growth medium was changed to differentiated medium (Ham's F-10 supplemented with 10% HS). After another 5 d, myotubes were treated with AB (0.1, 0.2, 0.5, 1, and 2 mM) for 48 h. Utrophin expression was determined by Western blot analysis. The histone acetylation state of the myotubes was determined after 48 h of treatment with AB (0.1, 0.5, and 1 mM) or L-arginine (0.066, 0.33, and 0.66 mM) or butyrate (0.034, 0.17, and 0.34 mM).

Statistics

Data are shown as means ± SE and are from ≥3 different experiments. Statistical group comparisons were performed using Student's *t* test with the level of significance set at $P < 0.05$.

RESULTS

In vivo protocol I: continuous-chronic intraperitoneal administration of AB

Utrophin and β*-dystroglycan are up-regulated in muscles from newborn and adult* mdx *mice*

The effects of AB were first evaluated in adult *mdx* mice after 6 series of injections (5 consecutive days per week for 6 wk, at 5 to 300 mg/kg/d). After the treatment, utrophin immunostaining was increased in an apparent dose-dependent manner from 5 to 100 mg/kg/d, reaching comparable levels at the doses of 100 and 200 mg/kg/d (data not shown). We selected the dose of 100 mg/kg/d for the following experiments. Utrophin immunoreactivity appeared in large areas of muscle sarcolemma in gastrocnemius, soleus, tibialis anterior (TA), and diaphragm (**Fig. 1*A***). Utrophin labeling was also increased in the capillaries (Fig. 1*B*). Experiments were also performed in newborn mice with the same protocol (5 d/wk for 6 wk). In newborn mice, utrophin staining at the sarcolemma was weak in TA, soleus, and diaphragm in saline-injected mice, while pronounced staining was obtained after injections of a dose of AB adapted to newborn animals, as determined in a pilot study (25 mg/kg/d AB for 6 wk; Fig. 1*C*).

The putative relocalization of β-dystroglycan, a transmembrane dystrophin-associated protein (33), which is

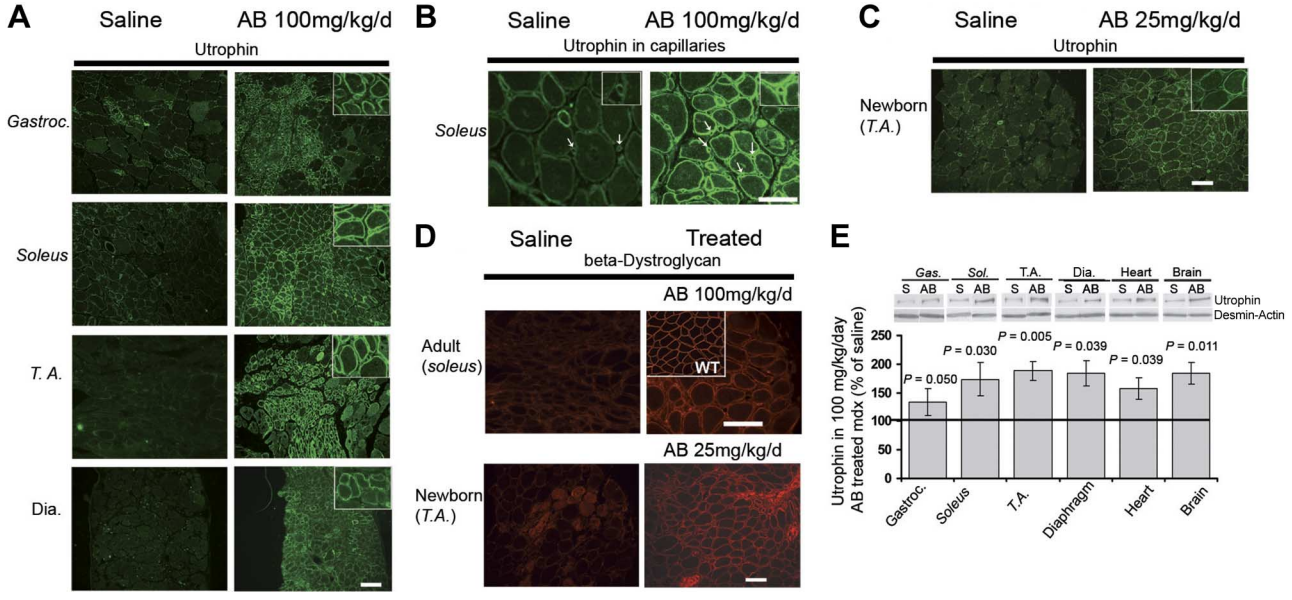

Figure 1. Utrophin in adult and newborn *mdx* mice subjected to the 6-wk continuous-chronic AB treatment protocol. *A*) Utrophin immunostaining in gastrocnemius (gastroc.), soleus, TA, and diaphragm (dia.) of adult *mdx* mice (n=10) after AB treatment (100 mg/kg/d, the dose that produced maximal staining) or saline injections. *B*) Utrophin immunostaining in capillaries of soleus muscle in adult *mdx* mice after AB (100 mg/kg/d) or saline treatments. *C*) Utrophin immunostaining in the TA of *mdx* mice treated from birth with AB (25 mg/kg/d; n=5) compared with the saline group. *D*) β-Dystroglycan immunostaining in soleus muscles of adult *mdx* or WT (inset) mice treated with AB (100 mg/kg/d) and in TA of newborn *mdx* mice treated with AB (25 mg/kg/d). Scale bars = 100 μm. Original view: ×3. *E*) Utrophin levels expressed as a percentage of the level in the saline group were increased in gastrocnemius (gas.; 1.3-fold), soleus (sol.; 1.7-fold), TA (1.9-fold), diaphragm (1.8-fold), heart (1.6-fold), and brain (1.8-fold) in *mdx* mice at the dose of 100 mg/kg/d (n=3/treatment) of AB. Loading controls: desmin for muscle and actin for brain extracts.

not properly integrated into the sarcolemma in patients with DMD, was also assessed. Gastrocnemius, soleus (Fig. 1*D*), TA, and diaphragm muscles of treated adult *mdx* mice showed more pronounced β-dystroglycan staining at the sarcolemma compared with saline-injected mice. Similarly, in treated newborn *mdx* mice, soleus, TA (Fig. 1*D*), and diaphragm muscles showed more pronounced staining for β-dystroglycan as compared with saline-injected mice (dose 25 mg/kg/d).

Semiquantitative Western blot analyses revealed a near 2-fold increase in utrophin expression in the gastrocnemius, soleus, TA, diaphragm, heart, and brain tissues, in *mdx* mice treated with AB at the dose of 100 mg/kg/d (Fig. 1*E*), as compared with mice injected with a saline solution. The relative increase was lower (1.7-fold) at 5 mg/kg/d, whereas no further increase was found at a higher dose of 200 mg/kg/d (data not shown).

Decreased serum CK levels in adult and newborn mdx mice: synergistic effect

In adult *mdx* mice treated with AB at 50 and 100 mg/kg/d, CK level was reduced to about half the level observed in saline-injected *mdx* mice (**Fig. 2*A***), indicating a reduction of muscle necrosis. AB treatment had no effect on CK levels in WT mice injected at 100 mg/kg/d in the same conditions (n=10/treatment group; data not shown). The inverted bell-shaped dose response curve for CK indicated that AB's beneficial effect was obtained from dose 50 mg/kg/d (ratio of 1: a combination that corresponds to 33 mg/kg/d arginine plus 17 mg/kg/d butyrate). The beneficial effect with butyrate (alone) was obtained at 55 mg/kg/d, while the minimal effective dose for arginine (alone) was 200 mg/kg/d, thus demonstrating a synergistic action of arginine and butyrate when used in combination. The effect of AB on CK levels was also evaluated in newborn *mdx* mice. AB reduced CK levels by ~70% compared with saline-injected *mdx* mice at doses of 25, 50, and 60 mg/kg/d (Fig. 2*B*), suggesting that AB treatment was more effective in immature than mature tissues.

Improvement of respiratory function and diaphragm structure in adult mdx mice

In vivo ventilatory function depends on neural control and drive, as well as on blood flow regulation and muscle production. Respiratory function, a major parameter affected in patients with DMD, was, here, evaluated in mice treated with a 100 mg/kg/d dose of AB. The V_T, f_R, and V_E were all lower in control *mdx* mice than in WT mice (**Fig. 3*A***, top panels). During exposure to 6 and 8% CO_2, the V_T was increased in *mdx* mice treated with AB as compared with saline-injected mdx mice. In contrast, the f_R was unaffected. Consequently, the V_E was not modified by treatment (Fig. 3*A*, bottom panels). There was no effect of AB on ventilatory function in WT mice (data not shown).

An enhanced V_T may reflect improved structure of the diaphragm muscle. To confirm this hypothesis, we analyzed the extent of diaphragm necrosis using Evan's blue dye, a vital stain used to identify areas of necrosis and cell damage. We found so few fibers stained by Evan's blue dye in diaphragm from treated *mdx* mice that we considered that quantification was not justified (Fig. 3*B*). Infiltration of diaphragm by collagen, another marker of tissue damage, was visualized using Masson's trichrome stain. As shown in Fig. 3*C*, *mdx* mice treated with AB displayed reduced collagen infiltration (stained blue) in the diaphragm along with improved myofiber organization.

Improvement of hind-limb muscle structure and function in adult mdx *mice*

The body weight of adult *mdx* mice receiving continuous-chronic AB administration increased modestly (~10%) at

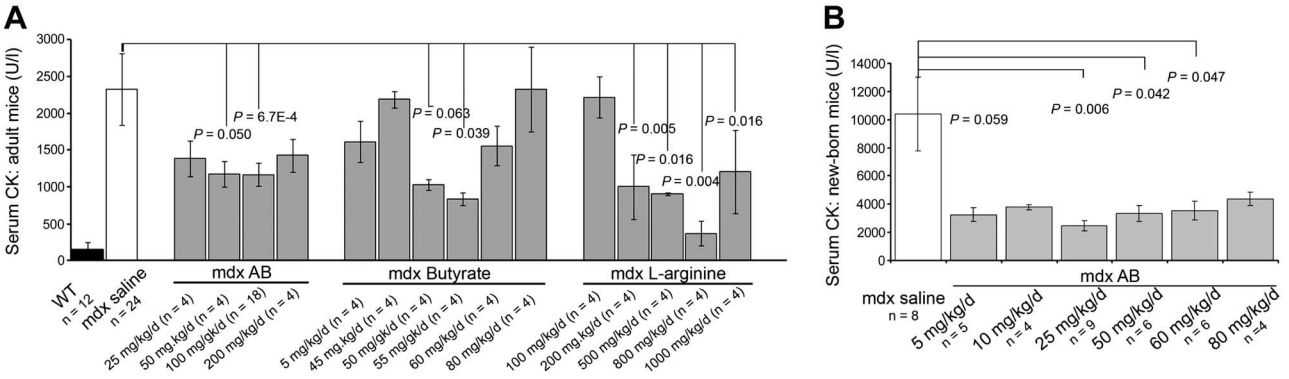

Figure 2. Serum CK level in adult and newborn *mdx* mice subjected to the 6-wk continuous-chronic AB treatment protocol. *A*) Adult untreated *mdx* mice exhibited high levels of serum CK activity (2322±312 U/L) compared with WT mice (153±100 U/L). However, serum CK levels decreased to 40–50% of those of saline-injected *mdx* mice after treatment with AB at 50 and 100 mg/kg/d. AB dose of 50 mg/kg/d corresponds to 33 mg/kg/d of L-arginine plus 17 mg/kg/d of butyrate, while reduction of CK with L-arginine was obtained from dose of 200 mg/kg/d and with butyrate from dose of 55 mg/kg/d, demonstrating a synergistic action of both drugs when used in combination. *B*) Newborn serum CK levels decreased to 70% of those of saline-injected *mdx* mice when the *mdx* mice were injected from birth from 25 to 60 mg/kg/d. Reduction of CK was nearly significant at a dose of 5 mg/kg/d (P=0.059).

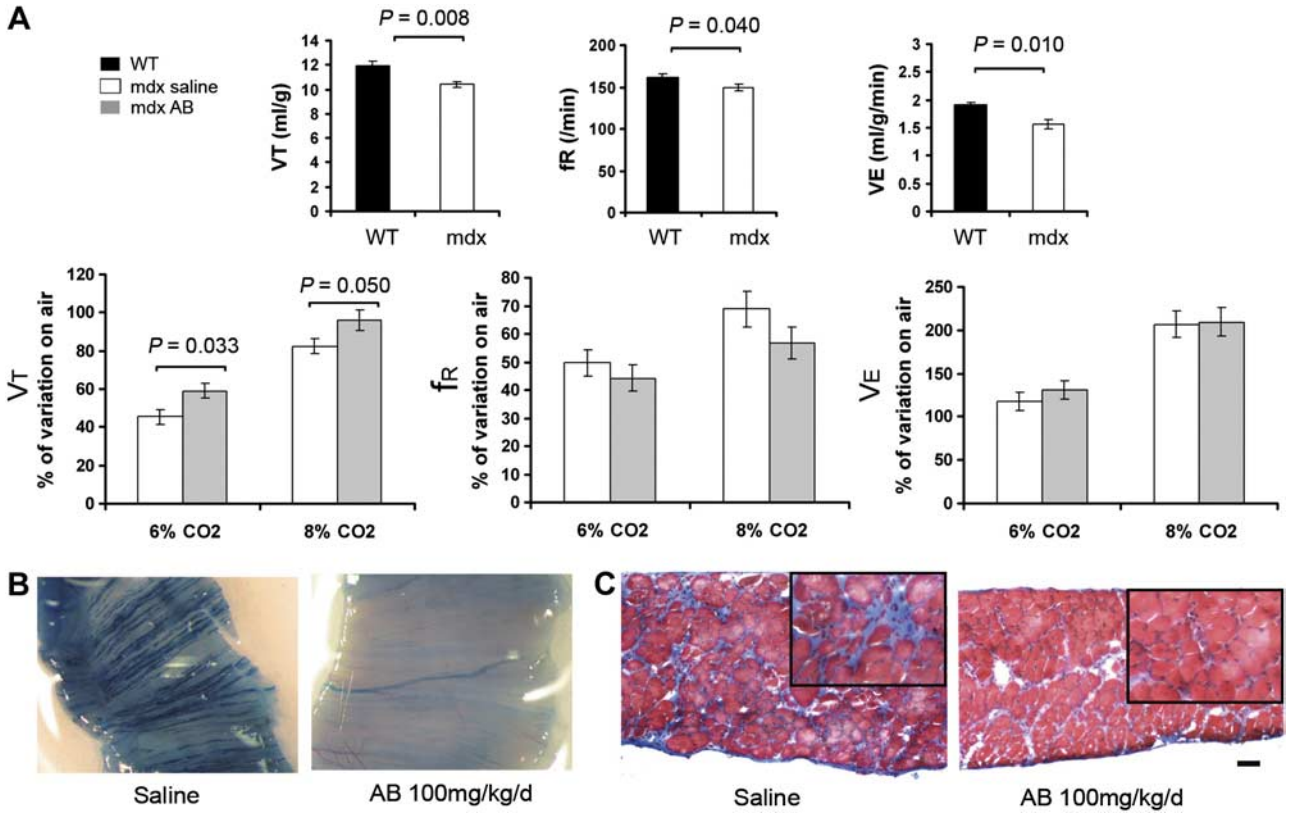

Figure 3. Improved respiratory function and diaphragm muscle structure in *mdx* mice subjected to the 6-wk continuous-chronic AB treatment protocol (100 mg/kg/d). *A*) Top panels: basal ventilatory function at rest in *mdx* mice and WT mice (n=10/group). During exposure to room air, V_T, f_R, and V_E ($V_T \times f_R$) were reduced by 13, 7.5, and 20%, respectively, in *mdx* compared with WT mice. Bottom panels: ventilatory function in adult-treated and saline-injected *mdx* mice (n=10/group) was assessed when muscles were strongly solicited under hypercapnic conditions (6 and 8% CO_2). During hypercapnia, V_T showed a greater increase (14% more) in AB-treated than in saline-injected *mdx* mice. The f_R and, consequently, V_E were not modified. *B*) Reduction of necrosis in the diaphragm after treatment with AB, as demonstrated by the exclusion of Evans's blue dye from the treated muscle, as compared with saline. Diaphragm of saline-injected *mdx* mice (n=3) had numerous necrotic fibers, as evidenced by extensive areas stained by Evan's blue dye. In contrast, necrotic fibers were almost absent in *mdx* mice (n=5) after AB injections. *C*) Masson's trichrome staining of diaphragm in untreated *vs.* treated *mdx* mice (n=6). AB treatment in *mdx* mice reduced the amount of collagen infiltration (stained in blue) in the diaphragm compared with untreated mice. Scale bar = 50 μm. Original view: ×3.

doses 50, 100, and 200 mg/kg/d as compared with saline-injected mice (Supplemental Fig. S1*A*). This was associated with an increased weight of TA and soleus muscles (Supplemental Fig. S1*B*), but not of gastrocnemius.

An MRI study was performed in *mdx* mice before (T_0) and after (T_0+6 wk) treatment with AB (100 mg/kg/d), providing an *in situ* evaluation of muscle necrotic areas in living animals. Reduced necrosis was readily visible in tissue sections (**Fig. 4*A***) and in 3D reconstitutions of the hind limb (Fig. 4*B*), and the quantification of the necrotic areas confirmed the significant reduction in *mdx* mice treated with AB compared with those injected with a saline solution (Fig. 4*C*). As shown in Fig. 4*D*, this was associated with reduced fibrosis and improved structure of the hind-limb muscles, which more closely resembled healthy tissue (as illustrated for the soleus muscle in the figure).

To document further the alleviation of myopathy by AB treatment, we measured the isometric force in soleus muscles of *mdx* mice injected with AB or NaCl. *Mdx* mice treated with AB showed a 23% increase in the isometric force (n=19 muscles), as compared with saline-injected *mdx* mice (n=13 muscles). Although this improvement was statistically significant (P<0.03), the isometric force in treated *mdx* mice did not reach the levels of healthy WT mice (n=8 muscles; Fig. 4*E*).

In vivo protocol II: intermittent intraperitoneal AB_{cf} administration

In this series of experiments with adult mice, the frequency of injections was reduced, and preliminary experiments demonstrated that higher doses could then be used. The AB formulation used in this protocol was different to that used in the previous experiments: it was based on the formulation recently applied in patients suffering from β-globin disorders, *i.e.*, it corresponded to a 0.76 M arginine instead of 1 M. This distinct formulation is referred to as AB_{cf} in all parts of the text and in the figures.

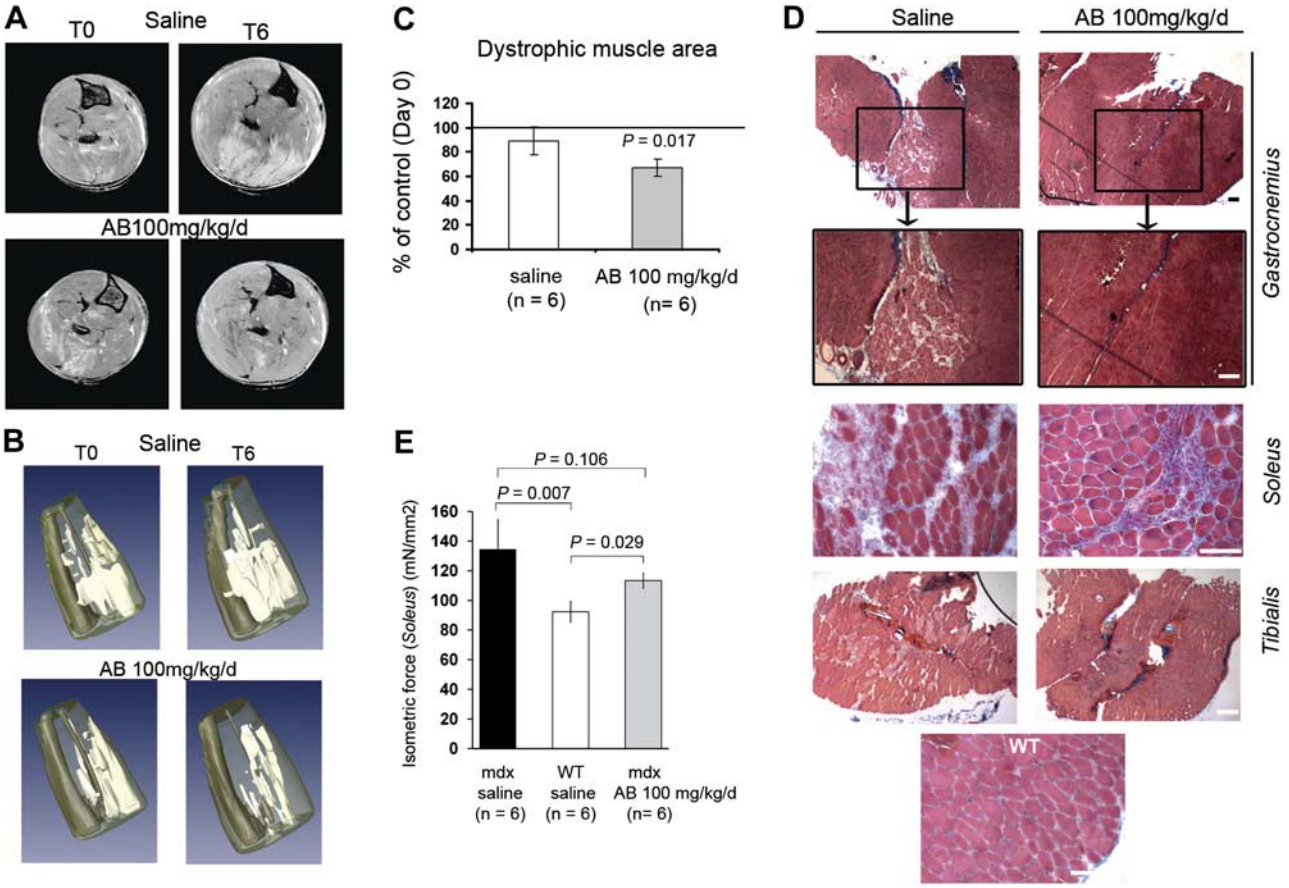

Figure 4. Muscle structure and function in adult *mdx* mice subjected to the 6-wk continuous-chronic AB treatment protocol (100 mg/kg/d). *A*) Lower limbs of adult *mdx* mice were examined by cross-sectional MRI before (T_0) and after [T_0+6 wk (T_6)] treatment with saline solution or AB (n=6/case). Black, bone cavities; white, fat and damaged tissues; gray, healthy muscle tissue. For each animal, the percentage of areas containing healthy muscle (gray) and damaged muscle (white) were measured in 4 consecutive slices corresponding to the median part of the hind limb, at T_0 and T_6 (subcutaneous fat was excluded). A large decrease in damaged tissue areas was observed after treatment. *B*) Amira-3D reconstitution data analysis enabled visualization of the reduction of necrotic zones in the whole hind limb (brown, bone; white, damaged tissues). *C*) Quantification of necrotic surfaces from MRI study; results are presented as percentages of control (d 0). A large reduction of necrotic areas (30%) was observed after treatment with AB. *D*) Masson's trichrome staining of gastrocnemius (original view: ×2), soleus, and tibialis anterior (TA) in untreated *vs.* treated mice (n=10/treatment). Muscles from saline-injected *mdx* mice had extensive areas of necrosis characterized by extensive areas of connective tissue invasion. Following AB treatment, the muscle more closely resembled healthy tissue (WT; illustrated: soleus muscle). Scale bars = 250 μm. *E*) Isometric force production. Isometric force was slightly (23%) increased in soleus muscles of treated *mdx*, compared with untreated mice.

Series of 4 injections (every 2 wk for 6 wk)

The body weight of *mdx* mice treated for 4 consecutive days every 2 wk for 6 wk (3 series of injections) increased by up to 21% at doses from 500 to 1000 mg/kg/d (Supplemental Fig. S1*C*), which is greater than the changes induced by continuous-chronic injections (~10%). No change in body weight was detected in WT mice (data not shown).

An effect of AB_{cf} on muscle strength was first evaluated using a grip-strength meter. AB_{cf} treatment improved *mdx* mice grip strength at doses 600 and 800 mg/kg/d in a dose-dependent manner (**Fig. 5*A***). In the inverted grid test, the ability of AB_{cf}-treated *mdx* mice to maintain a grip on an inverted grid (grip latency) varied according to mice but was significantly improved at the dose of 600 mg/kg/d (Fig. 5*B*).

Intermittent treatment with AB_{cf} also significantly reduced the serum CK levels at doses of 200, 500, 600, 800, and 1000 mg/kg (Fig. 5*C*). However, CK levels in AB_{cf}-treated *mdx* mice never reached the very low levels that are typically measured in the WT mice, thus showing again that AB alleviates myopathy but does not lead to complete rescue of the dystrophic phenotype. Increasing the interval between the series of 4 daily injections from 2 to 3 wk (2 series of injections during the 6 wk of the protocol) induced a reduction of CK levels of ~30% in *mdx* mice treated with the higher doses (600, 800, and 1000 mg/kg/d), though this group difference did not reach statistical significance (data not shown).

Western blot analyses showed that in TA muscle, AB_{cf} increased expression levels of utrophin at doses of 200, 600, 800, and 1000 mg/kg/d (EC_{50}=284 mg/ml; Fig.

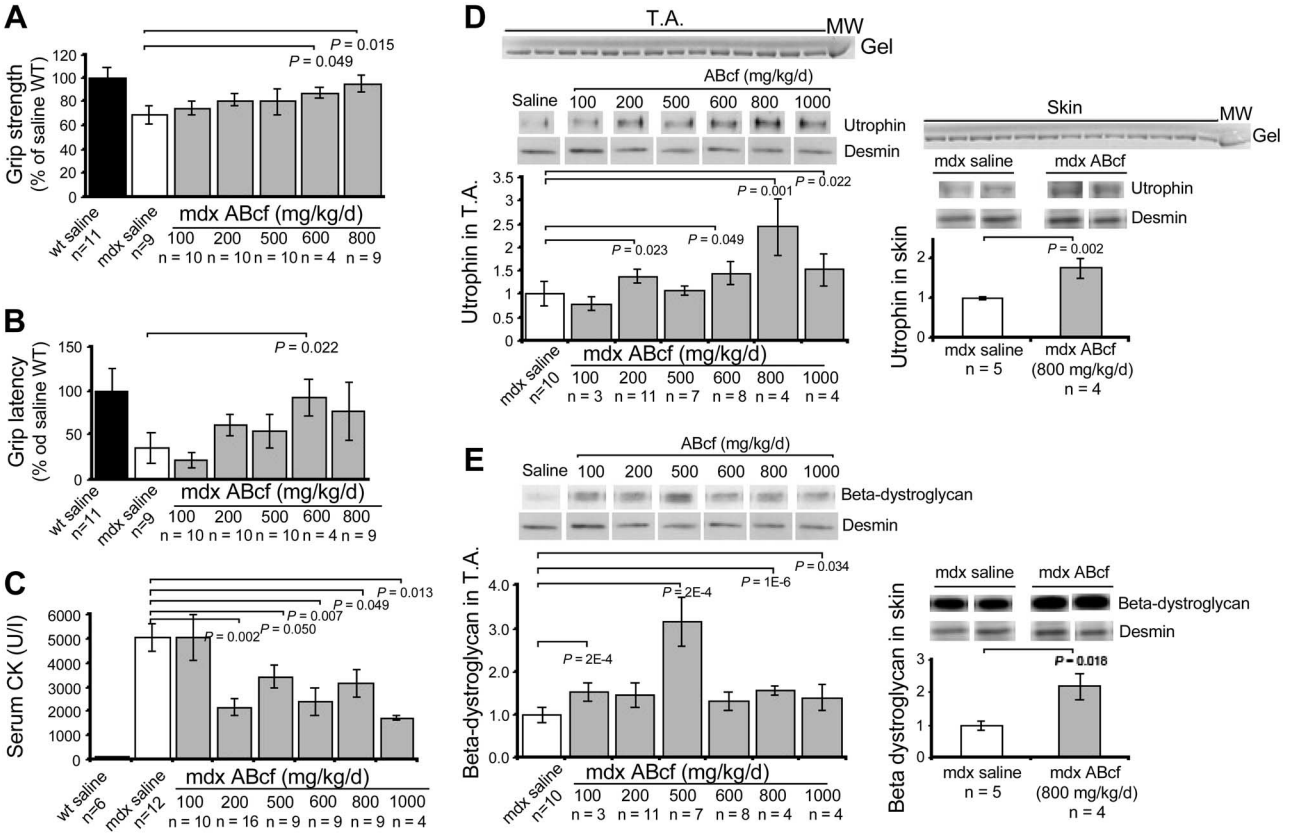

Figure 5. Beneficial effects of AB_{cf} (100 to 1000 mg/kg/d) administered to adult *mdx* mice for 6 wk following an intermittent protocol. *A*) Grip strength of saline-injected *mdx* mice was 70% of that of WT mice. AB_{cf} treatment (100–800 mg/kg/d) at doses of 600 and 800 mg/kg/d improved *mdx* mouse grip strength, which reached 88 and 95% of the WT value, respectively. *B*) In the inverted grid test, grip latency in WT mice was 3-fold longer than in the saline-injected *mdx* mice. Treatment at 600 mg/kg/d improved grip latency, which reached 92% of the WT value. *C*) AB_{cf} treatment reduced serum CK levels by ~50% at doses of 200 to 1000 mg/kg as compared with saline. *D*, *E*) Utrophin (*D*) and β-dystroglycan (*E*) expression was assessed by Western blot in TA muscle of *mdx* mice receiving 100 to 1000 mg/kg/d of AB_{cf}. Equal loading was verified by staining protein gels with Coomassie blue (MW, molecular weight marker). Graph shows the mean values for ≥3 different experiments. Results were normalized to saline values (treated/saline ratio). Values are representative of 3 independent experiments. *D*) Utrophin expression level was increased in TA from treated mice compared with saline-injected mice at 200 (1.9-fold), 600 (1.45-fold), 800 (2.45-fold), and 1000 (1.5-fold) mg/kg/d. In skin from mice injected with AB_{cf} at 800 mg/kg/d, utrophin levels were increased 1.8-fold compared with saline. *E*) β-Dystroglycan levels were increased in TA from treated mice at 100 (1.5-fold), 500 (3-fold), 800 (1.6-fold), and 1000 (1.4-fold) mg/kg/d. In skin samples, β-dystroglycan expression level was increased 1.7-fold at 800 mg/kg/d as compared with saline. Increased utrophin and β-dystroglycan expression levels in soleus are shown in Supplemental Fig. S2.

5*D*) and that of β-dystroglycan at doses of 100, 500, 800, and 1000 mg/kg/d (Fig. 5*E*). In the soleus, utrophin (at doses of 800 and 1000 mg/kg/d) and β-dystroglycan (at doses of 200, 500, 600, and 1000 mg/kg/d) were also overexpressed (Supplemental Fig. S2). Moreover, we also showed that AB_{cf} could increase utrophin expression in mouse skin samples (Fig. 5*D*, *E*), reflecting widespread effects of AB in various tissues and organs and raising the possibility of using skin biopsies to monitor treatment effects over time.

One single series of 4 injections of AB_{cf}

In a clinical trial, a biopsy performed shortly after the beginning of the treatment could be useful to validate the first expected effect of AB_{cf} in muscles of the patient, *i.e.*, an increase in expression of utrophin and associated proteins, such as β-dystroglycan or embryonic myosin (a putative marker of regeneration). In anticipation of the biopsies that could be scheduled in clinical trials, we determined the time frame in which utrophin expression could be clearly up-regulated in muscle tissues from treated *mdx* mice. Mice were sacrificed 24 h after a single series of 4 consecutive daily injections (d 5) or 1 wk later (d 12).

Expression of utrophin, β-dystroglycan, and embryonic myosin was analyzed by Western blot in the same muscle extracts. Utrophin expression was increased 24 h after the end of the treatment in the TA of *mdx* mice treated with AB_{cf} at 800 mg/kg/d (**Fig. 6*A***). This overexpression of the utrophin protein was associated with an increased expression of utrophin-A mRNA, as evaluated by qPCR (Fig. 6*B*). No increases were observed for the utrophin-B mRNA level (ratio: 0.93±0.019, range: 0.88–1.10; $P>0.05$; data not shown)

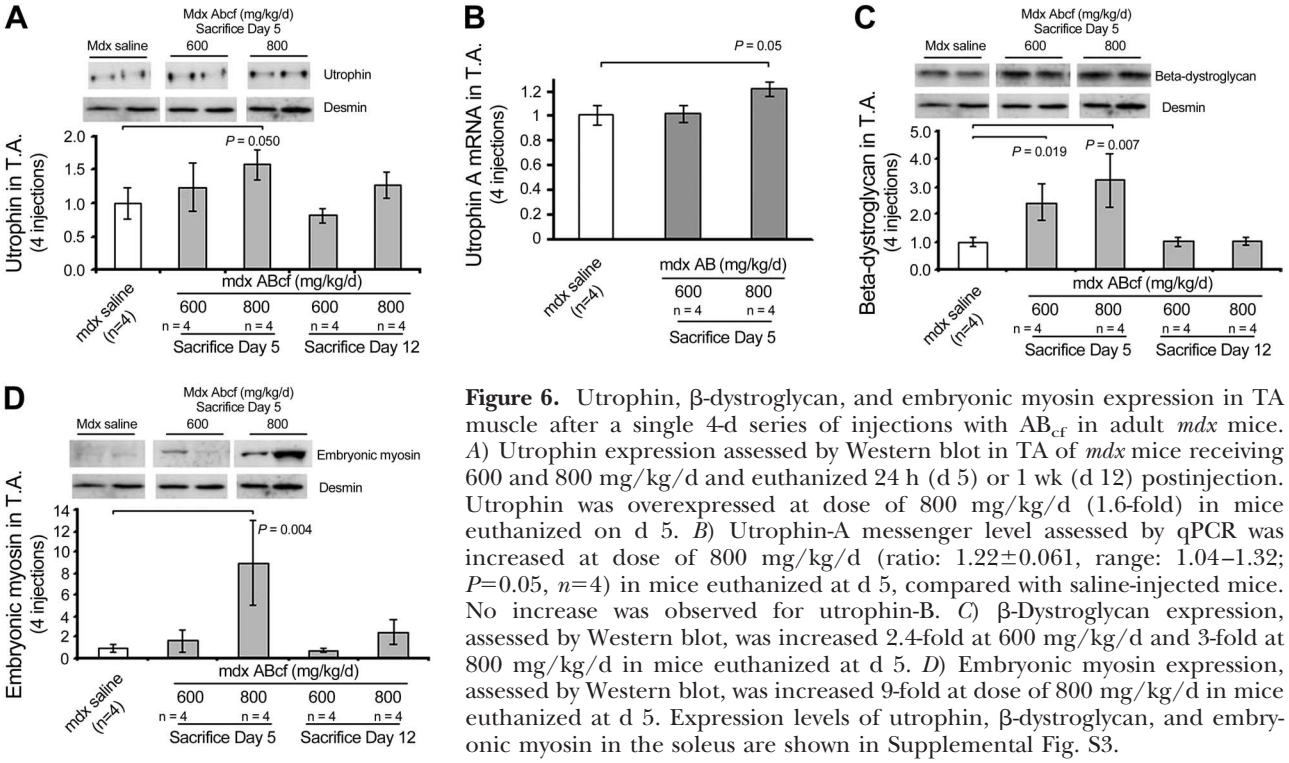

Figure 6. Utrophin, β-dystroglycan, and embryonic myosin expression in TA muscle after a single 4-d series of injections with AB_{cf} in adult *mdx* mice. *A*) Utrophin expression assessed by Western blot in TA of *mdx* mice receiving 600 and 800 mg/kg/d and euthanized 24 h (d 5) or 1 wk (d 12) postinjection. Utrophin was overexpressed at dose of 800 mg/kg/d (1.6-fold) in mice euthanized on d 5. *B*) Utrophin-A messenger level assessed by qPCR was increased at dose of 800 mg/kg/d (ratio: 1.22±0.061, range: 1.04–1.32; P=0.05, n=4) in mice euthanized at d 5, compared with saline-injected mice. No increase was observed for utrophin-B. *C*) β-Dystroglycan expression, assessed by Western blot, was increased 2.4-fold at 600 mg/kg/d and 3-fold at 800 mg/kg/d in mice euthanized at d 5. *D*) Embryonic myosin expression, assessed by Western blot, was increased 9-fold at dose of 800 mg/kg/d in mice euthanized at d 5. Expression levels of utrophin, β-dystroglycan, and embryonic myosin in the soleus are shown in Supplemental Fig. S3.

β-dystroglycan expression levels were significantly increased at doses of 600 and 800 mg/kg/d in tissues analyzed 24 h after the end of treatment (Fig. 6*C*). Expression of embryonic myosin was strongly increased at 800 mg/kg/d 24 h after the end of treatment (Fig. 6*D*). Similarly in the soleus, utrophin, and β-dystroglycan, expression levels were increased 24 h after the end of treatment in *mdx* mice treated with AB_{cf} at 800 mg/kg/d (Supplemental Fig. S3*A*, *B*), while expression of embryonic myosin was increased at both 600 and 800 mg/kg/d (Supplemental Fig. S3*C*). Utrophin and β-dystroglycan immunostaining revealed localization in the soleus sarcolemma, and the staining for embryonic myosin was strongly increased in treated mice (Supplemental Fig. S4).

However, in both TA and soleus muscles, none of these changes were maintained when mice were sacrificed 1 wk after the fourth injections, thus confirming the need for a chronic regimen to maintain the effects of AB.

Interestingly, utrophin and β-dystroglycan were also overexpressed in the brain of treated *mdx* mice: utrophin protein was overexpressed by 37% (P<0.03) and β-dystroglycan by 74% (P<0.001) at the dose of 800 mg/kg/d, 24 h after the end of treatment. In contrast to the muscle tissues, these changes were persistent, as mice euthanized 1 wk after the fourth injections still showed significant overexpression of utrophin (216%; P=0.001) and β-dystroglycan (200%; P<0.001) (data not shown). This delay could reflect better diffusion of AB in brain tissues due to the blood-brain barrier dysfunction reported in *mdx* mice (34), or unidentified differences in the dynamics of AB metabolism and/or regulation of utrophin expression and stabilization in muscle *vs.* brain tissues.

In vitro AB treatment in human cultured myotubes

How AB affects utrophin expression in human tissue was determined by Western blot analysis of myotube extracts obtained from myoblasts isolated from DMD volunteers. Treatment with 0.1–2 mM AB for 2 d increased utrophin expression around 2-fold in human myotubes (**Fig. 7*A***), in an apparent dose-dependent manner at doses from 0.1 to 1 mM. Localization of utrophin in myotubes was observed after immunostaining of utrophin: little utrophin labeling was visible in untreated myotubes, but staining was slightly increased in the sarcolemma after treatment (Fig. 7*B*). This increase of utrophin in human myotubes suggests that the treatment may have a similar effect in muscles of patients with DMD. In addition, the synergistic effect of AB was also demonstrated by analyzing the chromatin acetylation state in Western blot experiments using an antibody against the acetylated part of histone H3 (Lys 9). An increased acetylation level was expected after treatment with butyrate, due to its histone deacetylase inhibitor properties. This was, however, not directly expected following treatment with L-arginine alone, although recent studies suggest that NO may also be involved in epigenetic histone modification and gene expression regulation in *mdx* mice, as well as in C2C12 myoblasts from patients with DMD (35). Here, human myotubes were treated with different doses of AB or L-arginine or butyrate alone. In a first group, we compared AB (0.1 mM) with the corresponding doses of L-arginine (0.066 mM) or butyrate (0.034 mM) alone; in a second group, we compared AB (0.5 mM) with the corresponding doses of L-arginine (0.33 mM) or butyrate (0.17 mM) alone; and in a last group, we com-

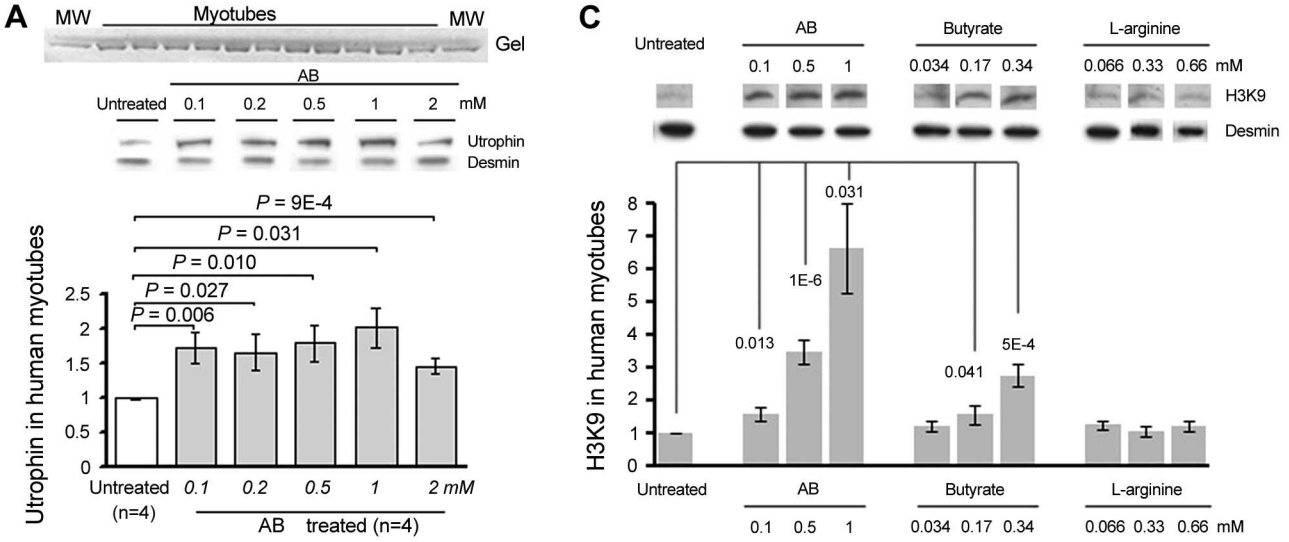

Figure 7. Primary cultures of myotubes prepared from DMD patient myoblasts under control conditions (untreated) and after 48-h treatment with AB, L-arginine, or butyrate. Utrophin analysis after treatment with AB. *A*) For immunoblot analyses, equal loading was verified by staining protein gels with Coomassie blue (MW, molecular weight marker). Graph shows the mean values for ≥3 different experiments. Results are expressed as treated/untreated ratios. Values are representative of 3 independent experiments. Utrophin level was increased (~2-fold) after treatment with AB (0.1–2 mM). *B*) For immunostaining, little staining was observed in untreated myotubes, but utrophin was clearly detected under the sarcolemma in treated myotubes (AB, 0.5 mM). Scale bar = 68 μm. *C*) Level of histone H3 acetylated at Lys 9 (H3K9) after treatment with AB, L-arginine, and butyrate. Results are expressed as treated/untreated ratios. Values are representative of 3 independent experiments. H3 acetylation levels were increased in myotubes treated with AB (0.5–1 mM; 2- to 6-fold) or with butyrate (0.034–0.34 mM; 1.5- to 3-fold), but not with L-arginine (0.066–0.66 mM). Note the dose-dependent effect of AB and butyrate on H3 acetylation level.

pared AB (1 mM) with the corresponding doses of L-arginine (0.66 mM) or butyrate (0.34 mM) alone. A dose-dependent increase in the acetylation of histones was observed following treatment with AB and butyrate (Fig. 7*C*), which is reminiscent of the effects on utrophin expression level (Fig. 7*A*). In contrast, L-arginine alone did not induce any chromatin change. When myotubes were treated with 0.1 mM AB the level of acetylation was increased, while this was not observed with the corresponding doses of L-arginine (0.066 mM) or butyrate (0.034 mM) alone. Similarly, with 0.5 mM AB the level of acetylation was strongly increased, not with the corresponding doses of L-arginine alone (0.33 mM) and only modestly with butyrate alone (0.17 mM). The same tendency was obtained with 1 mM AB compared with the corresponding doses of L-arginine (0.66 mM) and butyrate (0.34 mM). These results demonstrate a synergistic effect of arginine and butyrate on chromatin acetylation level when used in combination.

DISCUSSION

In the present study, arginine and butyrate were associated in a salt in two distinct but close formulations, AB and AB_{cf}, and tested for preclinical efficacy as a potential treatment option for patients with DMD. Previous studies have demonstrated the beneficial effects of arginine (11, 12, 14, 15, 18, 19) and of histone deacetylase inhibitors [trichostatin (25) and valproic acid (26)] used separately in *mdx* mice. Besides, recently published results support the clinical use of AB in pediatric patients (29, 36–39).

In our experimental setting, chronic continuous treatment of *mdx* mice with AB for 6 wk induced an up-regulation of utrophin expression in skeletal muscles, heart, brain, and skin. Utrophin overexpression was associated with dose-dependent beneficial effects on the dystrophic phenotype.

In *mdx* mice, as in patients with DMD, the mRNAs of dystrophin-associated protein (DAP) and dystrophin-associated glycoprotein (DAG) complexes are expressed at normal levels. However, in the absence of dystrophin, these proteins are no longer integrated into the sarcolemma and are subsequently degraded, leading to a reduction of DAGs and DAPs in muscle tissues (40). Our results indicate that utrophin and β-dystroglycan are properly localized to the sarcolemma after AB treatment, suggesting that the treatment may be sufficient to restore sarcolemmal integrity.

This is supported by the associated decreases in serum CK levels and the incorporation of Evans blue dye in myofibers. The bell-shaped dose response curve demonstrated by body weight index is mirrored by the inverted bell shape of CK release. Changes in CK level indicate a beneficial effect obtained from the dose of 50 mg/kg/d with AB (33 mg/kg/d arginine plus 17 mg/kg/d butyrate), from the dose of 200 mg/kg/d with L-arginine alone and from the dose of 55 mg/kg/d with butyrate alone, as expected in a multiple-targeting situation. These results demonstrate synergistic effects of a low-dose combination of arginine and butyrate, and they support the effectiveness of a combination treatment regimen for the management of patients with DMD, minimizing potential adverse events. In our MRI study, we observe a decrease in both necrosis and proliferation of connective tissue in AB-treated *mdx* mice. Necrosis and extensive proliferation of connective tissue in skeletal muscles are characteristics in human DMD, and treatment with AB may be expected to induce a similar improvement in patients. The MRI analysis provides anatomical evidence of an improved phenotype by a noninvasive procedure, which may also be useful in clinical settings where tissue biopsies cannot be readily obtained. All of these results have been confirmed by Masson's trichrome staining and measurement of the isometric force in excised muscles.

Respiratory function is compromised in *mdx* mice compared with WT mice. However, we show here that AB can improve tidal volume capacity, possibly through a direct effect on the diaphragm, as suggested by the associated decrease in the density of necrotic fibers and connective tissue invasion in this muscle. This suggests that AB could have a positive effect on the respiratory symptoms in patients with DMD.

To further evaluate whether AB may be used for the early treatment of DMD in pediatric patients, we also studied its effects in newborn *mdx* pups. After slight dose adjustments, the results in the males were similar to those found in adult animals. Therefore, it is anticipated that early treatment with AB in pediatric patients with DMD could be well tolerated and might protect muscles against deterioration. Moreover, AB treatment improved muscle function in *mdx* mice as assessed by measurement of isometric force, thus showing that AB does not solely reduce biochemical alterations and improve the structure of muscle tissues, but also leads to substantial improvement in the physiological functions of muscle.

Increases in utrophin expression in other tissues, such as heart and brain could also have positive consequences. It is known that although the lack of dystrophin results in mild cardiomyopathy in *mdx* mice (41), the chronic treatment with L-arginine was shown to ameliorate cardiac function and to reduce necrosis in the heart in *mdx* mice (15). In patients with DMD, the heart can be severely affected, resulting in degeneration of the myocardium, heart failure, and sudden death in 10–30% of patients (42, 43). We also noted an up-regulation of utrophin in the brain of treated *mdx* mice, suggesting that AB may compensate, at least partially, for the lack of brain dystrophin and potentially ameliorate some of the brain and cognitive abnormalities associated with DMD (44). However, we recently showed that this does not overcome behavioral alterations in *mdx* mice (45). This lack of effects in brain is potentially linked to the cellular expression profiles of utrophin and dystrophin, which do not seem to overlap any more in adult brain tissues, unlike their expression in muscle fibers. However, one may hypothesize that AB could have a greater impact when administered to younger mice, when developmental plasticity is still occurring in the immature brain. Moreover, the increased expression of utrophin in the brain is in favor of a direct effect of AB on the mechanisms regulating utrophin expression. This suggests that, in general, the effects of AB are not indirect, such as the differentiation of myoblasts during regeneration processes. Because overexpression of utrophin in a broad range of nonmuscle tissues in transgenic *mdx* mice is not detrimental (46), the use of AB is expected to be a safe therapeutic approach, even if utrophin regulation by this treatment is not tissue-specific.

To be closer to conditions of use of the product in clinical trials, we also evaluated an intermittent protocol that reduces the frequency of injections. This protocol has been developed and applied in clinical trials to treat patients with β-globin disorders. In *mdx* mice, we found that this administration regimen elicits dose-dependent beneficial effects similar to those with the continuous-chronic protocol of injections. This includes changes in utrophin and β-dystroglycan expression, reduction of serum CK levels, and partial increase in muscle strength and alleviation of fatigue. This intermittent protocol also has the advantage of allowing better tolerability at high doses. Indeed, while continuous-chronic injections of AB_{cf} at the dose of 300 mg/kg/d led to a decrease in body weight, suggesting suboptimal tolerability of the product, such detrimental effects were not observed with the intermittent protocol up to a dose of 1000 mg/kg/d. After treatment with high doses of AB, the loss of beneficial effects on body weight (Supplemental Fig. S1*A*) and on CK level (Fig. 2*B*) might explain the modest beneficial effects reported in an initial study performed in *mdx* mice with 250 mg/kg/d of AB (27). Indeed, the optimal dose selected in the current study for chronic-continuous injections was only 100 mg/kg/d. Another explanation could be that the treatment in our initial study (27) was prolonged for several months, which could have induced tolerance to the effects of AB, thus making prolonged treatment ineffective. Other factors could also be responsible for the differences between the two studies, including differences in the age of the animals at the start of treatment. In the present study, mice were aged 8 wk, which is a reliable time to induce treatment since *mdx* mice display important necrosis and regeneration cycles at this age, while in the former study mice were aged 12 wk at the start of treatment. Sex could also be a misleading factor; using only males

reduces variability and better reflects the human condition as DMD affects boys, and sexual dimorphism has been shown in the *mdx* line (47).

A single series of 4 injections of AB_{cf} was sufficient to overexpress utrophin (both protein and mRNA expression), β-dystroglycan, and embryonic myosin in adult *mdx* mice. Thus, in the course of clinical trials using AB_{cf} in humans, biopsies could be performed shortly after the beginning of the treatment, and utrophin expression could be used as a biochemical marker of treatment efficacy. Utrophin is also expressed in the smooth muscle of skin (arrector pili muscle; ref. 48), and we found that AB_{cf} treatment increases utrophin and β-dystroglycan expression in the skin of *mdx* mice, which opens the possibility of easily monitoring utrophin induction in patients along with diagnosis of myopathy using skin samples (49), which could limit the frequency of the more invasive muscle biopsies. The proportion of centronucleated fibers (75% in *mdx* mice) was not reduced in soleus and TA after treatment (data not shown). This result suggests cell replication and muscle regeneration continued at least up to the time at which the mice were sacrificed and is supported by the increase of embryonic myosin observed in treated mice. Increased expression of embryonic myosin may reflect a regeneration process, which is in line with the effects of L-arginine on the activation of satellite cells during muscle repair after injury (50). Unlike previous studies (27, 45), in which no quantitative changes in utrophin mRNA expression were detected, we found here that utrophin-A mRNA was up-regulated in skeletal muscle of treated *mdx* mice. The reasons for this discrepancy could be linked to the assessment of mRNA expression several weeks or months after the start of the product administration. Here, the level of utrophin mRNA was measured after a single series of 4 injections of AB_{cf} and with a 24-h delay after the last injection.

Finally, the beneficial effect on the animal's body weight suggests that AB and AB_{cf} are well tolerated by *mdx* mice, which is consistent with the anabolic effect of L-arginine on muscles (51). Moreover, we show that AB increases utrophin expression in human myotubes, with correct localization at the sarcolemma, suggesting that the beneficial effects of utrophin up-regulation on muscle structure and function could also be achieved in patients with DMD. A comparison of the chromatin acetylation state in human myotubes treated with L-arginine, butyrate, and AB confirmed that the combined formula of AB acts synergistically, as observed in the measurements of CK serum levels *in vivo*. Taken together, our data suggest that AB is a good candidate for systemic up-regulation of utrophin in DMD and deserves to be tested as a proof of concept in clinical trials.

FJ

The authors thank Francesca Consolaro for technical assistance for the experiments on the chromatin acetylation state. The authors thank the French Banque de Tissus pour la Recherche (BTR; Institut de Myologie) for providing surgical residues of human paravertebral striated muscles. BTR is a partner of the EuroBioBank network funded by the European Community under the Fifth Framework Program (QLRI-CT-2002-02769). The authors thank M. Bonora (Paris) for help with the respiration protocols and the Imagif qPCR platform. This work was supported by the Association Française contre les Myopathies (2004.001/10689, 2007.1563/12507, 2008.0797/13466); and the Muscular Dystrophy Association (MDA3561, MDA4078). The authors declare no conflicts of interest.

REFERENCES

1. Fairclough, R. J., Bareja, A., and Davies, K. E. (2011) Progress in therapy for Duchenne muscular dystrophy. *Exp. Physiol.* **96,** 1101–1113
2. Voisin, V., and de la Porte, S. (2004) Therapeutic strategies for Duchenne and Becker dystrophies. *Int. Rev. Cytol.* **240,** 1–30
3. Love, D. R., Hill, D. F., Dickson, G., Spurr, N. K., Byth, B. C., Marsden, R. F., Walsh, F. S., Edwards, Y. H., and Davies, K. E. (1989) An autosomal transcript in skeletal muscle with homology to dystrophin. *Nature* **339,** 55–58
4. Karpati, G., Carpenter, S., Morris, G. E., Davies, K. E., Guerin, C., and Holland, P. (1993) Localization and quantitation of the chromosome 6-encoded dystrophin-related protein in normal and pathological human muscle. *J. Neuropathol. Exp. Neurol.* **52,** 119–128
5. Rafael, J. A., Tinsley, J. M., Potter, A. C., Deconinck, A. E., and Davies, K. E. (1998) Skeletal muscle-specific expression of a utrophin transgene rescues utrophin-dystrophin deficient mice. *Nat. Genet.* **19,** 79–82
6. Tinsley, J. M., Potter, A. C., Phelps, S. R., Fisher, R., Trickett, J. I., and Davies, K. E. (1996) Amelioration of the dystrophic phenotype of mdx mice using a truncated utrophin transgene. *Nature* **384,** 349–353
7. Tinsley, J., Deconinck, N., Fisher, R., Kahn, D., Phelps, S., Gillis, J. M., and Davies, K. (1998) Expression of full-length utrophin prevents muscular dystrophy in *mdx* mice. *Nat. Med.* **4,** 1441–1444
8. Chaubourt, E., Fossier, P., Baux, G., Leprince, C., Israel, M., and De La Porte, S. (1999) Nitric oxide and L-arginine cause an accumulation of utrophin at the sarcolemma: a possible compensation for dystrophin loss in Duchenne muscular dystrophy. *Neurobiol. Dis.* **6,** 499–507
9. Chaubourt, E., Voisin, V., Fossier, P., Baux, G., Israel, M., and De La Porte, S. (2002) Muscular nitric oxide synthase (muNOS) and utrophin. *J. Physiol. Paris* **96,** 43–52
10. Anderson, J. E., and Vargas, C. (2003) Correlated NOS-Imu and myf5 expression by satellite cells in mdx mouse muscle regeneration during NOS manipulation and deflazacort treatment. *Neuromuscul. Disord.* **13,** 388–396
11. Archer, J. D., Vargas, C. C., and Anderson, J. E. (2006) Persistent and improved functional gain in mdx dystrophic mice after treatment with L-arginine and deflazacort. *FASEB J.* **20,** 738–740
12. Barton, E. R., Morris, L., Kawana, M., Bish, L. T., and Toursel, T. (2005) Systemic administration of L-arginine benefits *mdx* skeletal muscle function. *Muscle Nerve* **32,** 751–760
13. Brunelli, S., Sciorati, C., D'Antona, G., Innocenzi, A., Covarello, D., Galvez, B. G., Perrotta, C., Monopoli, A., Sanvito, F., Bottinelli, R., Ongini, E., Cossu, G., and Clementi, E. (2007) Nitric oxide release combined with nonsteroidal antiinflammatory activity prevents muscular dystrophy pathology and enhances stem cell therapy. *Proc. Natl. Acad. Sci. U. S. A.* **104,** 264–269
14. Chazalette, D., Hnia, K., Rivier, F., Hugon, G., and Mornet, D. (2005) α7B integrin changes in mdx mouse muscles after L-arginine administration. *FEBS Lett.* **579,** 1079–1084
15. Hoey, A. J., and Erp, C. V. (2006) Effect of L-arginine on cardiac function and fibrosis in *mdx* mice. *Proc. Aust. Physiol. Soc.* **37,** 57
16. Marques, M. J., Luz, M. A., Minatel, E., and Neto, H. S. (2005) Muscle regeneration in dystrophic mdx mice is enhanced by isosorbide dinitrate. *Neurosci. Lett.* **382,** 342–345
17. Segalat, L., Grisoni, K., Archer, J., Vargas, C., Bertrand, A., and Anderson, J. E. (2005) CAPON expression in skeletal muscle is regulated by position, repair, NOS activity, and dystrophy. *Exp. Cell. Res.* **302,** 170–179

18. Voisin, V., Sebrie, C., Matecki, S., Yu, H., Gillet, B., Ramonatxo, M., Israel, M., and De la Porte, S. (2005) L-arginine improves dystrophic phenotype in mdx mice. *Neurobiol. Dis.* **20,** 123–130
19. Hnia, K., Gayraud, J., Hugon, G., Ramonatxo, M., De La Porte, S., Matecki, S., and Mornet, D. (2008) L-arginine decreases inflammation and modulates the nuclear factor-κB/matrix metalloproteinase cascade in mdx muscle fibers. *Am. J. Pathol.* **172,** 1509–1519
20. Benabdellah, F., Yu, H., Brunelle, A., Laprevote, O., and De La Porte, S. (2009) MALDI reveals membrane lipid profile reversion in *MDX* mice. *Neurobiol. Dis.* **36,** 252–258
21. Thomas, G. D., Sander, M., Lau, K. S., Huang, P. L., Stull, J. T., and Victor, R. G. (1998) Impaired metabolic modulation of alpha-adrenergic vasoconstriction in dystrophin-deficient skeletal muscle. *Proc. Natl. Acad. Sci. U. S. A.* **95,** 15090–15095
22. Sander, M., Chavoshan, B., Harris, S. A., Iannaccone, S. T., Stull, J. T., Thomas, G. D., and Victor, R. G. (2000) Functional muscle ischemia in neuronal nitric oxide synthase-deficient skeletal muscle of children with Duchenne muscular dystrophy. *Proc. Natl. Acad. Sci. U. S. A.* **97,** 13818–12823
23. Perrine, S. P., Miller, B. A., Faller, D. V., Cohen, R. A., Vichinsky, E. P., Hurst, D., Lubin, B. H., and Papayannopoulou, T. (1989) Sodium butyrate enhances fetal globin gene expression in erythroid progenitors of patients with Hb SS and beta thalassemia. *Blood* **74,** 454–459
24. Perrine, S. P. (2008) Fetal globin stimulant therapies in the β-hemoglobinopathies: principles and current potential. *Pediatr. Ann.* **37,** 339–346
25. Minetti, G. C., Colussi, C., Adami, R., Serra, C., Mozzetta, C., Parente, V., Fortuni, S., Straino, S., Sampaolesi, M., Di Padova, M., Illi, B., Gallinari, P., Steinkuhler, C., Capogrossi, M. C., Sartorelli, V., Bottinelli, R., Gaetano, C., and Puri, P. L. (2006) Functional and morphological recovery of dystrophic muscles in mice treated with deacetylase inhibitors. *Nat Med* **12,** 1147–1150
26. Gurpur, P. B., Liu, J., Burkin, D. J., and Kaufman, S. J. (2009) Valproic acid activates the PI3K/Akt/mTOR pathway in muscle and ameliorates pathology in a mouse model of Duchenne muscular dystrophy. *Am. J. Pathol.* **174,** 999–1008
27. Guerron, A. D., Rawat, R., Sali, A., Spurney, C. F., Pistilli, E., Cha, H. J., Pandey, G. S., Gernapudi, R., Francia, D., Farajian, V., Escolar, D. M., Bossi, L., Becker, M., Zerr, P., de la Porte, S., Gordish-Dressman, H., Partridge, T., Hoffman, E. P., and Nagaraju, K. (2010) Functional and molecular effects of arginine butyrate and prednisone on muscle and heart in the *mdx* mouse model of Duchenne muscular dystrophy. *PLoS One* **5,** e11220
28. Jeng, M. R., Feusner, J., Skibola, C., and Vichinsky, E. (2002) Central venous catheter complications in sickle cell disease. *Am. J. Hematol.* **69,** 103–108
29. Perrine, S. P., and Faller, D. V. (1993) Butyrate-induced reactivation of the fetal globin genes: a molecular treatment for the beta-hemoglobinopathies. *Experientia* **49,** 133–137
30. Baby, S. M., Bogdanovich, S., Willmann, G., Basu, U., Lozynska, O., and Khurana, T. S. (2010) Differential expression of utrophin-A and -B promoters in the central nervous system (CNS) of normal and dystrophic mdx mice. *Brain Pathol.* **20,** 323–342
31. Straub, V., Rafael, J. A., Chamberlain, J. S., and Campbell, K. P. (1997) Animal models for muscular dystrophy show different patterns of sarcolemmal disruption. *J. Cell Biol.* **139,** 375–385
32. Edom, F., Mouly, V., Barbet, J. P., Fiszman, M. Y., and Butler-Browne, G. S. (1994) Clones of human satellite cells can express in vitro both fast and slow myosin heavy chains. *Dev. Biol.* **164,** 219–229
33. Ozawa, E., Yoshida, M., Suzuki, A., Mizuno, Y., Hagiwara, Y., and Noguchi, S. (1995) Dystrophin-associated proteins in muscular dystrophy. *Hum. Mol. Genet.* **4,** 1711–1716
34. Nico, B., Paola Nicchia, G., Frigeri, A., Corsi, P., Mangieri, D., Ribatti, D., Svelto, M., and Roncali, L. (2004) Altered blood-brain barrier development in dystrophic MDX mice. *Neuroscience* **125,** 921–935
35. Colussi, C., Gurtner, A., Rosati, J., Illi, B., Ragone, G., Piaggio, G., Moggio, M., Lamperti, C., D'Angelo, G., Clementi, E., Minetti, G., Mozzetta, C., Antonini, A., Capogrossi, M. C., Puri, P. L., and Gaetano, C. (2009) Nitric oxide deficiency determines global chromatin changes in Duchenne muscular dystrophy. *FASEB J.* **23,** 2131–2141
36. Faller, D. V., and Perrine, S. P. (1995) Butyrate in the treatment of sickle cell disease and β-thalassemia. *Curr. Opin. Hematol.* **2,** 109–117
37. Perrine, S. P., Ginder, G. D., Faller, D. V., Dover, G. H., Ikuta, T., Witkowska, H. E., Cai, S. P., Vichinsky, E. P., and Olivieri, N. F. (1993) A short-term trial of butyrate to stimulate fetal-globin-gene expression in the beta-globin disorders. *N. Engl. J. Med.* **328,** 81–86
38. Perrine, S. P., Olivieri, N. F., Faller, D. V., Vichinsky, E. P., Dover, G. J., and Ginder, G. D. (1994) Butyrate derivatives. New agents for stimulating fetal globin production in the β-globin disorders. *Am. J. Pediatr. Hematol. Oncol.* **16,** 67–71
39. Sher, G. D., Ginder, G. D., Little, J., Yang, S., Dover, G. J., and Olivieri, N. F. (1995) Extended therapy with intravenous arginine butyrate in patients with β-hemoglobinopathies. *N. Engl. J. Med.* **332,** 1606–1610
40. Matsumura, K., and Campbell, K. P. (1994) Dystrophin-glycoprotein complex: its role in the molecular pathogenesis of muscular dystrophies. *Muscle Nerve* **17,** 2–15
41. Bia, B. L., Cassidy, P. J., Young, M. E., Rafael, J. A., Leighton, B., Davies, K. E., Radda, G. K., and Clarke, K. (1999) Decreased myocardial nNOS, increased iNOS and abnormal ECGs in mouse models of Duchenne muscular dystrophy. *J. Mol. Cell. Cardiol.* **31,** 1857–1862
42. Finsterer, J., and Stollberger, C. (2003) The heart in human dystrophinopathies. *Cardiology* **99,** 1–19
43. Ishikawa, K. (1997) Cardiac involvement in progressive muscular dystrophy of the Duchenne type. *Jpn. Heart J.* **38,** 163–180
44. Anderson, J. L., Head, S. I., Rae, C., and Morley, J. W. (2002) Brain function in Duchenne muscular dystrophy. *Brain* **125,** 4–13
45. Perronnet, C., Chagneau, C., Le Blanc, P., Samson-Desvignes, N., Mornet, D., Laroche, S., De La Porte, S., and Vaillend, C. (2012) Upregulation of brain utrophin does not rescue behavioral alterations in dystrophin-deficient mice. *Hum. Mol. Genet.* **21,** 2263–2276
46. Fisher, R., Tinsley, J. M., Phelps, S. R., Squire, S. E., Townsend, E. R., Martin, J. E., and Davies, K. E. (2001) Non-toxic ubiquitous over-expression of utrophin in the *mdx* mouse. *Neuromuscul. Disord.* **11,** 713–721
47. Salimena, M. C., Lagrota-Candido, J., and Quirico-Santos, T. (2004) Gender dimorphism influences extracellular matrix expression and regeneration of muscular tissue in *mdx* dystrophic mice. *Histochem. Cell Biol.* **122,** 435–444
48. Marbini, A., Gemignani, F., Bellanova, M. F., Guidetti, D., and Ferrari, A. (1996) Immunohistochemical localization of utrophin and other cytoskeletal proteins in skin smooth muscle in neuromuscular diseases. *J. Neurol. Sci.* **143,** 156–160
49. Tanveer, N., Sharma, M. C., Sarkar, C., Gulati, S., Kalra, V., Singh, S., and Bhatia, R. (2009) Diagnostic utility of skin biopsy in dystrophinopathies. *Clin. Neurol. Neurosurg.* **111,** 496–502
50. Anderson, J. E. (2000) A role for nitric oxide in muscle repair: nitric oxide-mediated activation of muscle satellite cells. *Mol. Biol. Cell* **11,** 1859–1874
51. Guilhermet, R. G. (1996) Fonctions nutritionnelles et métaboliques de l'arginine. *INRA Prod. Anim.* **9,** 265–272

Received for publication August 20, 2012.
Accepted for publication February 11, 2013.

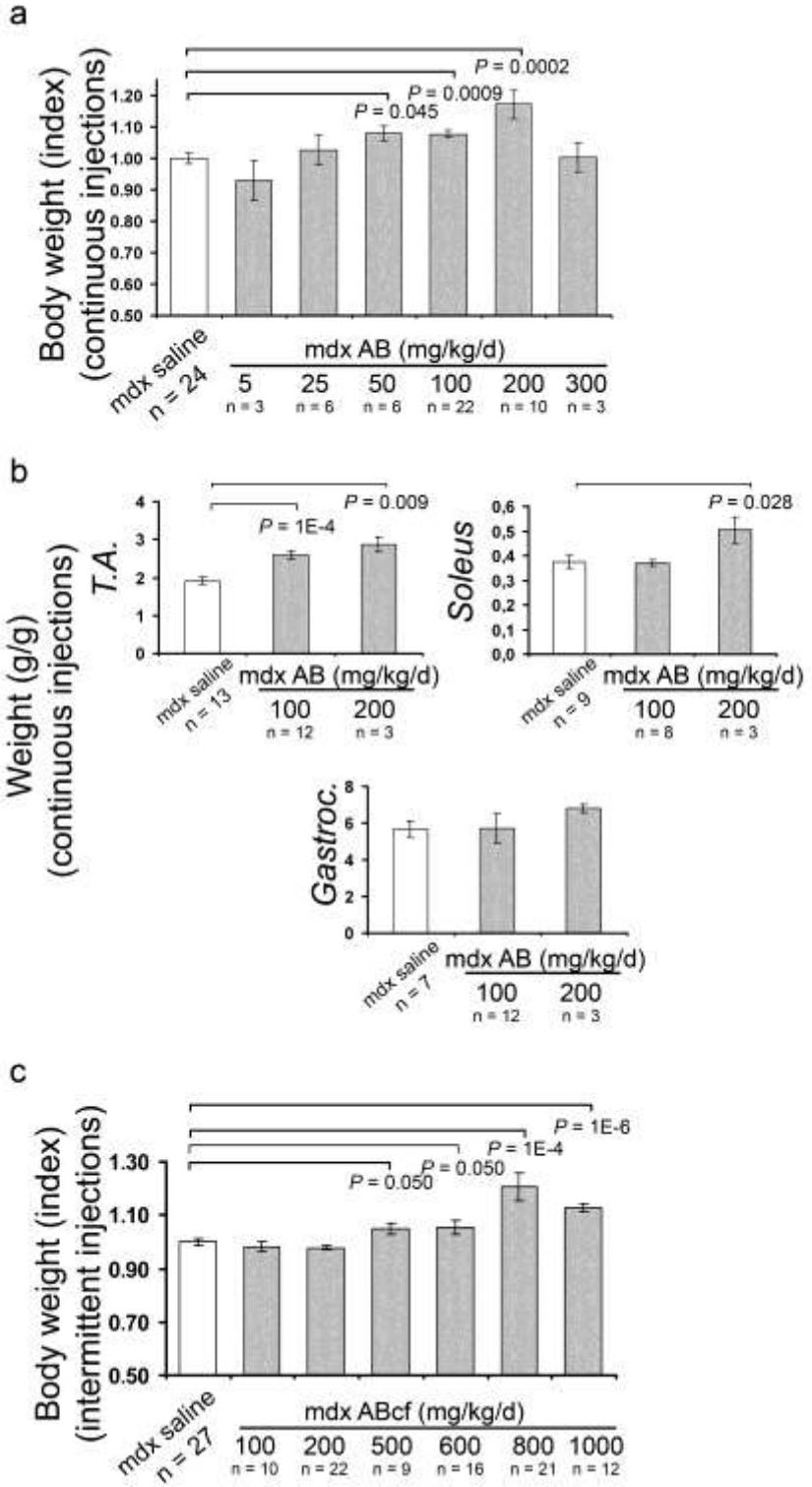

Figure S1: Effects of AB on muscle and body weight (*normalized weight = weight at the end of the treatment / weight at the start of the injections*) in *mdx* mice treated for 6 weeks. (**a**) Continuous-chronic treatment protocol in adult *mdx* mice. The body weight of AB-treated adult *mdx* mice increased by 8-17% after treatment (50, 100, or 200 mg/kg/day) as compared with saline-injected *mdx* mice. (**b**) AB increased the weight of *tibialis anterior (T.A.)* (1.4-fold at dose 100 mg/kg/day and 1.5-fold at dose 200 mg/kg/d) and the weight of *soleus* (1.35-fold at dose 200 mg/kg/day) muscles, but not that of *gastrocnemius*. (**c**) Intermittent treatment protocol in adult *mdx* mice. The body weight of AB-treated adult *mdx* mice increased by 5-21% following treatment with doses of 500 to 1000 mg/kg/day compared with saline.

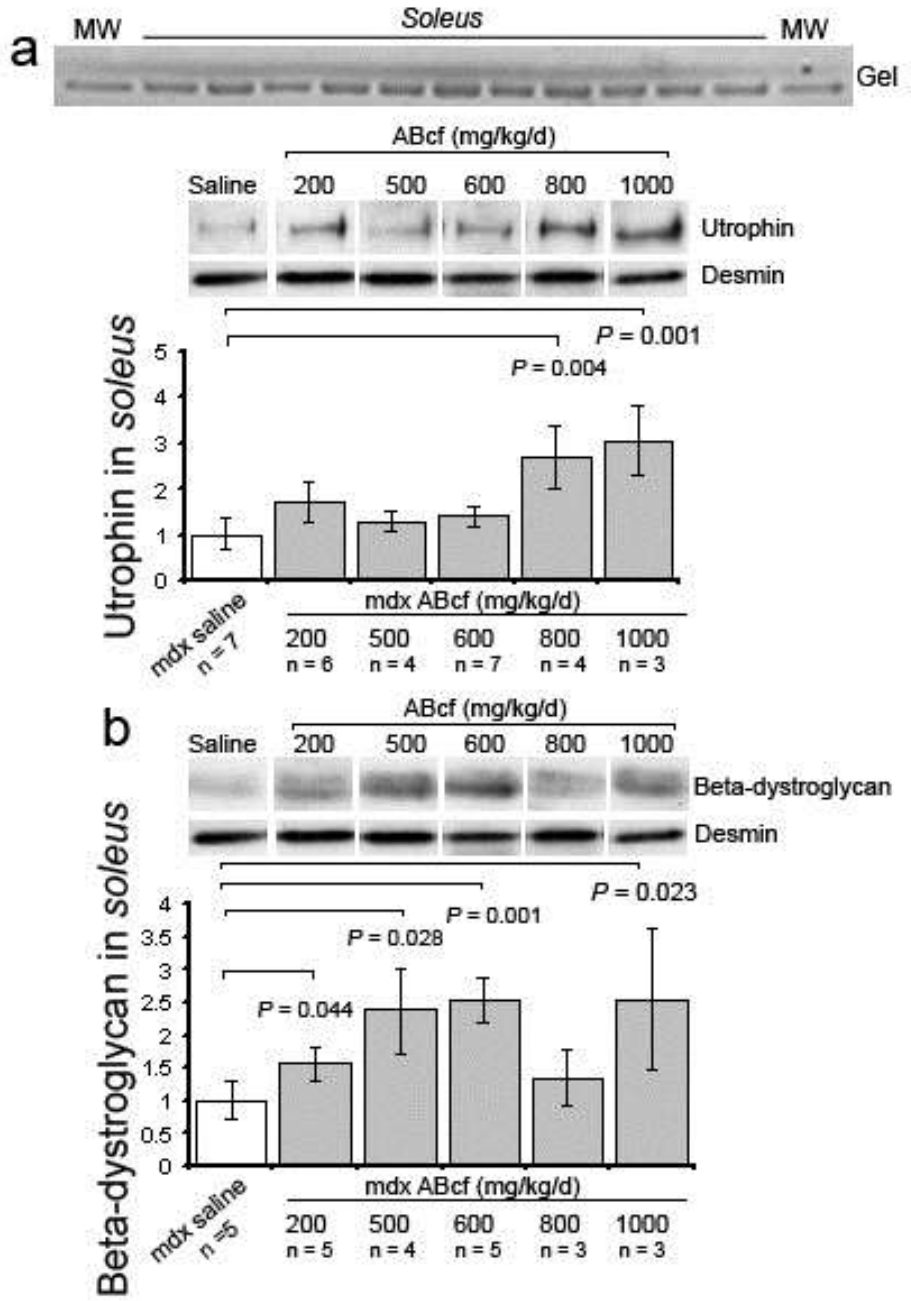

Figure S2: Effects of the clinical AB formulation (AB_{cf}) (100 to 1000 mg/kg/day) in adult *mdx* mice subjected to the 6-week intermittent AB_{cf} treatment protocol (4 injections every 2 weeks): utrophin and beta-dystroglycan expression assessed by western blot in *soleus*. (**a**) Equal loading was verified by staining protein gels with Coomassie blue (MW: molecular weight marker). Utrophin expression was increased at doses 800 (2.7-fold), and 1000 (3-fold) mg/kg/day compared with the saline group. (**b**) Beta-dystroglycan was increased at doses 200 (1.6-fold), 500 (2.4-fold), 600 (2.5-fold), and 1000 (2.6-fold) mg/kg/day compared with saline-injected mice.

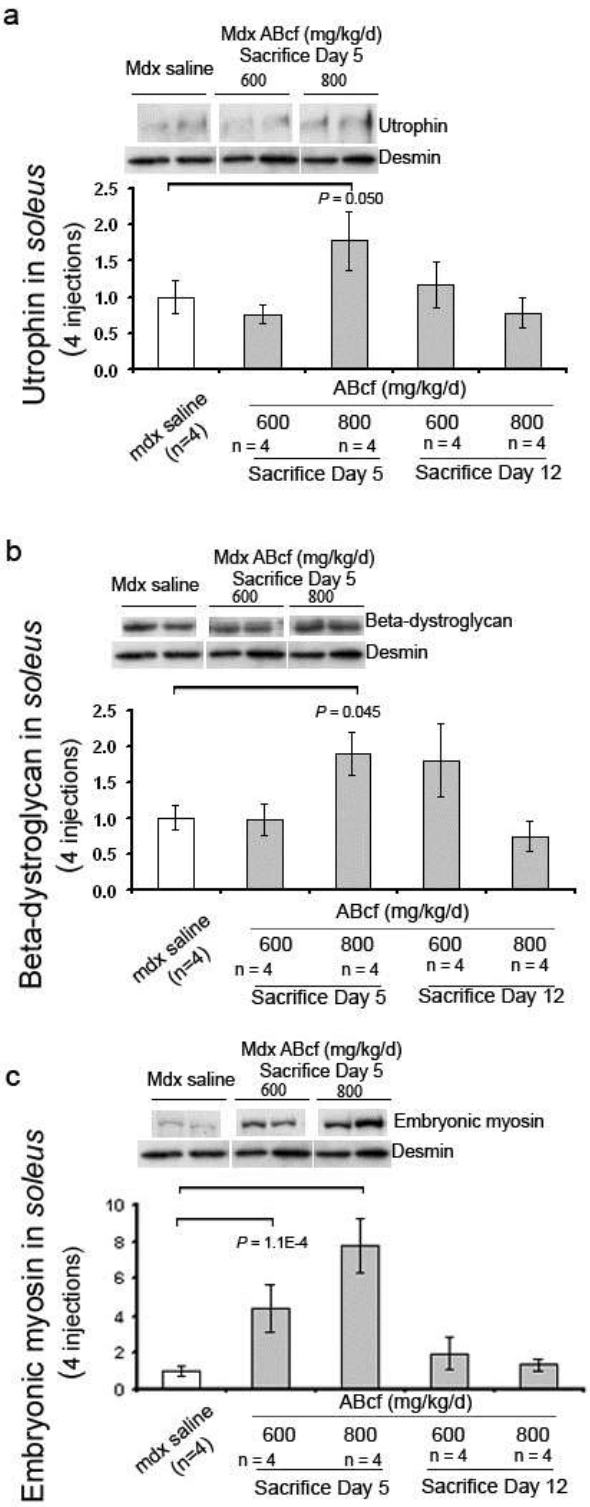

Figure S3: Utrophin, beta-dystroglycan and embryonic myosin expression levels in *soleus* of adult *mdx* mice after a single 4-day series of injections with the clinical AB_{cf} formulation. (**a**) Utrophin level was increased at dose 800 mg/kg/day (1.7-fold) in mice sacrificed at day 5 (one day after the 4^{th} injection), compared with saline. (**b**) Beta-dystroglycan expression was increased at dose 800 mg/kg/day (1.6-fold) in mice sacrificed at day 5 compared with saline-injected mice. (**c**) Embryonic myosin expression was increased at doses 600 (4.4-fold) and 800 mg/kg/day (8-fold) in mice sacrificed at day 5, as compared with saline-injected mice.

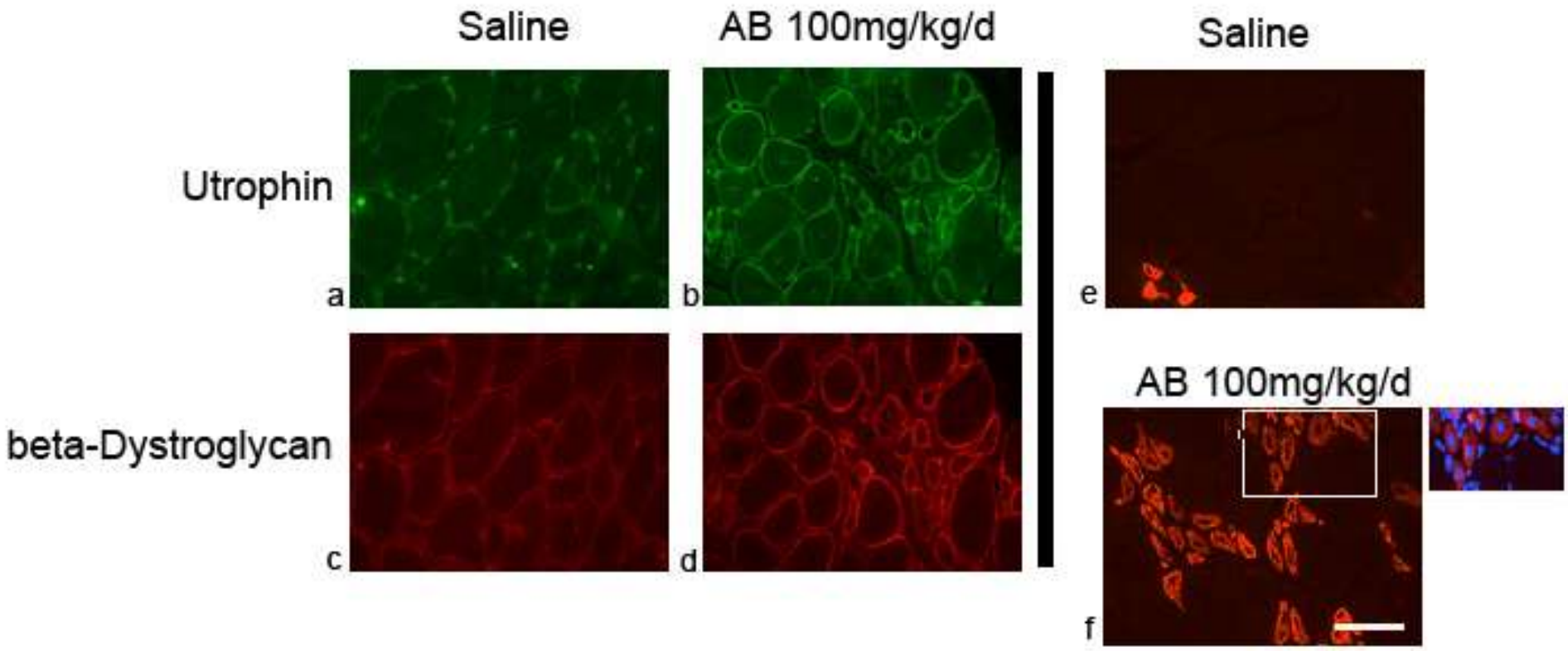

Figure S4: Immunofluorescent staining of utrophin, beta-dystroglycan and embryonic myosin in *soleus* of adult *mdx* mice after a single 4-day series of injections with the clinical AB_{cf} formulation (800 mg/kg/d). Utrophin (**a,b**), beta-dystroglycan staining (**c,d**) at the sarcolemma and new fibers expressing embryonic myosin (**e,f**) were increased in treated mice (**b,d, and f**) compared with saline-injected mice (**a,c and e**) (Dapi: inserted picture). Scale bar, 100 µm.

3.2 Manuscript 2. “*Per os* administration of arginine butyrate preserve *mdx* mice from cardiomyopathy, kyphosis and axonal excitability defaults.”

Per os administration of arginine butyrate preserve *mdx* mice from cardiomyopathy, kyphosis and axonal excitability defaults.

Sara Vianello[1], Sophie Bouyon[2], Evelyne Benoit[1], Catherine Sebrié[3], Delphine Boerio[1], Marc Herbin[4], Morgane Roulot[1], Yves Fromes[2,5] and Sabine de la Porte[1].

[1] CNRS, Institut de Neurobiologie Alfred Fessard – FRC2118, Neurobiologie & Développement, UPR 3294, Gif sur Yvette, F-91198, France, [2] UPMC, Université Paris 6, UMR 974, Institut de Myologie, F-75013 Paris, France, [3] CNRS, IR4M – UMR8081, Orsay, F-91405, France, [4] CNRS, Muséum National d'Histoire Naturelle, CNRS - UMR7179, Pavillon d'anatomie comparée, BP 55, 52 Rue Cuvier 75231 Paris Cedex 05, France, [5] ONIRIS, Centre de Boisbonne, Nantes, F-44307, France

Correspondence should be addressed to Sabine de la Porte: CNRS, Avenue de la Terrasse, Bat.32/33, Institut de Neurobiologie Alfred Fessard, Neurobiologie & Développement, UPR 3294, Gif sur Yvette, F-91198, France. Phone: 33 1 69 82 36 27, fax: 33 1 69 82 34 47, E-mail: sabine.delaporte@inaf.cnrs-gif.fr

ABSTRACT

Duchenne muscular dystrophy (DMD) is a progressive neuromuscular disease due to the lack of dystrophin, a sub-sarcolemmal protein, which leads to dramatic muscle deterioration. Although various curative therapeutic approaches, such as cell, gene and pharmacological therapies, are currently investigated, they still show some limitations. We addressed in *mdx* mice, the potential profits of the oral administration of arginine butyrate (AB), a compound currently used for the treatment of sickle cell anemia in children, on the main noticeable deficits in DMD patients: cardiomyopathy, vertebral column deformation and electromyogram defaults. A monthly follow-up study by echocardiography from the 8th to the 14th month evidenced that a treatment with AB preserves the *mdx* mice from the drastic reduction of ejection fraction and fractional shortening, but also from the ventricular dilatation and hypertrophy observed in saline-treated *mdx* mice. Moreover, AB treatment protected from the progressive spinal deformity observed in *mdx* mice, another similarity with DMD patients. Finally axonal excitability parameters that were modified in saline-treated *mdx* mice, did not show any significant difference, compared with wild type animals, in AB-treated *mdx* mice. All of these results make us confident of a possible clinical study of AB in order to treat DMD patients.

ABBREVIATIONS

AB: arginine butyrate; CK: creatine kinase; CMAP: compound muscle action potential; DMD: Duchenne muscular dystrophy; EF: ejection fraction; FS: fractional shortening; HDAC: histone deacetylases; IVS,s: interventricular septum, systole; KI: kyphotic index; LV: left ventricle; LVPW,s: left ventricular posterior wall, systole; LVID: left ventricular inner diameter; LVOD: left ventricular outer diameter; MRI: magnetic resonance imaging ; NO: nitric oxide; NOS: nitric oxide synthase; TEd: depolarizing threshold electrotonus; TEh: hyperpolarizing threshold electrotonus

INTRODUCTION

DMD is a progressive neuromuscular disease affecting 1/3500 male at birth, caused by the lack of dystrophin, a sub-sarcolemmal protein. Dystrophin, is the central component of a complex that links cytoskeletal actin to extracellular matrix, thus maintaining muscle fiber membrane integrity. The lack of this protein induces a weakness of skeletal, smooth and cardiac cells, due to mechanical muscle contraction and leading to dramatic muscle deterioration. In addition to this principal cause, Ca^{2+} leakage, oxidative stress, inflammatory response and fat infiltration are observed in human dystrophic muscle *(1)*.

Although various curative therapeutic approaches, such as cell, gene and pharmacological therapies, are currently investigated, they still show some limitations (2–5). Despite significant progress, the problem of targeting all muscles (40% of the total body mass), including diaphragm and heart at sufficiently high efficiency, remains a

challenge. Currently the only treatment approved to try to stem the relentless progression of muscle wasting in DMD is with corticosteroids, which have very limit benefits and are plagued by a number of side effects. Whatever the pharmacological strategy foreseen for reversing the dystrophic phenotype in DMD patients, it cannot be effective without restoration of dystrophin expression or overexpression of utrophin, the autosomal paralogue of dystrophin.

Recently we successfully tested arginine butyrate (AB) (6), which combines two pharmacological activities described as a possible way to alleviate dystrophic phenotype in DMD models (*mdx* mice and human DMD myotubes) (7–21): NO-pathway activation by arginine.and histone deacetylase (HDAC) inhibition by butyrate. AB is currently used for the treatment of sickle cell anemia in children by intermittent intravenous administration *(22)*. *In vivo* and *in vitro* experiments demonstrate that the drug combination acts synergistically. In particular, intermittent administration of AB (800 mg/kg/d) to dystrophin-deficient *mdx* mice resulted in a near 2-fold increase in utrophin accompanied by an improvement of the dystrophic phenotype in skeletal muscles of both adult and newborn mice. Together these data constitute a proof-of-principle of the beneficial effects of AB on muscular dystrophy.

In the present work we focused our attention on three main deficit described in DMD patients: cardiomyopathy, kyphosis and electromyogram defaults.

In DMD patients, preclinical abnormalities are detectable by electrocardiogram in 59% of patients between 6 and 10 years of age and progressively develop into clinically apparent cardiomyopathy in 100% of patients over 18 years of age. Cardiomyopathy begins by affecting particularly the posterobasal segment of the left ventricle (LV) *(23)* that leads to a rise in wall stress and to an after load excess *(24)*. Progressively, systolic LV function decreases and myocardial oxygen consumption increases, leading finally to LV dilation dysfunction. Moreover, post-mortem examination of cardiac tissue shows that extreme fibrosis is the most histological feature of the pathology *(25)*. Hearts of *mdx* mice share many features of the DMD cardiomyopathy, although the pathology is less severe. In particular any signs of cardiomyopathy could be observed in young animals (6 weeks old) compared with age-matched wild-type mice and only slight difference are present in *mdx* mice at the age of 29 weeks. At the age of 42/43 weeks a patent cardiomyopathy could be detected and electrocardiogram abnormalities, autonomic dysfunctions, impaired conduction, arrhythmias and dilated cardiomyopathy coul be observed. *Mdx* hearts also experience accumulation of connective tissue, suggesting that fibrosis may also be responsible for some features of the cardiomyopathy. (26–28).

In addition to cardiomyopathy, DMD patients performe progressive progression of spinal cord deformity *(29)*. As well as exacerbating respiratory dysfunction in affected boys, kyphosis negatively impacts their quality of life in their wheel-chair dependent years, leading to surgery or chronic pain. A recent longitudinal study on *mdx* mice has shown that starting at 9 month a significant difference on vertebral colum became apparent compared with C57BL/10. The kyphotic index (KI) of dystrophic animals decreases progressively up to the age of 11 months and then stabilizes, while the C57BL/10 one remains stable during all time window study *(30)*.

Finally, electromyography and nerve conduction studies have been performed in DMD patients. Although nerve conduction is normal in early DMD, the compound muscle action potential (CMAP), which idealizes the summation of a group of action potentials from several muscle fibers in the same area, decreases in amplitude as the disease progresses *(31)*. *Mdx* mice display a broadly normal axonal transport *(32)* as are innervation and myelinisation but, in degenerating zones, nerve terminals fragment into subunits *(11)*. Although there is no direct injury of motoneurons, the frequency of the miniature endplate potentials, their quantal content, and their amplitude are or not modified, depending to the authors (33–35). There is a decrease in the number of subneuronal folds, simplification of the

postsynaptic membrane *(36, 37)*, widening of the synaptic zone *(35)* and redistribution of the postsynaptic molecules. In summary, the absence of dystrophin in the postsynaptic membrane has little effect on the function of the neuromuscular junction, but the degeneration and regeneration of the fibers lead to remodeling of the pre- and postsynaptic components.

To address in *mdx* mice the benefit of AB treatment on these three main defaults associated to dystrophynopathies, we used an intermittent protocol (one week on/one week off) and force-feeding as mode of administration. The dose of AB used (800 mg/kg/d) was validated by intraperitoneal injection in our previous work *(6)*. With a range of functional and structural approaches, we demonstrated that AB plays a protective role on the progressive cardiomyopathy and on vertebral column deformation. We observed a significant attenuation of the kyphosis that settles down, by measuring by magnetic resonance imaging (MRI) and radioscopy the index of deformity in treated animals. Moreover, in order to assess whether excitability properties of the neuromuscular system are disorganized when dystrophin is lacking, a multimodal evaluation of excitability was performed in *mdx* mice using a minimally invasive method that has been developed to supplement conventional electrophysiological methods and to investigate ion conductance and membrane properties in human *(38)* and then adapted to mouse models *(39)*. The protocol includes different tests designated to measure, more than 30 parameters of nerve excitability. Clearly, the abnormalities detected in untreated *mdx* mice were corrected by the treatment with AB. Finally, because we used for the first time force-feeding procedure (instead of intraperitoneal injection) to treat mice with AB, we compared some functional parameters to verify that both modes of administration were equivalent in efficiency.

The goal of a treatment plan is to improve the patient's quality of life and the survey thanks to a well-tolerated protocol. Here we demonstrated that cardiomyopathy, postural stability, and electromyographic defaults could be ameliorated by AB treatment in DMD patients.

Results

Long- and short-term protocols were used, depending of the addressed deficit, for instance: cardiomyopathy is detected from the age of 8/9 months, while neuromuscular excitability defaults concern young adult animals.

Long-term protocol

Two groups of 6-week-old *mdx* mice (n = 10 per group) were administered by means of a force-feeding procedure with saline (0.9% NaCl) or AB (800 mg/kg/day) solutions for 4 consecutive days every 2 weeks until 14 months of age. No change in body weight was detected in AB-treated mice, compared with saline-treated animals.

AB treatment alleviates heart function and structure in *mdx* mice:

- *AB maintains cardiac function in mdx mice*

Serial measurements of cardiac morphology and function were made monthly in the same animals of each group, from age 8 to 14 months. A continuous decrease of ejection fraction (EF) was monitored by echocardiography in saline-treated *mdx* mouse hearts from the first time point at 8 months to the last one at 14 months, in comparison with C57BL/10 mice who had stable EF during this period. EF values decreased by about 20% in saline-treated *mdx* mice over the 6 months study window (**Fig. 1A**), whereas in AB-treated *mdx* mice, cardiac function was maintained stable. The same profiles were observed for the fractional shortening (FS).

- *AB preserves heart from ventricular dilatation in mdx mice*

In order to investigate LV dilatation, left ventricular inner and outer diameters (LVID, LVOD) were measured. An increase of about 20% of LVID was observed in saline-treated *mdx* mice over the 6 months study window, whereas the LVID values remained stable in C57BL/10 and in AB-treated *mdx* mice, suggesting that a treatment with BA, when initialized early, preserves from ventricular dilatation (**Fig. 1B**). The same profiles were observed for the LVOD.

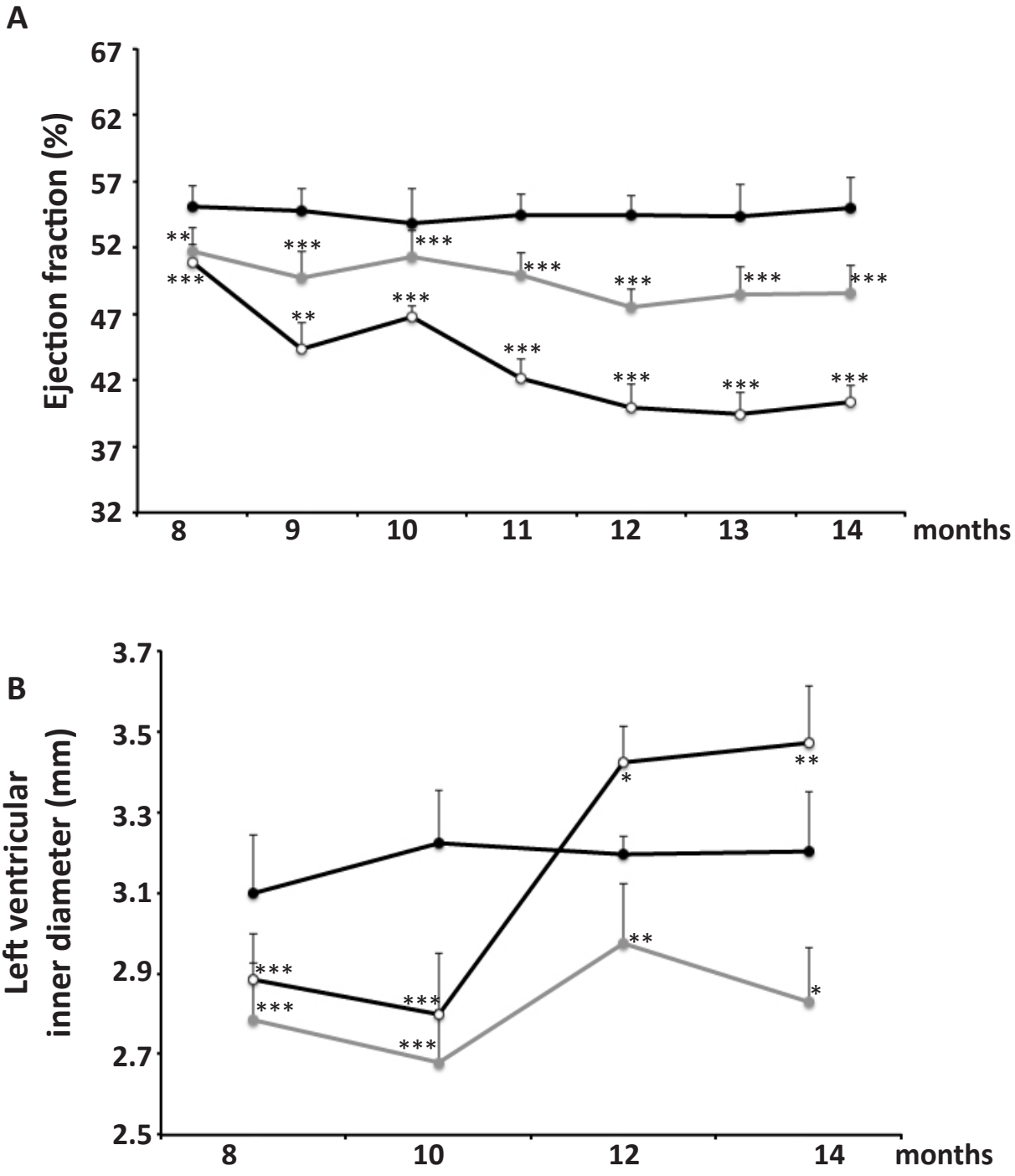

Figure 1: Ejection fraction (EF) and ventricular inner diameter (LVID) of mdx mice treated with AB by force-feeding for 12 months. (A) EF in C57BL/10 (black circles), AB-treated *mdx* (grey circles) and saline-treated *mdx* (white circles) mice monitored from 8 to 14 months old by echocardiography. (B) M-mode measurements of LVID in C57BL/10 mice, and saline- and AB-treated *mdx* mice at 8, 10, 12 and 14 months old. Note that the LVID values in AB-treated *mdx* mice are maintained all along the 7 months of recording, compared with the 20% increase in saline-treated *mdx* mice. Statistical test with the level of significance set at 0.05.

- *No fibrotic change occurs in heart after one year of AB treatment in mdx mice*

Masson's trichrome staining was used to investigate the structure of the heart tissue. Any necrosis was observed in C57BL/10 mice. Rare focal necrosis was present in saline- and AB-treated *mdx* mice, and the two groups of mice were indistinguishable by histology (**Fig. 2A**). Necrotic surface of the samples was measured and quantified by ImageJ software. The treatment of *mdx* mice with AB, one year after the initiation of therapy, did not modify the rare focal necrosis (3% of the surface, **Fig. 2B**).

-AB preserves heart from ventricular hypertrophy in mdx mice

In order to further investigate if AB-treated mice developed cardiac hypertrophy, hearts have been weighted immediately after the sacrifice. Saline-treated mice display an about 25% increase in heart weight compared with C57BL/10 animals. Heart weight was equivalent between C57BL/10 and AB-treated *mdx* mice (**Fig. 2C**), suggesting that AB treatment preserved heart from hypertrophy. In agreement with this result no alterations of interventricular septum (IVS,s) or left ventricular posterior wall (LVPW,s) thickness, at systole, were detected in saline-treated *mdx.*

Moreover, no change of body weight was observed in AB-treated, compared with saline-treated, *mdx* mice. This later observation and the rescue of a heart weight equivalent to C57BL/10 mice support the safety of the product.

AB treatment alleviates global functional and biochemical parameters in *mdx* mice

An about 70% decrease of serum CK level in AB-treated *mdx* mice was measured compared with saline-treated *mdx* mice value (**Supplementary Material, Fig. S1A**). The effect of AB on muscle strength was evaluated using a grip-strength meter. No difference of muscular strength was observed in *mdx* mice (AB- and saline-treated animals) compared with C57BL/10 animals at 14 months old (**Supplementary Material, Fig. S1B**), suggesting also a good safety of the product. Concerning the inverted grid test, 14-month-old *mdx* mice displayed half of the value of C57BL/10 mice with high variability among animals. The ability of AB-treated *mdx* mice to maintain a grip on an inverted grid was improved (**Supplementary Material, Fig. S1C**) to reach values of C57BL/10 mice, demonstrating a specific resistance of AB-treated *mdx* mice to the fatigue.

AB treatment alleviates spinal deformity in *mdx* mice

The same group of mice used to evaluate the benefit on heart was used to address the spinal deformity by magnetic resonance imaging (MRI). Vertebral column distortion was measured after 3D reconstruction, on AMIRA software (TGS Inc., San Diego, CA). Semiautomatic segmentation was performed on spinal cord, and inter-vertebral spaces were identified and delineated using magnetic resonance TurboRARE/FLASH imaging sequences (**Fig. 3A**). The KI was calculated in C57BL/10 mice and in saline- and AB-treated *mdx* mice (**Fig. 3B**). The KI in 14-month-old saline-treated *mdx* animals was reduced by 24% compared with C57BL/10 mice. In AB-treated mice, the value of KI increased by about 17% compared with saline-treated animals, rescuing 94% of C57BL/10 mice value (**Fig. 3C**). This suggests that the treatment considerably limits the spinal deformity. In order to verify that the adopted a lordosis-like posture in response to anesthesia didn't interfere with the measure of KI, we performed complementary experiments by radiographic pictures with mice free of movements in a physiological moderately extended posture. The results obtained were comparable with those from radiographic procedure technique (**Supplementary Material, Fig. S2**).

Short-term protocol

Three groups of 6-week-old *mdx* mice (n = 7 *per* group) were administered by intraperitoneal injection with AB (800 mg/kg/day) or by means of force-feeding procedure with saline (0.9% NaCl) or AB (800 mg/kg/day) solution for 4 consecutive days, every 2 weeks for 7 weeks. Mice were 13 weeks old at the end of treatment. As in the case of long-term protocol, no change in body

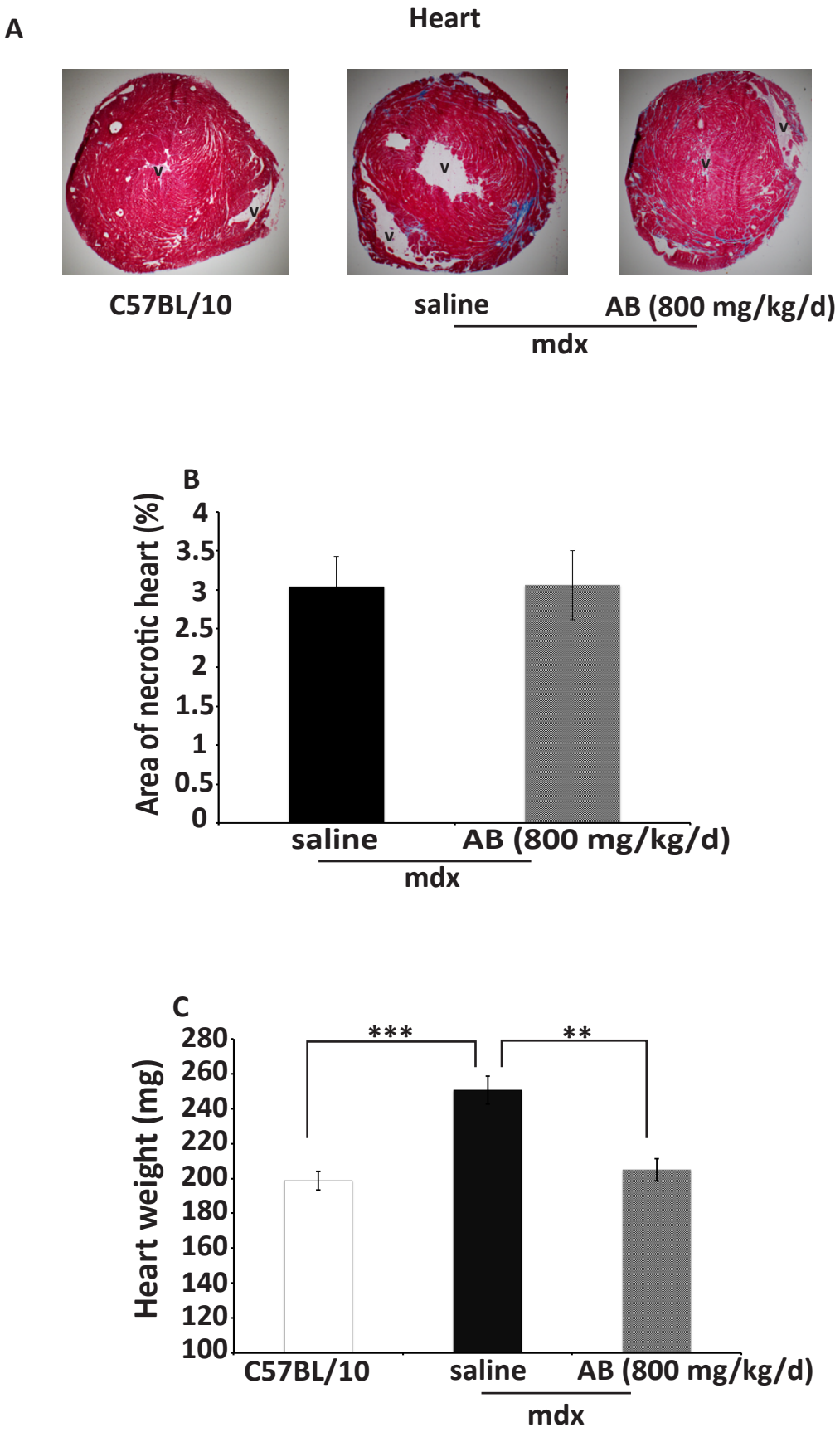

Figure 2: Muscle structure and weight in mdx mice treated with AB by force-feeding for 12 months. (A) Masson's trichrome staining of heart slices in 14-month-old C57BL/10, saline- and AB-treated mdx mice. Focal fibrotic zones are stained in blue in mdx mice. V: ventricle. Magnification, 2X. (B) Percentage of fibrotic tissue quantified by ImageJ software. The rare focal necrosis (3% of the surface) is similar in saline- and AB-treated mdx mice, supporting the safety of AB in long-term treatment. (C) Heart weight (mg) of C57BL/10, saline-and AB-treated mdx mice after sacrifice. The strong increase in weight measured in saline-treated mdx mice does not occur in AB-treated mdx animals, suggesting that AB preserves the heart against hypertrophy. Statistical test with the level of significance set at 0.05.

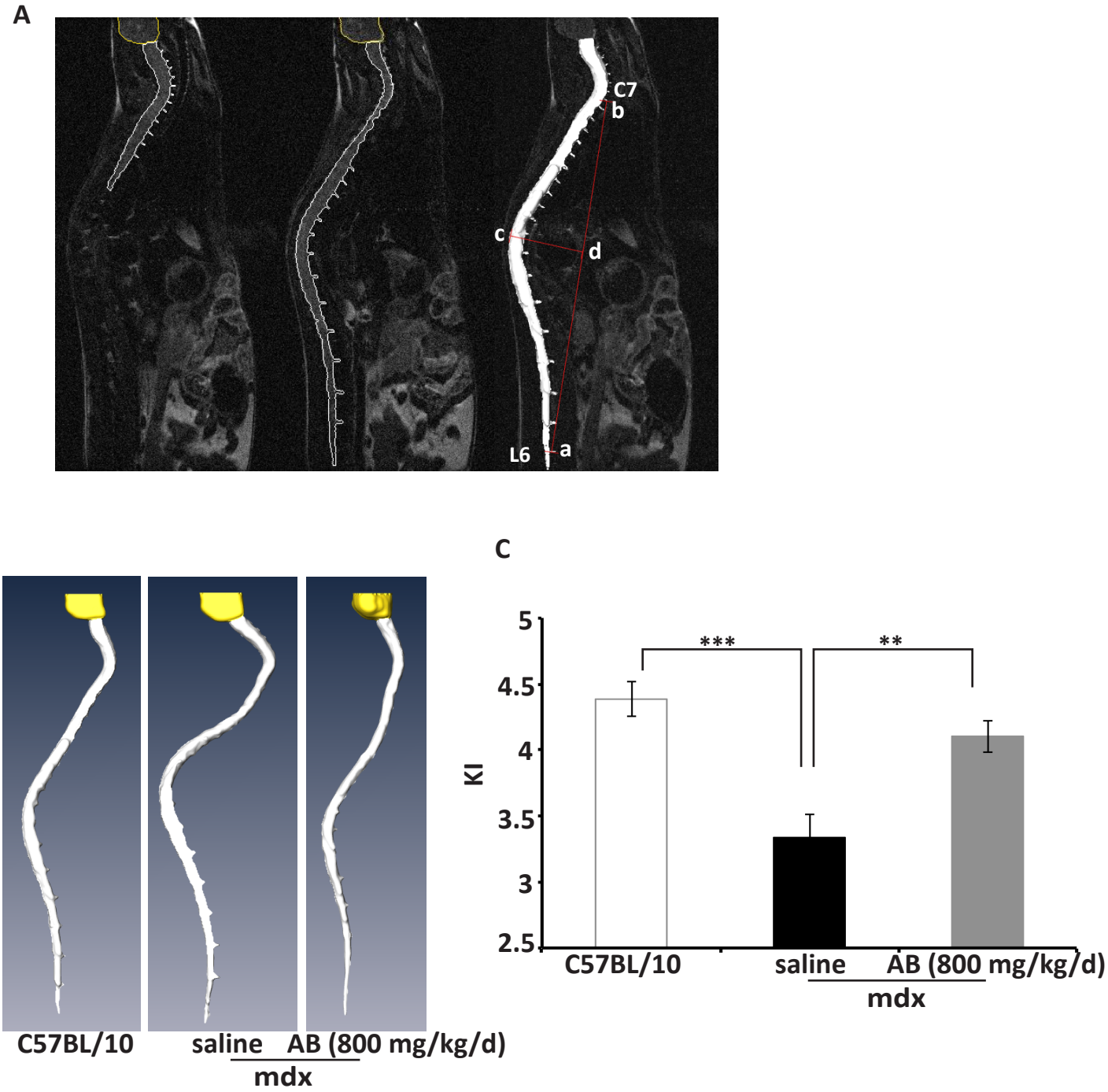

Figure 3: AB treatment alleviates spinal deformity in mdx mice treated by force-feeding for 12 months: MRI procedure. (A) Vertebral column distortion was measured after semiautomatic segmentation and 3D reconstruction to indentify intervertebral spaces. The kyphotic index (KI) was calculated as follows: line “ab”, the length of a line drawn from posterior edge of C7 to the posterior edge of L6; line “cd” is the distance from line “ab” to the dorsal border of the vertebral body (KI = ab/cd). (B) 3D reconstruction of vertebral column in C57BL/10 mice, and saline- and AB-treated mdx mice. (C) The KI value is lower in saline-treated *mdx* mice than in C57BL/10 animals and comparable in AB-treated *mdx* mice with C57BL/10 animals value, suggesting that the early treatment with AB preserves from the spinal deformity. Statistical test with the level of significance set at 0.05.

weight was detected in AB-treated mice, compared with saline-treated animals.

AB treatment alleviates axonal excitability parameters in *mdx* mice

The caudal muscle of saline-treated *mdx* mice displayed some significant differences in excitability waves forms (**Fig. 4**) and associated parameters (**Table 1**), when compared with C57BL/10 animals. These differences consisted in (i) a reduced CMAP amplitude, an enhanced latency (measured from 1 ms stimulation onset to peak amplitude) and a higher threshold (*i.e.* an increased intensity of the stimulation that has to be applied to evoke 50% of maximal CMAP amplitude), determined from the stimulus - response relationship (**Table 1**); (ii) an increased rheobase (*i.e.* minimum intensity of a maximum duration stimulation necessary to evoke a CMAP) and a decreased chronaxis (duration of a twice rheobase intensity stimulation necessary to evoke a CMAP) determined from the strength-duration relationship (**Fig. 4A** and **Table 1**); (iii) a higher minimum current-threshold (I-V) slope, determined as the three smallest slope values calculated from the I-V slope-threshold curve derived from the current-threshold relationship (**Fig. 4B** and **Table 1**), while the resting and hyperpolarizing I-V slopes were not significantly modified (**Fig. 4B**, **Table 1**; **Supplementary Material, Table S3**); (iv) less threshold changes in response to a constant depolarizing long - duration current of sub - threshold intensity, as determined from the threshold electrotonus that allows studying the altered excitability state of a given membrane when a such depolarizing or hyperpolarizing current is passed through it (**Fig. 4C** and **Table 1**); and (v) increased refractoriness (the property of excitable tissue that determines how closely together two action potentials can occur) as calculated by the duration of the relative refractory period and the percents of refractoriness for an interstimulus delay of 2 and 2.5 ms, determined from the recovery cycle and indicating a more longer and important loss of excitability following an action potential (**Fig. 4D** and **Table 1**). All the other parameters were not markedly different between the two groups of animals ($p \geq 0.056$; **Fig. 4** and **Supplementary Material, Table S3**). Similar results were obtained from plantar muscle recordings of saline-treated *mdx* mice (**Table 2, Supplementary Material, Table S3**), except for the CMAP amplitude and the latency that are not different from C57BL/10 animal values.

Very interestingly, when treated with AB, most (tail, **Table 1**) if not all (foot, **Table 2**) excitability parameters in saline-treated *mdx* mice did no longer differ significantly from C57BL/10 animals ($p \geq 0.053$). However, the CMAP amplitude and latency recorded from the tail muscle of AB-treated *mdx* mice were similar to saline-treated *mdx* animals. It is worth noting that no significant difference was observed between excitability properties of untreated and saline-treated *mdx* mice ($p \geq 0.056$, **Supplementary Material, Table S4),** indicating that the force-feeding procedure had, by itself, no effect on the excitability parameters.

Intraperitoneal injection and force-feeding procedure induce similar effects

The effects of administration mode were observed by comparing the AB-treated *mdx* mice using oral administration and intraperitoneal injection of AB, according to similar treatment protocol (dose, frequency and duration). Surface of necrosis in heart, muscular force values and neuromuscular excitability parameters were used to compare the two ways of administration.

Once again, no change of body weight was detected for the two ways of administration. A reduction of the areas of necrosis was clearly visible in cross-sectional sections of heart stained by Masson's trichrome in AB-treated *mdx* mice, with both modes of administration (**Supplementary Material, Fig. S5A**) and confirmed by quantification using ImageJ software (**Supplementary Material, Fig. S5B**). Muscle strength was evaluated using a grip-strength meter and the inverted grid test (grip latency) in the mouse. AB treatment improved *mdx* mice grip strength in both conditions of administration to reach values equivalent to C57BL/10 animals (**Supplementary Material, Fig. S5C,D**). Finally, utrophin and beta-dystroglycan up-regulation in muscles was

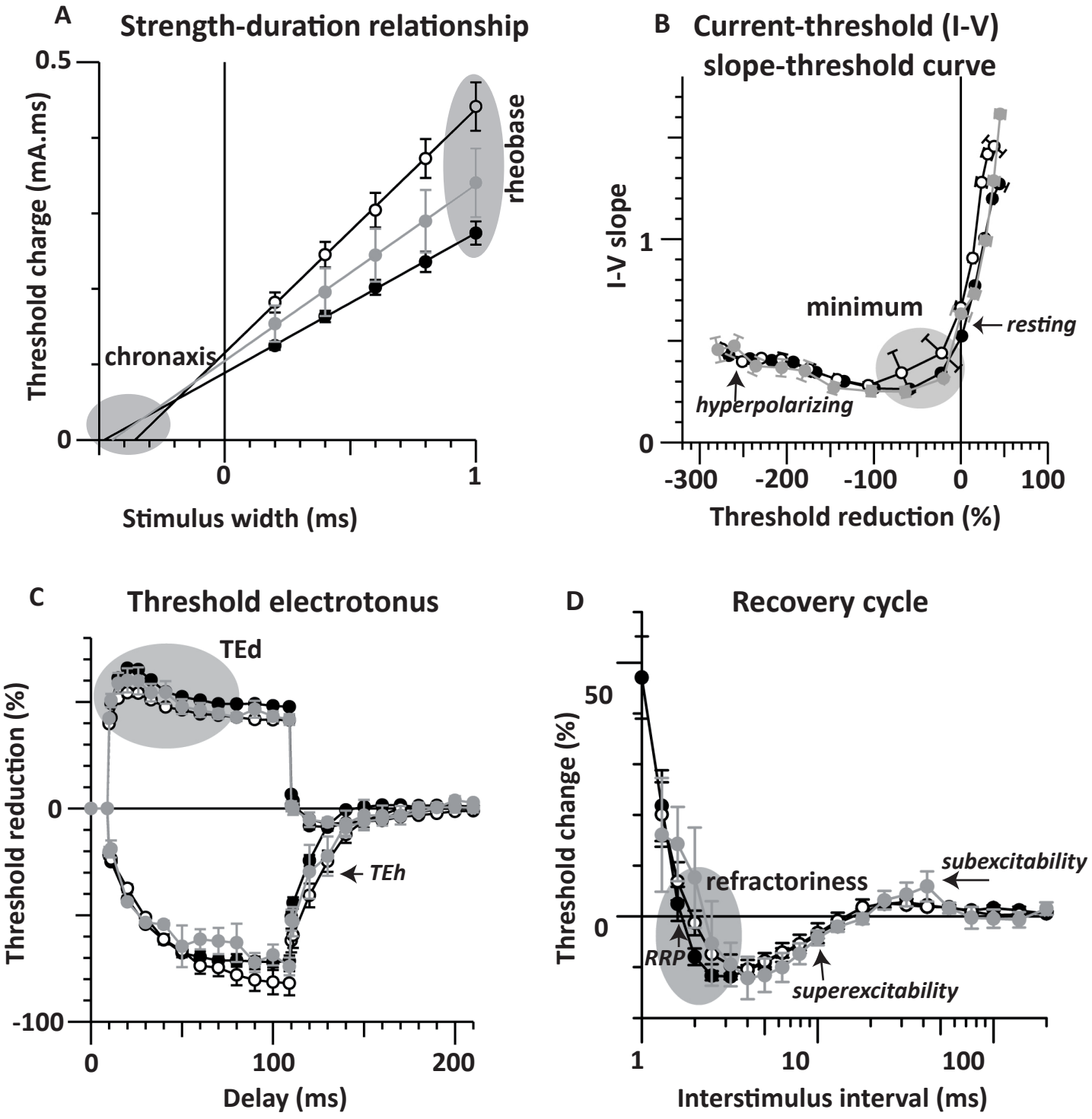

Figure 4: Excitability waveforms obtained by stimulating the caudal motor nerve and recording the compound muscle action potential from tail muscle in 13-week-old *mdx* mice treated with AB by force-feeding for 7 weeks. C57BL/10 mice (black circles), and AB-treated (grey circles) and saline-treated (white circles) *mdx* mice (A) Strength-duration relationship. (B) Current-threshold (I-V) slope-threshold curve derived from the current-threshold relationship. AB main effects are indicated in grey. (C) Threshold electrotonus (TEd and TEh are threshold electrotonus in response to constant depolarizing and hyperpolarizing long-duration currents of sub-threshold intensity, respectively). (D) Recovery cycle (RRP: relative refractory period). AB main effects are indicated in grey areas, while non modified parameters by arrows. Statistical test with the level of significance set at 0.05.

Caudal muscle	C57BL/10	*mdx*	
		saline	AB (800 mg/kg/d)
CMAP amplitude (mV) [1]	3.68 ± 0.11	1.11 ± 0.12**	1.05 ± 0.12***
Latency (ms) [1]	3.16 ± 0.06	3.62 ± 0.13*	4.03 ± 0.11****
Stimulus (mA) for 50% max response [1]	0.28 ± 0.06	0.38 ± 0.09*	0.35 ± 0.11
Strength-duration time constant (ms) [2]	0.49 ± 0.03	0.36 ± 0.02**	0.44 ± 0.06
Rheobase (mA) [2]	0.18 ± 0.08	0.26 ± 0.11*	0.22 ± 0.13
Minimum I-V slope [3]	0.26 ± 0.01	0.22 ± 0.01**	0.21 ± 0.03
S2 accommodation [4]	15.30 ± 0.70	11.43 ± 0.77**	16.94 ± 2.56
TEd (10-20ms) [4]	64.77 ± 1.01	53.80 ± 1.75***	55.32 ± 4.89
TEd (40-60ms) [4]	50.79 ± 0.88	44.73 ± 1.25**	46.17 ± 3.02
TEd (peak) [4]	63.32 ± 0.91	53.00 ± 1.58***	54.95 ± 4.29
TEd20 (peak) [4]	37.68 ± 0.69	32.19 ± 1.07**	34.05 ± 2.20
Relative refractory period (ms) [5]	1.65 ± 1.06	2.18 ± 1.13*	2.26 ± 1.17*
Refractoriness at 2ms (%) [5]	-7.96 ± 1.65	3.42 ± 3.70*	8.46 ± 9.49
Refractoriness at 2.5ms (%) [5]	-11.67 ± 0.88	-2.59 ± 2.66*	-3.00 ± 5.87

Table 1: Excitability parameters obtained by stimulating the caudal motor nerve and recording the CMAP from tail muscle in 13-week-old C57BL/10, saline- and AB-*mdx* mice treated by force-feeding for 7 weeks. Compared with C57BL/10 mice, most excitability parameters that are modified in saline-treated *mdx* mice, do no longer show any significant difference when *mdx* mice were treated with AB ($p \geq 0.054$). Statistical test with the level of significance set at 0.05.

Exponent numbers correspond to parameters of: (1) Stimulus-response relationship, (2) strength-duration relationship, (3) current-threshold (I-V) relationship, (4) threshold electrotonus (TEd and TEh are threshold electrotonus in response to constant depolarizing and hyperpolarizing long-duration currents of sub-threshold intensity, respectively), (5) recovery cycle.

Plantar muscle	C57BL/10	*mdx*	
		saline	AB (800 mg/kg/d)
Stimulus (mA) for 50% max response [1]	0.28 ± 1.03	0.41 ± 1.09*	0.27 ± 1.19
Strength-duration time constant (ms)[2]	0.47 ± 0.01	0.35 ± 0.03*	0.43 ± 0.05
Rheobase (mA)[2]	0.18 ± 1.05	0.27 ± 1.09*	0.19 ± 1.22
Minimum I-V slope[3]	0.48 ± 0.01	0.42 ± 0.01*	0.47 ± 0.04
S2 accommodation [4]	14.24 ± 1.35	7.81 ± 1.58*	10.85 ± 0.88
TEd (10-20ms) [4]	50.06 ± 1.62	41.72 ± 1.61*	50.99 ± 3.37
TEd (peak) [4]	49.26 ± 1.61	42.30 ± 1.43*	47.09 ± 2.36
TEd20 (peak) [4]	26.19 ± 1.41	22.42 ± 0.76*	23.54 ± 0.97
Refractoriness at 2ms (%) [5]	1.54 ± 3.09	17.95 ± 3.02*	7.32 ± 4.14
Refractoriness at 2.5ms (%) [5]	-8.41 ± 1.90	0.79 ± 1.69*	-13.25 ± 3.79

Table 2: Excitability parameters obtained by stimulating the tibial branch of the sciatic nerve and recording the CMAP from plantar muscle in 13-week-old C57BL/10, saline- and AB-*mdx* mice treated by force-feeding for 7 weeks. Compared with C57BL/10 mice, all excitability parameters that are modified in saline-treated mdx mice, do no longer show any significant difference when *mdx* mice were treated with AB ($p \geq 0.053$). Statistical test with the level of significance set at 0.05

Exponent numbers correspond to parameters of: (1) Stimulus-response relationship, (2) strength-duration relationship, (3) current-threshold (I-V) relationship, (4) threshold electrotonus (TEd and TEh are threshold electrotonus in response to constant depolarizing and hyperpolarizing long-duration currents of sub-threshold intensity, respectively), (5) recovery cycle.

reported to be one of the major effects of AB in mice when intraperitoneally injected *(6)*. A similar increase was observed when AB was orally administered: semi-quantitative western blot analyses revealed an about 2-fold increase in utrophin and beta-dystroglycan expression in the heart tissues, in AB-treated *mdx* mice compared with saline-treated *mdx* animals (**Supplementary Material, Fig. S6A,B**). No significant difference in neuromuscular excitability parameters was detected between the two administration modes (**Supplementary Material, Table S7**).
Taken together, these data indicate that intraperitoneal injection and force-feeding procedures give similar results.

DISCUSSION

In the present paper, we address the potential benefits of the oral administration of AB, a combination of L-arginine (NO-pathway activation) and butyrate (an HDAC inhibitor), on cardiomyopathy, spinal deformity and excitability defaults, three noticeable alterations in DMD patients. Each of these alterations is partially directly or indirectly responsible for death and/or additionally contributes to the onset of symptoms that reduce the quality of life of DMD patients.

To explore the effect of AB on heart structure and function, the animals were treated before the appearance of functional symptoms of cardiomyopathy, and echocardiography was recorded in a follow-up study monthly from the 8^{th} to the 14^{th} month of age. In particular, EF and FS have been monitored in order to investigate heart function. As expected, any changes for C57BL/10 mice were visible during the monitored period but saline-treated *mdx* mice displayed about 20% progressive decrease of EF (23% for FS), over the studied period. EF and FS in AB-treated *mdx* mice were maintained all along the 7 months of recording, indicating that the cardiac function is preserved in treated animals. This strongly suggests that AB compensates, at least partially, the lack of dystrophin in heart and could ameliorate some of heart dysfunctions in DMD patients. Cardiac enlargement was also investigated to examine the effect of AB on left ventricular dilatation: as observed for EF and FS, treatment with AB protects heart from the ventricular dilatation that progressively set up in *mdx* mice. In addition, the heart weight in 14 month-old saline-treated *mdx* mice was increased by about 25% compared with C57BL/10 mice. The treatment with AB maintained a value similar to C57BL/10 mice, supporting that AB treatment protects heart from hypertrophy. Surprisingly, the percentage of necrotic surface remained very low (3-4%) in 14 month-old saline-treated *mdx* mice. These results indicate that, in *mdx* mice, the percentage of necrotic surface does not increase meanwhile cardiac function deteriorates. Moreover, the very low percentage of necrotic tissue in heart of 14 month-old saline-treated *mdx* mice was not modified in treated *mdx* mice, suggesting that AB does not influenced necrotic process. Taken together, these results suggest strongly that the maintaining cardiac function in AB-treated mice results of a better functioning of the heart muscle.
Several hypotheses could be advanced to explain the strong benefit of AB treatment on cardiac function. In heart of *mdx* mice, the decrease of NO production is about 75-80%, which is similar to the loss of NO synthase (NOS) activity that occurs in skeletal muscle *(40, 41)*. While in skeletal muscles nNOS is located at the sarcolemma, in heart tissue the enzyme can be found at the sarcolemma but also in the sarcoplasmic reticulum and mitochondria (42–44). Thus deficiency in nNOS activity in heart may primarily reflect defects in its regulation and/or the loss of binding to the dystrophin complex.
In addition a deregulation of L-arginine transporters at the membrane of dystrophic cardiomyocyte in *mdx* mice has been observed. Ramachandran et al. (2012) observed a spontaneous/intrinsic increase of CATs (cationic amino acid transporters) expression in *mdx* mice and *mdx:utro* mice in order to improve the transport inside the cell and produce NO. In particular, they have shown that the lower-affinity CAT (CAT-2A) is more expressed and a possible compensatory mechanism could be develop by DMD cardiac muscle cells to oppose the effects of nNOS reduction *(41)*. Moreover it is known that NO pathway is implicated in utrophin expression

through cGMP *(45)* and that cGMP, when enhanced, improves contractile function, energy metabolism and sarcolemmal integrity of dystrophin deficient mice heart *(46, 47)* In our case the fetal homologue of dystrophin, utrophin, is re-expressed and we can suppose that the correct re-organization of the plasmatic membrane stop or reverse dystrophic features. In particular our results indicate that utrophin and beta-dystroglycan are properly localized in heart membrane after AB treatment, suggesting that the treatment may be sufficient to restore sarcolemmal integrity. Besides, HDAC inhibitors could regulate the HDAC/acetylase functional balance which is altered in *mdx* mice *(20)*.

Nowadays cardiomyopathy management in DMD patients relies on steroids, angiotensin-converting-enzyme inhibitors and beta-blockers. The combination of this type of molecules delay the onset of LV dysfunction and improve the LV function in DMD patients (Abdallah Fayssoil et al., 2010; Politano and Nigro, 2012). So, the beneficial effect of AB on cardiac function could be related to (i) an increase of NO production, (ii) an enhanced utrophin expression through L-arginine *via* cGMP and the relocalization at the membrane of dystrophine/utrophin associated proteins such beta-dystroglycan, and (iii) the regulation of the HDAC/acetylase balance *via* butyrate. Because heart muscle is not able to generate new cells, any technique that could reverse the progressive decline of the tissues is welcome.

The effect of AB on the spinal cord deformity that settles down in *mdx* mice was evaluated by measuring the index of kyphosis, calculated by RMI (anesthetized mice) and by radiography (awaked mice). The measures clearly indicated that the deformity described in saline-treated *mdx* mice did not appear in AB-treated mice. This strongly suggests that the treatment could stop the progression of spinal deformity in patients and, indirectly, reduces respiratory complications *(29)*, thus avoiding surgery for spinal fusion and stabilization.

Moreover, we evaluated the benefit of AB on the neuromuscular excitability, *i.e.* on the CMAP recorded from tail and plantar muscles, in response to excitability tests applied *via* the caudal and tibial motor nerves in 13 week-old *mdx* mice. We observed that saline-treated *mdx* mice displayed changes in neuromuscular excitability, compared with C57BL/10 animals. These changes mainly consisted in (i) a higher threshold, an enhanced latency and a reduced CMAP amplitude, (ii) an increased rheobase and a reduced chronaxis, (iii) a reduced minimum I-V slope, (iv) less threshold changes in response to a constant depolarizing long‐duration current of sub‐threshold intensity, and (v) increased refractoriness. It is worth nothing that the above parameters are related to peripheral nerve excitability, and not muscle excitability *(39, 38)*. The changes in recovery cycle and strength-duration relationship could be explained by different contribution of sodium channels (both transient and persistent) in *mdx* and C57BL/10 animals. Hence, it is likely that longer transient inactivation of voltage-gated sodium channels induces the longer refractory period and greater refractoriness in saline-treated *mdx* mice. Beside, threshold electrotonus and current-threshold relationship provide an assessment of intermodal properties *in vivo*. Abnormalities in these later parameters imply the functioning of different subtypes of potassium channels. Altogether, these changes could reflect structural alterations of both paranodal and intermodal regions and, thereby, may suggest a subtle disorganization of the myelin sheath of the peripheral nerve *(51, 52)*, which could result in modifications of repartition and density of ion channels in *mdx* mice. This hypothesis is also in line with previous findings suggesting an important role of sarcoglycans in the stability of peripheral nerve myelin in a hamster model *(53)*. Very interestingly, in AB-treated *mdx* mice, most (tail) if not all (foot) excitability parameters did no longer differ significantly from C57BL/10 animals.

In addition, the CMAP amplitude was reduced and the latency prolonged in the tail muscle recordings of saline-treated *mdx* mice compared with C57BL/10 animals. These

modifications remained abnormal despite AB treatment. Although persistent (background) channels may be more abundant in *mdx* mice, allowing thus a decreased threshold and an increased current intensity able to evoke a CMAP, a decreased number of voltage-gated sodium channels could also explain the decrease of the CMAP amplitude. In accordance with this hypothesis, it has been described that neuromuscular junction of *mdx* mice present fragmentation, excessive nerve sprouting *(11)*, and a decrease of the number and depth of synaptic folds that promote the decrease of the density of voltage-gated sodium channels to the synapse *(36)*. The increased latency of CMAP in saline-treated *mdx* mice may reflect the morphological alterations at the neuromuscular junction that influence action potential propagation. In contrast, in the plantar muscle recordings of saline-treated *mdx* mice, the CMAP amplitude and the latency did not change when compared with C57BL/10 animals.

The non-invasive automatized sequential acquisition of multiple excitability tests developed in clinical neurophysiology could be used to explore the neuromuscular excitability in DMD patients and to monitor treatment effects over time.

In a previous study where we have tested a pharmaceutical approach to treat DMD with AB, in *mdx* mice *(6)*, we have shown that many of the structural, biochemical and functional hallmarks of the principal animal model of DMD were improved by AB treatment after intraperitoneal administration and that L-arginine and butyrate act synergically. Therefore, one of the most important points of the present work was to verify if the positive effects observed after the intreperitoneal injection of AB were maintained after oral administration, in order to treat DMD children. Different parameters have been studied with this aim. In particular, the reduction of the percentage of necrotic surface in heart observed after i.p. injection is the same after oral administration and is close to C57BL/10 value, suggesting that starting the treatment in young animals temporally protect heart from structural deterioration processes such as necrosis/fibrosis. In addition, force and fatigue measures displayed similar performances in AB-treated *mdx* mice compared with C57BL/10 mice. Finally, the majority of tail and foot excitability parameters that were modified in saline-treated *mdx* mice did not show any significant difference when *mdx* mice were treated with AB, whatever the way of administration. Taken together these data indicated that whatever the way of administration, structural and functional positive effect are visible after AB treatment, and the oral way could be considered as the way of treatment for DMD children.

The global benefit of AB after long force-feeding protocol was supported by the decrease of CK level in the serum and by a better tirelessness. We can suppose that the decrease of CK level belongs from skeletal muscle enzyme rather than cardiac contribution because the percentage of necrotic tissue in the heart of AB treated mice is 3%, similar to saline-treated *mdx* mice. The safety of AB was reinforced by the fact that any change on body weight was observed during both types of treatments. A sign that in case of clinical trial AB administration should be well tolerate by patients. Moreover the benefit on cardiac function was not accompanied by heart hypertrophy, which could be noxious in the long-term administration. On the contrary, the global benefit of AB was strengthened by a protective effect on heart ventricular dilatation and hypertrophy. Any major limitation is expected because the components of the pro-drugs are already widely used in clinical applications.

In conclusion, we have shown that AB orally administered performs the same beneficial effect yet observed after intraperitoneal administration in *mdx* mice. Moreover the molecule reveals a protective role in postural, structural and functional parameters in *mdx* mice treated for a long period, with a very interesting result for heart cardiomyopathy. Taken together these effects give arguments to proceed towards clinical evaluation of a long-term treatment.

MATERIALS & METHODS

AB preparation

L-arginine and n-butyric acid (Sigma-Aldrich, Lyon, France) were added in miliQ water to make a 26% stock solution (1 M arginine – 1 M butyrate, pH = 7), as previously described *(54)*. The stock solution was diluted before use in 0.9% NaCl to obtain the injectable and force-feeding solution.

Mouse experimental procedures

Since DMD is an X-linked genetic disorder, studies were performed using male mice. All experiments were performed in accordance with the guidelines established by the European Communities Council Directive (Guide for the Care and Use of Laboratory Animals: EEC86/609 Council Directive - Decree 2001-131). The experimental protocols were approved by the local review board "Comité d'Ethique Cuvier du Museum National d'Histoire Naturelle" (number 68-024) and by the French Departmental Direction of Animal Protection (number A91-453).

Adult *mdx* and wild-type mice of the C57Bl/10 strain were 6 weeks old at the beginning of the experiments. Animals were weighed before each treatment administration. Dystrophic animals were treated by force-feeding procedure (1 mL/100 g body weight) with flexible cannulas (PHYMEP, Paris, France). Animals were assigned to the saline group (0.9% NaCl) or to the treated group (AB: 800 mg/kg/day), the optimal dose determined by intraperitoneal injection *(6)* in an intermittent protocol: a series of 4 consecutive daily administrations every 2 weeks for 7 weeks or 14 months, depending on the addressed parameters. The cardiomyopathy and the distortion of the vertebral column are two defects never evidenced in mice *mdx* before the age of 9 months. We recorded the cardiac functioning monthly, by echocardiography, in *mdx* mice from 8 to 14 months, which corresponds to one year of treatment. At this age, X-ray and MRI of the animals were carried out to measure a radiographic index of kyphosis, KI. Analysis of neuromuscular excitability properties was performed in 13-week-old mice, which corresponds to 7 weeks of treatment. Global functional and biochemical parameters were used to complete the evaluation of the benefit: a measure of force (grip test) and of fatigue (inverted grid test). At the end of the protocol, mice were anesthetized with 10% pentobarbital, blood samples were taken from the heart for measurement of serum CK levels, and at the end were sacrificed by cervical dislocation. Hearts were dissected, weighted and frozen for structural analysis. Finally, we compared the effectiveness of AB force-feeding as mode of administration with intraperitoneal injections, the mode used in our previous studies *(55, 56, 6)*.

Echocardiography

All *in vivo* studies were performed using a high resolution Vevo 770 system, including a high-frequency (40 MHz) transducer (Visualsonics, Toronto, Canada). Briefly, mice were anesthetized using an isoflurane gas anesthesia system, with isoflurane concentrations reaching 2-3% in oxygen during the exam. Animals were placed in dorsal position. Heart rate and body temperature were monitored. Echographic studies were performed in parasternal long and short axis views. All images were recorded, and measurements were made off-line using analytic software of the system (Visualsonics, Toronto, Canada). 2D and M-mode measurements were performed at the level of papillary muscles in order to obtain the diameters of LVID and LVOD during systole and diastole. In addition interventricular septum thickness (IVS,s) and left ventricular posterior wall thickness at systole (LVPW,s) were measured. Left ventricular systolic function was assessed by EF and FS which were calculated using M-mode, according to the usual formulas: EF (%) = 100*(LV Vol,d - LV, Vol,s)/LV Vol,d and FS (%) = 100*(LVID,d - LVID,s)/LVID,d. The average of at least three representative cardiac cycles was considered.

Magnetic resonance imaging

Mice were imaged under isoflurane anesthesia (induction 1.5%; flow rate 1.5-0.8% in compressed air) and controlled on the basis of respiratory parameters. The body temperature was maintained at 37°C using

heated mattress. MRI measurements were performed on a 7-T horizontal bore magnet (Oxford, UK) driven by Paravision (Bruker, Wissembourg, France), equipped with a 300 mT/m actively shielded gradient device (internal diameter [ID] = 90 mm, Bruker). For MRI examination, animals were introduced in a ''bird-cage'' 1-H coil (ID = 63 mm). After scouting gradient-echo images in the 3 orthogonal directions and shimming process, the spinal cord and intervertebral spaces were explored using 2D- multi-slice Turbo Spin Echo Bruker MRI sequence (2D-TurboRARE) (Repetition time (TR)/echo time (TE)/effective echo time (TEeff) = 3700/15.89/47.69 ms, number of averages (NA) = 12, fat and motion suppression' ON') and Flash MRI sequence (Fast Low Angle SHot) (TR/TE = 385/6.94ms; excitation pulse angle 30°). In both MRI sequences, matrix size = 512*256, field of view (FOV) = 60×30 mm^2, slice thickness (ST) = 0.250 mm, slice gap = 0 mm, number of slices = 24, voxel size =117*117*250 μm^3. The total time spent by the mouse in the magnet never exceeds 1 h. After each experiment, mice were recovered from anesthesia and returned to their home cages with free access to food and water.

Radiographic pictures

The KI was calculated from series of radiography obtained by video-radiographic apparatus (Philips Medical Systems) constituted by a generator, an image intensifier with a field of 23 cm, combined to high-speed video camera (Motionscope), with resolution of 1040x1024 pixels. As the X-rays were emitted periodically through the positive portion of a filtered sinusoidal current, the use of high-speed videoradiography required a low intensity (5 mA) to smooth the sine curves and avoid periodic fading of the image. This was obtained by using a voltage (56 kV) higher than the optimum with respect to the thickness of the object being viewed. The camera was run at 20 frames per second, with a shutter speed off set at 30 000µ seconds. Each mouse was set (free of movements) in a small cardboard box of 20 x 5 x 5 cm. The box was then placed between the x-ray generator and as close as possible to the input surface of the image intensifier to avoid magnification effects and loss of resolution. After one minute the animal was familiarized in its new environment and, adopted a natural rest position. From this moment, a series of radiographic pictures was done in lateral view. In these conditions, no signs of distress were observed in the mice during the capture of image.

Five radiographs of the same animals in a rest position were hind limbs and forelimbs placed in moderate extension *(57)*, showed there was few differences in measured KI. Care was then taken to avoid overextension or flexion of limbs and to ensure that limbs were only moderately extended.

Kyphotic index

The KI was calculated with ImageJ software from a line drawn between the caudal margin of the last cervical vertebra to the caudal margin of the sixth lumbar vertebra (usually corresponding to the cranial border of the wing of the ilium) (line ab) divided by a line perpendicular to this from the dorsal edge of the vertebra at the point of greatest curvature (line cd), as performed in DMD patients (KI = ab/cd).

Combined forelimb and hindlimb grip strength measurement

In vivo functional evaluations were performed blind and carried out 24 h after the end of the treatment. Grip strength was measured using a grip-strength meter (Bioseb). The apparatus consisted of a grid connected to a digital dynamometer. The animals were gently lowered over the top of the grid so that both sets of front paws and hind paws could grip the grid. While the torso of the animal was kept parallel to the grid, the animal was gently pulled back by the tail until it released its grip. This procedure was repeated three times and the values were averaged and normalized to mouse body weight.

Inverted grid test

Mice were placed individually on a cage wire grid about 35 cm above a table. After slowly turning the grid through 180°, the length of time the mice continued to grip the grid was monitored (grip latency), a maximum score of

180 s being given if the animal did not fall. This procedure was repeated three times. The values were averaged and normalized to mouse body weight.

Neuromuscular excitability recordings

The multimodal evaluation of neuromuscular excitability was assessed, *in vivo*, by means of a minimally-invasive electrophysiological method, using the QTrac© software (written by Prof. Hugh Bostock, Institute of Neurology, London, UK), on mice under isoflurane anesthesia as previously described *(39)*. Briefly, an anesthetized mouse was placed on a heating pad to maintain body temperature between 35.2 and 35.8°C (measured using a rectal probe), and submitted to two sessions of excitability testing (TRONDE protocol) applied consecutively on the tail and rear leg. Electrical stimulations were delivered to either the caudal motor nerve or the tibial branch of sciatic nerve, by means of surface electrodes, and the CMAP was recorded using needle electrodes inserted into the tail or plantar muscle, respectively. Excitability measurements consisted in five different tests (stimulus-response, strength-duration and current-threshold relationships, as well as threshold electrotonus and recovery cycle) from which more than thirty parameters were determined and analyzed. It is worth noting that each specific excitability test provides additional and complementary information regarding the functional status of ion channels and electrogenic pumps, as well as membrane properties *(51, 52)*. Hence, the first group of parameters, obtained from the stimulus-response relationship, describes the amplitude of the CMAP in relation with the intensity of the stimulation (*i.e.* the current applied). The second group is obtained from the strength-duration relationship derived from the intensity-duration curve that determines the intensity in relation with the duration of the stimulation necessary to evoke a CMAP. The third group is obtained from the current-threshold relationship establishing the excitability modifications in response to depolarizing and hyperpolarizing currents. The fourth group is obtained from the threshold electrotonus that allows, in particular, studying the accommodation properties of axonal membranes in response to depolarizing and hyperpolarizing long-duration currents applied at sub-threshold intensity. Finally, the fifth group of parameters is obtained from the recovery cycle that characterizes the excitability fluctuations (as the percent of threshold change) during (*i.e.* the duration of the relative refractory period determined as the first intercept on the x-axis, and the refractoriness determined as percents of threshold change for an interstimulus delay of 2 and 2.5 ms) and after an action potential (*i.e.* the superexcitability, produced by the depolarizing after potential and determined as percents of threshold change for an interstimulus delay of 5 and 7 ms, and the late subexcitability determined as percent of threshold change for an interstimulus delay over 10 ms).

Masson's trichrome stain

Cryostat muscle sections (8 µm) were stained with Masson's trichrome stain to visualize connective tissue and muscle fibers in pink and collagen in blue (Sigma kit #HT15, USA) and then observed using a Leica DM RXA2 microscope (Leica Microsystems, Germany). The sections were photographed using a CoolSNAP camera (Roper Scientific, USA) and Openlab acquisition software (Improvision, UK).

Immunoblot analyses

The proteins were extracted from muscles samples in a buffer containing 10 mM Tris-HCl, 1mM EDTA and 10% SDS (pH 6.8). Total protein content was determined according to DC Protein Assay protocol (Bio-Rad). Proteins were separated by SDS-PAGE on a 6-12% multiplex gel (X-Cell II Mini Cell, Invitrogen, France) with a molecular weight marker (Rainbow^{TM}, Amersham Pharmacia Biotech) and then electroblotted into an immobilon-P polyvinyl membrane. We applied Coomassie G250 stain to verify the equal loading of gels.

The membrane was incubated with monoclonal antibodies against utrophin (NCL-DRP 2, 1/250 dilution, Novocastra), and beta-dystroglycan (NCL-beta-DG, 1/50 dilution, Novocastra) and then with a secondary sheep anti-mouse antibody linked to horseradish peroxidase (1/4000 dilution, Biorad, USA).

Immunostaining was revealed by a chemiluminescent reaction (ECL, Amersham Pharmacia Biotech). Desmin (53 kD), actin (43 kD) and GAPDH (38 kD) were used as loading controls. Band intensity was quantified using the 'Claravision' analyzer software. Experiments were repeated at least three times. For each experiment the results in treated mice were normalized to the values obtained in saline-treated mice (treated/saline ratio). Quantification was performed on films obtained after different exposure times for distinct proteins (around 30 seconds for beta-dystroglycan, 2 min for desmin and utrophin), but within quantifications of a given target protein the same exposure times were used for the different doses shown on the histograms.

Serum CK determination

Blood samples were taken from hearts of anaesthetized mice immediately before sacrifice. Serum CK activity was determined using a bioMérieux kit (enzyline CK NAC optimized 10).

Statistics

In general, data are shown as means ± SEM from at least three different experiments, and statistical group comparisons were performed using Student's t-test. For multimodal evaluation of neuromuscular excitability, data are expressed as means ± SD, and differences between values were tested using the parametric unpaired two-tailed t-test, two-way ANOVA, or the non parametric Mann-Whitney U-test, depending on the equality of variances estimated using the Lilliefors test. Differences were considered significant when $p < 0.05$.

ACKNOWLEDGEMENTS

We thank Jordi Molgó (Transferts ioniques et Pharmacologie du système neuromusculaire, UPR CNRS 3294, Gif sur Yvette) for continuous support of this work, and Thierry Decamps (Plateforme d'analyse du mouvement, UMR 7179, Paris) for technical assistance in the radiographic experiments.

Conflicts of Interest statement: none declared.

REFERENCES

1. Blake,D.J., Weir,A., Newey,S.E. and Davies,K.E. (2002) Function and genetics of dystrophin and dystrophin-related proteins in muscle. *Physiol. Rev.*, **82**, 291–329.
2. Finkel,R.S. (2010) Read-through strategies for suppression of nonsense mutations in Duchenne/ Becker muscular dystrophy: aminoglycosides and ataluren (PTC124). *J. Child Neurol.*, **25**, 1158–1164.
3. Goyenvalle,A. and Davies,K.E. (2011) Challenges to oligonucleotides-based therapeutics for Duchenne muscular dystrophy. *Skelet. Muscle*, **1**, 8.
4. Meregalli,M., Farini,A., Parolini,D., Maciotta,S. and Torrente,Y. (2010) Stem cell therapies to treat muscular dystrophy: progress to date. *BioDrugs Clin. Immunother. Biopharm. Gene Ther.*, **24**, 237–247.
5. Pichavant,C., Aartsma-Rus,A., Clemens,P.R., Davies,K.E., Dickson,G., Takeda,S., Wilton,S.D., Wolff,J.A., Wooddell,C.I., Xiao,X., et al. (2011) Current status of pharmaceutical and genetic therapeutic approaches to treat DMD. *Mol. Ther. J. Am. Soc. Gene Ther.*, **19**, 830–840.
6. Vianello,S., Yu,H., Voisin,V., Haddad,H., He,X., Foutz,A.S., Sebrié,C., Gillet,B., Roulot,M., Fougerousse,F., et al. (2013) Arginine butyrate: a therapeutic candidate for Duchenne muscular dystrophy. *FASEB J. Off. Publ. Fed. Am. Soc. Exp. Biol.*, 10.1096/fj.12-215723.
7. Anderson,J.E. (2000) A role for nitric oxide in muscle repair: nitric oxide-mediated activation of muscle satellite cells. *Mol. Biol. Cell*, **11**, 1859–1874.
8. Archer,J.D., Vargas,C.C. and Anderson,J.E. (2006) Persistent and improved functional gain in mdx dystrophic mice after treatment with L-arginine and deflazacort. *FASEB J. Off. Publ. Fed. Am. Soc. Exp. Biol.*, **20**, 738–740.
9. Barton,E.R., Morris,L., Kawana,M., Bish,L.T. and Toursel,T. (2005) Systemic

administration of L-arginine benefits mdx skeletal muscle function. *Muscle Nerve*, **32**, 751–760.
10. Chazalette,D., Hnia,K., Rivier,F., Hugon,G. and Mornet,D. (2005) alpha7B integrin changes in mdx mouse muscles after L-arginine administration. *FEBS Lett.*, **579**, 1079–1084.
11. Marques,M.J., Taniguti,A.P.T., Minatel,E. and Neto,H.S. (2007) Nerve terminal contributes to acetylcholine receptor organization at the dystrophic neuromuscular junction of mdx mice. *Anat. Rec. Hoboken NJ 2007*, **290**, 181–187.
12. Ségalat,L., Grisoni,K., Archer,J., Vargas,C., Bertrand,A. and Anderson,J.E. (2005) CAPON expression in skeletal muscle is regulated by position, repair, NOS activity, and dystrophy. *Exp. Cell Res.*, **302**, 170–179.
13. Voisin,V., Sébrié,C., Matecki,S., Yu,H., Gillet,B., Ramonatxo,M., Israël,M. and De la Porte,S. (2005) L-arginine improves dystrophic phenotype in mdx mice. *Neurobiol. Dis.*, **20**, 123–130.
14. Hnia,K., Gayraud,J., Hugon,G., Ramonatxo,M., De La Porte,S., Matecki,S. and Mornet,D. (2008) L-arginine decreases inflammation and modulates the nuclear factor-kappaB/matrix metalloproteinase cascade in mdx muscle fibers. *Am. J. Pathol.*, **172**, 1509–19.
15. Benabdellah,F., Yu,H., Brunelle,A., Laprévote,O. and De La Porte,S. (2009) MALDI reveals membrane lipid profile reversion in MDX mice. *Neurobiol. Dis.*, **36**, 252–258.
16. Brunelli,S., Sciorati,C., D'Antona,G., Innocenzi,A., Covarello,D., Galvez,B.G., Perrotta,C., Monopoli,A., Sanvito,F., Bottinelli,R., et al. (2007) Nitric oxide release combined with nonsteroidal antiinflammatory activity prevents muscular dystrophy pathology and enhances stem cell therapy. *Proc. Natl. Acad. Sci. U. S. A.*, **104**, 264–269.
17. Sciorati,C., Miglietta,D., Buono,R., Pisa,V., Cattaneo,D., Azzoni,E., Brunelli,S. and Clementi,E. (2011) A dual acting compound releasing nitric oxide (NO) and ibuprofen, NCX 320, shows significant therapeutic effects in a mouse model of muscular dystrophy. *Pharmacol. Res. Off. J. Ital. Pharmacol. Soc.*, **64**, 210–217.
18. Thomas,G.D., Ye,J., De Nardi,C., Monopoli,A., Ongini,E. and Victor,R.G. (2012) Treatment with a nitric oxide-donating NSAID alleviates functional muscle ischemia in the mouse model of Duchenne muscular dystrophy. *PloS One*, **7**, e49350.
19. Gurpur,P.B., Liu,J., Burkin,D.J. and Kaufman,S.J. (2009) Valproic acid activates the PI3K/Akt/mTOR pathway in muscle and ameliorates pathology in a mouse model of Duchenne muscular dystrophy. *Am. J. Pathol.*, **174**, 999–1008.
20. Colussi,C., Illi,B., Rosati,J., Spallotta,F., Farsetti,A., Grasselli,A., Mai,A., Capogrossi,M.C. and Gaetano,C. (2010) Histone deacetylase inhibitors: keeping momentum for neuromuscular and cardiovascular diseases treatment. *Pharmacol. Res. Off. J. Ital. Pharmacol. Soc.*, **62**, 3–10.
21. Consalvi,S., Mozzetta,C., Bettica,P., Germani,M., Fiorentini,F., Del Bene,F., Rocchetti,M., Leoni,F., Mascagni,P., Puri,P.L., et al. (2013) Preclinical studies in the mdx mouse model of Duchenne Muscular Dystrophy with the Histone Deacetylase inhibitor Givinostat. *Mol. Med. Camb. Mass*, 10.2119/molmed.2013.00011.
22. Perrine,S.P. (2008) Fetal globin stimulant therapies in the beta-hemoglobinopathies: principles and current potential. *Pediatr. Ann.*, **37**, 339–346.
23. Goodwin,F.C. and Muntoni,F. (2005) Cardiac involvement in muscular dystrophies: molecular mechanisms. *Muscle Nerve*, **32**, 577–588.
24. Colan,S.D. (2005) Evolving therapeutic strategies for dystrophinopathies: potential for conflict between cardiac and skeletal needs. *Circulation*, **112**, 2756–2758.
25. Moriuchi,T., Kagawa,N., Mukoyama,M. and Hizawa,K. (1993)

Autopsy analyses of the muscular dystrophies. *Tokushima J. Exp. Med.*, **40**, 83–93.
26. Quinlan,J.G., Hahn,H.S., Wong,B.L., Lorenz,J.N., Wenisch,A.S. and Levin,L.S. (2004) Evolution of the mdx mouse cardiomyopathy: physiological and morphological findings. *Neuromuscul. Disord. NMD*, **14**, 491–496.
27. Spurney,C.F., Knoblach,S., Pistilli,E.E., Nagaraju,K., Martin,G.R. and Hoffman,E.P. (2008) Dystrophin-deficient cardiomyopathy in mouse: expression of Nox4 and Lox are associated with fibrosis and altered functional parameters in the heart. *Neuromuscul. Disord. NMD*, **18**, 371–381.
28. Au,C.G., Butler,T.L., Sherwood,M.C., Egan,J.R., North,K.N. and Winlaw,D.S. (2011) Increased connective tissue growth factor associated with cardiac fibrosis in the mdx mouse model of dystrophic cardiomyopathy. *Int. J. Exp. Pathol.*, **92**, 57–65.
29. Oda,T., Shimizu,N., Yonenobu,K., Ono,K., Nabeshima,T. and Kyoh,S. (1993) Longitudinal study of spinal deformity in Duchenne muscular dystrophy. *J. Pediatr. Orthop.*, **13**, 478–488.
30. Laws,N. and Hoey,A. (2004) Progression of kyphosis in mdx mice. *J. Appl. Physiol. Bethesda Md 1985*, **97**, 1970–1977.
31. Yiu,E.M. and Kornberg,A.J. (2008) Duchenne muscular dystrophy. *Neurol. India*, **56**, 236–247.
32. Yamashita,S., Takenaka,H., Sugimoto,S., Chihara,E., Sawada,A., Matsukura,S. and Hamada,M. (1989) Axonal transport in mdx mouse sciatic nerve. *J. Neurol. Sci.*, **92**, 267–79.
33. Hollingworth,S., Marshall,M.W. and Robson,E. (1990) Excitation contraction coupling in normal and mdx mice. *Muscle Nerve*, **13**, 16–20.
34. Lyons,P.R. and Slater,C.R. (1991) Structure and function of the neuromuscular junction in young adult mdx mice. *J. Neurocytol.*, **20**, 969–981.
35. Nagel,A., Lehmann-Horn,F. and Engel,A.G. (1990) Neuromuscular transmission in the mdx mouse. *Muscle Nerve*, **13**, 742–749.
36. Banks,G.B., Chamberlain,J.S. and Froehner,S.C. (2009) Truncated dystrophins can influence neuromuscular synapse structure. *Mol. Cell. Neurosci.*, **40**, 433–441.
37. Torres,L.F. and Duchen,L.W. (1987) The mutant mdx: inherited myopathy in the mouse. Morphological studies of nerves, muscles and end-plates. *Brain*, **110 (Pt 2)**, 269–99.
38. Bostock,H., Cikurel,K. and Burke,D. (1998) Threshold tracking techniques in the study of human peripheral nerve. *Muscle Nerve*, **21**, 137–158.
39. Boerio,D., Greensmith,L. and Bostock,H. (2009) Excitability properties of motor axons in the maturing mouse. *J Peripher Nerv Syst*, **14**, 45–53.
40. Bia,B.L., Cassidy,P.J., Young,M.E., Rafael,J.A., Leighton,B., Davies,K.E., Radda,G.K. and Clarke,K. (1999) Decreased myocardial nNOS, increased iNOS and abnormal ECGs in mouse models of Duchenne muscular dystrophy. *J. Mol. Cell. Cardiol.*, **31**, 1857–62.
41. Ramachandran,J., Schneider,J.S., Crassous,P.-A., Zheng,R., Gonzalez,J.P., Xie,L.-H., Beuve,A., Fraidenraich,D. and Peluffo,R.D. (2012) Nitric Oxide Signaling Pathway in Duchenne Muscular Dystrophy Mice: Upregulation of L-arginine Transporters. *Biochem. J.*, 10.1042/BJ20120787.
42. Wehling-Henricks,M., Jordan,M.C., Roos,K.P., Deng,B. and Tidball,J.G. (2005) Cardiomyopathy in dystrophin-deficient hearts is prevented by expression of a neuronal nitric oxide synthase transgene in the myocardium. *Hum. Mol. Genet.*, **14**, 1921–1933.
43. Xu,K.Y., Huso,D.L., Dawson,T.M., Bredt,D.S. and Becker,L.C. (1999) Nitric oxide synthase in cardiac sarcoplasmic reticulum. *Proc. Natl. Acad. Sci. U. S. A.*, **96**, 657–662.
44. Kanai,A.J., Pearce,L.L., Clemens,P.R., Birder,L.A., VanBibber,M.M., Choi,S.Y.,

de Groat,W.C. and Peterson,J. (2001) Identification of a neuronal nitric oxide synthase in isolated cardiac mitochondria using electrochemical detection. *Proc. Natl. Acad. Sci. U. S. A.*, **98**, 14126–14131.
45. Chaubourt,E., Fossier,P., Baux,G., Leprince,C., Israël,M. and De La Porte,S. (1999) Nitric oxide and l-arginine cause an accumulation of utrophin at the sarcolemma: a possible compensation for dystrophin loss in Duchenne muscular dystrophy. *Neurobiol. Dis.*, **6**, 499–507.
46. Adamo,C.M., Dai,D.-F., Percival,J.M., Minami,E., Willis,M.S., Patrucco,E., Froehner,S.C. and Beavo,J.A. (2010) Sildenafil reverses cardiac dysfunction in the mdx mouse model of Duchenne muscular dystrophy. *Proc. Natl. Acad. Sci. U. S. A.*, **107**, 19079–19083.
47. Khairallah,M., Khairallah,R.J., Young,M.E., Allen,B.G., Gillis,M.A., Danialou,G., Deschepper,C.F., Petrof,B.J. and Des Rosiers,C. (2008) Sildenafil and cardiomyocyte-specific cGMP signaling prevent cardiomyopathic changes associated with dystrophin deficiency. *Proc. Natl. Acad. Sci. U. S. A.*, **105**, 7028–7033.
48. Fayssoil,A. (2010) Angiotensin-converting enzyme inhibitors and beta-blockers in cardiac asymptomatic patients with Duchenne muscular dystrophy. *Indian Heart J.*, **62**, 273.
49. Fayssoil,A., Nardi,O., Orlikowski,D. and Annane,D. (2010) Cardiomyopathy in Duchenne muscular dystrophy: pathogenesis and therapeutics. *Heart Fail. Rev.*, **15**, 103–107.
50. Politano,L. and Nigro,G. (2012) Treatment of dystrophinopathic cardiomyopathy: review of the literature and personal results. *Acta Myol. Myopathies Cardiomyopathies Off. J. Mediterr. Soc. Myol. Ed. Gaetano Conte Acad. Study Striated Muscle Dis.*, **31**, 24–30.
51. Kiernan,M.C., Burke,D., Andersen,K.V. and Bostock,H. (2000) Multiple measures of axonal excitability: a new approach in clinical testing. *Muscle Nerve*, **23**, 399–409.
52. Krishnan,A.V., Lin,C.S.-Y., Park,S.B. and Kiernan,M.C. (2008) Assessment of nerve excitability in toxic and metabolic neuropathies. *J. Peripher. Nerv. Syst. JPNS*, **13**, 7–26.
53. Cai,H., Erdman,R.A., Zweier,L., Chen,J., Shaw,J.H.,4th, Baylor,K.A., Stecker,M.M., Carey,D.J. and Chan,Y.M. (2007) The sarcoglycan complex in Schwann cells and its role in myelin stability. *Exp. Neurol.*, **205**, 257–269.
54. Perrine,S.P. and Faller,D.V. (1993) Butyrate-induced reactivation of the fetal globin genes: a molecular treatment for the beta-hemoglobinopathies. *Experientia*, **49**, 133–7.
55. Guerron,A.D., Rawat,R., Sali,A., Spurney,C.F., Pistilli,E., Cha,H.-J., Pandey,G.S., Gernapudi,R., Francia,D., Farajian,V., et al. (2010) Functional and molecular effects of arginine butyrate and prednisone on muscle and heart in the mdx mouse model of Duchenne Muscular Dystrophy. *PLoS ONE*, **5**, e11220.
56. Perronnet,C., Chagneau,C., Le Blanc,P., Samson-Desvignes,N., Mornet,D., Laroche,S., De La Porte,S. and Vaillend,C. (2012) Upregulation of brain utrophin does not rescue behavioral alterations in dystrophin-deficient mice. *Hum. Mol. Genet.*, **21**, 2263–2276.
57. Herbin M., Jeanne V., Gasc J. P. and Vidal P. P. (2001) Stereotyped skeletal configurations of cervical column and rest to motion transition underly the motor repertoire in rodent.

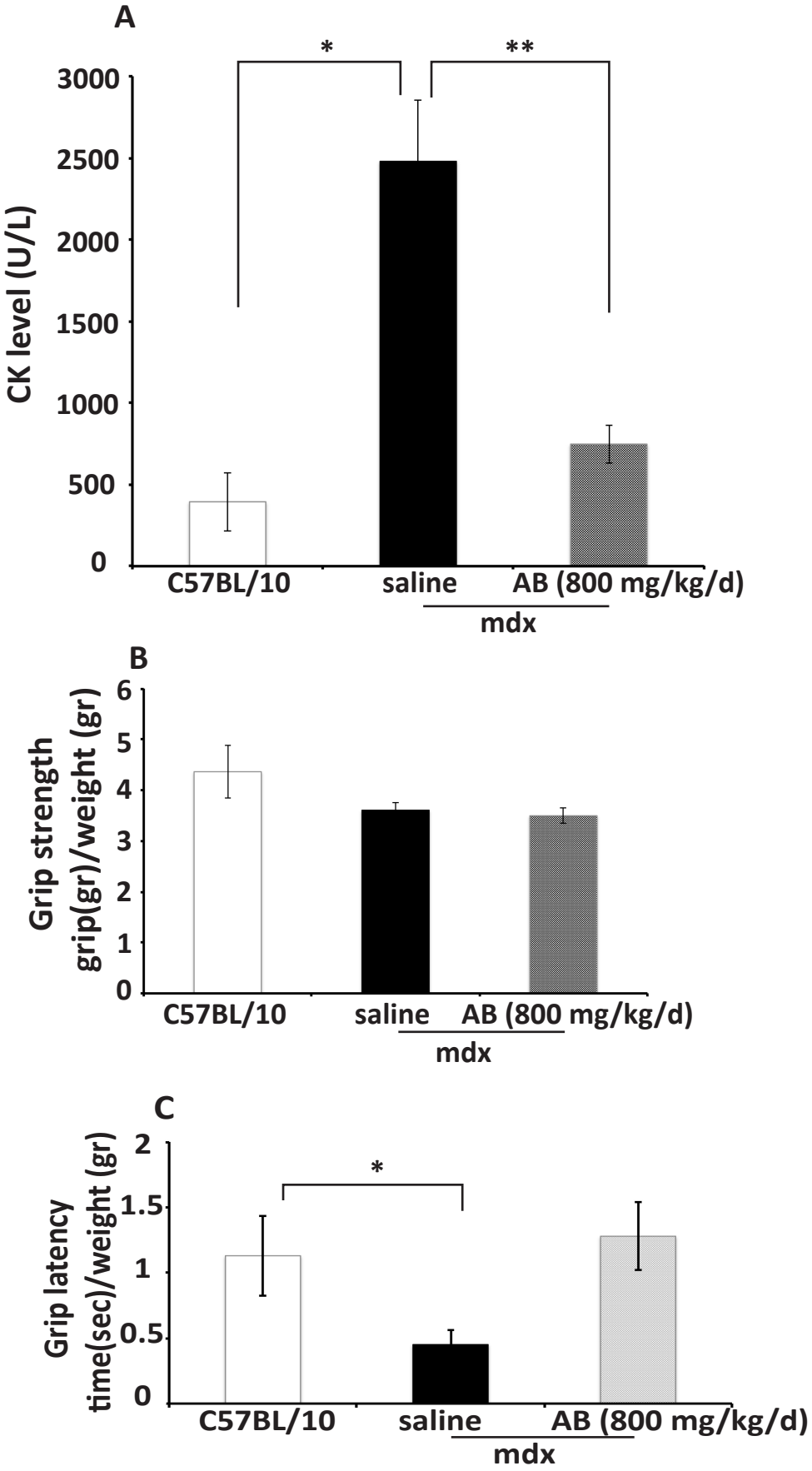

Supplementary Material, Fig. S1: AB treatment alleviates global functional and biochemical parameters in 14-month-old *mdx* mice treated for 7 weeks. (A) Serum CK level. The high value in saline-treated mdx mice (2500 U/l) is decreased about 70% in AB-treated *mdx* mice. (B) Normalized grip strength (grip strength/weight at the end of the treatment) in C57BL/10 mice, and saline- and AB-treated *mdx* mice. No difference is observed between the groups, suggesting a good safety of the product. (C) Normalized inverted grid test shows a complete rescue of performance in AB-treated *mdx* mice compared with saline-treated mdx mice. Statistical test with the level of significance set at 0.05.

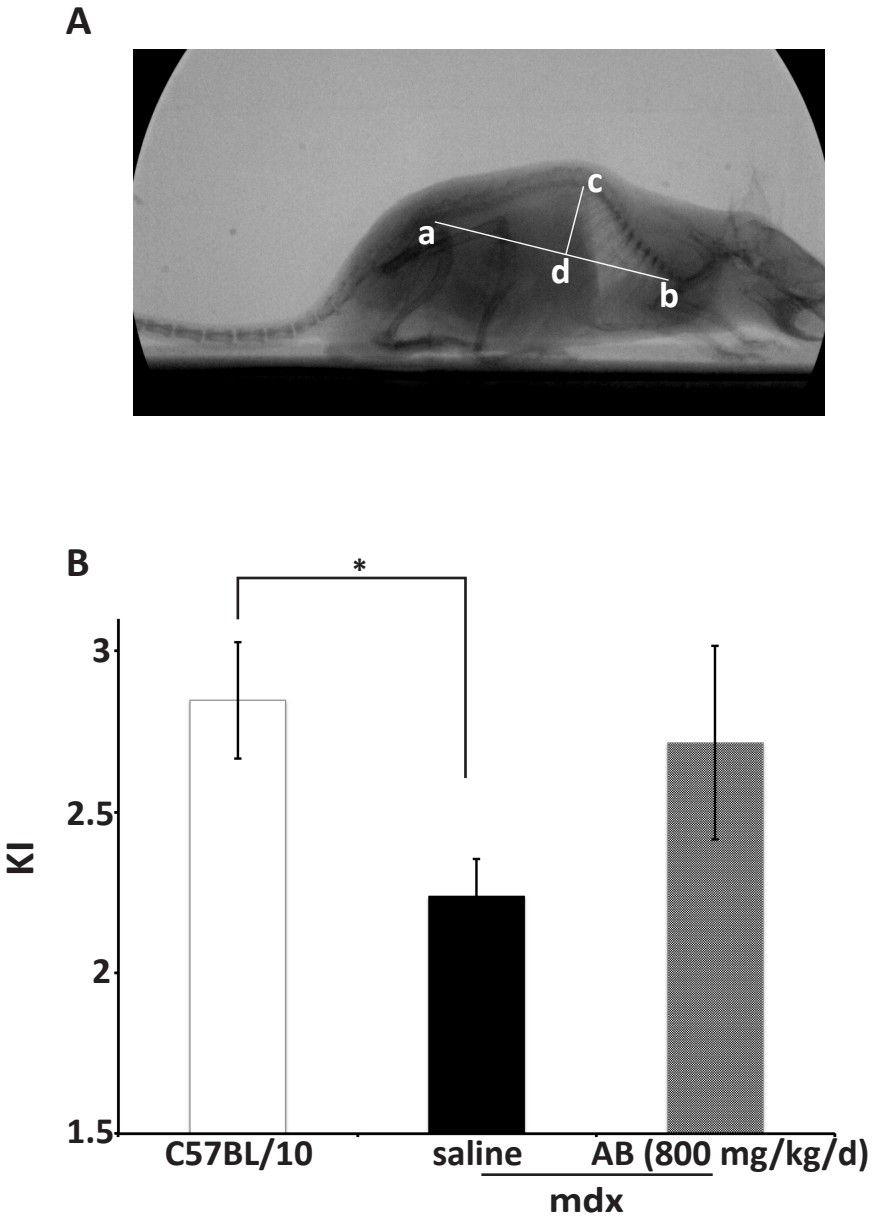

Supplementary Material, Fig. S2: AB treatment alleviates spinal deformity in *mdx* mice treated with AB by force-feeding for 12 months: radiographic procedure. (A) Example of mouse whole body radiography used for the calculation of kyphotic index (KI). Line “ab”, the length of a line drawn from posterior edge of C7 to the posterior edge of L6; line “cd” is the distance from line “ab” to the dorsal border of the vertebral body (KI = ab/cd). (B) The KI value is lower in saline-treated *mdx* mice than in C57BL/10 mice, and comparable in AB-treated *mdx* mice with C57BL/10 value. The rescue of spinal deformity after AB treatment, calculated by MRI, is confirmed with radiographic procedure. Statistical test with the level of significance set at 0.05.

Caudal muscle	C57BL/10	mdx saline
Accommodation half-time (ms) [4]	30.66 ± 1.28	35.85 ± 2.49
S3 (-70%) [4]	93.33 ± 5.49	91.44 ± 6.11
TEd (90-100ms) [4]	47.97 ± 0.73	45.68 ± 1.28
TEd (undershoot) [4]	-8.50 ± 1.26	-8.42 ± 1.07
TEh (10-20ms) [4]	-99.13 ± 1.88	-97.25 ± 2.30
TEh (20-40ms) [4]	-135.40 ± 2.80	-135.60 ± 3.90
TEh (90-100ms) [4]	-177.80 ± 6.10	-198.80 ± 10.50
TEh (overshoot) [4]	8.15 ± 0.81	7.11 ± 0.70
TEh (peak,-70%)[4]	-321.90 ± 10.30	-302.90 ± 16.20
TEh (slope 101-140ms) [4]	3.43 ± 0.14	3.49 ± 0.17
Stimulus-response slope [1]	3.23 ± 1.19	3.92 ± 1.20
Superexcitability (%) [5]	-11.80 ± 0.60	-10.79 ± 1.67
Superexcitability at 5ms (%) [5]	-9.10 ± 0.89	-8.81 ± 1.63
Superexcitability at 7ms (%) [5]	-6.50 ± 0.89	-6.27 ± 1.83
Subexcitability (%) [5]	2.93 ± 0.59	4.70 ± 1.20
Resting I-V slope [3]	0.52 ± 0.03	0.51 ± 0.04
Hyperpolarizing I-V slope [3]	0.43 ± 0.01	0.45 ± 0.02

Plantar muscle	C57BL/10	mdx saline
Accommodation half-time (ms) [4]	29.29 ± 1.12	32.14 ± 8.67
S3 (-70%) [4]	40.33 ± 4.66	22.53 ± 8.14
TEd (40-60ms) [4]	37.71 ± 2.24	35.62 ± 0.89
TEd (90-100ms) [4]	35.02 ± 1.90	34.49 ± 0.35
TEd (undershoot) [4]	-12.47 ± 0.87	-7.80 ± 1.78
TEh (10-20ms) [4]	-68.13 ± 0.29	-64.16 ± 3.07
TEh (20-40ms) [4]	-75.76 ± 1.35	-72.40 ± 5.41
TEh (90-100ms) [4]	-72.11 ± 2.94	-68.94 ± 4.81
TEh (overshoot) [4]	7.58 ± 1.67	3.50 ± 1.25
TEh (peak,-70%) [4]	-174.00 ± 1.05	-154.00 ± 11.00
TEh (slope 101-140ms) [4]	0.71 ± 0.09	0.55 ± 0.08
CMAP amplitude (mV) [1]	2.45 ± 0.14	1.90 ± 0.15
Latency (ms) [1]	2.54 ± 0.12	2.31 ± 0.12
Stimulus-response slope [1]	3.79 ± 1.25	2.15 ± 1.22
Superexcitability (%) [5]	-3.45 ± 1.15	-1.70 ± 0.97
Superexcitability at 5ms (%) [5]	-2.10 ± 1.32	2.47 ± 2.24
Superexcitability at 7ms (%) [5]	-2.94 ± 0.67	3.69 ± 2.66
Subexcitability (%) [5]	6.05 ± 0.31	5.04 ± 2.70
Resting I-V slope [3]	0.82 ± 0.03	0.89 ± 0.05
Hyperpolarizing I-V slope [3]	0.54 ± 0.01	0.61 ± 0.13

Supplementary Material, Table S3: Excitability parameters obtained by stimulating the caudal motor nerve and the tibial branch of the sciatic nerve in 13-week-old C57BL/10 mice and saline-treated mdx mice treated by force-feeding for 7 weeks. Records of the CMAPs from tail and plantar muscles. Complementary table to Tables 2 and 3: List of not modified parameters. Statistical test with the level of significance set at 0.05.

Exponent numbers correspond to parameters of: (1) Stimulus-response relationship, (2) strength-duration relationship (all parameters of this test are modified), (3) current-threshold (I-V) relationship, (4) threshold electrotonus (TEd and TEh are threshold electrotonus in response to constant depolarizing and hyperpolarizing long-duration currents of sub-threshold intensity, respectively), (5) recovery cycle.

	Caudal-*mdx*		Plantar-*mdx*	
	saline-treated	un-treated	saline-treated	un-treated
Strength-duration time constant (ms) [2]	0.36 ± 0.02	0.47 ± 0.06	0.35 ± 0.03	0.33 ± 0.04
Rheobase (mA) [2]	0.26 ± 0.11	0.18 ± 0.18	0.27 ± 1.09	0.28 ± 1.23
Accommodation half-time (ms) [4]	35.85 ± 2.49	40.85 ± 3.28	32.14 ± 8.67	26.87 ± 2.84
S2 accommodation [4]	11.43 ± 0.77	12.29 ± 0.76	7.81 ± 1.58	7.30 ± 1.23
S3 (-70%) [4]	91.44 ± 6.11	98.32 ± 13.90	22.53 ± 8.14	26.46 ± 3.56
TEd (10-20ms) [4]	53.80 ± 1.75	54.28 ± 2.14	41.72 ± 1.61	42.51 ± 1.53
TEd (40-60ms) [4]	44.73 ± 1.25	46.34 ± 1.85	35.62 ± 0.89	31.26 ± 4.01
TEd (90-100ms) [4]	45.68 ± 1.28	41.51 ± 2.06	34.49 ± 0.35	31.24 ± 2.90
TEd (undershoot) [4]	-8.42 ± 1.07	-12.22 ± 1.81	-7.80 ± 1.78	-9.48 ± 1.59
TEd (peak) [4]	53.00 ± 1.58	53.71 ± 1.81	42.30 ± 1.43	42.57 ± 1.11
TEd20 (peak) [4]	32.19 ± 1.07	32.58 ± 2.38	22.42 ± 0.76	22.82 ± 0.44
TEh (10-20ms) [4]	-97.25 ± 2.30	-103.30 ± 4.35	-64.16 ± 3.07	-61.67 ± 3.51
TEh (20-40ms) [4]	-135.60 ± 3.90	-142.10 ± 5.98	-72.40 ± 5.41	-67.44 ± 3.42
TEh (90-100ms) [4]	-198.80 ± 10.50	-195.10 ± 5.97	-68.94 ± 4.81	-61.98 ± 3.56
TEh (overshoot) [4]	7.11 ± 0.70	10.49 ± 3.17	3.50 ± 1.25	8.56 ± 1.61
TEh (peak,-70%) [4]	-302.90 ± 16.20	-350.80 ± 10.40	-154.00 ± 11.00	-161.00 ± 12.78
TEh (slope 101-140ms) [4]	3.49 ± 0.17	3.38 ± 0.14	0.55 ± 0.08	0.60 ± 0.07
CMAP amplitude (mV) [1]	1.11 ± 0.12	1.45 ± 0.11	1.904 ± 0.15	2.572 ± 0.13
Latency (ms) [1]	3.62 ± 0.13	3.57 ± 0.09	2.31 ± 0.12	2.54 ± 0.06
Stimulus (mA) for 50% max response [1]	0.38 ± 0.09	0.36 ± 0.03	0.41 ± 1.09	0.36 ± 1.22
Stimulus-response\slope [1]	3.92 ± 1.20	2.70 ± 1.12	2.15 ± 1.22	2.86 ± 1.15
Relative refractory period (ms) [5]	2.18 ± 1.13	2.66 ± 1.25	nd	nd
Refractoriness at 2ms (%) [5]	3.42 ± 3.70	3.79 ± 3.61	17.95 ± 3.02	28.01 ± 4.00
Refractoriness at 2.5ms (%) [5]	-2.59 ± 2.66	-3.91 ± 2.86	0.79 ± 1.69	-1.79 ± 0.95
Superexcitability (%) [5]	-10.79 ± 1.67	-13.80 ± 2.44	-1.70 ± 0.97	-1.34 ± 0.70
Superexcitability at 5ms (%) [5]	-8.81 ± 1.63	-9.51 ± 3.44	2.47 ± 2.24	0.21 ± 1.44
Superexcitability at 7ms (%) [5]	-6.27 ± 1.83	-6.04 ± 2.11	3.69 ± 2.66	1.87 ± 1.26
Subexcitability (%) [5]	4.70 ± 1.20	3.28 ± 0.72	5.04 ± 2.70	5.50 ± 1.52
Resting I-V slope [3]	0.51 ± 0.04	0.60 ± 0.09	0.89 ± 0.05	1.07 ± 0.12
Minimum I-V slope [3]	0.22 ± 0.01	0.20 ± 0.01	0.42 ± 0.01	0.41 ± 0.02
Hyperpolarizing I-V slope [3]	0.45 ± 0.02	0.46 ± 0.02	0.61 ± 0.13	0.46 ± 0.04

Supplementary Material, Table S4: Excitability parameters obtained by stimulating the caudal motor nerve and the tibial branch of the sciatic nerve in 13-week-old untreated and saline-treated *mdx* mice treated by force-feeding for 7 weeks. Records of the CMAPs from tail and plantar muscles. No significant difference is detected, indicating the absence of effect of the force-feeding procedure by itself ($p \geq 0.056$). Statistical test with the level of significance set at 0.05.
Exponent numbers correspond to parameters of: (1) Stimulus-response relationship, (2) strength-duration relationship, (3) current-threshold (I-V) relationship, (4) threshold electrotonus (TEd and TEh are threshold electrotonus in response to constant depolarizing and hyperpolarizing long-duration currents of sub-threshold intensity, respectively), (5) recovery cycle. Nd: not determined

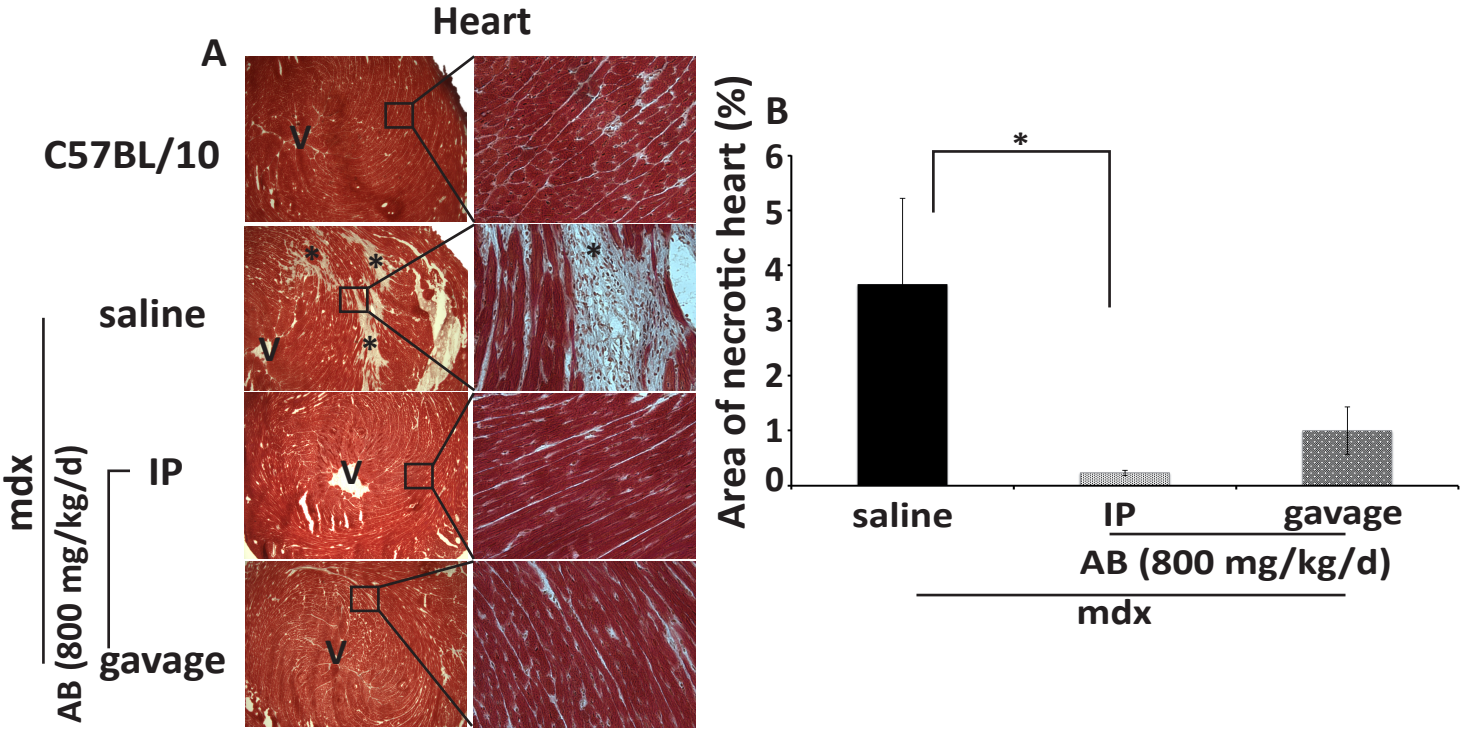

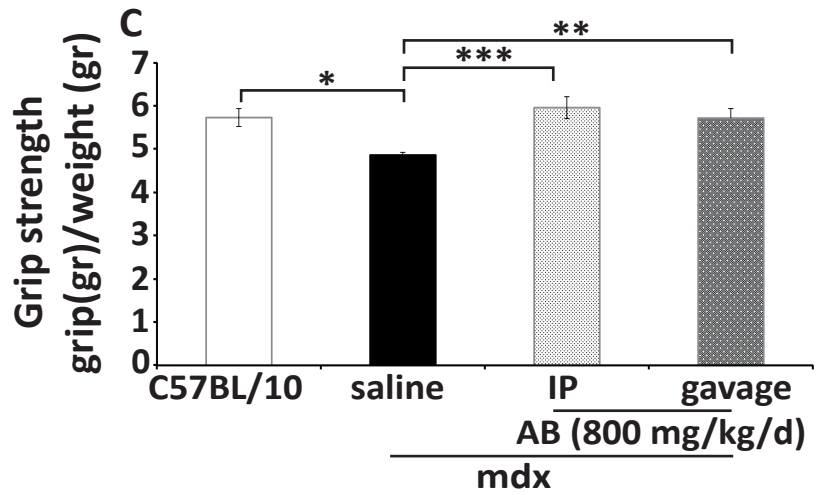

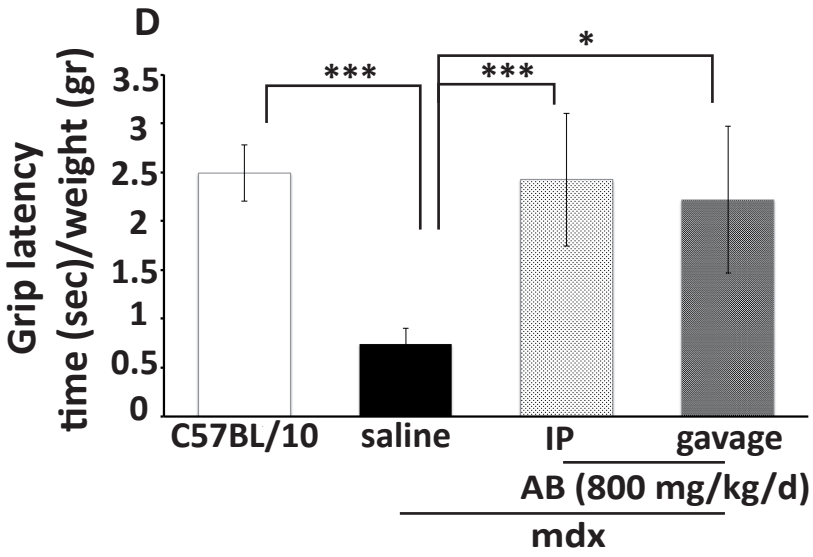

Supplementary Material, Figure S5: Comparison of the profits of force-feeding procedure and intraperitoneal injection of AB. The two ways of administration of AB provide comparable profits in 13-week-old mdx mice. (A) Masson's trichrome staining of heart slices from C57BL/10, saline- and AB-treated mdx mice. Necrotic zones are clearly visible (stars) in saline-treated mdx mice and absent in AB-treated mdx mice for both ways of administration. V: ventricle. Magnification, 5X and 40 X. (B) The quantification, by using ImageJ software, confirms the reduction of the surface of necrotic zones in AB-treated mdx mice. Normalized (value/weight at the end of the treatment) grip strength (C) and inverted grip (D) tests in C57BL/10 mice, and saline- and AB-treated mdx mice. The values in saline-treated mdx mice are reduced by about 15% and 30%, respectively, compared those of C57BL/10 mice. AB treatment improves values of saline-treated mdx mice, reaching those of C57BL/10 animals, for both ways of administration. Statistical test with the level of significance set at 0.05.

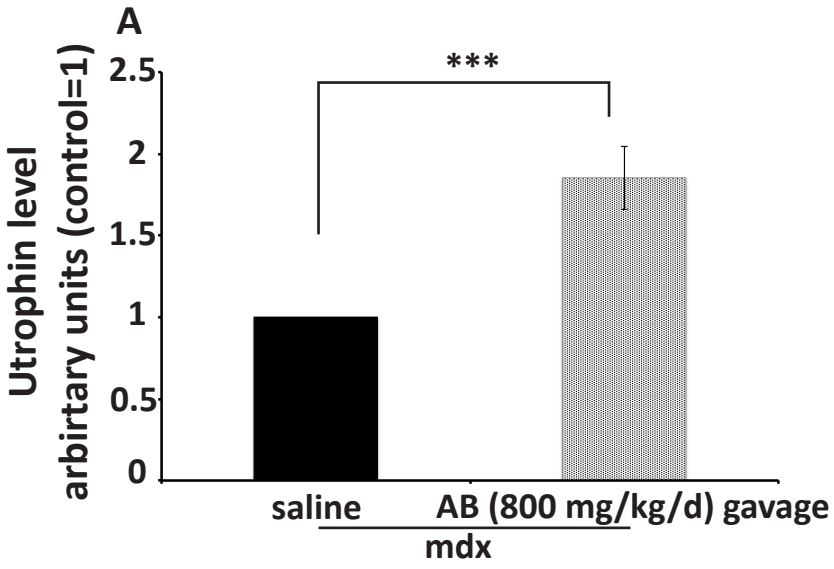

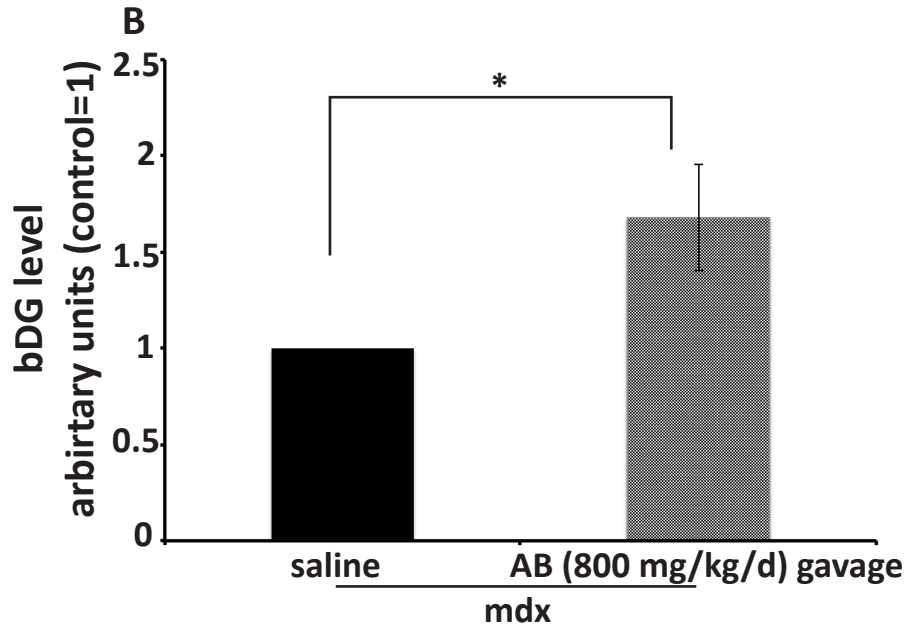

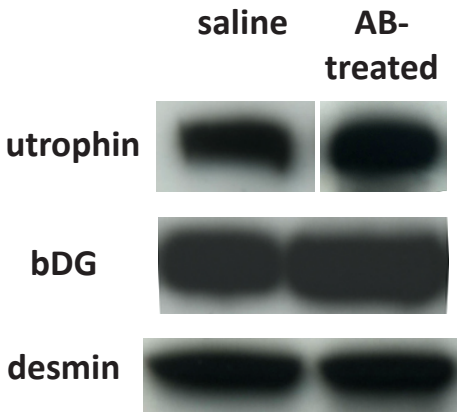

Supplementary Material, Fig. S6: Effect of AB on utrophin and beta-dystroglycan (bDG) levels in heart in 13-week-old *mdx* mice treated for 7 weeks. Semi-quantitative western-blot analysis of utrophin (A) and bDG (B) proteins. An about 2-fold increase in utrophin and bDG levels is detected in AB-treated *mdx* mice. (C) Example of western blot membrane of heart protein extract from saline- and AB-treated *mdx* mice.

	Caudal-*mdx*		Plantar-*mdx*	
	AB-gavage	AB-i.p.	AB-gavage	AB-i.p.
Strength-duration time constant (ms)[2]	0.44 ± 0.06	0.56 ± 0.09	0.43 ± 0.05	0.42 ± 0.10
Rheobase (mA)[2]	0.22 ± 0.13	0.22 ± 0.14	0.19 ± 1.22	0.18 ± 1.33
Accommodation half-time (ms)[4]	38.95 ± 5.12	34.45 ± 4.82	26.06 ± 1.70	24.02 ± 1.85
S2 accommodation[4]	16.94 ± 2.56	13.45 ± 1.40	10.85 ± 0.88	18.26 ± 1.03
S3(-70%)[4]	79.06 ± 12.20	99.37 ± 6.83	31.89 ± 3.31	34.54 ± 2.42
TEd (10-20ms)[4]	55.32 ± 4.89	58.20 ± 3.13	50.99 ± 3.37	53.37 ± 1.03
TEd (40-60ms)[4]	46.17 ± 3.02	47.24 ± 1.69	35.65 ± 1.21	36.62 ± 1.14
TEd (90-100ms)[4]	42.52 ± 2.36	43.63 ± 1.42	34.51 ± 1.52	35.94 ± 1.22
TEd (undershoot)[4]	-11.53 ± 1.92	-8.01 ± 1.22	-8.17 ± 1.38	-7.54 ± 1.45
TEd (peak)[4]	54.95 ± 4.29	57.07 ± 1.93	47.09 ± 2.36	46.21 ± 1.81
TEd 20(peak)[4]	34.05 ± 2.20	34.78 ± 1.22	23.54 ± 0.97	23.84 ± 0.44
TEh (10-20ms)[4]	-91.16 ± 5.55	-100.60 ± 3.73	-67.78 ± 1.80	-65.83 ± 1.56
TEh (20-40ms)[4]	-132.70 ± 3.75	-136.80 ± 4.86	-68.43 ± 1.98	-70.15 ± 2.70
TEh (90-100ms)[4]	-185.10 ± 7.88	-180.50 ± 9.66	-65.21 ± 2.44	-65.52 ± 3.46
TEh (overshoot)[4]	9.35 ± 2.33	9.19 ± 0.60	5.63 ± 0.87	5.27 ± 0.66
TEh (peak,-70%)[4]	-346.20 ± 10.50	-333.90 ± 12.40	-165.80 ± 14.78	-153.40 ± 8.00
TEh (slope 101-140ms)[4]	3.49 ± 0.19	3.21 ± 0.30	0.65 ± 0.07	0.48 ± 0.08
CMAP amplitude (mV)[1]	1.05 ± 0.12	1.20 ± 0.11	2.29 ± 0.13	2.19 ± 0.12
Latency (ms)[1]	4.03 ± 0.11	3.71 ± 0.07*	2.44 ± 0.12	2.40 ± 0.08
Stimulus (mA) for 50% max response[1]	0.35 ± 0.11	0.36 ± 0.10	0.27 ± 1.19	0.27 ± 1.25
Stimulus-response slope[1]	2.20 ± 1.26	1.93 ± 1.24	2.20 ± 1.18	2.06 ± 1.20
Relative refractory period (ms)[5]	2.26 ± 1.17	1.73 ± 1.08	2.27 ± 1.06	nd
Refractoriness at 2ms (%)[5]	8.46 ± 9.49	-3.84 ± 2.17	7.32 ± 4.14	7.38 ± 1.98
Refractoriness at 2.5ms (%)[5]	-3.00 ± 5.87	-10.02 ± 1.41	-13.25 ± 3.79	6.80 ± 4.66
Superexcitability (%)[5]	-10.11 ± 2.76	-16.60 ± 2.70	-2.30 ± 0.83	-1.64 ± 1.26
Superexcitability at 5ms (%)[5]	-9.35 ± 2.55	-10.99 ± 0.83	1.12 ± 1.90	0.48 ± 1.76
Superexcitability at 7ms (%)[5]	-6.27 ± 2.17	-7.92 ± 0.78	2.69 ± 1.56	2.40 ± 1.99
Subexcitability (%)[5]	4.07 ± 0.90	5.90 ± 2.49	3.70 ± 1.00	5.71 ± 1.53
Resting I-V slope[3]	0.53 ± 0.03	0.59 ± 0.10	0.96 ± 0.06	0.83 ± 0.06
Minimum I-V slope[3]	0.21 ± 0.03	0.24 ± 0.01	0.47 ± 0.04	0.44 ± 0.03
Hyperpolarizing I-V slope[3]	0.55 ± 0.11	0.40 ± 0.02	0.55 ± 0.02	0.48 ± 0.03

Supplementary Material, Table S7: Excitability parameters obtained by stimulating the caudal motor nerve and recording the CMAP from caudal muscle in 13-weeks-old treated *mdx* mice treated with AB by intraperitoneal (i.p.) injection or force-feeding procedure for 7 weeks. No significant difference is detected between the two administration modes. Statistical test with the level of significance set at 0.05.

Exponent numbers correspond to parameters of: (1) Stimulus-response relationship, (2) strength-duration relationship, (3) current-threshold (I-V) relationship, (4) threshold electrotonus (TEd and TEh are threshold electrotonus in response to constant depolarizing and hyperpolarizing long-duration currents of sub-threshold intensity, respectively), (5) recovery cycle. Nd: not determined.

3.3 Manuscript 3. “Low doses of arginine butyrate derivatives alleviate dystrophic phenotype and restore the membrane integrity in *DMD* murine model.”

Low doses of arginine butyrate derivatives alleviate dystrophic phenotype and restore the membrane integrity in *DMD* murine model.

Sara Vianello[1], Francesca Consolaro[1], Claudia Bich[2], José-Manuel Cancela[3], Morgane Roulot[1], Erwan Lanchec[3], David Touboul[2], Alain Brunelle[2], Maurice Israël[1], Evelyne Benoit[1], Sabine de la Porte[1]

[1] CNRS, Institut de Neurobiologie Alfred Fessard – FRC2118, Neurobiologie & Développement, UPR 3294, Gif sur Yvette, F-91198, France; [2] Centre de Recherche de Gif, Institut de Chimie des Substances Naturelles, CNRS UPR2301, Avenue de la Terrasse, Gif sur Yvette, F-91198, France; [3] CNRS- Université Paris Sud, Centre de Neurosciences Paris-Sud, UMR 8195, Orsay, F-91405 France

Correspondence should be addressed to Sabine de la Porte: CNRS, Avenue de la Terrasse, Bat.32/33, Institut de Neurobiologie Alfred Fessard, Neurobiologie & Développement, UPR 3294, Gif sur Yvette, F-91198, France. Phone: 33 1 69 82 36 27, fax: 33 1 69 82 34 47, E-mail: sabine.delaporte@inaf.cnrs-gif.fr

Short title: DMD per os *AB* derivatives

ABSTRACT

A curative/palliative approach was investigated to treat Duchenne muscular dystrophy through the covalent association of two pharmacological activities, the nitric oxide (NO)-pathway, activated by arginine, and histone deacetylase (HDAC) inhibition, thanks to butyrate action, in *mdx* mice and patient's myotubes. Two prodrugs were synthesised, with arginine and butyrate linked by ester or amide bounds and the beneficial effects on dystrophic phenotype were addressed. A non-invasive automatized method has been applied to measure nerve excitability parameters in *mdx* mice. The abnormalities detected in saline-treated mice were quasi totally rescued in treated animals with a maximum effect at low doses (50-100 mg/kg/d) tested. In addition, force measured by grip strength test and tirelessness measured by inverted grid test were improved by about 60% and 3.5 fold, respectively. The percentage of surface of necrosis in heart section was reduced by about 90% in treated mice. More than 50% decreased of creatine kinase level in the serum attested a global improvement of muscles. The restoration of membrane integrity was directly addressed by measuring the reduction (about 74%) of the Evans blue incorporation in myofibers of limb in treated animals, and by the observation of the normalisation of the lipid composition in heart membrane through mass spectrometry imaging techniques. In addition two new cardiac markers (the deprotonated fatty acid C16:0 and the ratio R3 (C18:1 over C18:2 fatty acid ion signals)) of dystrophy were identified by mass spectrometry.

In cultures of human myotubes both prodrugs increase by around 2-4 fold utrophin and related proteins (β-dystroglycan and embryonic myosin) levels and utrophin was correctly addressed at the membrane. The potential ability of the HDAC inhibitor function of the prodrugs to increase the expression of utrophin and related proteins by around 2-4 fold was demonstrated. Finally, the 50% reduction in number of DMD myotubes showing spontaneous Ca^{2+} spikes after treatment acting on the NO-pathway activation and/or with HDAC inhibitors, suggest that drug treatments has also an effect on Ca^{2+} homeostasis critically perturbed in DMD cells.

Globally, the beneficial effect on many structural and functional dystrophic parameters, in particular on membrane integrity, previously obtained with high doses of arginine butyrate (AB, the salted formulation) administered per os, was observed with doses 10 and 5 times lower, *in vivo* and *in vitro*, respectively, with both compounds.

ABBREVIATION: *AB*: arginine butyrate, *ABA*: N-butyrylarginine, *ABE*: 3-hydroxybutyrate arginate, CK: creatine kinase, CMAP: compound muscle action potential, DMD: Duchenne muscular dystrophy, HDAC: histone deacetylases, MALDI-TOF: matrix-assisted laser desorption/ionization time-of-flight , NO: nitric oxide, NOS: nitric oxide

synthase, TOF-SIMS: time-of-flight secondary ion mass spectrometry

KEY WORDS: DMD, *mdx*, therapy, pharmacology, utrophin, NO, histone deacetylase, mass spectrometry imaging, MALDI-TOF, TOF-SIMS, calcium homeostasis, neuromuscular excitability.

INTRODUCTION

Duchenne muscular dystrophy (DMD) is a progressive neuromuscular disease affecting 1/3500 male at birth. It is caused by a mutation of a gene located at the *Xp21* locus coding for dystrophin, a sub-sarcolemmal protein. Dystrophin, a 427 kDa protein, is the central component of the dystrophin-associated protein complex that links cytoskeletal actin to extracellular matrix, thus maintaining muscle fiber membrane integrity. The lack of this protein induces a weakness of skeletal, smooth and cardiac cells, due to mechanical muscle contraction, leading to dramatic muscle deterioration. In addition to this principal alteration, Ca^{2+} leakage, oxidative stress, inflammatory response and fat infiltration were observed in human dystrophic muscle (Blake et al., 2002).

Curative approaches, such as cell, gene and pharmacological therapies, are currently investigated, but they still show some limitations (Finkel, 2010; Goyenvalle and Davies, 2011; Meregalli et al., 2010; Pichavant et al., 2011). Pharmacological approaches aim to alleviate the pathology downstream of the primary membrane defect, target abnormal calcium influx, oxidative stress, inflammation, fibrosis and necrosis (Fairclough et al., 2011). Currently, the only treatment approved to try to stem the relentless progression of muscle wasting in DMD patient is in the form of corticosteroids which have very limited benefits and are plagued by a number of side effects.

In a previous work, we successfully tested arginine butyrate (*AB*), which combines two pharmacological activities [nitric oxide (NO)-pathway activation by arginine and histone deacetylase (HDAC) inhibition by butyrate] in *mdx* mice (the murine model for DMD) and DMD myotubes (Vianello et al., 2013). The assumption of studying *AB* in *mdx* mice originates from the observation that butyrate is able to re-express foetal forms of proteins, such as the foetal form of hemoglobin, in erythroid progenitors of patients with beta globin disorders (Perrine and Faller, 1993a). Sodium butyrate was first used for the treatment of sickle cell anemia in children, then substituted by *AB*, to limit the volume of sodium injected (Perrine, 2008). Many of the structural, biochemical and functional hallmarks of the *mdx* mice were improved by *AB* treatment after intraperitoneal administration. In addition, we demonstrated that both components, L-arginine and butyrate, act synergically (Vianello et al., 2013). The benefits of the oral administration of *AB* have been recently addressed in *mdx* mice, on the three main noticeable deficits of DMD patients (cardiomyopathy, vertebral column deformation and electromyogram defaults), with a range of functional and structural approaches. We demonstrated that *AB* plays a protective role on the progressive cardiomyopathy, which worsens over age in *mdx* mice. We also observed a significant attenuation of the kyphosis that settles down, by measuring the index of deformity in *AB*-treated animals. Finally, we applied a minimal invasive method that has been developed in human and then adapted to animals, to supply conventional extracellular electrophysiological procedures (Boerio et al., 2009; Bostock et al., 1998), in order to investigate ion conductance and membrane properties. We have shown that the abnormalities detected in saline-

treated *mdx* mice are corrected after *AB* treatment (Vianello et al., submitted). All these results make us confident of a possible clinical study of *AB* in order to treat DMD patients.

Based on the fact that nowadays AB is administered as an infusion twice a month to sickle cell anemia patients, and intraperitoneally to animals, and regarding the positive results obtained with *mdx* mice orally treated, it would be very useful to have products "of second generation" that could be administrated *per os* and at lower doses than those currently applied, for future non-invasive clinical trials in DMD patients. Two products based on *AB* formulation have been synthesised: 3-hydroxybutyrate arginate, with an ester link (referenced as *ABE*), and N-butyrylarginine with an amide link (referenced as *ABA*). A covalent link confers more stability to the molecules, which could thus pass the gastric barrier without being decomposed, in particular by the intestinal arginase, and allow predicting efficiency at lower doses. In the present study, *ABE* and *ABA* were tested *in vivo* on *mdx* mice to estimate their capacity to ameliorate dystrophic phenotype and improve utrophin expression. Mice were treated for an intermittent period by force-feeding using escalating doses of *ABE* and *ABA* to address the expected benefit and to determine the optimal dose.

Electromyography and nerve conduction studies have been performed in DMD patients and in *mdx* mice (reviewed in (Vianello et al., 2013)). Globally, although nerve conduction is normal in early DMD patients, the compound muscle action potential (CMAP), which idealizes the summation of a group of action potentials from several muscle fibers in the same area, decreases in amplitude as the disease progresses (Yiu and Kornberg, 2008). In *mdx* mice the absence of dystrophin in the postsynaptic membrane has little effect on the function of the neuromuscular junction, but the degeneration and regeneration of the fibers lead to remodeling of the pre- and postsynaptic components. A multimodal evaluation of excitability was performed in *mdx* mice using a minimally invasive method that has been developed to supplement conventional electrophysiological methods and to investigate ion conductance and membrane properties in human (Bostock et al., 1998) and then adapted to mouse models (Boerio et al., 2009). The protocol includes different tests designated to measure, in particular, a great number (more than 30) of nerve excitability parameters.

The functional improvement of skeletal muscle was completed by an evaluation of muscle function in treated-*mdx* mice using a measure of force (grip strength test) and tirelessness (inverted grid test). The increase in utrophin expression, already demonstrated with AB (Vianello et al., 2013) was checked in ABE-treated *mdx* mice. In addition, because 100% of DMD patients over 18 years develop a cardiomyopathy, we addressed the benefit of *ABE* and *ABA* on cardiac necrosis, at this age because any functional signs of cardiomyopathy could be observed in young *mdx* mice (Quinlan et al., 2004; Spurney et al., 2008).

Whatever the pharmacological strategy envisaged to reverse dystrophic phenotype in DMD patients, it cannot be effective without restoration of sarcolemmal integrity through dystrophin re-expression or utrophin overexpression. The restoration of the membrane integrity was addressed dosing creatine kinase (CK) level in the serum, measuring Evans blue incorporation in myofibers in limb, and completed by an analysis of the lipid

composition of the heart membrane using two mass spectrometry imaging techniques: matrix-assisted laser desorption/ionization time-of-flight (MALDI-TOF) and cluster-time-of-flight secondary ions mass spectrometry (cluster-TOF-SIMS). These two techniques were previously applied with success to study lipid composition in *mdx* mouse limb muscle (Benabdellah et al., 2009; Tahallah et al., 2008; Touboul et al., 2004, 2005).

In parallel, *ABE* and *ABA* were tested *in vitro* on human muscular cell cultures to investigate their capacity to promote the increase of utrophin level and to address it at the membrane. Because of the ability of butyrate to re-express foetal forms of hemoglobin, we also addressed the potential faculty of HDAC inhibitors to increase, by themselves, the expression of utrophin in human myotubes. In particular, butyrate, valproic acid (2-n-propylpentanoic acid), trichostatin A and isobutyramide, currently used in medicine, increase the level of utrophin that is correctly localised at the membrane.

Finally, we explore the effects of the treatment, associating the NO-pathway activation and/or the HDAC inhibition, on calcium homeostasis in DMD myotubes, recording spontaneous Ca^{2+} spikes. It is well-known that the alteration of calcium homeostasis in dystrophic fibers is largely implicated in the cascades leading to muscle necrosis/degeneration, in particular Ca^{2+} could accumulate through membrane tears due to the lack of dystrophin (Whitehead et al., 2006). Persistent Ca^{2+} influx activates Ca^{2+}-dependent proteolytic and phospholipolytic activities result in the degradation of dystrophic muscle fibres (Constantin et al., 2006). In this study, the recording of spontaneous Ca^{2+} spikes was also performed to complete the *in vivo* results on the restoration of sarcolemmal integrity.

MATERIALS & METHODS

Drugs

In vivo and *in vitro* doses and concentrations used are indicated in **Table 1**. *ABE* and *ABA* were synthethised by Syntheval (Caen, France) (**Supplementary data 1**).

AB preparation

L-arginine and n-butyric acid (Sigma-Aldrich, Lyon, France) were added in miliQ water to make a 26% stock solution (1 M arginine – 1 M butyrate, pH = 7), as previously described (Perrine and Faller, 1993b). The stock solution was diluted in phosphate buffer solution (PBS) (Sigma-Aldrich, Lyon, France) for cell cultures and in 0.9% NaCl for force-feeding procedures.

Mouse experimental procedures

Since DMD is an X-linked genetic disorder, studies were performed using male mice. All experiments were carried out in accordance with the guidelines established by the European Communities Council Directive (Guide for the Care and Use of Laboratory Animals: EEC86/609 Council Directive - Decree 2001-131). The experimental protocols have been approved by the French Departmental Direction of Animal Protection (number A91-453).

Adult *mdx* and wild-type (C57Bl/10) mice were aged 6 weeks at the start of experiments. Animals were weighed before each treatment administration. Treatment was administered by means of a force-feeding procedure (1 mL/100 g body weight), with flexible canulas (PHYMEP, Paris, France). Animals were assigned to the saline (0.9% NaCl) or treated group (*ABE* or *ABA* at doses 50, 80, 100, 200, 400 or 800 mg/kg/d,

Table 1: Drugs, concentrations and doses used

Drug name	Abbreviation	*In vitro* doses****	*In vivo* doses
Arginine butyrate*	*AB*	0.002, 0.005, 0.02, 0.05, 0.1, 0.2, 0.5, 1 and 2 mM	
3-Hydroxybutyrate arginate**	*ABE*		50, 80, 100, 200, 400 and 800 (mg/kg/d) (20, 30, 37, 77, 154, 308 mM)
N-Butyryl arginine**	*ABA*		50, 80, 100, 200, 400 and 800 (mg/kg/d) (18, 28, 35, 71, 143, 285 mM)
Trichostatin A***	*TSA*	0.05, 0.1, 0.5 and 1 µM	
Valproic acid***	*VPA*	0.25, 0.5, 1 and 2 mM	
Sodium butyrate***	*B*	0.1, 0.5, 1 and 5 mM	
Isobutyramide***	*ISO*	0.5, 1, 2 and 5 mM	

* See the preparation in in section Materials & Methods.
**Synthesised by Syntheval, Caen, France.
*** Purchased from Sigma-Aldrich, Lyon, France
****Doses used in vitro are 200 times lower than doses used in vivo

corresponding to 20-308 mM for *ABE* and 18-285 mM for *ABA*) in an intermittent protocol consisting in a series of 4 consecutive daily administrations every 2 weeks for 7 weeks. *In vivo* global functional evaluations were performed blind and carried out 24 h after the end of the treatment by measuring muscle force (grip strength test) and tirelessness (inverted grid test), then neuromuscular excitability. Mice were anesthetised with 10% pentobarbital, blood samples were taken from the heart for measurement of serum CK levels, and animals were sacrificed by cervical dislocation. Heart and *gastrocnemius* muscle were dissected out and frozen for structural and biochemical analyses. Two additional groups of animals (saline and *ABE* 80 mg/kg/d) were treated for specific visualization of Evans blue dye incorporation in necrotic fibres after intraperitoneal injection of the dye in living animal.

Neuromuscular excitability recordings

The multimodal evaluation of neuromuscular excitability was assessed, *in vivo*, by means of a minimally-invasive electrophysiological method, using the QTrac© software (written by Prof. Hugh Bostock, Institute of Neurology, London, UK), on mice under isoflurane anesthesia as previously described (Boerio et al., 2009). Briefly, an anesthetized mouse was placed on a heating pad to maintain body temperature between 35.2 and 35.8°C (measured using a rectal probe), and submitted to two sessions of excitability testing (TRONDE protocol) applied consecutively on the tail and rear leg. Electrical stimulations were delivered to either the caudal motor nerve or the tibial branch of sciatic nerve, by means of surface electrodes, and the CMAP was recorded using needle electrodes inserted into the caudal or plantar muscle, respectively. Excitability measurements consisted in five different tests (stimulus-response, strength-duration and current-threshold relationships, as well as threshold electrotonus and recovery cycle) from which more than thirty parameters were determined and analyzed. It is worth noting that each specific excitability test provides additional and complementary information regarding the functional status of ion channels and electrogenic pumps, as well as membrane properties (Kiernan et al., 2000; Krishnan et al., 2008). Hence, the first group of parameters, obtained from the stimulus-response relationship, describes the amplitude of the CMAP in relation with the intensity of the stimulation (*i.e.* the current applied). The second group is obtained from the strength-duration relationship derived from the intensity-duration curve that determines the intensity in relation with the duration of the stimulation necessary to evoke a CMAP. The third group is obtained from the current-threshold relationship establishing the excitability modifications in response to depolarizing and hyperpolarizing currents. The fourth group is obtained from the threshold electrotonus that allows, in particular, studying the accommodation properties of axonal membranes in response to depolarizing and hyperpolarizing long-duration currents applied at sub-threshold intensity. Finally, the fifth group of parameters is obtained from the recovery cycle that characterizes the excitability fluctuations (as the percent of threshold change) during (*i.e.* the duration of the relative refractory period determined as the first intercept on the x-axis, and the refractoriness determined as percents of threshold change for an interstimulus delay of 2 and 2.5 ms) and after an action potential (*i.e.* the superexcitability, produced by the depolarizing after

potential and determined as percents of threshold change for an interstimulus delay of 5 and 7 ms, and the late subexcitability determined as percent of threshold change for an interstimulus delay over 10 ms).

Grip strength test

In vivo functional evaluations of combined forelimb and hindlimb grip strength was performed blind and carried out 24 h after the end of the treatment. The muscle force was measured using a grip-strength meter (Bioseb). The apparatus consisted of a grid connected to a digital dynamometer. The animals were gently lowered over the top of the grid so that both sets of front paws and hind paws could grip the grid. While the torso of the animal was kept parallel to the grid, the animal was gently pulled back by the tail until it released its grip. This procedure was repeated three times and the values were averaged and normalized to mouse body weight.

Inverted grid test

Mice were placed individually on a cage wire grid, about 35 cm above a work-top. After slowly turning the grid through 180°, the length of time the mice continued to grip the grid was monitored (grip latency), a maximal score of 180 sec being given if the animal did not fall. This procedure was repeated three times. The values were averaged and normalised to mouse body weight.

Serum CK determination

Blood samples were taken from hearts of anaesthetized mice immediately before sacrifice. Serum CK activity was determined using a bioMerieux kit (enzyline CK NAC optimized 10).

Immunoblot analyses

The proteins were extracted from muscle samples and myotubes extract in a buffer containing 10 mM Tris-HCl, 1 mM EDTA and 10% SDS (pH 6.8). The total protein content was determined according to DC Protein Assay protocol (Bio-Rad). Proteins were separated into a multiplex NuPAGE® 4-12% Bis-Tris Gel (X-Cell II Mini Cell, Invitrogen, France) with a molecular weight marker (Rainbow™, Amersham Pharmacia Biotech) and then electroblotted onto an immobilon-P polyvinyl membrane in order to obtain the display of utrophin (395 kD); the protein of interest, embryonic myosin (220 kD); a marker of regeneration, β-dystroglycan (43 kD); a member of the dystrophin complex, desmin, actin, and GAPDH (53 kD, 42 kD, 37 kD, respectively); proteins of reference used as loading controls and protein normalization). We applied Coomassie G250 stain to verify the equal loading of gels.

After transfert, the membranes were incubated for 90 min with tris buffered saline with Tween 20 (TBST) added with 4% milk to saturate sites of non-specific binding. Then, they were incubated for 2 h with a mix of primary antibodies specific for monoclonal utrophin (NCL-DRP 2, 1/250 dilution, Novocastra Laboratories), β-dystroglycan (NCL-beta-DG, 1/50 dilution, Novocastra Laboratories), and/or embryonic myosin (*in vivo*: NCL-MHCd, 1/50 dilution, Novocastra; *in vitro*: ALX-805-504, 1/50 dilution, Enzo Life Sciences, Villeurbanne, France), desmin (D33, 1/500 dilution, Dako, Les Ulis, France), GAPDH (1/200 dilution, Sigma-Aldrich, Lyon, France), actin (1/2666 dilution, Dako, Les Ulis, France) and then for 1 h with a secondary sheep anti-mouse antibody linked to horseradish peroxidase (1/4000 dilution, Biorad, Marnes-la-Coquette, France). The chemiluminescence detection was done with SuperSignal® West Pico

(Thermo scientific) or SuperSignal® West Phemto (Thermo scientific). Quantification of band intensity on film (GE Healthcare, Aulnay-sous-Bois, France) was performed using the 'Claravision' analyser software. Results were expressed as a percentage of values obtained in saline-treated mice. Experiments were repeated at least three times. For each experiment, the results in treated mice were normalized to the values obtained in saline-treated mice (treated/saline ratio). Quantification was performed on films obtained after different exposure times for distinct proteins (around 30 sec for β-dystroglycan, 2 min for desmin and utrophin) but, within quantifications of a given target protein, the same exposure times were used for the different doses shown on the histograms.

Masson's trichrome stain

Cryostat muscle sections (8 µm) were stained with Masson's trichrome stain to visualize connective tissue and muscle fibers in pink and collagen in blue (Sigma kit #HT15, USA), then observed using a Leica DM RXA2 microscope (Leica Microsystems, Germany). The sections were photographed using a CoolSNAP camera (Roper Scientific, USA) and Openlab acquisition software (Improvision, UK).

Evans blue dye

Evans blue dye (10 mg/mL) in PBS was prepared extemporaneously and filtered through paper (Straub et al., 1997). A volume of 100 µL/10 g body weight was injected 9 h prior to sacrifice. Limbs were excised, frozen for cryostat sections and fixed in 3% paraformaldehyde for 5 min before mounting. Tissue sections were observed using a Leica DM RXA2 fluorescent-imaging microscope (Leica Microsystems, Germany). Image capture was performed with a CoolSNAP camera (Roper Scientific, USA) and Openlab software (Improvision, UK).

MALDI-ToF imaging and TOF-SIMS

Cryostat muscle sections (16 µm) were deposited onto stainless steel MALDI plates for MALDI imaging or onto silicon wafers (2 in. diameter polished silicon wafers, ACM, Villiers-Saint-Frédéric, France) for TOF-SIMS analyses. Immediately before analyses, samples were dried under a pressure of a few hPa for 15 min without any further treatment, and optical images were then recorded with an Olympus BX51 microscope (Rungis, France), monitored by Cell^{B} software (Soft Imaging System, GmbH, Münster, Germany).

For the MALDI-MS imaging, the matrix solution (10 mg/mL in acetonitrile/water/trifluoroacetic acid, 70/30/0.1 for α-cyano-4-hydroxy-cinnamic acid for the positive ion mode and in ethanol/water 70/30 for 9-aminoacridine for the negative ion mode) was deposited homogeneously on the sample plate using a TM sprayer (HTX Imaging, Carrboro, NC, USA). The coated sample plates were thus analysed with a 4800 MALDI ToF/ToF mass spectrometer (AB Sciex, Les Ulis, France) equipped with a 200 Hz Nd/YAG pulsed laser. The data were acquired in the positive ion mode at an accelerating potential of 20 kV and a delayed extraction time of 250 ns. The number of laser shots per pixel was set to 120, and the distance between two adjacent pixels was fixed to 50 µm, which is a bit more than the diameter of the crater formed onto the tissue surface. Mass spectra were recorded between *m/z* 400 and *m/z* 1000. In the case of the negative ion mode, the delayed extraction time was set to 300 ns, the number of laser shots per pixel to 150 and the mass range was between *m/z* 300 and *m/z* 1500. For both ion modes, the spatial resolution was set to 50 µm.

Images were processed with TissueView software (*AB* Sciex, Les Ulis, France).
The TOF-SIMS analyses were performed with a commercial TOF-SIMS IV mass spectrometer (ION-TOF GmbH, Münster, Germany). Positive and negative ion images were always recorded with the same parameters, *i.e.* 500 µm x 500 µm (256 × 256 pixels) under a primary ion (Bi_3^+ ions) dose density of 4.9×10^{11} ions/cm^2.

Human myotube cultures

Satellite cell populations were isolated, as previously described (Edom et al., 1994), from surgical samples obtained from 4 DMD patients aged 14 to 25 years (Banque de Tissus pour la Recherche, Paris). After 5 days, when the first mononucleated cells migrated out of the explants, the explants were removed and the cells were trypsinized (trypsin-EDTA, Invitrogen), collected by centrifugation and counted. Cells were seeded in 35 mm diameter dishes previously coated with Matrigel® (BD Biosciences, Le Pont de Claix, France) solution, at the density of 7×10^4/dish. The cell cultures were incubated at 37°C in a humid atmosphere containing 5.5% CO_2. Cultures were grown in a medium consisting of PromoCell® skeletal muscle cell basal medium, 4% of PromoCell® (Heidelberg, Germany) skeletal muscle cell growth medium supplement, 13% of fetal bovin serum and antobiotics (gentamycine + steptomycine 0.5mL/L). After 5 days, growth medium was changed to differentiated medium. For primary cells, the medium was composed of Dulbecco's modified eagle medium (DMEM) with 4.5 gr/L of glucose and added with 10% of horse serum and antibiotics (gentamycine + steptomycine 0.5 mL/L) (Sigma-Aldrich, Lyon, France). For the cell lines the differentiation medium was composed of DMEM 4.5 gr/L of glucose supplemented with antibiotics (gentamycine + streptomycine 0.5 mL/L), 10 µg/mL of bovine insuline and 100 µg/mL of human transferine (Sigma-Aldrich, Lyon, France). After 5 more days, myotubes were treated with drugs at various concentrations (**Table 1**) for 48 h and then analysed.

Utrophin immunostaining

Culture cell dishes were washed two times with PBS/BAS (bovine serum albumin) 0.2% and fixed in cold methanol (+4°C for 5 min). After two washes, they were incubated for 5 h with a polyclonal anti-utrophin antibody (N19, 1/100 dilution; Santa Cruz Biotechnology, USA). Dishes were washed four times with PBS/BSA 0.2%, and then incubated for 1 h with fluorescent secondary antibody (polyclonal anti-goat Cy2 antibody diluted 1/1000). After 4 washes with PBS/BSA 0.2% and one wash with PBS, the cells were mounted. DAPI dye (Sigma-Aldrich, St Quentin Fallavier, France) (1 mg/mL aquamount, Polysciences, Warrington, PA, USA) was used to tag the nuclei, as it is a fluorescent dye interacting selectively with DNA. Dishes were observed using a Leica DM RXA2 fluorescent-imaging microscope (Leica Microsystems, Germany). Image capture was performed with a CoolSNAP camera (Roper Scientific, USA) and Openlab software (Improvision, UK).

Calcium imaging

Culture cells were washed two times with Krebs buffer solution (145 mM NaCl, 5 mM KCl, 1 mM $CaCl_2$, 1 mM $MgCl_2$, 5.6 mM glucose and 10 mM HEPES, pH 7.4) and then loaded with Fluo-4 AM (4 µM) (Invitrogen Molecular probes, USA) for 45 min at 37°C. Cells were then washed twice again with Krebs buffer solution and maintained in 1 mL/dish of the same buffer for imaging experiments at room temperature. Changes in cytosolic Ca^{2+} concentration at rest were recorded

during 10 min. Calcium imaging was performed with a confocal microscope (Leica SP2) equipped with an oil immersion objective (40X). Fluo-4 was excited at 488 nm, and emitted fluorescence was recorded between 515-530 nm. Images were analysed with a Leica Confocal Software. Frame pixel size was 512 × 512.

Statistics

In general, data are shown as means ± SEM from at least three different experiments, and statistical group comparisons were performed using Student's t-test. For multimodal evaluation of neuromuscular excitability, data are expressed as means ± SD, and differences between values were tested using the parametric unpaired two-tailed t-test, two-way ANOVA, or the non parametric Mann-Whitney U-test, depending on the equality of variances estimated using the Lilliefors test. Differences were considered significant when $p < 0.05$.

RESULTS

IN VIVO STUDIES

Thirteen groups of 6-week-old *mdx* mice (n = 7 by group) were administered by means of a force-feeding procedure with saline (0.9% NaCl), ABE or ABA (at doses of 50, 80, 100, 200, 400 and 800 mg/kg/d) for 4 consecutive days every 2 weeks for 7 weeks.

Profits of* ABE *and* ABA *on neuromuscular excitability properties, muscle strength and tirelessness, and heart tissue

ABE *and* ABA *treatments counteract the neuromuscular excitability changes observed in* mdx *mice*

The caudal muscle of saline-treated *mdx* mice displayed some significant differences in excitability waves forms (**Fig. 1**) and associated parameters (**Tables 2**-**3**), when compared with C57BL/10 animals. These differences consisted in (i) a reduced CMAP (the summation of a group of almost simultaneous action potentials from several muscle fibers in the same area) amplitude, an enhanced latency (measured from 1 ms stimulation onset to peak amplitude) and a higher threshold (*i.e.* an increased intensity of the stimulation that has to be applied to evoke 50% of maximal CMAP amplitude), determined from the stimulus-response relationship (**Tables 2-3**); (ii) an increased rheobase (*i.e.* minimum intensity of a maximum duration stimulation necessary to evoke a CMAP) and a decreased chronaxis (duration of a twice rheobase intensity stimulation necessary to evoke a CMAP) determined from the strength-duration relationship (**Fig. 1A** and **Tables 2-3**); (iii) a higher minimum current-threshold (I-V) slope, determined as the three smallest slope values calculated from the I-V slope-threshold curve derived from the current-threshold relationship (**Fig. 1B** and **Tables 2-3**), while the resting and hyperpolarizing I-V slopes were not significantly modified (**Fig. 1B** and **Tables 2-3**); (iv) less threshold changes in response to a constant depolarizing long-duration current of sub-threshold intensity, as determined from the threshold electrotonus that allows studying the altered excitability state of a given membrane when a such depolarizing or hyperpolarizing current is passed through it (**Fig. 1C** and **Tables 2-3**); and (v) increased refractoriness (the property of excitable tissue that determines how closely together two action potentials can occur) as calculated by the duration of the relative refractory period and the percents of refractoriness for an interstimulus delay of 2 and 2.5 ms, determined from the recovery cycle and indicating a more longer and important loss of excitability

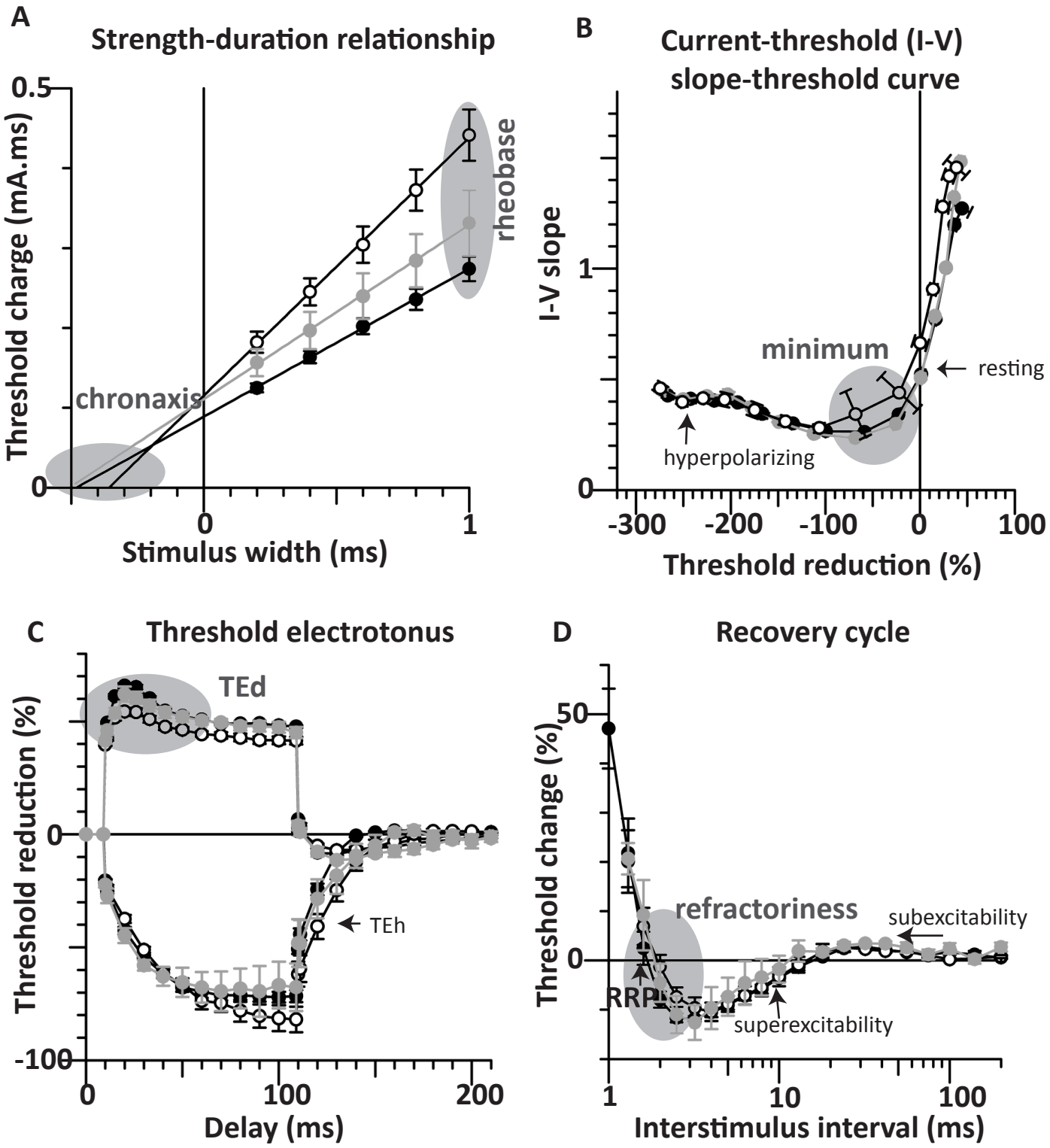

Figure 1: Excitability waveforms obtained by stimulating the caudal motor nerve and recording the compound muscle action potential from caudal muscle in 13-week-old *mdx* mice treated with *ABE* by force-feeding for 7 weeks. C57BL/10 mice (black circles), and *ABE* -treated (grey circles) and saline-treated (white circles) *mdx* mice (A) Strength-duration relationship. (B) Current-threshold (I-V) slope-threshold curve derived from the current-threshold relationship. *ABE* main effects are indicated in grey. (C) Threshold electrotonus (TEd and TEh are threshold electrotonus in response to constant depolarizing and hyperpolarizing long-duration currents of sub-threshold intensity, respectively). (D) Recovery cycle (RRP: relative refractory period). *ABE* main significative effects are indicated in grey areas, and non significantly modified parameters by arrows. Statistical test with the level of significance set at 0.05..

Caudal muscle

			mdx					
			ABE (mg/kg/d)					
	C57BL/10	saline	50	80	100	200	400	800
CMAP amplitude (mV) [1]	3.68 ± 0.12	1.11 ± 0.12**	2.95 ± 0.15	3.38 ± 0.41	3.86 ± 0.10	2.72 ± 0.19	3.36 ± 0.25*	2.98 ± 0.34
Latency (ms) [1]	3.16 ± 0.06	3.62 ± 0.13*	3.30 ± 0.18	3.29 ± 0.13	3.27 ± 0.12	3.06 ± 0.07	3.10 ± 0.07	nd
Stimulus (mA) for 50% max response [1]	0.28 ± 0.06	0.38 ± 0.09*	0.45 ± 1.07**	0.32 ± 1.13	0.35 ± 1.09	0.42 ± 1.10**	0.43 ± 1.10**	0.44 ± 1.25*
Strength-duration time constant (ms) [2]	0.49 ± 0.03	0.36 ± 0.02**	0.23 ± 0.07**	0.62 ± 0.07	0.48 ± 0.09	0.49 ± 0.02	0.61 ± 0.04*	0.70 ± 0.10*
Rheobase (mA) [2]	0.18 ± 0.08	0.26 ± 0.11*	0.34 ± 1.03**	0.23 ± 1.09	0.18 ± 1.19	0.24 ± 1.20	0.26 ± 1.13*	0.26 ± 1.08**
Minimum I-V slope [3]	0.26 ± 0.01	0.22 ± 0.01**	0.24 ± 0.03	0.23 ± 0.02	0.22 ± 0.02	0.30 ± 0.08	0.26 ± 0.04	0.26 ± 0.09
S2 accommodation [4]	15.30 ± 0.70	11.43 ± 0.77**	10.26 ± 1.77*	15.83 ± 3.77	15.92 ± 1.25	15.17 ± 1.85	12.81 ± 2.61	12.53 ± 7.80
TEd(10-20ms) [4]	64.77 ± 1.01	53.80 ± 1.75***	52.89 ± 4.87*	55.48 ± 5.05	50.83 ± 4.60	51.39 ± 2.44**	52.07 ± 2.39***	50.77 ± 4.70**
TEd(40-60ms) [4]	50.79 ± 0.88	44.73 ± 1.25**	45.17 ± 4.58*	48.43 ± 3.48	47.05 ± 4.94	47.53 ± 2.12	43.14 ± 2.02**	40.34 ± 3.43**
TEd(peak)	63.32 ± 0.91	53.00 ± 1.58***	51.42 ± 4.87*	53.75 ± 5.06	56.55 ± 5.17	51.40 ± 3.33**	53.70 ± 1.52***	51.16 ± 2.60***
TEd20(peak) [4]	37.68 ± 0.69	32.19 ± 1.07**	29.72 ± 3.13*	31.87 ± 4.05	30.79 ± 3.48	35.51 ± 4.34	36.66 ± 4.24	30.24 ± 1.78**
Relative refractory period (ms) [5]	1.65 ± 1.06	2.18 ± 1.13*	2.57 ± 1.09	2.11 ± 1.14	1.97 ± 1.16	1.82 ± 1.17	2.65 ± 1.30	nd
Refractoriness at 2ms (%) [5]	-7.96 ± 1.65	3.42 ± 3.70*	-0.51 ± 3.30	-8.27 ± 7.95	5.03 ± 12.90	-4.83 ± 5.94	-8.63 ± 7.74	8.37 ± 6.88*
Refractoriness at 2.5ms (%) [5]	-11.67 ± 0.88	-2.59 ± 2.66*	-1.12 ± 3.59**	-4.75 ± 3.95	-10.68 ± 7.76	-10.40 ± 4.22	-3.56 ± 7.35	4.30 ± 5.65*
Stimulus-response slope [1]	3.23 ± 1.19	3.92 ± 1.20	3.70 ± 1.57	3.76 ± 1.27	3.09 ± 1.22	3.36 ± 1.13	3.29 ± 1.16	2.94 ± 1.37
Resting I-V slope [3]	0.52 ± 0.03	0.51 ± 0.04	0.53 ± 0.05	0.64 ± 0.06	0.99 ± 0.29	0.52 ± 0.01	0.65 ± 0.11	0.71 ± 0.09*
Hyperpolarizing I-V slope [3]	0.43 ± 0.01	0.45 ± 0.02	0.46 ± 0.05	0.47 ± 0.03	0.41 ± 0.10	0.53 ± 0.07	0.47 ± 0.02	0.50 ± 0.04*
Accommodation half-time (ms) [4]	30.66 ± 1.28	35.85 ± 2.49	29.87 ± 3.89	30.88 ± 0.43	31.77 ± 0.97	43.18 ± 9.36	38.69 ± 3.16*	nd
S3(-70%) [4]	93.33 ± 5.49	91.44 ± 6.11	64.95 ± 18.60	86.60 ± 17.90	80.83 ± 3.75	53.62 ± 22.10	60.14 ± 9.77**	nd
TEd(90-100ms) [4]	47.97 ± 0.73	45.68 ± 1.28	47.37 ± 4.18	46.19 ± 2.15	46.72 ± 2.16	40.9 ± 3.3	34.88 ± 3.64**	nd
TEd(undershoot) [4]	-8.50 ± 1.26	-8.42 ± 1.07	-8.87 ± 2.31	-9.06 ± 2.99	-10.26 ± 3.01	-10.11 ± 0.10	-13.74 ± 4.83	-12.61 ± 1.26*
TEh(10-20ms) [4]	-99.13 ± 1.88	-97.25 ± 2.30	-98.67 ± 1.55	-98.36 ± 2.51	-97.26 ± 3.77	-72.51 ± 16.70	-98.93 ± 9.10	-90.84 ± 1.24*
TEh(20-40ms) [4]	-135.40 ± 2.80	-135.60 ± 3.90	-127.90 ± 2.72	-137.90 ± 18.00	-133.10 ± 4.74	-97.48 ± 23.00	-135.90 ± 4.39	-130.90 ± 9.77
TEh(90-100ms) [4]	-177.80 ± 6.10	-198.80 ± 10.50	-168.60 ± 4.39	-169.30 ± 4.09	-180.20 ± 10.10	-177.50 ± 13.10	-180.40 ± 7.83	nd
TEh(overshoot) [4]	8.15 ± 0.81	7.11 ± 0.70	8.24 ± 2.52	8.45 ± 2.81	8.71 ± 3.26	6.69 ± 1.50	7.32 ± 0.38	nd
TEh(peak,-70%) [4]	-321.90 ± 10.30	-302.90 ± 16.20	-315.10 ± 27.20	-294.20 ± 11.30	-337.40 ± 13.40	-316.10 ± 13.70	-296.50 ± 26.70	-316.50 ± 11.00
TEh(slope 101-140ms) [4]	3.43 ± 0.14	3.49 ± 0.17	3.13 ± 0.14	3.20 ± 0.08	3.60 ± 0.21	3.15 ± 0.23	3.31 ± 0.19	nd
Superexcitability (%) [5]	-11.80 ± 0.60	-10.79 ± 1.67	-10.61 ± 3.43	-16.20 ± 3.22	-12.73 ± 4.13	-12.39 ± 3.22	-12.83 ± 5.20	-26.87 ± 4.80**
Superexcitability at 5ms (%) [5]	-9.10 ± 0.89	-8.81 ± 1.63	-8.49 ± 2.11	-9.28 ± 2.24	-5.54 ± 4.78	-8.80 ± 1.88	-7.03 ± 1.37	-11.52 ± 6.97
Superexcitability at 7ms (%) [5]	-6.50 ± 0.89	-6.27 ± 1.83	-6.68 ± 1.65	-6.44 ± 0.74	-6.92 ± 2.23	-6.88 ± 1.59	-6.32 ± 1.14	nd
Subexcitability (%) [5]	2.93 ± 0.59	4.70 ± 1.20	3.04 ± 0.69	4.45 ± 1.06	4.54 ± 1.98	4.42 ± 1.72	2.735 ± 0.376	3.39 ± 1.92

Table 2: Excitability parameters obtained by stimulating the caudal motor nerve and recording the CMAP from caudal muscle in C57BL/10, saline- and *ABE*-treated *mdx* mice. Compared with C57BL/10 mice, all excitability parameters that are modified in saline-treated *mdx* mice (above the black line), do no longer show any significant difference when *mdx* mice were treated with 80 mg/kg/d ABE. A clear dose-response effect is observed since some improvements occur at 50 mg/kg/d, 80 mg/kg/d is the optimal concentration and the beneficial effect is progressively lost with high doses (400-800 mg/kg/d).

Exponent numbers correspond to parameters of: (1) Stimulus-response relationship, (2) strength-duration relationship, (3) current-threshold (I-V) relationship, (4) threshold electrotonus (TEd and TEh are threshold electrotonus in response to constant depolarizing and hyperpolarizing long-duration currents of sub-threshold intensity, respectively), (5) recovery cycle. Nd: not determined. Statistical test with the level of significance set at 0.05

Plantar muscle

		mdx						
			ABE (mg/kg/d)					
	C57BL/10	saline	50	80	100	200	400	800
Stimulus (mA) for 50% max response [1]	0.28 ± 1.03	0.41 ± 1.09*	0.26 ± 1.12	0.23 ± 1.09	0.31 ± 1.06	0.29 ± 1.15	0.35 ± 1.21	nd
Strength-duration time constant (ms) [2]	0.47 ± 0.01	0.35 ± 0.03*	0.35 ± 0.02*	0.43 ± 0.09	0.45 ± 0.08	0.49 ± 0.16	0.52 ± 0.15	nd
Rheobase (mA) [2]	0.18 ± 1.05	0.27 ± 1.09*	0.17 ± 1.16	0.16 ± 1.10	0.20 ± 1.07	0.18 ± 1.21	0.20 ± 1.18	nd
Minimum I-V slope [3]	0.48 ± 0.01	0.42 ± 0.01*	0.41 ± 0.03**	nd	0.52 ± 0.03	0.41 ± 0.01**	0.29 ± 0.01**	nd
S2 accommodation [4]	14.24 ± 1.35	7.81 ± 1.58*	10.95 ± 0.68*	8.35 ± 1.23*	12.92 ± 0.53	13.75 ± 2.35	7.41 ± 1.56*	nd
TEd(10-20ms) [4]	50.06 ± 1.62	41.72 ± 1.61*	41.78 ± 1.29**	41.54 ± 1.64*	44.03 ± 1.48	46.43 ± 1.73	38.49 ± 2.93*	nd
TEd(peak) [4]	49.26 ± 1.61	42.30 ± 1.43*	42.44 ± 1.41*	42.52 ± 1.09*	44.66 ± 1.50	46.93 ± 2.19	39.15 ± 2.57*	nd
TEd20(peak) [4]	26.19 ± 1.41	22.42 ± 0.76*	25.98 ± 1.49	25.83 ± 1.58	25.37 ± 0.88	26.21 ± 1.70	22.61 ± 1.43	nd
Relative refractory period (ms) [5]	1.99 ± 1.10	nd	2.61 ± 1.05*	2.34 ± 1.01	2.55 ± 1.09	2.38 ± 1.08	3.39 ± 1.55	nd
Refractoriness at 2ms (%) [5]	1.54 ± 3.09	17.95 ± 3.02*	13.29 ± 1.97*	6.25 ± 1.84	6.90 ± 2.52	8.02 ± 3.49	13.06 ± 2.10*	nd
Refractoriness at 2.5ms (%) [5]	-8.41 ± 1.90	0.79 ± 1.69*	-0.70 ± 1.26*	-0.83 ± 1.37*	-1.56 ± 2.74	-1.28 ± 1.55*	-0.75 ± 1.43*	nd
CMAP amplitude (mV) [1]	2.45 ± 0.14	1.90 ± 0.15	2.60 ± 0.21	2.92 ± 0.21	2.67 ± 0.19	2.42 ± 0.19	2.05 ± 0.21*	nd
Latency (ms) [1]	2.54 ± 0.12	2.31 ± 0.12	2.84 ± 0.17	2.91 ± 0.20	3.09 ± 0.22	2.83 ± 0.28	2.93 ± 0.06*	nd
Stimulus-response slope [1]	3.79 ± 1.25	2.15 ± 1.22	2.57 ± 1.26	2.40 ± 1.12	2.64 ± 1.23	4.01 ± 1.19	3.72 ± 1.13	nd
Resting I-V slope [3]	0.82 ± 0.03	0.89 ± 0.05	0.86 ± 0.05	0.83 ± 0.03	0.86 ± 0.04	0.88 ± 0.03	0.99 ± 0.04*	nd
Hyperpolarizing I-V slope [3]	0.54 ± 0.01	0.61 ± 0.13	0.54 ± 0.03	0.46 ± 0.04	0.55 ± 0.04	0.54 ± 0.02	0.81 ± 0.28	nd
Accommodation half-time (ms) [4]	29.29 ± 1.12	32.14 ± 8.67	25.69 ± 1.28	24.68 ± 3.08	28.38 ± 0.83	28.66 ± 2.46	21.08 ± 1.50**	nd
S3(-70%) [4]	40.33 ± 4.66	22.53 ± 8.14	40.13 ± 5.08	31.65 ± 7.57	26.47 ± 9.00	29.50 ± 14.70	15.10 ± 5.66*	nd
TEd(40-60ms) [4]	37.71 ± 2.24	35.62 ± 0.89	36.85 ± 1.38	35.01 ± 1.14	34.45 ± 0.96	35.30 ± 1.37	32.52 ± 3.23	nd
TEd(90-100ms) [4]	35.02 ± 1.90	34.49 ± 0.35	35.42 ± 1.25	34.10 ± 1.00	31.74 ± 0.98	34.57 ± 3.11	33.28 ± 3.81	nd
TEd(undershoot) [4]	-12.47 ± 0.87	-7.80 ± 1.78	-9.11 ± 1.10	-8.82 ± 1.78	-12.89 ± 1.16	-10.42 ± 2.02	-7.20 ± 1.38*	nd
TEh(10-20ms) [4]	-68.13 ± 0.29	-64.16 ± 3.07	-69.94 ± 2.65	-67.62 ± 4.83	-67.60 ± 2.62	-67.13 ± 3.97	-70.53 ± 2.59	nd
TEh(20-40ms) [4]	-75.76 ± 1.35	-72.40 ± 5.41	-83.03 ± 3.26	-85.12 ± 3.96	-73.55 ± 7.77	-80.03 ± 4.01	-89.84 ± 2.92*	nd
TEh(90-100ms) [4]	-72.11 ± 2.94	-68.94 ± 4.81	-67.82 ± 4.95	-71.40 ± 8.91	-92.44 ± 8.03	-92.88 ± 5.66*	-103.10 ± 6.03**	nd
TEh(overshoot) [4]	7.58 ± 1.67	3.50 ± 1.25	5.87 ± 0.79	3.59 ± 1.18	7.03 ± 1.13	6.05 ± 0.82	2.71 ± 0.39*	nd
TEh(peak,-70%) [4]	-174.00 ± 1.05	-154.00 ± 11.00	-184.90 ± 17.00	-206.10 ± 12.04	-175.00 ± 52.70	-197.30 ± 9.85	-194.90 ± 16.20	nd
TEh(slope 101-140ms) [4]	0.71 ± 0.09	0.55 ± 0.08	0.62 ± 0.23	0.78 ± 0.26	1.43 ± 0.18*	1.37 ± 0.19*	1.40 ± 0.14*	nd
Superexcitability (%) [5]	-3.45 ± 1.15	-1.70 ± 0.97	-4.76 ± 1.43	-3.38 ± 2.12	-4.95 ± 2.10	-4.21 ± 0.46	-6.02 ± 3.18	nd
Superexcitability at 5ms (%) [5]	-2.10 ± 1.32	2.47 ± 2.24	-4.39 ± 1.27	-2.68 ± 2.40	-2.15 ± 3.70	-4.72 ± 1.25	-1.10 ± 3.09	nd
Superexcitability at 7ms (%) [5]	-2.94 ± 0.67	3.69 ± 2.66	-2.45 ± 0.94	-0.63 ± 1.54	-3.05 ± 0.44	-2.36 ± 0.40	-2.69 ± 0.93	nd
Subexcitability (%) [5]	6.05 ± 0.31	5.04 ± 2.70	6.53 ± 1.02	5.70 ± 1.05	4.76 ± 0.44	6.56 ± 1.18	5.28 ± 1.45	nd

Table 3: Excitability parameters obtained by stimulating the tibial branch of the sciatic nerve and recording the CMAP from plantar muscle in C57BL/10, saline- and *ABE*-treated *mdx* mice. Compared with C57BL/10, all excitability parameters that are modified in saline-treated *mdx* mice (above the black line), do no longer show any significant difference when *mdx* mice were treated with 100 mg/kg/d *ABE*, with a clear dose-response effect. A progressive amelioration occurs at 50 and 80 mg/kg/d, and the beneficial effect is progressively lost with high doses (200-400 mg/kg/d)

Exponent numbers correspond to parameters of: (1) Stimulus-response relationship, (2) strength-duration relationship, (3) current-threshold (I-V) relationship, (4) threshold electrotonus (TEd and TEh are threshold electrotonus in response to constant depolarizing and hyperpolarizing long-duration currents of sub-threshold intensity, respectively), (5) recovery cycle; Nd: not determined. Statistical test with the level of significance set at 0.05.

following an action potential (**Fig. 1D** and **Tables 2-3**). All the other parameters were not markedly different between the two groups of animals (**Fig. 1** and **Tables 2-3**). Similar results were obtained from the plantar muscle recordings of saline-treated *mdx* mice (**Supplementary data 2 and 3**), except for the CMAP amplitude and the latency that are not different from C57BL/10 animal values.

Very interestingly, the number of modified excitability parameters decreased when *mdx* mice were treated with *ABE* and *ABA* in an apparent dose-dependent manner. In particular, all excitability parameters determined from the caudal muscle of *mdx* mice administered with 80 mg/kg/d *ABE* (**Fig. 1** and **Table 2)** or 100 mg/kg/d *ABA* (**Table 3)** did no longer differ significantly from C57BL/10 animals. Similarly, a complete rescue of most of, if not all, excitability parameters was observed from the plantar muscle of *mdx* mice administered with 100 mg/kg/d *ABE* (**Supplementary data 2)** or 50-80 mg/kg/d *ABA* (**Supplementary data 3).** It is worth noting that the treatment of *mdx* animals with higher doses (from 200 to 800 mg/kg/d) of *ABE* or *ABA* led to an increase in the number of modified excitability parameters determined from the caudal muscle (**Tables 2-3)** and the plantar muscles, (**Supplementary data 2 and 3),** including also parameters that were not different between C57BL/10 and saline-treated mice.

ABE *and* ABA *treatments alleviate skeletal muscle function in* mdx *mice*

Muscle strength was evaluated using a grip-strength meter. *ABE* treatment improved *mdx* mice grip strength at doses of 50, 80, 100 and 200 mg/kg/d with a maximal effect (60%) around 80 mg/kg/d (**Fig. 2A)**. *ABA* treatment improved *mdx* mice grip strength at all doses used (50, 80, 100, 200, 400 and 800 mg/kg/d), with a maximal effect (62%) at 50 mg/kg/d (**Fig. 2B**). Similarly to what was observed with the grip strength test, *ABE* and *ABA* treatments improved the tirelessness determined on inverted grid test, but with higher variability according to mice. Hence, *ABE* treatment improved *mdx* tirelessness at 50 and 80 mg/kg/d with a maximal effect (3-fold) at 50 mg/kg/d (**Fig. 2C)**, while *ABA* improved tirelessness at 50-100 mg/kg/d with a maximal effect (4-fold) at 100 mg/kg/d (**Fig. 2D).** Therefore, it appears that low doses of *ABE* or *ABA* are more efficient than intermediate doses. However, high doses (200-800 mg/kg/d for *ABE*, **Fig. 2C**; 400-800 mg/kg/d for *ABA*, **Fig. 2D**) are not effective, while no change in body weight was detected in treated mice for any dose. The expected increase of utrophin level was verified by semi-quantitative western blot analyses. An about 40% increase was quantified in the *gastrocnemius* muscle of *mdx* mice treated with *ABE* (80 mg/kg/d), compared with saline-treated mice (**Supplementary data 4**).

ABE *and* ABA *treatments alleviate cardiac heart structure in* mdx *mice*

In the absence of functional defect at this age we analyzed the necrotic achievement in heart. The areas of necrosis were determined with ImageJ software on heart sections stained by Masson's trichrome (**Supplementary data 5)**. *ABE* and *ABA* treatments reduced the percentage of necrotic areas in heart of *mdx* mice at doses of 80 (84%) and 100-200 mg/kg/d (about 94%), respectively (**Fig. 2E** and **F**).

In order to study membrane permeability, complementary analyses were performed on skeletal muscle and heart after the treatment:

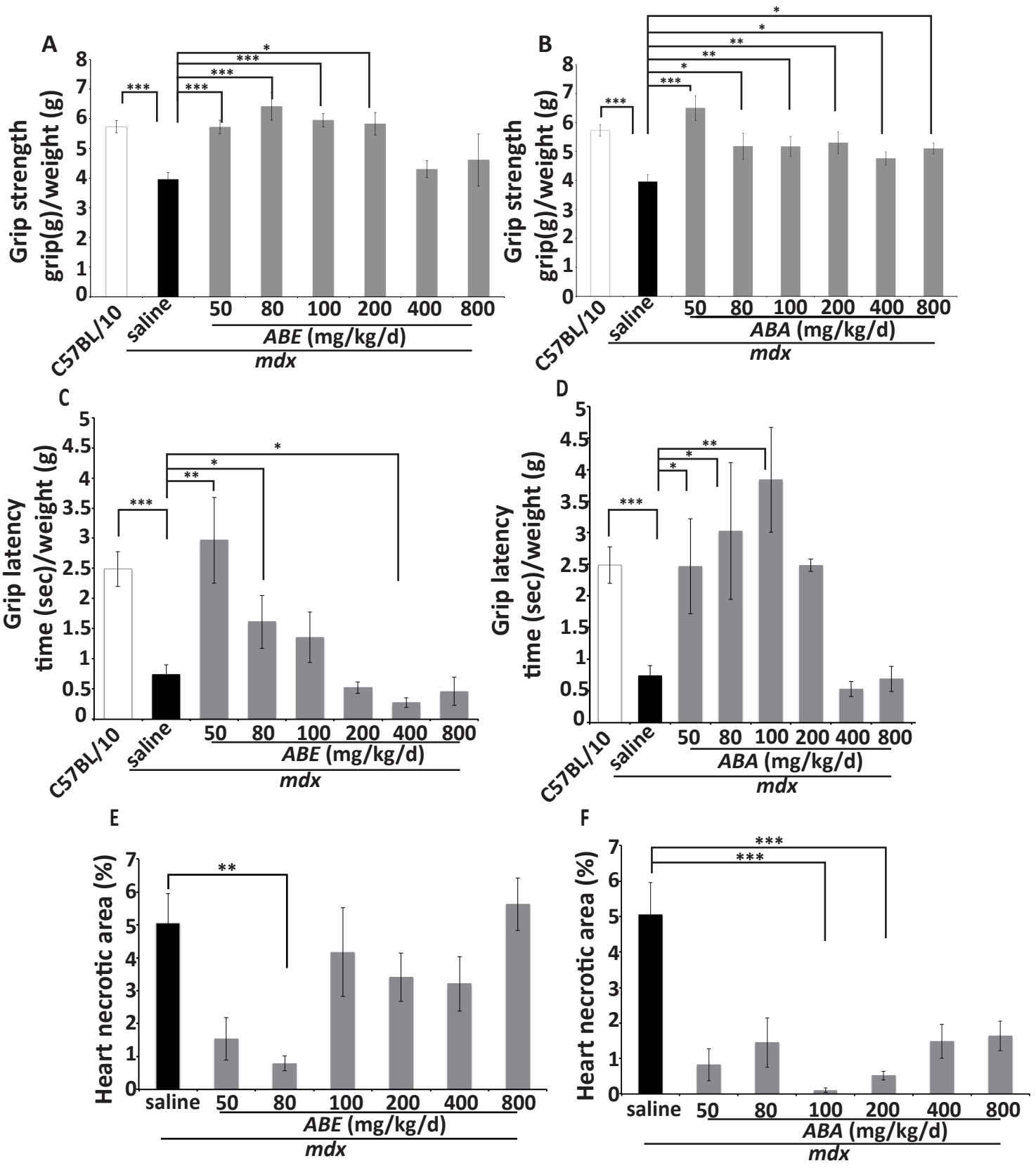

Figure 2: Dose-response effect of *ABE* and *ABA* (50-800 mg/kg/d) on muscle function and heart necrosis of *mdx* mice, compared to saline-treated *mdx* mice and C57BL/10 animals. (A-B) Grip strength test. The values are normalized to the weight of animals at the end of treatment. (A) *ABE* increases the grip strength at doses of 50, 80, 100 and 200 mg/kg/d, with a complete rescue at 80 mg/kg/d. (B) *ABA* increases the grip strength at each dose used, with a complete rescue at 50 mg/kg/d. (C-D) Inverted grid test. The values are normalized to the weight of animals at the end of the treatment. (C) *ABE* improves the tirelessness at doses of 50, 80 and 100 mg/kg/d, with a complete rescue at 50 mg/kg/d. (D) *ABA* improves the tirelessness with a complete rescue at 50-200 mg/kg/d. (E-F) Quantification by ImageJ software of necrotic area in heart section after Masson's trichrome staining. *ABE* (E) reduces the percentage of necrotic areas at doses 100-200 mg/kg/d, and *ABA* (F) at 50 mg/kg/d. Student's t-test with the level of significance set at 0.05.

- ABA *and* ABE *treatments decrease serum CK level in* mdx *mice*

In saline-treated *mdx* mice, the CK level was very high (7000 ± 1131 U/l), while *ABE*- and *ABA*-treated animals displayed more than about 50% reduction of the enzyme. In particular, the decrease was of 60% and 85% for 50 and 80 mg/kg/d *ABE* respectively, while it was of 47% and 60 % for 50 and 80 mg/kg/d *ABA* respectively (**Fig. 3A**).

- ABE *reduces the incorporation of Evans Blue dye in* mdx *mice fibres*

Based on the evidence that ABE 80 mg/kg/d seems to be the most effective dose, two additional groups of 6 *mdx* animals have been treated with saline solution and *ABE* respectively. At the end of the protocol Evans Blue dye has been injected and membrane integrity studied. On a transversal section in the middle part of the limb of saline-treated *mdx* mice, 11 ± 3% of the surface were damaged while in *ABE*-treated animals, only 3 ± 1.65% were damaged, as revealed by quantification with ImageJ software (**Fig. 3B**).

- ABE *protects heart membrane from degeneration in* mdx *mice*

The heart, a tissue not able to regenerate, is therefore a model of interest to look for a potential direct protective effect of *ABE*. To address the integrity of the cardiac membrane, by means of the analysis of the lipid composition of heart, TOF-SIMS and MALDI-ToF, two mass spectrometry imaging techniques, were applied on transversal heart slices. Experiments were performed in positive and negative ion modes at different locations chosen to be characteristic of necrotic and non-necrotic areas.

TOF-SIMS: With the positive ion mode any information, which may discriminate non-necrotic areas from necrotic one, could not be obtained from the ionic images or from mass spectra. In contrast, in the negative ion mode, among the fatty acid ions detected by TOF-SIMS, the ion signal detected at *m/z* 255.2, corresponding to the deprotonated fatty acid C16:0, was increased in non-necrotic areas of saline-treated *mdx* mice, compared with C57BL/10 mice, and decreased by around 30% in those of animals treated with 80 mg/kg/d *ABE*, compared with saline-treated mice, to reach the level of C57BL/10 mice (**Fig. 4A and corresponding spectra)**. In necrotic areas, only present in *mdx* mice, the fatty acid C16:0 was reduced by more than 50% in mice treated with 80 mg/kg/d *ABE*, compared with saline-treated animals (**Fig. 4B**).

Our recent study on skeletal muscle showed the variation of several ratios between fatty acid ion peak intensities (Tahallah et al., 2008). In heart, the ratio R2 (C18:0 at *m/z* 283.2 over C18:1 at *m/z* 281.3) did not vary. We thus focused on the ratio R3 of the intensity of the C18:1 fatty acid ion signal at *m/z* 281.3 signal over the intensity of the C18:2 fatty acid ion signal at *m/z* 279.2 signal. The variation of the ratio R3 in non-necrotic and necrotic areas followed the same pattern than that of the C16:0 signal. In non-necrotic areas, R3 was increased in saline-treated *mdx* mice and decreased by around 12% in animals treated with *ABE* (80 mg/kg/d) to reach the level comparable of C57BL/10 mice, (**Fig. 4C)**. In necrotic areas, R3 was reduced by about 30% in *mdx* treated with 80 mg/kg/d *ABE*, compared with saline-treated animals (**Fig. 4D**).

MALDI-ToF: According to the results previously obtained with skeletal muscle samples (limb) (Benabdellah et al., 2009; Tahallah et al., 2008; Touboul et al., 2004, 2005), the signals corresponding to the

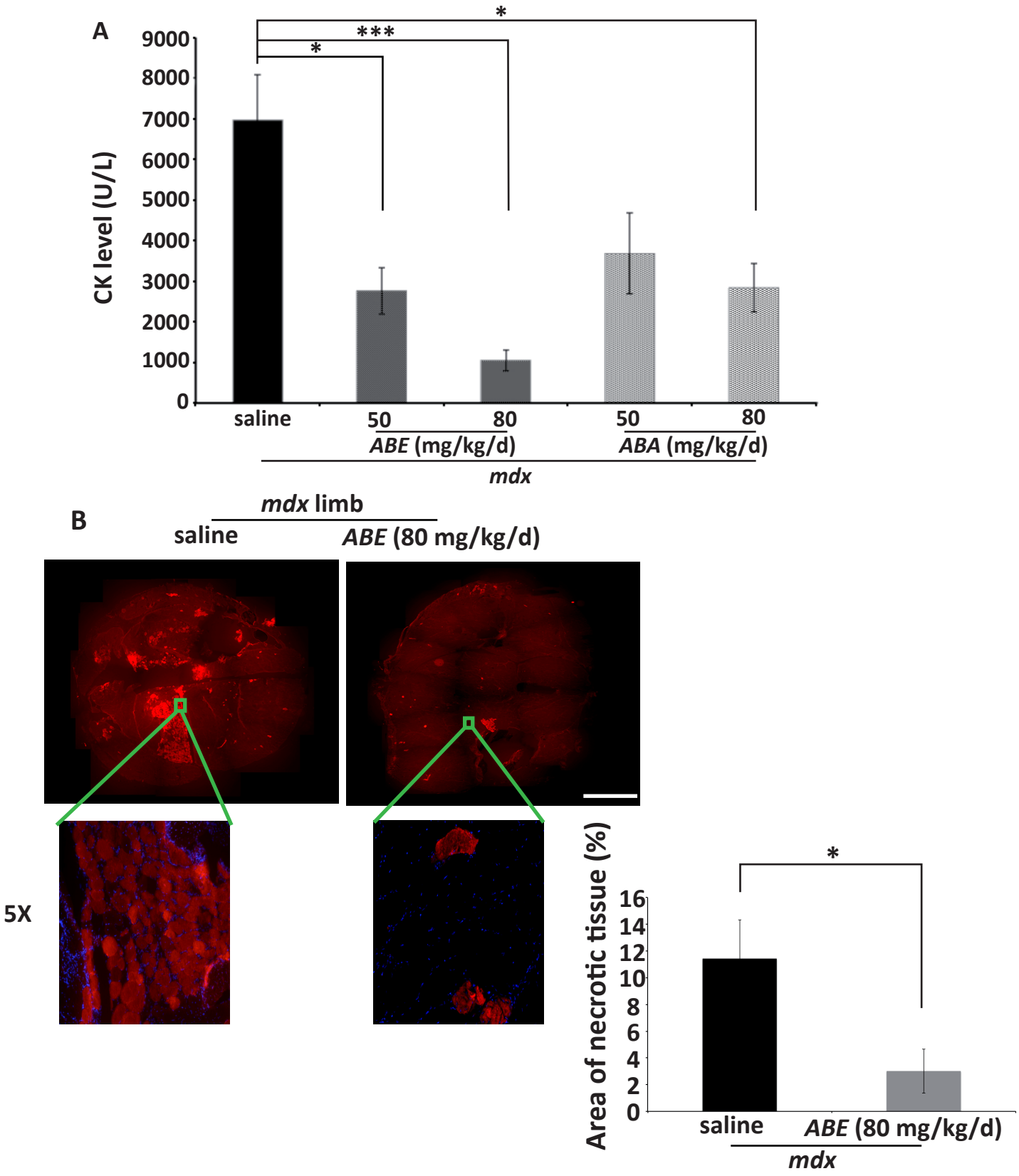

Figure 3: *ABE* and *ABA* induce the restoration of sarcolemmal integrity in *mdx* mice. (A) CK level in the serum. A meaningful decrease of CK in the serum is visible after the treatment with both *ABE* and *ABA*. The decrease for 80 mg/kg/d *ABE* is 85% compared with saline-treated animals. (B) Reduction of the incorporation of injected Evans blue dye in the limb of *ABE*-treated *mdx* mice compared to saline-treated animals. The limb of saline-injected mdx mice presents numerous necrotic fibers, as evidenced by extensive areas stained by Evans blue dye. In contrast, necrotic fibers are almost absent in *ABE*-treated *mdx* mice. Scale bar, 1.5 mm. A decrease of about 74% of the surface of tissue having incorporated the dye was observed in *ABE*-treated *mdx* mice, compared with saline-treated animals. Student's t-test with the level of significance set at 0.05.

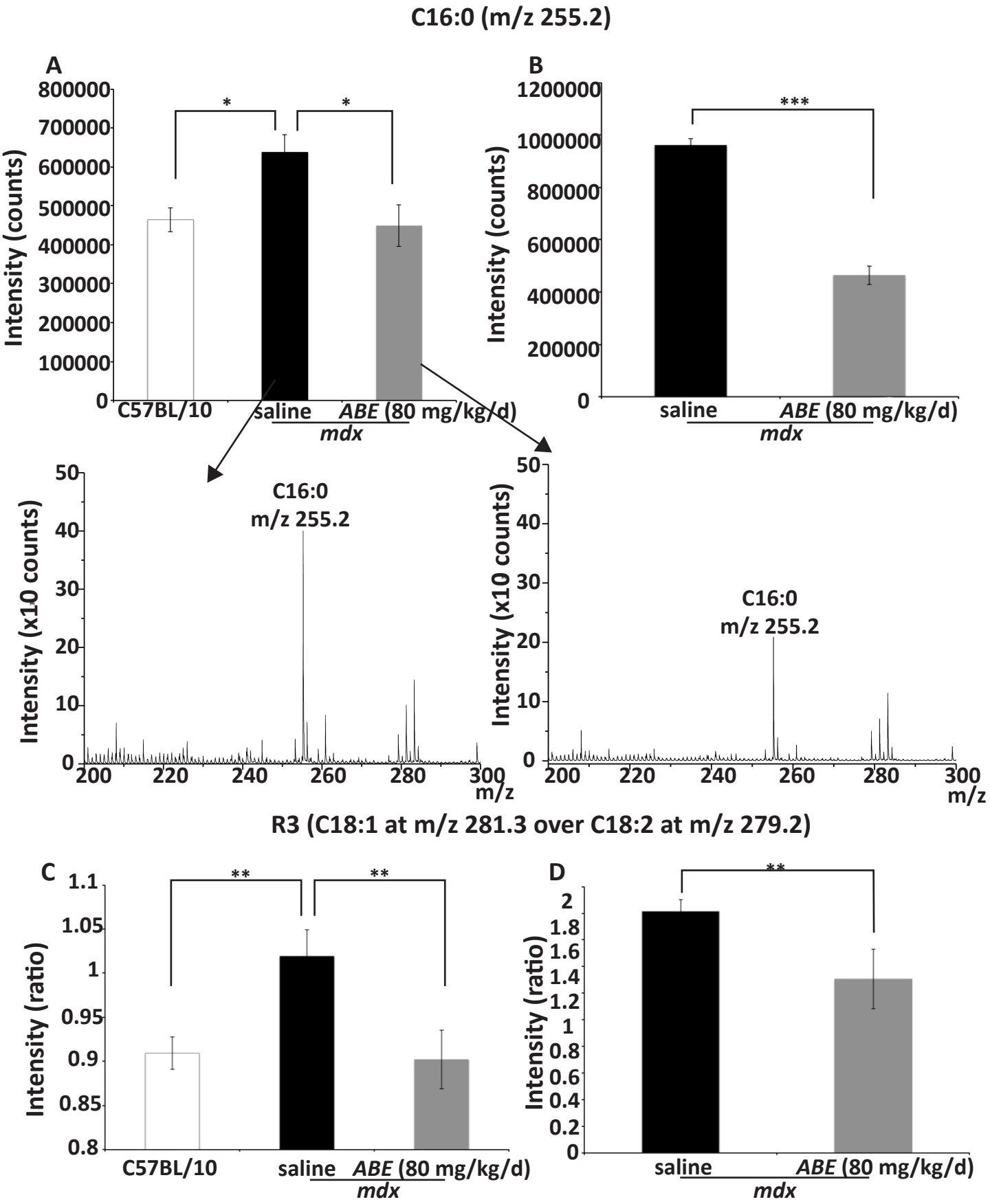

Figure 4: Fatty acid ions detected by TOF-SIMS mass spectrometry in heart sections of C57BL/10, saline- and 80 mg/kg/d *ABE*-treated *mdx* mice. (A) Non-necrotic areas: the fatty acid C16:0 (corresponding to the m/z 255.2 ion signal) is increased in sections of saline-treated *mdx* mice, compared with C57BL/10 animals, and decreased in *ABE*-treated *mdx* mice to a level comparable to the C57BL/10 mice value. Parts of TOF-SIMS negative ion mass spectra showing C16:0 ion peaks from saline- and *ABE*-treated *mdx* mice. (B) Necrotic areas: the fatty acid C16:0, absent in section of C57BL/10 mice, is detected in saline-treated *mdx* mice and reduced by more than 50% in *ABE*-treated animals. (C-D) Ratio R3 (C18:1 fatty acid ion at m/z 281.3 signal over C18:2 fatty acid ion at m/z 279.2 signal) in structured (C) and necrotic (D) areas. Same profile of distribution as C16:0. The global decrease of these differents makers was around 30%. Student's t-test with the level of significance set at 0.05.

glycerophosphatidylcholine (PC) positive ions were particularly sought by MALDI mass spectrometry imaging. PC34:2 and PC34:1 were detected as the potassium cationized species $[M+K]^+$ at *m/z* 796.6 and *m/z* 798.6, respectively, instead of the expected $[M+H]^+$ protonated ion species. Unfortunately, the signal was not intense enough to evaluate the ratio of intensities. However, a clear difference in lipid composition was evidenced in the negative ion mode, and two ions at *m/z* 885.6 and *m/z* 1447.8 were identified by tandem mass spectrometry (MS/MS): The *m/z* 885.6 ion, corresponds to a phosphatidylinositol (PI) 18:0/20:4 and is only present in necrotic areas. An opposite distribution was observed for the *m/z* 1447.8 ion which is attributed to cardiolipine (CL, 18:2/18:2/18:2/18:2) since this specific lipid from heart tissue was detected everywhere in the heart excepted in the necrotic areas (**Fig. 5A, B**). These two ion species can be considered as specific markers of non-necrotic areas or necrotic.

IN VITRO STUDIES

In vitro studies were performed to investigate beneficial effect of *ABE* and *ABA* on human DMD myotubes, an essential step before envisaged clinical trial. Cell culture were also use to complete the data on membrane permeability by analysis of the spontaneous Ca^{2+} spikes.

AB*,* ABA *and* ABE *increase utrophin, β-dystroglycan and embryonic myosin levels in human DMD myotubes.*

Primary myotubes: The levels of utrophin, β-dystroglycan and embryonic myosin were quantified in human primary differentiate myotubes treated for 48 h with nine doses (from 0.002 to 2 mM) of *AB*, *ABA* and *ABE*. The treatment with the three products increased utrophin, β-dystroglycan and embryonic myosin levels by around 2-3 fold, compared with untreated myotubes (**Fig. 6**).

For *AB* clear dose-response effects were observed for utrophin, β-dystroglycan and embryonic myosin levels, with a maximal increase at doses over 0.2 mM (**Fig. 6A**). Concerning *ABE*, dose-response effects were also observed for utrophin, β-dystroglycan and embryonic myosin levels, with a maximal increase at lower doses compared with *AB*, *i.e.* 0.05 mM *versus* 0.2 mM (**Fig. 6B**). Concerning the third formulation, *ABA*, although no clear dose-effect response was observed a maximal increase was obtained with doses from 0.1 to 0.5 mM (**Fig. 6C**). Localization of utrophin in myotubes was observed after immunostaining of utrophin: little utrophin labeling was visible in untreated myotubes, but staining was slightly increased in the sarcolemma after treatment (**Fig. 7**).

Cell line: Fibroblast cells are well-known to contaminate primary muscle cell cultures. To verify that the increase in utrophin nevel could be attributed to myogenic cells and not to fibroblasts, experiments were carried out on a muscular cell line from DMD patient. We focussed on utrophin and β-dystroglycan levels. The increase was confirmed by western blot analysis performed on differentiate myotubes obtained from a human DMD cell line and treated for 48 h with *AB* or *ABE*, at doses with which the maximal level increase was obtained on primary myotubes, *i.e.* 0.1-0.5 mM (**Fig. 8**). Very interestingly, the increases were more than 2 fold higher in cell line of myotubes, compared with primary cell cultures.

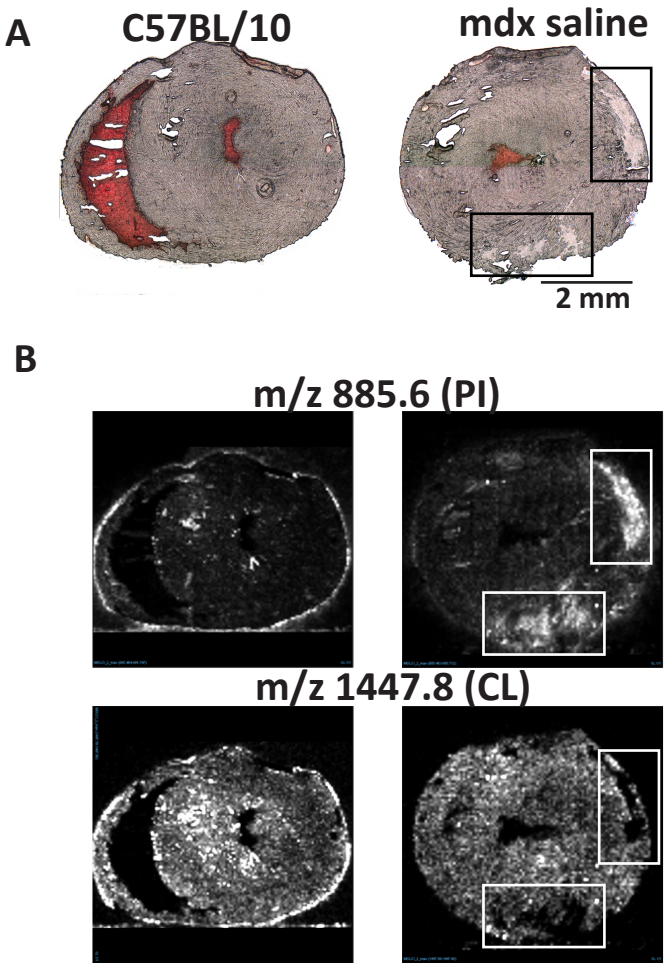

Figure 5: MALDI-ToF mass spectrometry images of two new ionic markers specific of the lipid composition of membranes in heart necrotic areas of *mdx* mice (right column) and healthy tissue (left column). The squares indicate two large zones of necrosis. (A) Optical images of heart section in C57BL/10 and *mdx* mice. (B) Ion imaging of the m/z 885.6 and m/z 1447.8 ions. The m/z 885.6 ion, identified by MS/MS as a phosphatidylinositol (PI) 18:0/20:4, is exclusively detected in necrotic areas of *mdx* mice. At the opposite, the m/z 1447.8 ion, identified by MS/MS as the cardiolipine (CL) 18:2/18:2/18:2/18:2, is detected everywhere in the heart section excepted in the necrotic areas.

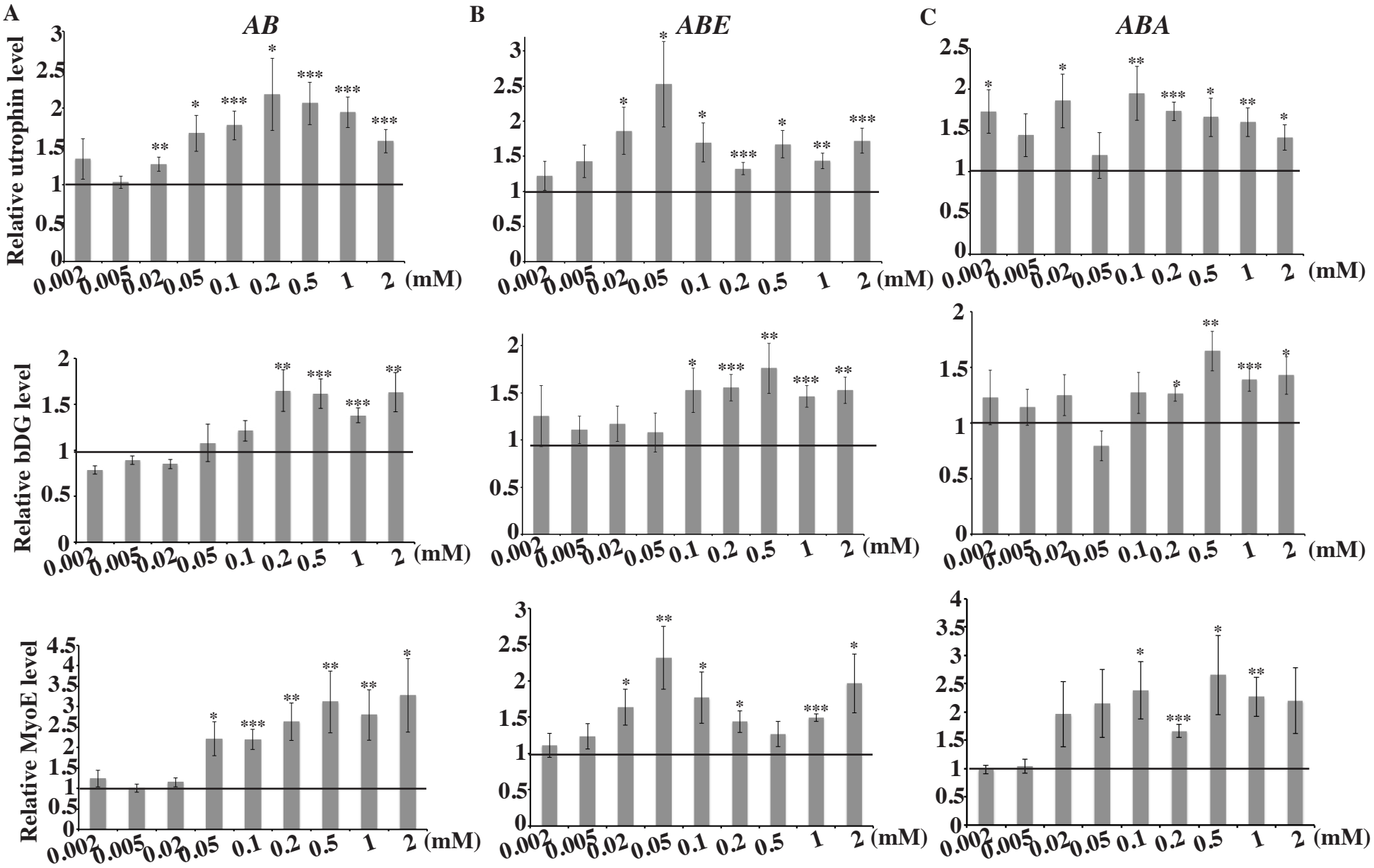

Figure 6: Semi-quantitative western-blot analysis of utrophin, β-dystroglycan (bDG) and embryonic myosin (MyoE) levels in primary skeletal muscle cells derived from DMD patients and treated for 48 h with (A) *AB*, (B) *ABE* and (C) *ABA*, at concentration ranging from 0.002 to 2 mM. Results were normalized to saline values (treated/saline ratio with saline = 1, black line). Values are representative of three independent experiments. Dose-response relationships are clearly visible after the treatment with *AB*. Globally, an about 2 fold increase in the three protein levels is observed with the three drugs. Student's t-test with the level of significance set at 0.05.

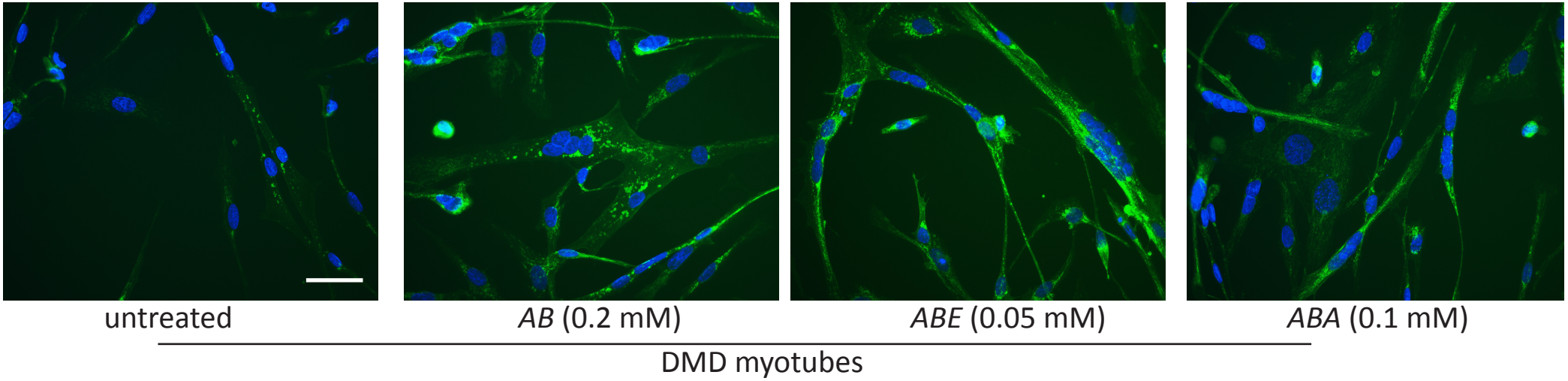

Figure 7: Immunostaining of utrophin in skeletal muscle cell line derived from DMD patients and treated for 48 h with *AB* (0.2 mM), *ABE* (0.05 mM) and *ABA* (0.1 mM). Little staining was observed in untreated myotubes, but utrophin was clearly detected at the sarcolemma in treated myotubes. Scale bar, 150 µm.

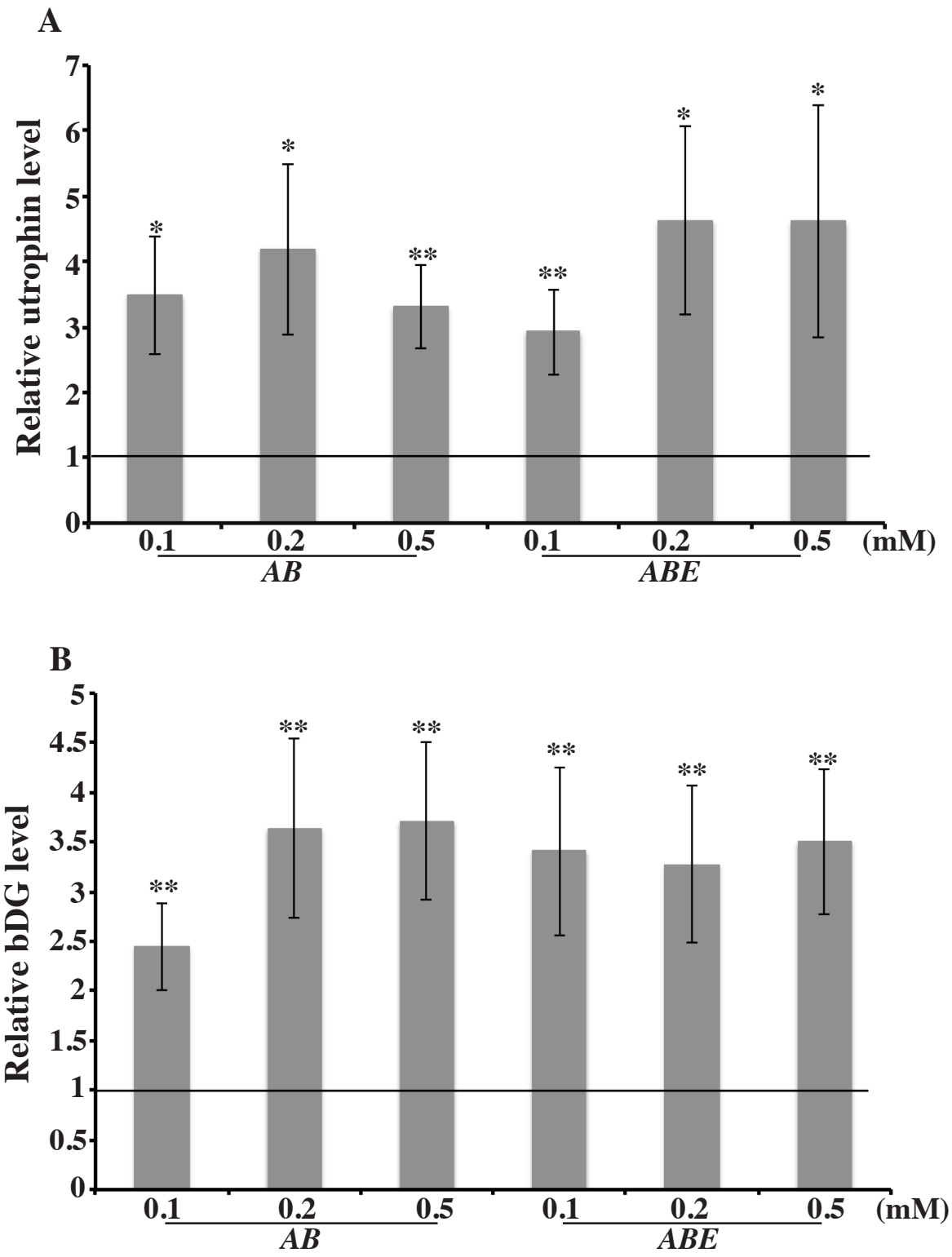

Figure 8: Semi-quantitative western-blot analysis of (A) utrophin and (B) β-dystroglycan (bDG) in skeletal muscle cell line derived from DMD patients and treated for 48 h with *AB* and *ABE* at concentration ranging from 0.1 to 0.5 mM. Results were normalized to saline values (treated/saline ratio with saline = 1, black line). Values are representative of three independent experiments. Increases of about 4 fold for utrophin level and 3 fold for bDG level are detected with both drugs. Student's t-test with the level of significance set at 0.05.

HDAC inhibitors increase utrophin, β-dystroglycan and embryonic myosin levels in human DMD myotubes

To address the potential contribution of HDAC inhibitors to the increase in utrophin, β-dystroglycan and embryonic myosin levels in myotubes treated with *AB*, *ABE* or *ABA*, we directly tested the effects of a selection of HDAC inhibitors among those currently used as medicinal products. The levels of utrophin, β-dystroglycan and embryonic myosin were quantified by western blot in human differentiate myotubes derived from cell line, treated for 48 h with trichostatin (0.05-1 µM), valproate acid (0.25-2 mM), butyrate (0.1-5 mM) or isobutyramide (0.5-5 mM). All treatments increased utrophin, β-dystroglycan and embryonic myosin levels by 2-3 fold, compared with untreated myotubes (**Fig. 9**). These results demonstrate that HDAC inhibitors, by themselves, increase the levels of these proteins. Moreover, the correct localisation of utrophin at the membrane of treated-myotubes has been checked by immunofluorescence staining. The results reveal that few immunostaining was observed in untreated myotubes compared to the clear straining detected under the sarcolemma in treated cells (**Supplementary data 6**).

L-arginine and HDAC inhibitors reduce the spontaneous Ca^{2+} spikes in human DMD myotubes

Human differentiate myotubes derived from cell line were used to address the effects of drugs (*AB*, *ABE*, *ABA* but also trichostatin, L-arginine and butytate) on Ca^{2+} spikes at rest. Recordings were performed for 10 min, with a confocal microscope, on healthy, untreated- and 48 h treated-DMD myotubes, loaded with Fluo-4 AM. Healthy myotubes displayed no spontaneous Ca^{2+} spikes (**Fig. 10A, C)**. In contrast, 64% of untreated-DMD myotubes displayed spontaneous Ca^{2+} spikes (**Fig. 10A and B**) of amplitude of 2 fold above the basal activity and with a frequency of 2 ± 0.14 spikes/min (**Fig. 10C**). In DMD cell cultures treated for 48 h with L-arginine (5 mM), butyrate (1 mM), *AB* (1 mM), *ABE* (0.1 mM), *ABA* (0.1 mM) or trichostatin (0.1 µM), the number of myotubes displaying spontaneous Ca^{2+} spikes was reduced by around 50%, *i.e.* less than 20-30% of cells were active (**Fig. 10A**), compared with untreated DMD myotubes. In those 30% of active cells, the amplitude and frequency of Ca^{2+} oscillations were comparable to untreated myotubes as illustrated in (**Fig. 10C**).

DISCUSSION

We explored a pharmacological approach to treat DMD patients, by investigating the potential benefit of two new prodrugs, *ABE* and *ABA*. *ABE* corresponds to 3-hydroxybutyrate arginate, the association of L-arginine and butyrate *via* a covalent ester link, while *ABA* corresponds to N-butyrylarginine where the covalent link is an amine. Both have been designed to be administrated *per os* to patients, protected from gastric degradation and expected to be effective and beneficial at lower doses than *AB*. Indeed, the dose optimal of AB for mice corresponds to 16 g/d for a 20 kg boy.

In vivo effects of increasing doses of *ABE* and *ABA*, ranging from 50 to 800 mg/kg/d (rationale: 800 mg/kg/d is the optimal dose determined for *AB*), were addressed by using a minimally invasive protocol dedicated to the analysis of neuromuscular excitability parameters, designed first in patients and then adapted to laboratory animals. As demonstrated previously (Vianello *et al.*, submitted), numerous neuromuscular excitability parameters exhibited some significant differences in saline-treated *mdx* mice, when compared with C57BL/10

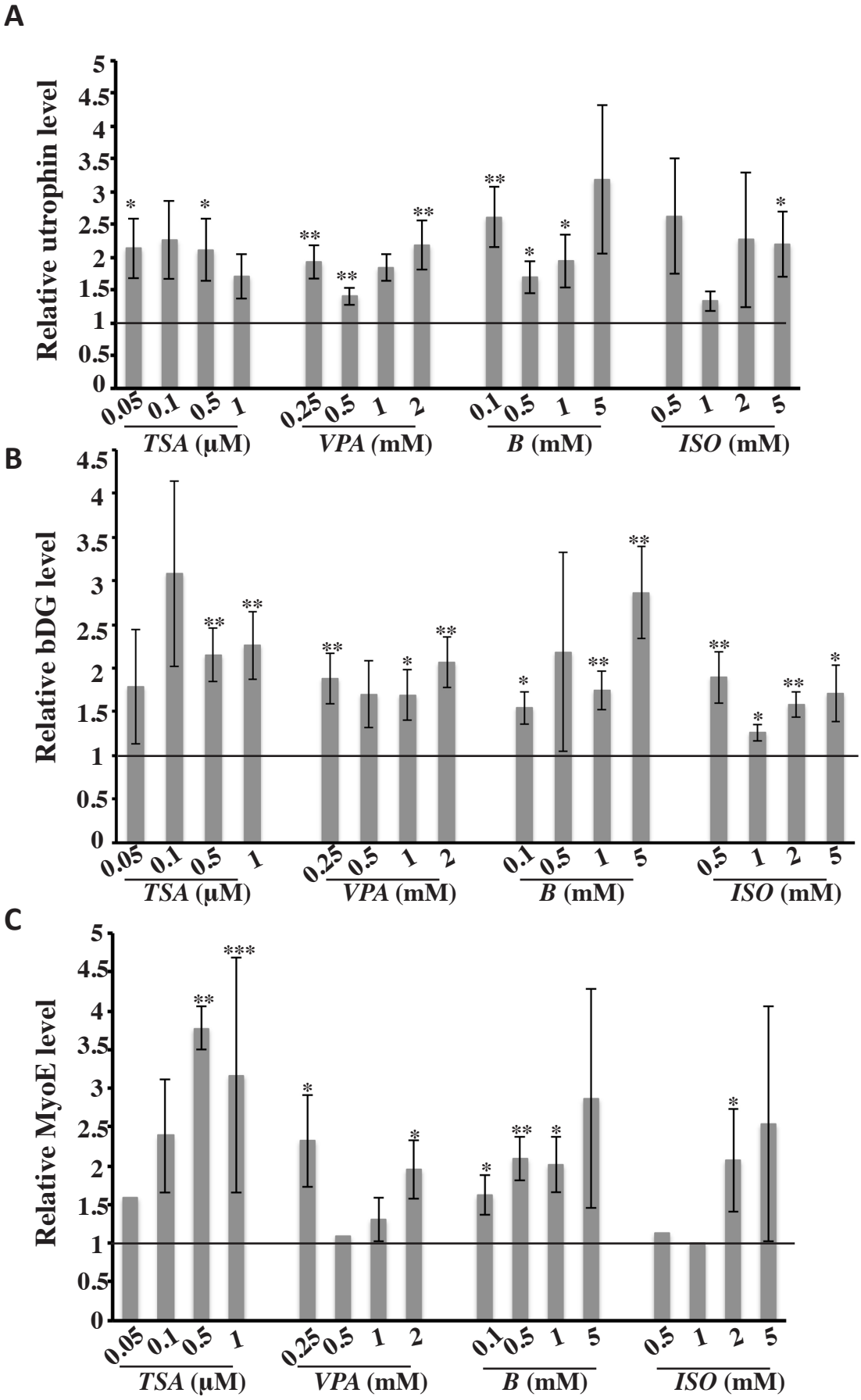

Figure 9: Semi-quantitative western-blot analysis of (A) utrophin, (B) β-dystroglycan (bDG) and (C) embryonic myosin (MyoE) levels in a skeletal muscle cell line derived from DMD patients and treated for 48 h with HDAC inhibitors of clinical use at various concentrations: trichostatin A (*TSA*), valproic acid (*VPA*), butyrate (*B*) and isobutyramide (*ISO*). Results were normalized to saline values (treated/saline ratio with saline = 1, black line). Values are representative of three independent experiments. Increases of about by 2-3 fold fold for utrophin, bDG and embryonic myosin level are detected with all drugs. Note that *TSA* is efficient at low dose (µM versus mM). Student's t-test with the level of significance set at 0.05.

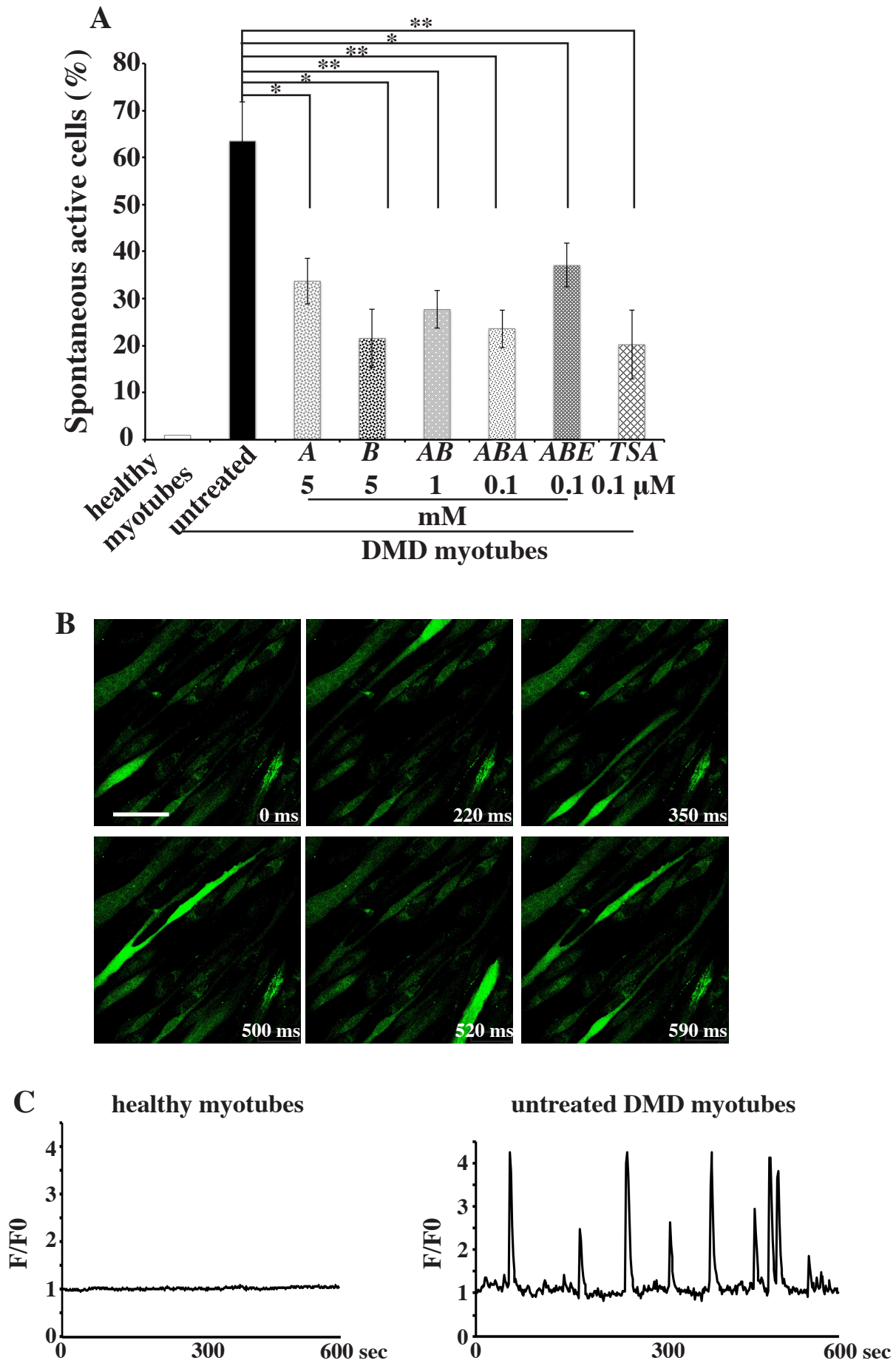

Figure 10: Spontaneous Ca^{2+} spikes in healthy, untreated- and treated-DMD myotubes (cell lines). (A) Quantification of spontaneous spikes: healthy myotubes display only basal activity, while 64% of DMD myotubes display spontaneous Ca^{2+} spikes. In cell cultures treated for 48 h with L-arginine (5 mM), butyrate (1 mM), *AB* (1 mM), *ABE* (0.1 mM), *ABA* (0.1 mM) or trichostatin (0.1 µM), the number of myotubes displaying spontaneous Ca2+ spikes was reduced by about 50%. (B) Illustration of the spontaneous spikes recorded in untreated DMD myotubes. (C) Examples of recording tracks in representative region of interest in healthy and untreated-DMD myotubes. These data suggest that the treatments strongly ameliorate Ca^{2+} homeostasis. Student's t-test with the level of significance set at 0.05. Scale bar, 150 µm.

animals. These changes mainly consisted in (i) a higher threshold, an enhanced latency and a reduced CMAP amplitude, (ii) an increased rheobase and a reduced chronaxis, (iii) a reduced minimum I-V slope, (iv) less threshold changes in response to a constant depolarizing long-duration current of sub-threshold intensity, and (v) increased refractoriness which were modified in the caudal muscle recordings. Most of the parameters modified in the plantar muscle were also modified in the caudal muscle, except the CMAP amplitude and the latency values which are not different. These changes could be explained by a different contribution of sodium and potassium channels in *mdx* and C57BL/10 animals that could result from a subtle disorganization of the myelin sheath of the peripheral nerve, leading to modifications of repartition and density of ion channels in *mdx* mice, which may influence also the CMAP amplitude. The fragmentation of the neuromuscular junction, the excessive nerve sprouting (Marques et al., 2007) and the decrease of the number and depth of synaptic folds that promote the decrease of the density of voltage-gated sodium channels to the synapse (Banks et al., 2009), described in *mdx* mice, support our explanation. Moreover, the increased latency of CMAP in saline-treated *mdx* mice may reflect the morphological alterations at the neuromuscular junction that influence action potential propagation. In *ABE*- and *ABA*-treated *mdx* mice, all abnormal excitability parameters return to C57BL/10 animal values, in a dose-dependent manner, with a maximum of efficiency at doses around 80 mg/kg/d. Higher doses (200-800 mg/kg/d) of both prodrugs outcome to a progressive re-increase in the number of modified excitability parameters, compared with C57BL/10 mice, probably resulting from a toxic effect of the two molecules**.**

The skeletal muscle strength and tirelessness were also improved in *ABE* and *ABA*-treated mice, with a maximal effect around 80 mg/kg/d. Semi-quantitative western blot analyses revealed an increase of about 40% of utrophin level in the *gastrocnemius* muscle of *ABE*-treated *mdx* mice, confirming the data obtained with AB (Vianello et al., 2013). Moreover, the surface of necrosis in heart sections is clearly reduced in *mdx* mice treated with *ABE* or *ABA* at doses of 80 mg/kg/d and 100-200 mg/kg/d, respectively. The increase in necrotic surface at higher doses supports the hypothesis that the molecules may be noxious.

Based on the evidence of dose-response relationships indicating that *ABE* and *ABA* were efficient at low doses, further studies were undertaken with the doses 50 and 80 mg/kg/d of both prodrugs to investigate membrane integrity of skeletal and cardiac membranes. The results reveal that (i) the CK level in the serum of *ABE*- or *ABA*-treated mice was reduced by about 70%, (ii) *ABE* reduces the incorporation of Evans's Blue dye and finally. These results confirm that low doses (around 80 mg/kg/d) of the covalently forms produce the same benefit than high doses (800 mg/kg/d) of the salted formulation ((Vianello et al., 2013) Vianello *et al.* submitted). And (iii) the analysis of the effect of *ABE* (80 mg/kg/d) treatment on the lipid composition of heart membranes, by mass spectrometry imaging evidenced a direct effect on ABE on membrane lipid composition and suggested a stabilisation of the membrane.

Indeed, the restoration of a normal phosphatidylcholine PC34:2/PC34:1 ion peak intensity ratio in the skeletal muscle membrane of *mdx* mice treated with molsidomine (a NO donor), has been

hypothetically related to incorporation of fatty acids in the membrane and/or to the process of muscle regeneration (Benabdellah et al., 2009). To address this point, the heart is a good model, since newborn are able to produce new heart cells to replace injured ones. However, this ability is lost early in life (generally, seven days after birth), and the adult heart lacks this regenerative capacity (Kikuchi and Poss, 2012). The analysis of the effect of *ABE* (80 mg/kg/d) treatment on the lipid composition of heart membranes, by TOF-SIMS imaging, permits to demonstrate that a specific fatty acid (C16:0), highly expressed in non-necrotic areas in saline-treated *mdx* mice, comebacks to a level comparable that of C57BL/10 animals in *ABE*-treated *mdx* mice. Similar results were observed in necrotic areas with nevertheless a difference: C16:0 ion and remains expressed but to low level in ABE-treated *mdx* mice. The same profile of variation was observed for the ratio R3 corresponding to the intensity of the C18:1 fatty acid ion signal at *m/z* 281.3 over that of the C18:2 fatty acid ion signal at *m/z* 279.2. Our data indicate that treatment with *ABE* (80 mg/kg/d) induces a direct modification of lipid composition in heart membrane, independently of the regeneration process. A consequence of deficit in the composition of the lipid bilayer in dystrophic membrane is that the molecules of CK are able to pass through the plasmic membrane (Ozawa et al., 1999). The reestablishment of a correct lipid composition in membranes could participate to the global benefit obtained after ABE or ABA treatment, and to the functional benefit on heart function observed in *mdx* mice chronically treated with *AB* (Vianello *et al.*, submitted). The benefit of *ABE* treatment on heart in *mdx* mice is particularly important because DMD patients progressively develop into clinically apparent cardiomyopathy over 18 years of age. Very interestingly, the two signals, C16:0 ion and R3 ratio, where decrease in ABE-treated *mdx* mice. In addition, two new markers were evidenced by MALDI-ToF mass spectrometry imaging: (1) the cardiolipine (CL, 18:2/18:2/18:2/18:2), specifically detected in non-necrotic areas tissue and (2) the phosphatidylinositol (PI,18:0/20:4), specifically detected in necrotic tissue. These four new markers could be used, in dystrophic animals (*mdx* mice and presumably canine model), to separate necrotic/structured areas and specifically follow the benefit of a given treatment. Together these data strongly suggest that *ABE* protects the integrity of the membrane.

Overall, these results indicate that *ABE* and *ABA* are efficient at low doses (50 and 80 mg/kg/d) compared with the optimal dose of *AB* (800 mg/kg/d) (Vianello et al., 2013) (Vianello *et al.*, submitted). In particular, *ABE* was efficient at 80 mg/kg/d, *i.e.* 10 times lower compared with *AB*. With the limitation to start before the dystrophic phenotype establishment irreversibility occurrence, *ABE* (or *ABA*, for which further complementary preclinical analyses are necessary) treatment could bring a real profit to the patients.

In parallel to *in vivo* studies and with the objective of a clinical application, we addressed some aspects of the beneficial effect of *ABE* and *ABA* on myotubes from DMD patients. The levels of utrophin, β-dystroglycan and embryonic myosin were quantified in cultures of human primary myotubes, which contain contaminating fibroblasts, treated for 48 h with *AB* (used as reference), *ABA* and *ABE*. The treatments with these three products increase utrophin, β-dystroglycan and embryonic myosin levels by around 2 fold,

compared with untreated myotubes. For *ABE* treatment, dose-response effects were observed with utrophin, β-dystroglycan and embryonic myosin levels, with a maximal increase at doses 4 times as low as *AB*. Concerning *ABA*, a maximal increase was obtained with doses from 0.1 to 0.5 mM, although no clear dose-effect response was observed. Utrophin immunostaining revealed localization in myotube membranes, and the staining strongly increased in *ABE*-treated myotubes. This strongly suggests that up-regulation of utrophin level compensates for the absence of dystrophin and stabilises the sarcolemma.

A 4-fold increase was obtained in cultures of pure myotubes, suggesting a better answer to the treatment of the myotubes from cell line, than that of primary cultures, which are contaminated by fibroblasts. Nevertheless, the overexpression of utrophin in fibroblasts could not be excluded. Fortunately the forced overexpression of utrophin in a broad range of non-muscle tissues in transgenic *mdx* mice appears innocuous (Fisher et al., 2001). Other hypothesis could be that fibroblasts inhibit ABE/ABA processing.

To explain the better global beneficial effect of *ABE* than *ABA* treatment both *in vivo* and *in vitro,* several hypotheses can be formulated. Amidases and esterases are widespread but the major problem in designing amine prodrugs is the general robustness of amine derivatives. Ester prodrugs are in general readily hydrolysed by the rich variety of hydrolase enzymes present in the human body, while cetylation of amines is more robust (Simplício et al., 2008). In this context, preclinical pharmacokinetic/pharmacodynamics analysis would be helpful to confirm the relationship.

Inhibitors of HDAC ameliorate dystrophin phenotype in *mdx* mice: trichostatin (Minetti et al., 2006), valproic acid (Gurpur et al., 2009), givinostat (Consalvi et al., 2013) and, indirectly, silent mating type information regulator 2 homolog 1 (SIRT1) (*via* resveratrol) (Gordon et al., 2013; Hori et al., 2011). In these studies contradictory results were obtained concerning utrophin level: no increase with trichostatin, and an increase in utrophin mRNA but not of the protein with reverastrol. We directly addressed, in an *in vitro* model, the possible participation to the benefit of an increase of utrophin induced by HDAC inhibitor, a plausible hypothesis because utrophin can be considered as the embryonic form of the dystrophin. Supporting this hypothesis, it has been demonstrated that butyrate, the second component of *AB*, (i) increases embryonic globin gene expression in chickens pretreated with 5-azacytidine, (ii) causes higher levels of fœtal hemoglobin at birth in infants born from diabetic mothers, (iii) delays the switch from fœtal to adult haemoglobin in sheep exposed to butyrate *in utero* and finally (iii) increases fœtal hemoglobin levels in adult baboons (Weinberg et al., 2005). We addressed the potential capacity of HDAC inhibitors to increase utrophin expression in an *in vitro* model, and demonstrated that butyrate, trichostatin, isobutyramide and valproic acid increase around 2-3 fold utrophin, β-dystroglycan and embryonic myosin levels in human DMD myotubes. The comparison of doses used with butyrate used alone or in combination with L-arginine confirms the synergic effect (Vianello et al., 2013). We also observed a clear increase of utrophin in *mdx* mice treated with those HDAC inhibitors (unpublished data). In the 1970s, butyrate was shown to induce histone hyperacetylation through inhibition of HDAC so it is widely assumed, although never proven, that it is able to

increase fœtal hemoglobin levels expression through changes in histone acetylation. Concerning utrophin, the increase of chromatin acetylation state in human myotubes treated with, butyrate and *AB* has been demonstrated (Vianello et al., 2013)

Finally, *AB*, *ABE*, *ABA* and HDAC reduce the spontaneous Ca^{2+} activity, which characterizes human DMD myotubes, suggesting a better regulation of Ca^{2+} homeostasis probably related to the restoration of normal membrane, in accordance to *in vivo* results that demonstrated that *ABE* treatment reduces the incorporation of Evans Blue dye, and protects heart membrane from degeneration. *ABE* and *ABA* treatment could prevent or delay cellular damages resulting from the disruption of calcium homeostasis described in *mdx* mice and DMD patient. This hypothesis is in agreement with the observation that forced expression of mini-dystrophin in dystrophic myotubes, reactivates appropriate sarcolemmal expression of dystrophin-associated proteins and restores normal calcium handling in the cytosol (Constantin et al., 2006). Furthermore, the forced expression of full-length dystrophin (by plasmid microinjection) in myotubes, prevents the development of the calcium-handling abnormalities by maintaining the resting Ca^{2+} concentration at low levels and decreasing global calcium-release amplitudes (Marchand et al., 2004). Further studies are necessary to address these parameters in case of utrophin up-regulation but our results are in favour of this hypothesis. Moreover, it has been described that resting intracellular Ca^{2+} is indirectly implicated in the nitric oxide (NO) production through the modulation of NF-*k*B pathway in *mdx* mice (Altamirano et al., 2012). A decrease of inflammation and a restoration of the NF-*k*B pathway, likely *via* utrophin up-regulation, has been described in L-arginine-treated *mdx* mice (Hnia et al., 2008). It could be interesting to directly undertake parameters of the NF-*k*B pathway in myotubes with Ca^{2+} activity normalized by ABE.

In conclusion, the abnormalities detected in saline-treated *mdx* mice were corrected by the treatment with *ABE* or *ABA* at doses 5 (*in vitro*) and 10 (*in vivo*) fold lower than the salted formulation (*AB*), reflecting probably that AB is rapidly degraded and that amidase and esterase levels are different *in vivo* and *in vitro*. In particular, sarcolemmal integrity is restored. In addition the non-invasive automatized sequential acquisition of multiple excitability tests developed in clinical neurophysiology could be useful to monitor treatment effects, in DMD patients, over time. All these data making us confident for a future clinical trial.

ACKNOWLEDGEMENTS

We thank the French *"Banque de Tissus pour la Recherche"* (*BTR, Institut de Myologie*) for providing surgical residues of human paravertebral striated muscles. *BTR* is a partner of the EuroBioBank network funded by the EC under the Fifth Framework Program (QLRI-CT-2002-02769). We thank Dr. D. Boërio for having introduced the techniques of recording the neuromuscular excitability to the laboratory, Drs Mouly (Hôpital Pitié-Salpêtrière, Paris, France) and Muntoni (Center for neuromuscular disease, London, UK) for providing human cell lines, and K. Mamchaoui (Hôpital Pitié-Salpêtrière, Paris, France) for his technical help.

Conflicts of Interest statement: none declared.

REFERENCES

Altamirano, F., López, J.R., Henríquez, C., Molinski, T., Allen, P.D., and Jaimovich, E. (2012). Increased resting intracellular calcium modulates NF-κB-dependent inducible nitric-oxide synthase gene expression in dystrophic mdx skeletal myotubes. J. Biol. Chem. *287*, 20876–20887.

Banks, G.B., Chamberlain, J.S., and Froehner, S.C. (2009). Truncated dystrophins can influence neuromuscular synapse structure. Mol. Cell. Neurosci. *40*, 433–441.

Benabdellah, F., Yu, H., Brunelle, A., Laprévote, O., and De La Porte, S. (2009). MALDI reveals membrane lipid profile reversion in MDX mice. Neurobiol. Dis. *36*, 252–258.

Blake, D.J., Weir, A., Newey, S.E., and Davies, K.E. (2002). Function and genetics of dystrophin and dystrophin-related proteins in muscle. Physiological Reviews *82*, 291–329.

Boerio, D., Greensmith, L., and Bostock, H. (2009). Excitability properties of motor axons in the maturing mouse. J Peripher Nerv Syst *14*, 45–53.

Bostock, H., Cikurel, K., and Burke, D. (1998). Threshold tracking techniques in the study of human peripheral nerve. Muscle Nerve *21*, 137–158.

Consalvi, S., Mozzetta, C., Bettica, P., Germani, M., Fiorentini, F., Del Bene, F., Rocchetti, M., Leoni, F., Mascagni, P., Puri, P.L., et al. (2013). Preclinical studies in the mdx mouse model of Duchenne Muscular Dystrophy with the Histone Deacetylase inhibitor Givinostat. Mol. Med.

Constantin, B., Sebille, S., and Cognard, C. (2006). New insights in the regulation of calcium transfers by muscle dystrophin-based cytoskeleton: implications in DMD. Journal of Muscle Research and Cell Motility *27*, 375–386.

Edom, F., Mouly, V., Barbet, J.P., Fiszman, M.Y., and Butler-Browne, G.S. (1994). Clones of human satellite cells can express in vitro both fast and slow myosin heavy chains. Dev Biol *164*, 219–229.

Fairclough, R.J., Bareja, A., and Davies, K.E. (2011). Progress in therapy for Duchenne muscular dystrophy. Exp. Physiol. *96*, 1101–1113.

Finkel, R.S. (2010). Read-through strategies for suppression of nonsense mutations in Duchenne/ Becker muscular dystrophy: aminoglycosides and ataluren (PTC124). J. Child Neurol. *25*, 1158–1164.

Fisher, R., Tinsley, J.M., Phelps, S.R., Squire, S.E., Townsend, E.R., Martin, J.E., and Davies, K.E. (2001). Non-toxic ubiquitous over-expression of utrophin in the mdx mouse. Neuromuscul Disord *11*, 713–721.

Gordon, B.S., Delgado Díaz, D.C., and Kostek, M.C. (2013). Resveratrol decreases inflammation and increases utrophin gene expression in the mdx mouse model of duchenne muscular dystrophy. Clin Nutr *32*, 104–111.

Goyenvalle, A., and Davies, K.E. (2011). Challenges to oligonucleotides-based therapeutics for Duchenne muscular dystrophy. Skelet Muscle *1*, 8.

Gurpur, P.B., Liu, J., Burkin, D.J., and Kaufman, S.J. (2009). Valproic acid activates the PI3K/Akt/mTOR pathway in muscle and ameliorates pathology in a mouse model of Duchenne muscular dystrophy. Am. J. Pathol. *174*, 999–1008.

Hnia, K., Gayraud, J., Hugon, G., Ramonatxo, M., De La Porte, S., Matecki, S., and Mornet, D. (2008). L-arginine decreases inflammation and modulates the nuclear factor-kappaB/matrix metalloproteinase cascade in mdx muscle fibers. The American Journal of Pathology *172*, 1509–1519.

Hori, Y.S., Kuno, A., Hosoda, R., Tanno, M., Miura, T., Shimamoto, K., and Horio, Y. (2011). Resveratrol ameliorates muscular pathology in the dystrophic mdx mouse, a

model for Duchenne muscular dystrophy. J. Pharmacol. Exp. Ther. *338*, 784–794.
Kiernan, M.C., Burke, D., Andersen, K.V., and Bostock, H. (2000). Multiple measures of axonal excitability: a new approach in clinical testing. Muscle Nerve *23*, 399–409.
Kikuchi, K., and Poss, K.D. (2012). Cardiac regenerative capacity and mechanisms. Annu. Rev. Cell Dev. Biol. *28*, 719–741.
Krishnan, A.V., Lin, C.S.-Y., Park, S.B., and Kiernan, M.C. (2008). Assessment of nerve excitability in toxic and metabolic neuropathies. J. Peripher. Nerv. Syst. *13*, 7–26.
Marchand, E., Constantin, B., Balghi, H., Claudepierre, M.-C., Cantereau, A., Magaud, C., Mouzou, A., Raymond, G., Braun, S., and Cognard, C. (2004). Improvement of calcium handling and changes in calcium-release properties after mini- or full-length dystrophin forced expression in cultured skeletal myotubes. Exp. Cell Res. *297*, 363–379.
Marques, M.J., Taniguti, A.P.T., Minatel, E., and Neto, H.S. (2007). Nerve terminal contributes to acetylcholine receptor organization at the dystrophic neuromuscular junction of mdx mice. Anat Rec (Hoboken) *290*, 181–187.
Meregalli, M., Farini, A., Parolini, D., Maciotta, S., and Torrente, Y. (2010). Stem cell therapies to treat muscular dystrophy: progress to date. BioDrugs *24*, 237–247.
Minetti, G.C., Colussi, C., Adami, R., Serra, C., Mozzetta, C., Parente, V., Fortuni, S., Straino, S., Sampaolesi, M., Di Padova, M., et al. (2006). Functional and morphological recovery of dystrophic muscles in mice treated with deacetylase inhibitors. Nat. Med. *12*, 1147–1150.
Ozawa, E., Hagiwara, Y., and Yoshida, M. (1999). Creatine kinase, cell membrane and Duchenne muscular dystrophy. Mol. Cell. Biochem. *190*, 143–151.
Perrine, S.P. (2008). Fetal globin stimulant therapies in the beta-hemoglobinopathies: principles and current potential. Pediatr Ann *37*, 339–346.
Perrine, S.P., and Faller, D.V. (1993a). Butyrate-induced reactivation of the fetal globin genes: a molecular treatment for the beta-hemoglobinopathies. Experientia *49*, 133–137.
Perrine, S.P., and Faller, D.V. (1993b). Butyrate-induced reactivation of the fetal globin genes: a molecular treatment for the beta-hemoglobinopathies. Experientia *49*, 133–137.
Pichavant, C., Aartsma-Rus, A., Clemens, P.R., Davies, K.E., Dickson, G., Takeda, S., Wilton, S.D., Wolff, J.A., Wooddell, C.I., Xiao, X., et al. (2011). Current status of pharmaceutical and genetic therapeutic approaches to treat DMD. Mol. Ther. *19*, 830–840.
Quinlan, J.G., Hahn, H.S., Wong, B.L., Lorenz, J.N., Wenisch, A.S., and Levin, L.S. (2004). Evolution of the mdx mouse cardiomyopathy: physiological and morphological findings. Neuromuscul. Disord. *14*, 491–496.
Simplício, A.L., Clancy, J.M., and Gilmer, J.F. (2008). Prodrugs for amines. Molecules *13*, 519–547.
Spurney, C.F., Knoblach, S., Pistilli, E.E., Nagaraju, K., Martin, G.R., and Hoffman, E.P. (2008). Dystrophin-deficient cardiomyopathy in mouse: expression of Nox4 and Lox are associated with fibrosis and altered functional parameters in the heart. Neuromuscul. Disord. *18*, 371–381.
Straub, V., Rafael, J.A., Chamberlain, J.S., and Campbell, K.P. (1997). Animal models for muscular dystrophy show different patterns of sarcolemmal disruption. J Cell Biol *139*, 375–385.
Tahallah, N., Brunelle, A., De La Porte, S., and Laprevote, O. (2008). Lipid mapping in human dystrophic muscle by cluster-time-of-flight secondary ion mass spectrometry imaging. Journal of Lipid Research *49*, 438–454.

Touboul, D., Piednoel, H., Voisin, V., De La Porte, S., Brunelle, A., Halgand, F., and Laprevote, O. (2004). Changes of phospholipid composition within the dystrophic muscle by matrix-assisted laser desorption/ionization mass spectrometry and mass spectrometry imaging. European Journal of Mass Spectrometry (Chichester, England) *10*, 657–664.

Touboul, D., Brunelle, A., Halgand, F., De La Porte, S., and Laprévote, O. (2005). Lipid imaging by gold cluster time-of-flight secondary ion mass spectrometry: application to Duchenne muscular dystrophy. J. Lipid Res. *46*, 1388–1395.

Vianello, S., Yu, H., Voisin, V., Haddad, H., He, X., Foutz, A.S., Sebrié, C., Gillet, B., Roulot, M., Fougerousse, F., et al. (2013). Arginine butyrate: a therapeutic candidate for Duchenne muscular dystrophy. FASEB J.

Weinberg, R.S., Ji, X., Sutton, M., Perrine, S., Galperin, Y., Li, Q., Liebhaber, S.A., Stamatoyannopoulos, G., and Atweh, G.F. (2005). Butyrate increases the efficiency of translation of gamma-globin mRNA. Blood *105*, 1807–1809.

Whitehead, N.P., Yeung, E.W., and Allen, D.G. (2006). Muscle damage in mdx (dystrophic) mice: role of calcium and reactive oxygen species. Clin. Exp. Pharmacol. Physiol. *33*, 657–662.

Yiu, E.M., and Kornberg, A.J. (2008). Duchenne muscular dystrophy. Neurol India *56*, 236–247.

A

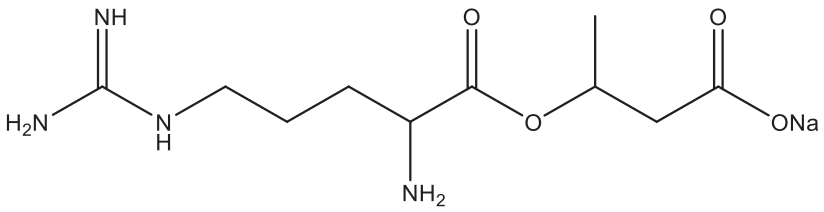

B

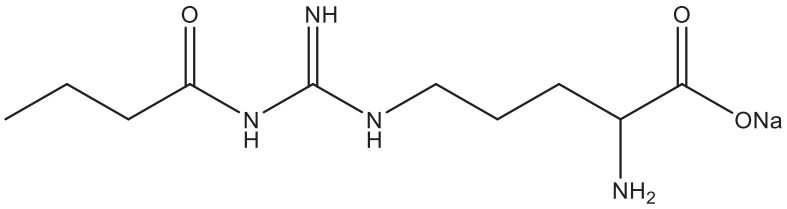

Supplementary data 1: Chemical structure of (A) 3-hydroxybutyrate arginate, referenced as *ABE* (ester link), and (B) N-butyrylarginine referenced as *ABA* (amide link). ChemDraw software.

Caudal muscle

		mdx						
			ABA (mg/kg/d)					
	C57BL/10	saline	50	80	100	200	400	800
CMAP amplitude (mV)[1]	3.68 ± 0.12	1.11 ± 0.12**	1.81 ± 0.12*	2.19 ± 0.48	3.38 ± 0.12	3.29 ± 0.55	2.40 ± 0.45*	2.54 ± 0.14*
Latency (ms)[1]	3.16 ± 0.06	3.62 ± 0.13*	3.38 ± 0.12	3.31 ± 0.14	3.26 ± 0.06	3.79 ± 0.16**	3.59 ± 0.13**	3.60 ± 0.15*
Stimulus (mA) for 50% max response[1]	0.28 ± 0.06	0.38 ± 0.09*	0.33 ± 0.07	0.33 ± 1.15	0.27 ± 1.12	0.34 ± 1.19	0.39 ± 1.10**	0.27 ± 1.12
Strength-duration time constant (ms)[2]	0.49 ± 0.03	0.36 ± 0.02**	0.52 ± 0.07	0.52 ± 0.05	0.49 ± 0.11	0.67 ± 0.14	0.58 ± 0.13	0.70 ± 0.07*
Rheobase (mA)[2]	0.18 ± 0.08	0.26 ± 0.11*	0.19 ± 0.10	0.20 ± 1.17	0.15 ± 1.16	0.21 ± 1.21	0.24 ± 1.28	0.16 ± 1.18
Minimum I-V slope[3]	0.26 ± 0.01	0.22 ± 0.01**	0.29 ± 0.06	0.28 ± 0.10*	0.26 ± 0.03	0.19 ± 0.03*	0.29 ± 0.06	0.19 ± 0.01**
S2 accommodation[4]	15.30 ± 0.70	11.43 ± 0.77**	11.74 ± 0.75**	12.70 ± 2.14	13.20 ± 1.00	14.58 ± 3.93	13.93 ± 2.13	18.37 ± 0.65*
TEd(10-20ms)[4]	64.77 ± 1.01	53.80 ± 1.75***	53.83 ± 1.83***	55.02 ± 3.41*	60.55 ± 2.81	60.77 ± 2.72	52.42 ± 3.55**	52.36 ± 4.88**
TEd(40-60ms)[4]	50.79 ± 0.88	44.73 ± 1.25**	47.82 ± 1.83	48.61 ± 4.38	50.56 ± 1.80	51.37 ± 2.66	44.15 ± 2.38*	38.43 ± 3.94**
TEd(peak)[4]	63.32 ± 0.91	53.00 ± 1.58***	54.22 ± 1.64***	55.17 ± 2.97*	59.42 ± 2.61	59.83 ± 2.75	52.18 ± 3.47**	51.37 ± 4.18**
TEd20(peak)[4]	37.68 ± 0.69	32.19 ± 1.07**	33.13 ± 1.10**	35.46 ± 1.27	34.18 ± 1.67	34.07 ± 1.90	31.34 ± 1.72**	31.61 ± 2.04**
Relative refractory period (ms)[5]	1.65 ± 1.06	2.18 ± 1.13*	2.08 ± 1.09*	2.09 ± 1.04*	1.77 ± 1.08	1.503 ± 1.04	2.11 ± 1.06*	nd
Refractoriness at 2ms (%)[5]	-7.96 ± 1.65	3.42 ± 3.70*	9.39 ± 5.82*	1.05 ± 5.42	-4.53 ± 3.88	-7.38 ± 0.86	5.61 ± 4.47**	6.24 ± 8.93*
Refractoriness at 2.5ms (%)[5]	-11.67 ± 0.88	-2.59 ± 2.66*	-0.27 ± 4.56*	-10.48 ± 4.05	-10.95 ± 2.77	-10.45 ± 2.09	-1.40 ± 2.62**	-0.45 ± 5.99*
Stimulus-response slope[1]	3.23 ± 1.19	3.92 ± 1.20	3.34 ± 1.25	3.34 ± 1.32	2.54 ± 1.36	2.67 ± 1.79	2.94 ± 1.30	4.18 ± 1.56
Resting I-V slope[3]	0.52 ± 0.03	0.51 ± 0.04	0.77 ± 0.20	0.53 ± 0.05	0.50 ± 0.05	0.51 ± 0.07	0.63 ± 0.13	1.06 ± 0.16**
Hyperpolarizing I-V slope[3]	0.43 ± 0.01	0.45 ± 0.02	0.54 ± 0.06	0.61 ± 0.11	0.46 ± 0.05	0.43 ± 0.06	0.45 ± 0.06	0.47 ± 0.03
Accommodation half-time (ms)[4]	30.66 ± 1.28	35.85 ± 2.49	41.44 ± 4.31	28.76 ± 3.63	40.47 ± 4.85	36.90 ± 7.18	40.45 ± 7.28	34.88 ± 3.65
S3(-70%)[4]	93.33 ± 5.49	91.44 ± 6.11	88.87 ± 8.52	82.01 ± 16.1	89.42 ± 13.90	nd	66.56 ± 20.00	61.27 ± 7.80*
TEd(90-100ms)[4]	47.97 ± 0.73	45.68 ± 1.28	43.62 ± 2.14	43.16 ± 3.17	46.22 ± 2.47	46.98 ± 0.48	39.95 ± 3.17*	38.15 ± 3.24**
TEd(undershoot)[4]	-8.50 ± 1.26	-8.42 ± 1.07	-7.45 ± 1.45	-9.56 ± 2.20	-11.96 ± 1.69	-9.43 ± 2.50	-7.63 ± 1.28	-13.44 ± 0.96*
TEh(10-20ms)[4]	-99.13 ± 1.88	-97.25 ± 2.30	-97.28 ± 3.36	-97.07 ± 3.38	-99.49 ± 6.41	-125.60 ± 7.06**	-95.69 ± 5.16	-91.19 ± 4.48
TEh(20-40ms)[4]	-135.40 ± 2.80	-135.60 ± 3.90	-137.60 ± 5.59	-134.40 ± 7.86	-132.80 ± 12.70	-170.00 ± 5.37***	-130.80 ± 9.75	-115.00 ± 6.51**
TEh(90-100ms)[4]	-177.80 ± 6.10	-198.80 ± 10.50	-156.20 ± 10.30	-179.50 ± 19.00	-152.90 ± 32.40	-229.90 ± 18.20**	-151.30 ± 10.10*	-143.80 ± 15.80*
TEh(overshoot)[4]	8.15 ± 0.81	7.11 ± 0.70	7.52 ± 1.93	7.83 ± 2.05	8.51 ± 1.51	9.19 ± 3.19	10.19 ± 1.01	10.00 ± 0.32
TEh(peak,-70%)[4]	-321.90 ± 10.30	-302.90 ± 16.20	-299.60 ± 14.50	-341.70 ± 9.01	-322.10 ± 20.30	-365.10 ± 19.50	-306.80 ± 21.70	-263.00 ± 36.10
TEh(slope 101-140ms)[4]	3.43 ± 0.14	3.49 ± 0.17	2.71 ± 0.28	3.43 ± 0.21	2.56 ± 0.68	4.48 ± 0.47*	2.75 ± 0.28*	2.68 ± 0.26*
Superexcitability (%)[5]	-11.80 ± 0.60	-10.79 ± 1.67	-21.76 ± 4.66	-23.87 ± 9.53	-12.46 ± 2.95	-11.95 ± 1.36	-7.19 ± 2.32*	-7.26 ± 1.65**
Superexcitability at 5ms (%)[5]	-9.10 ± 0.89	-8.81 ± 1.63	-6.85 ± 2.85	-8.76 ± 1.50	-8.61 ± 2.79	-10.40 ± 2.73	-6.27 ± 3.40	-2.76 ± 3.24*
Superexcitability at 7ms (%)[5]	-6.50 ± 0.89	-6.27 ± 1.83	-5.81 ± 2.27	-6.47 ± 2.15	-5.49 ± 2.97	-7.95 ± 2.49	-3.53 ± 2.73	-3.45 ± 0.62*
Subexcitability (%)[5]	2.93 ± 0.59	4.70 ± 1.20	3.99 ± 1.14	4.02 ± 1.10	3.65 ± 0.50	3.39 ± 0.82	4.17 ± 1.21	3.62 ± 0.58

Supplementary data 2: Excitability parameters obtained by stimulating the caudal motor nerve and recording the CMAP from caudal muscle in C57BL/10, saline- and *ABA*-treated *mdx* mice. Compared with C57BL/10 mice, all excitability parameters that are modified in saline-treated *mdx* mice (above the black line), do no longer show any significant difference when *mdx* mice were treated with 100 mg/kg/d ABA, with a clear dose-response effect. A progressive amelioration occurs at 50 and 80 mg/kg/d, and the beneficial effect is progressively lost with higher doses (200-800 mg/kg/d).
Exponent numbers correspond to parameters of: (1) Stimulus-response relationship, (2) strength-duration relationship, (3) current-threshold (I-V) relationship, (4) threshold electrotonus (TEd and TEh are threshold electrotonus in response to constant depolarizing and hyperpolarizing long-duration currents of sub-threshold intensity, respectively), (5) recovery cycle; nd: not determined. Statistical test with the level of significance set at 0.05.

Plantar muscle

		mdx					
		ABA (mg/kg/d)					
	C57BL/10	saline	50	80	100	200	400	800
Stimulus (mA) for 50% max response[1]	0.28 ± 1.03	0.41 ± 1.09*	0.24 ± 1.10	0.27 ± 1.20	0.26 ± 1.06	0.23 ± 1.26	0.30 ± 1.21	0.33 ± 1.09
Strength-duration time constant (ms)[2]	0.47 ± 0.01	0.35 ± 0.03*	0.45 ± 0.04	0.37 ± 0.06	0.33 ± 0.03*	0.39 ± 0.05	0.47 ± 0.10	0.36 ± 0.07
Rheobase (mA)[2]	0.18 ± 1.05	0.27 ± 1.09*	0.15 ± 1.11	0.16 ± 1.08	0.19 ± 1.06	0.16 ± 1.26	0.20 ± 1.18	0.22 ± 1.13
Minimum I-V slope[2]	0.48 ± 0.01	0.42 ± 0.01*	0.41 ± 0.01*	0.46 ± 0.07	0.47 ± 0.02	0.44 ± 0.02	0.43 ± 0.05	0.32 ± 0.03**
S2 accommodation[4]	14.24 ± 1.35	7.81 ± 1.58*	12.53 ± 1.77	10.54 ± 0.59*	9.18 ± 0.83*	6.08 ± 2.08*	8.30 ± 0.93**	12.79 ± 2.30
TEd(10-20ms)[4]	50.06 ± 1.62	41.72 ± 1.61*	48.77 ± 2.57	49.66 ± 0.73	43.34 ± 1.13*	44.69 ± 1.87	43.55 ± 0.90**	43.12 ± 1.12**
TEd(peak)[4]	49.26 ± 1.61	42.30 ± 1.43*	48.20 ± 2.16	49.84 ± 0.77	43.34 ± 1.06*	44.89 ± 1.75	44.00 ± 0.68**	44.29 ± 1.20*
TEd20(peak)[4]	26.19 ± 1.41	22.42 ± 0.76*	26.71 ± 2.12	26.81 ± 1.40	22.60 ± 0.31**	25.21 ± 1.47	24.80 ± 0.57	25.28 ± 1.06
Relative refractory period (ms)[5]	1.99 ± 1.10	nd	2.37 ± 1.05	2.26 ± 1.03	2.68 ± 1.11	2.17 ± 1.07	2.06 ± 1.07	2.22 ± 1.05
Refractoriness at 2ms (%)[5]	1.54 ± 3.09	17.95 ± 3.02*	7.47 ± 2.17	6.01 ± 1.30	13.14 ± 4.60	8.90 ± 2.95	3.68 ± 1.78	3.56 ± 2.68
Refractoriness at 2.5ms (%)[5]	-8.41 ± 1.90	0.79 ± 1.69*	-3.22 ± 1.85	-5.13 ± 1.62	2.88 ± 2.82*	1.67 ± 2.18*	-4.78 ± 1.82	-2.98 ± 1.31*
CMAP amplitude (mV)[1]	2.45 ± 0.14	1.90 ± 0.15	2.08 ± 0.38	2.46 ± 0.17	2.34 ± 0.14	2.34 ± 0.18	2.94 ± 0.37	2.85 ± 0.76
Latency (ms)[1]	2.54 ± 0.12	2.31 ± 0.12	2.93 ± 0.17	2.59 ± 0.17	2.54 ± 0.12	2.18 ± 0.09*	2.61 ± 0.15	2.93 ± 0.25
Stimulus-response slope[1]	3.79 ± 1.25	2.15 ± 1.22	2.64 ± 1.13	3.52 ± 1.59	3.14 ± 1.28	2.68 ± 1.23	4.03 ± 1.12	3.62 ± 1.40
Resting I-V slope[3]	0.82 ± 0.03	0.89 ± 0.05	0.77 ± 0.04	0.87 ± 0.05	0.93 ± 0.05	0.88 ± 0.07	0.89 ± 0.13	0.83 ± 0.08
Hyperpolarizing I-V slope[3]	0.54 ± 0.01	0.61 ± 0.13	0.76 ± 0.21	0.53 ± 0.04	0.53 ± 0.03	0.48 ± 0.03	0.46 ± 0.02*	0.59 ± 0.12
Accommodation half-time (ms)[4]	29.29 ± 1.12	32.14 ± 8.67	28.76 ± 1.68	30.53 ± 4.61	30.00 ± 4.19	28.68 ± 6.75	28.34 ± 4.24	28.20 ± 3.79
S3(-70%)[4]	40.33 ± 4.66	22.53 ± 8.14	33.27 ± 5.48	35.03 ± 1.09	26.98 ± 3.33	34.87 ± 2.19	27.12 ± 3.55	19.85 ± 5.73*
TEd(40-60ms)[4]	37.71 ± 2.24	35.62 ± 0.89	37.79 ± 2.03	38.96 ± 2.65	36.43 ± 0.94	40.63 ± 1.42	37.43 ± 0.95	35.05 ± 1.55
TEd(90-100ms)[4]	35.02 ± 1.90	34.49 ± 0.35	35.36 ± 1.84	34.65 ± 2.09	34.21 ± 0.96	38.81 ± 1.09	35.70 ± 0.76	34.38 ± 2.51
TEd(undershoot)[4]	-12.47 ± 0.87	-7.80 ± 1.78	-10.04 ± 1.35	-10.79 ± 1.27	-8.62 ± 0.77*	-4.62 ± 0.87***	-7.75 ± 1.36*	-10.88 ± 5.02
TEh(10-20ms)[4]	-68.13 ± 0.29	-64.16 ± 3.07	-73.57 ± 2.70	-69.41 ± 3.30	-58.78 ± 1.24**	-66.26 ± 1.91	-71.67 ± 2.55	-63.66 ± 3.52
TEh(20-40ms)[4]	-75.76 ± 1.35	-72.40 ± 5.41	-91.39 ± 4.94	-67.88 ± 13.50	-64.21 ± 1.96**	-69.35 ± 2.30	-84.25 ± 5.07	-77.28 ± 3.12
TEh(90-100ms)[4]	-72.11 ± 2.94	-68.94 ± 4.81	-111.00 ± 6.14**	-95.21 ± 11.30	-59.34 ± 1.70**	-61.95 ± 2.71	-89.29 ± 12.40	-95.39 ± 2.59**
TEh(overshoot)[4]	7.58 ± 1.67	3.50 ± 1.25	5.63 ± 1.15	6.23 ± 1.05	5.60 ± 0.65	4.99 ± 0.76	2.78 ± 0.53**	3.14 ± 0.28*
TEh(peak,-70%)[4]	-174.00 ± 1.05	-154.00 ± 11.00	-226.10 ± 9.78**	-210.80 ± 19.60	-141.90 ± 5.76**	-157.70 ± 4.80	-194.80 ± 18.60	-167.20 ± 35.20
TEh(slope 101-140ms)[4]	0.71 ± 0.09	0.55 ± 0.08	0.71 ± 0.17	0.69 ± 0.17	0.37 ± 0.03**	0.34 ± 0.07*	1.35 ± 0.28	1.40 ± 0.10**
Superexcitability (%)[5]	-3.45 ± 1.15	-1.70 ± 0.97	-5.33 ± 1.61	-5.97 ± 2.79	-3.01 ± 1.49	-1.81 ± 0.60	-1.64 ± 0.83	-1.48 ± 0.78
Superexcitability at 5ms (%)[5]	-2.10 ± 1.32	2.47 ± 2.24	-5.84 ± 1.30	-4.74 ± 1.91	-1.01 ± 1.52	1.42 ± 0.80**	1.97 ± 1.50*	3.60 ± 1.05*
Superexcitability at 7ms (%)[5]	-2.94 ± 0.67	3.69 ± 2.66	-3.34 ± 0.92	-3.36 ± 1.58	0.68 ± 1.27	3.74 ± 0.47***	1.79 ± 1.23*	-0.51 ± 0.76
Subexcitability (%)[5]	6.05 ± 0.31	5.04 ± 2.70	5.04 ± 0.57	6.35 ± 1.30	3.76 ± 0.80	3.91 ± 0.72	3.17 ± 0.99	2.21 ± 0.37**

Supplementary data 3: Excitability parameters obtained by stimulating the tibial branch of the sciatic nerve and recording the CMAP from plantar muscle in C57BL/10, saline- and *ABA*-treated *mdx* mice. Compared with C57BL/10 mice, most of excitability parameters that are modified in saline-treated *mdx* mice (above the black line), do no longer show any significant difference when *mdx* mice were treated with low doses of *ABA*, with a clear dose-response effect. A quasi complete rescue of most of excitability parameters occurs at 50-80 mg/kg/d, and the beneficial effect is progressively lost with high doses (100-800 mg/kg/d).

Exponent numbers correspond to parameters of: (1) Stimulus-response relationship, (2) strength-duration relationship, (3) current-threshold (I-V) relationship, (4) threshold electrotonus (TEd and TEh are threshold electrotonus in response to constant depolarizing and hyperpolarizing long-duration currents of sub-threshold intensity, respectively), (5) recovery cycle; nd: not determined. Statistical test with the level of significance set at 0.05.

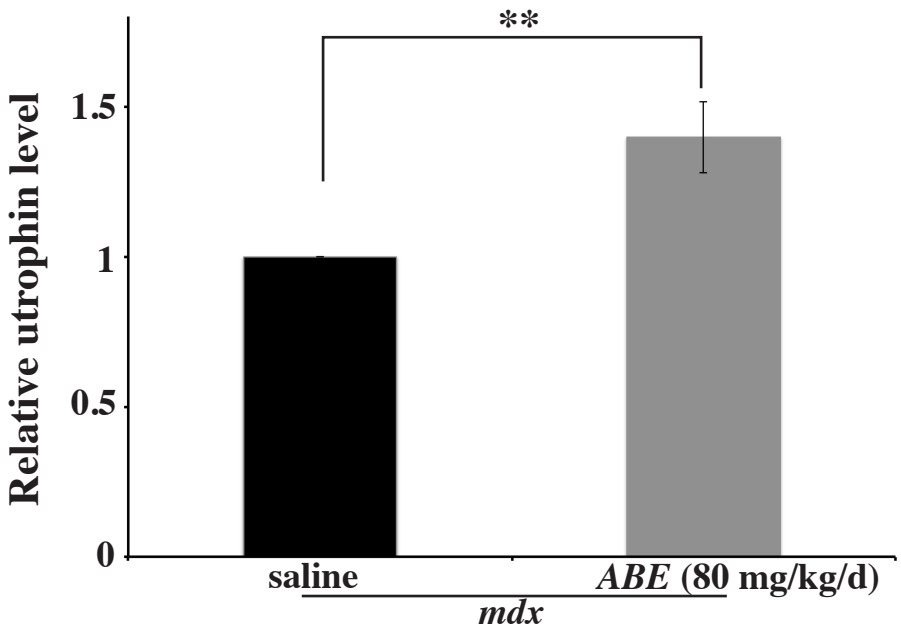

Supplementary data 4: Semi-quantitative analysis of utrophin level in the *gastrocnemius* muscle of saline- and *ABE*-treated *mdx* mice (dose 80 mg/kg/d). A 40% increase is observed. Student's t-test with the level of significance set at 0.05.

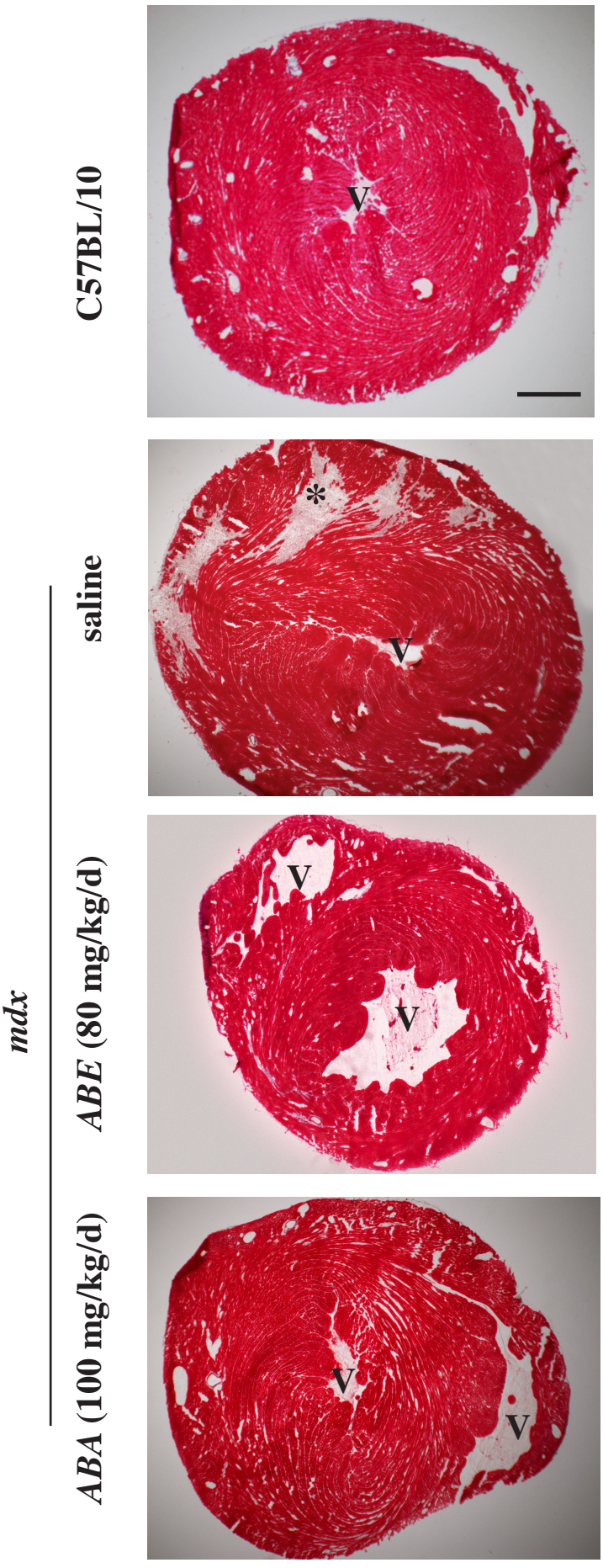

Supplementary data 5: Masson's trichrome staining of heart tissues from C57BL/10, saline-, *ABE*- and *ABA*-treated *mdx* mice. Focal fibrotic zones are stained in blue and and identified by stars. V: ventricle.

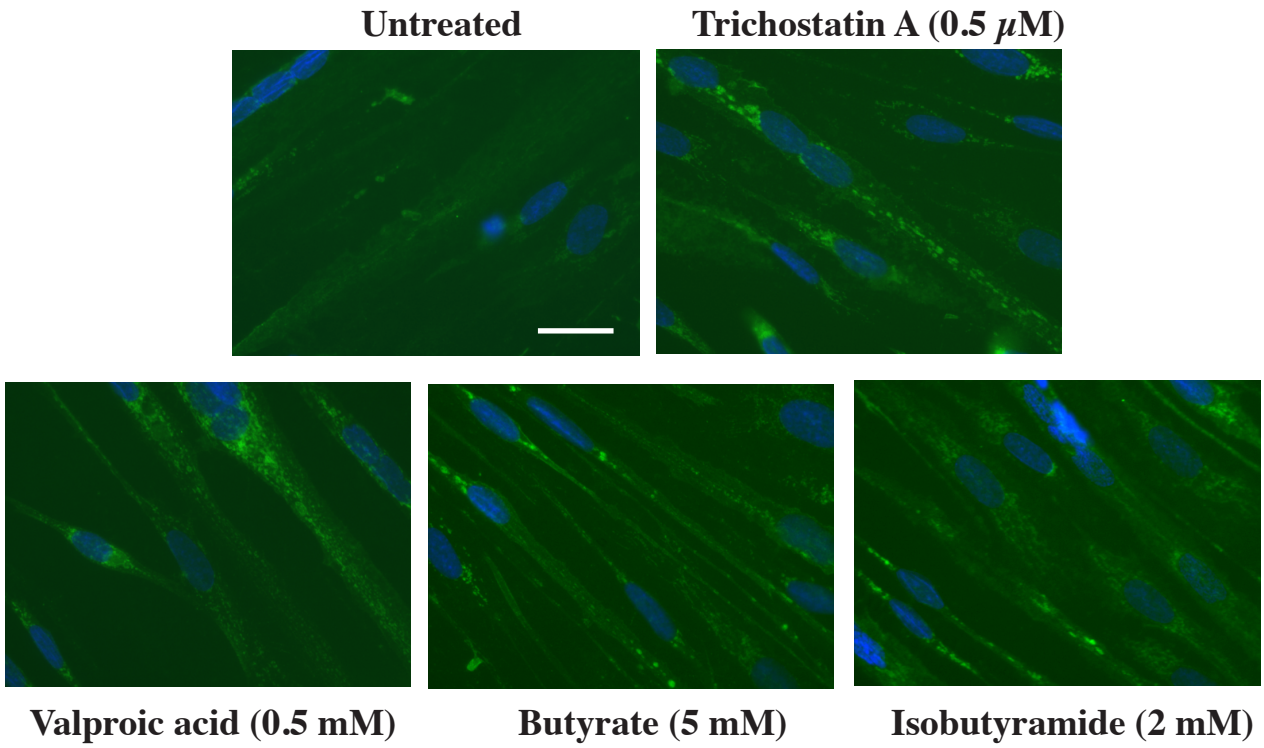

Supplementary data 6: Utrophin localization in a skeletal muscle cell line derived from DMD patients and treated for 48 h with HDAC inhibitors: trichostatin A (0.5 µM), valproic acid (0.5 mM), butyrate (5 mM) and isobutyramide (2 mM). Utrophin was clearly detected at the sarcolemma in treated myotubes while little immunostaining was observed in untreated cells. Nuclei were labeled with a DNA-selective fluorescent dye (DAPI). Scale bar, 70 µm.

SUPPLEMENTARY RESULTS

(**see M&M in Manuscript 2**)

Long term effect of ABE in *mdx* mice

In parallel to AB treated animals, another group of *mdx* mice have been treated with ABE at the dose 80mg/kg/d and the same analyses were performed. The global functional improvement described in AB-treated *mdx* mice, compared with saline-treated animals, was not observed in ABE-treated *mdx* mice, at the dose used.

Cardiac function and structure in ABE-treated* mdx *mice

- *ABE does not maintains cardiac function in mdx mice*

Serial measurements of cardiac morphology and function were made monthly from 8 to 14 months. A continuous decrease of EF was monitored by echocardiography in saline-treated *mdx* mouse all along the period monitored, in comparison with C57BL/10 mice, in which EF values are stable during this period. EF values were decreased by about 20% in saline-treated *mdx* mice over the 6 months study window (Supplementary Fig. 1A). In ABE-treated *mdx* mice, the continuous decrease was more or less comparable with the saline-treated animal values, suggesting that ABE treatment did not protect against cardiac function deterioration, with a further reduction of 8% at the end of the treatment compared with saline-treated animals, reaching a loss of 28% of EF. The same profiles were observed for the FS (not shown).

- *ABE does not preserve heart from ventricular dilatation in mdx mice*

LV dilatation was estimated *via* the measures of LVID and LVOD. An increased of about 20% of LVID was observed in saline-treated *mdx* mice over the 6 month study window, whereas the LVID values remained stable in C57BL/10. At 8 months, C57BL/10, saline - and ABE-treated *mdx* mice display similar values, then progressively the values increases in saline- and ABE-treated mice, suggesting that a treatment with ABE does not preserve them from ventricular dilatation (Supplementary Fig. 1B). The same profiles were observed for the LVOD (not shown).

- *ABE does not preserve heart from ventricular hypertrophy in mdx mice*

In ABE-treated mice, the weight of hearts was increased, but not statistically meaningful, compared with saline-treated *mdx* mice (mean: 275 ± 11.5 mg vs 250 ± 7.9 mg, respectively, Supplementary Fig. 2A). The histological analysis on ABE heart tissue revealed that the percentage of necrotic area was increased by about 52%, compared with saline-treated samples

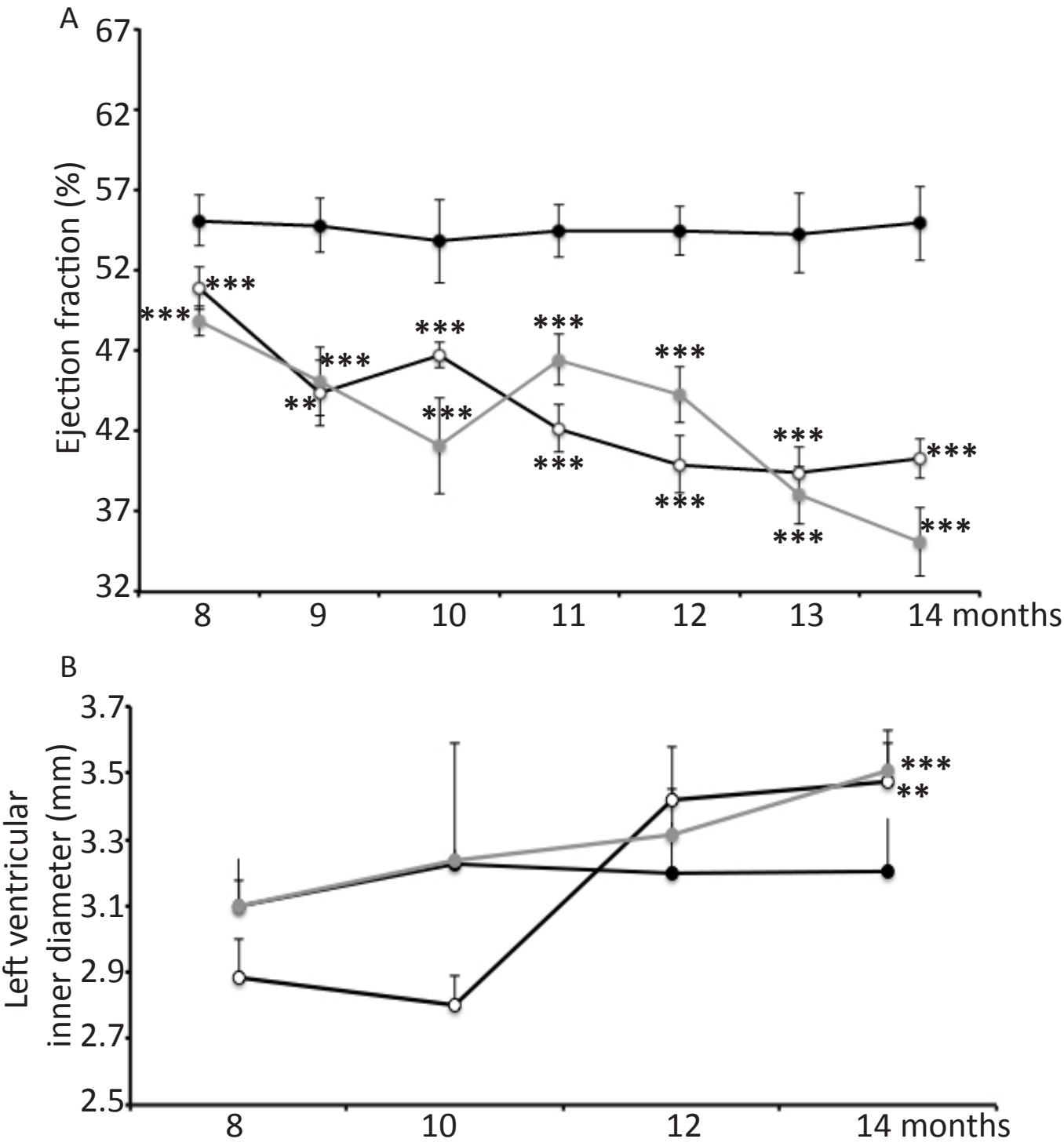

Supplementary Figure 1: (A) Ejection fraction (EF) and (B) left ventricular inner diameter (LVID) of *mdx* mice treated with ABE by force-feeding for 12 months. EF in C57BL/10 (black circles), ABE-treated (close grey circles) and saline-treated *mdx* (white circles) mice monitored from 8 to 14 months old by echocardiography analysis. Note that the EF values in ABE-treated mice decrease all along the time window study by about 28%, while LVID of the same animals increase progressively.*: statistically meaningful compared with C57BL/10 mice.

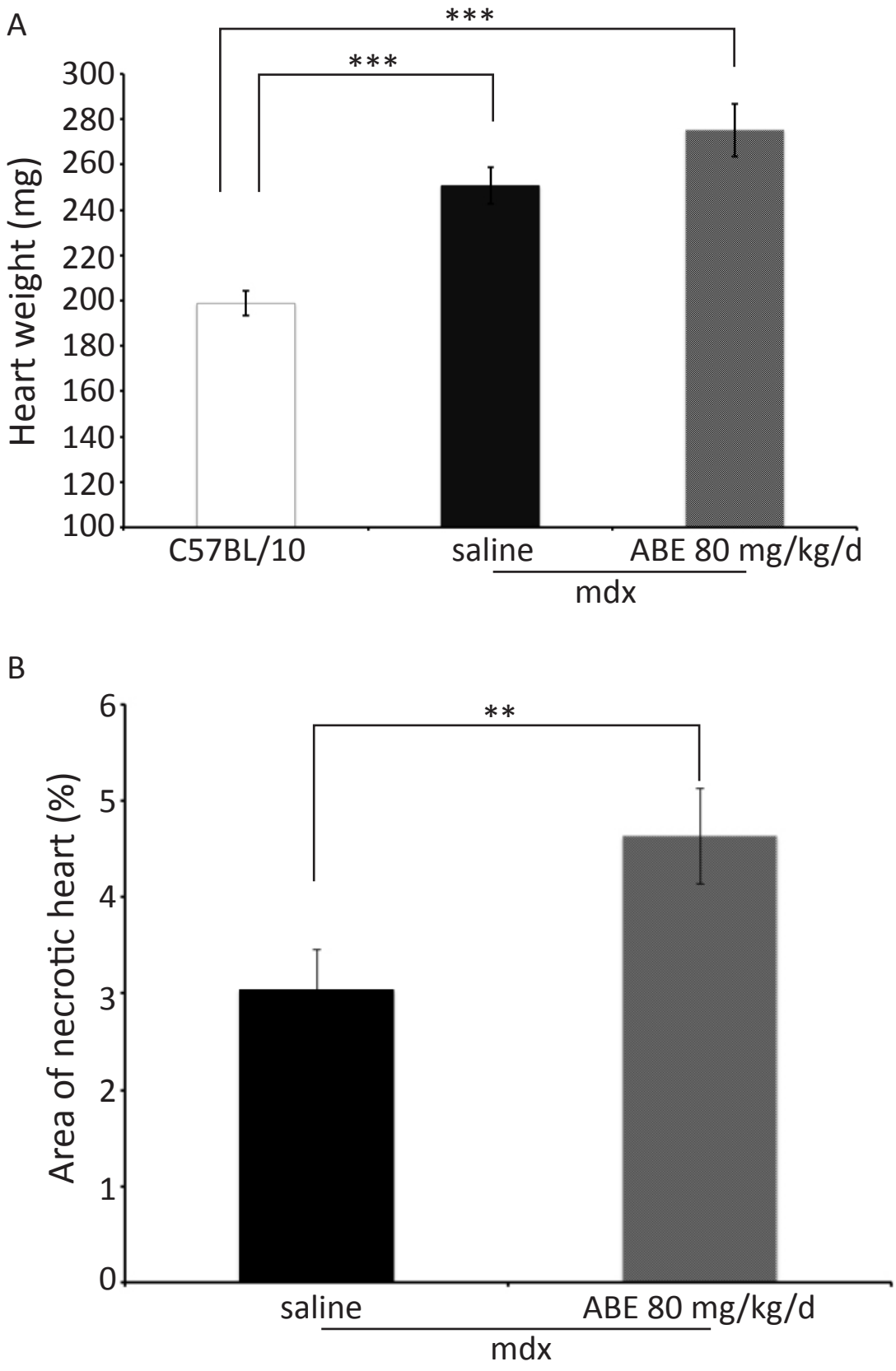

Supplementary Figure 2: (A) Heart (mg) of C57BL/10, saline- and ABE-treated mice after sacrifice. The strong increase in weight measured in saline-treated *mdx* mice is not rescue in ABE-treated *mdx* mice, suggesting that ABE may maintain hypertrophy (B) The percentage of fibrotic tissue in heart has been quantified by ImageJ software, after Masson's trichrome staining. The rare focal fibrosis (3% of the surface) observed in saline-treated animals is increased in ABE-treated *mdx* mice.

(Supplementary Fig. 2B). The ABE-treated animals did not display a decrease in weight or of the percentage of necrotic areas in the heart, compared with saline-treated *mdx* mice.

We conclude that ABE do not protect the heart of dystrophic animals from cardiomyopathy, contrary to what we observed after AB treatment.

Skeletal function and structure in ABE-treated* mdx *mice

- *ABE treatment does not alleviates spinal deformity in mdx mice*

After ABE treatment the KI does not change compared with saline-treated animals. We obtained the same result with two different approaches: MRI (magnetic resonance imaging; Supplementary Fig. 3A) and radiographic pictures (data not shown). In the first case the animals were awake while they were anesthetized in the second case. We conclude that ABE do not preserve from spinal deformity, contrary to what we observed after AB treatment.

- *ABE treatment does not alleviate global functional parameters in mdx mice*.

The effect of ABE on muscle strength was evaluated using a grip-strength meter. Muscular weakness was worse in ABE-treated *mdx* compared with saline-treated *mdx* mice and C57BL/10 animals, at 14 months of age (Supplementary Fig. 3B). Concerning the inverted grid test, *mdx* mice displayed half of the value of C57BL/10 mice with high variability among animals. The ability of ABE-treated *mdx* mice to maintain a grip on an inverted grid was not improved compared with C57BL/10 mice (Supplementary Fig. 3C). We conclude that ABE decreased the strength in *mdx* mice, and do not preserve the fatigability, results contrary to what was we observed after AB treatment.

- *ABE treatment tends to alleviate biochemical parameters in mdx mice.*

Meanwhile, a near significant (P = 0.072) 60% decrease of serum CK level in ABE-treated *mdx* mice was measured compared with saline-treated *mdx* mice value (Supplementary Fig. 4A).

Based on these data we concluded that the ameliorations determined after a long-term treatment with AB at the dose 80O mg/kg/d was not reproduced with ABE at the dose 80 mg/kg/d, a dose chosen for is capacity to improve the dystrophic phenotype in short-term treatment. A tendency for improvement was only observed on the CK level. No change in body weight was detected in

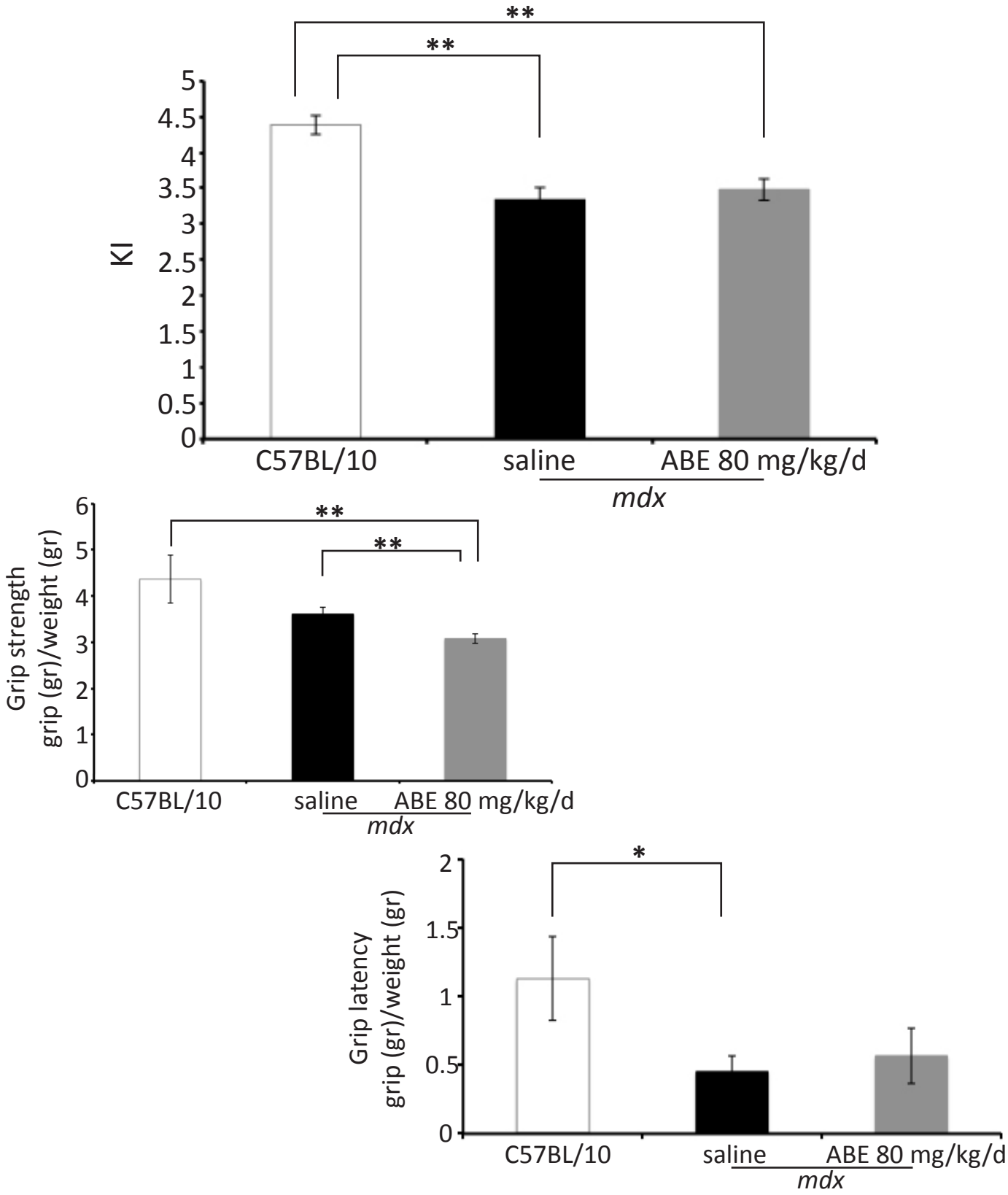

Supplementary Figure 3: (A) ABE treatment does not alleviates spinal deformity (MRI procedure) and it does not increase (B) muscular strength and (C) grip latancy in *mdx* mice treated by force-feeding for 12 months. The KI calculated in saline-treated mice is not rescued in ABE-treated mice.

ABE-treated mice, compared with saline-treated animals (data not shown), suggesting a global safety of ABE for *mdx* mice in long-term treatment.

Long term effect of AB on diaphragm structure in *mdx* mice

No fibrotic change occurs in diaphragm after one year of AB treatment in mdx mice

Histological analysis was performed on the diaphragm of *mdx* mice one-year-treated with AB. Masson's trichrome staining reveals that fibrotic tissue in AB-treated mdx mice did not differ from saline-treated group (Supplementary Fig. 4B). The expected benefit of AB on respiratory complications could not be direct but only *via* the protection against spinal deformity.

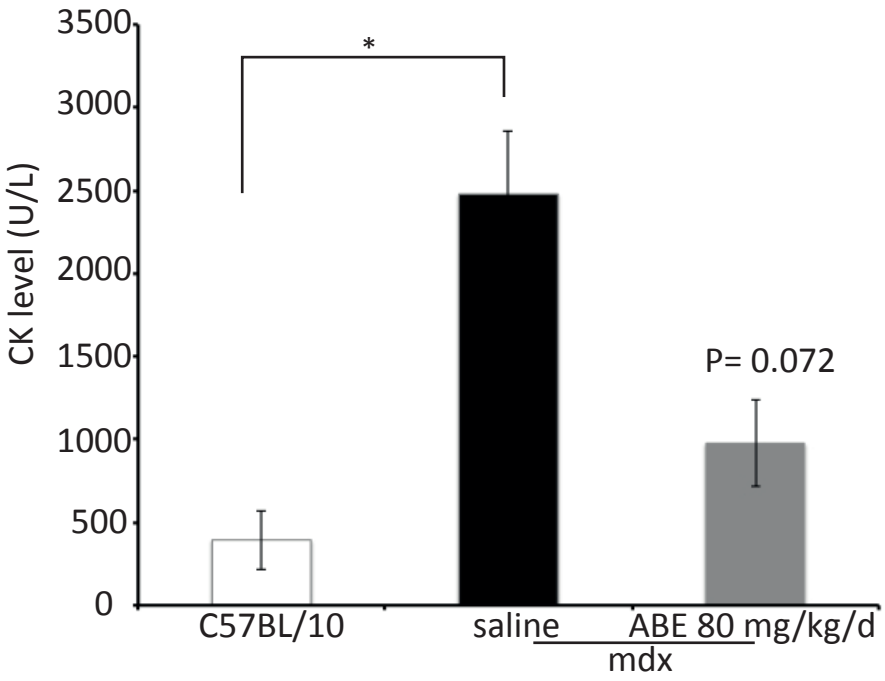

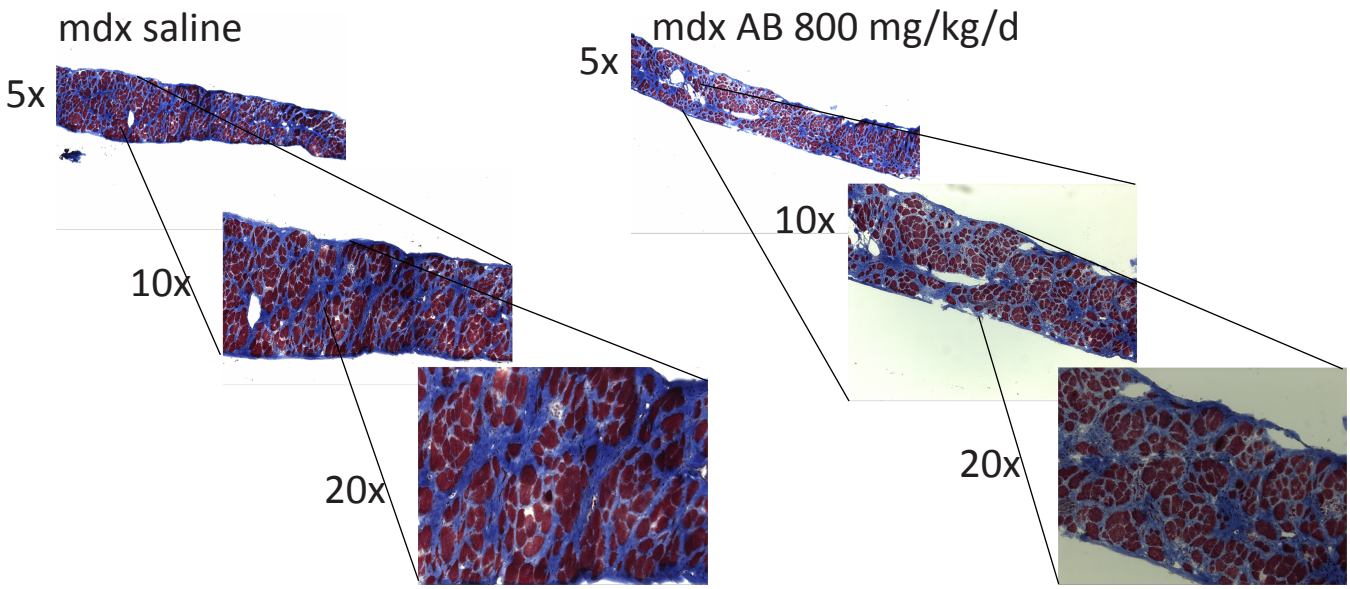

Supplementary figure 4: (A) ABE treatment alleviates CK level in the serum compared to saline-treated mice. The high value in saline-treated *mdx* mice (2500 U/L) is decreased about 60% in ABE-treated mice. (B) Masson's trichrome staining of diaphragm in saline- and AB-treated animals. The histological analysis reveals that the treatment does not modify the fibrosis observed in the saline-treated animals. Muscular fibers are stained in red, collagen in blue and nuclei in brown.

DISCUSSION

The aims of my PhD work were:

In vivo: (i) Investigate the benefit of AB, a compound currently used in children for another indication, and of two new compounds that we hope will be used in a future clinical trial on DMD patients. Dystrophic boys begin to show signs of muscle weakness as early as the age of 2, so it is of interest to design molecules that can be administered orally for a long term avoiding the source of infections, *i.e.*. catheter. We focussed our attention on parameters of neuromuscular excitability, using a non-invasive automatized method of sequential acquisition of multiple excitability tests, developed for neuropathies (Boerio et al., 2009). An investigation, that could be potentially applied in DMD patients in a follow-up study to estimate the long-term benefit associated with exposure to a concomitent treatment whatever it is. (ii) Monitor, in a large time window study, the evolution of the disease in saline-, AB- and ABE-treated animals, focusing in particular on heart, because clinical evaluation indicates that 90% of DMD patients develop dilated cardiomyopathy with progressive decline in cardiac functions that is the cause of more than 30% of deaths (Colussi et al., 2010b; Ferlini et al., 1999), and on spinal cord deformity (Oda et al., 1993).

Two types of protocols have been performed: a short-term and a long term one. The short-term protocol started at the age of 6 weeks until the 14^{th} week while the long one started at the same age but it ended at 14^{th} month of age. Weights of mice were monitored throughout the treatment. At the end of the protocols strength and fatigue tests were performed; the animals were then anesthetised, blood samples taken, cervical dislocation performed and muscles tissues frozen. Long- and short-term protocols were used, depending of the addressed deficit, for instance: cardiomyopathy is detected from the age of 8/9 months, while neuromuscular excitability defaults concern young adult animals.

In vitro: (i) Verify on human dystrophic myotubes the ability of our products (AB, ABE and ABA) to induce an increase of utrophin expression, β-dystroglycan and, in most of the cases, embryonic myosin, a marker of regeneration (ii) Investigate the contribution of butyrate and other HDAC inhibitors (trichostatin A, valproic acid, isobutyramide) on utrophin up-regulation (part of the F. Consolaro M2). Finally (iii), verify the hypothesis that the spontaneous spikes observed in untreated cultures cells could be related to the absence of dystrophin that could regulate the flows of calcium in/out the cell.

New drugs were designed for this work: 3-Hydroxybutyrate arginate (ABE) and N-butyryl arginine (ABA), two pro-drugs that were derived from the salt formulation, arginine butyrate (AB), frequently used as comparator. The differences with AB are the covalent links that bound L-arginine and butyrate. In the case of ABE an esteric bound is set, while for ABA an amidic bound. The presence of covalent links confers a more stable structure to the molecules, supposed to pass the gastric barrier being protected from massive degradation.

The choice to study a possible role of AB and its derivatives for DMD patients came from the similarity of the disease with the β-hemoglobinopathies. In these diseases, mutations on the β-chain of the adult form of the protein promote hemoglobinopathies characterized by defects on oxygen delivery in blood (Ingram V.M., 1956; Pauling C. et al., 1949). The foetal form of the protein (Hbf) is composed of chains α and γ and appears around the 12^{th} weeks of human gestation. Similar to what happened to utrophin, during the last months of gestation the expression of γ chain decreases and the production of β and δ start producing α2β2 and α2δ2 (Karlsson and Nienhuis, 1985). The clinical administration of AB has been tested to treat paediatric patients affected by β-hemoglobinopathies for its ability to induce the expression of the foetal form of the protein (Faller and Perrine, 1995; Perrine and Faller, 1993; Perrine et al., 1993, 1994; Sher et al., 1995). In the case of DMD only preclinical assays have been performed (Guerron et al., 2010; Perronnet et al., 2012; Vianello et al., 2013), in which the protein of interest is utrophin, the foetal form of dystrophin (Blake et al., 2002).

The AB compound

1. Rescue of neuromuscular excitability parameters

A non-invasive automatized sequential acquisition of multiple excitability tests has been applied in order to investigate neuromuscular excitability parameters in C57BL/10 mice, and in saline, AB (intraperitoneal and oral administration) treated *mdx* mice on the CMAP of tail and limb muscles, in response to excitability tests applied *via* the caudal and plantar motor nerves in 13 week-old mice. We observed that saline-treated *mdx* mice displayed changes on neuromuscular excitability, compared with C57BL/10 animals, with abnormal response to strength-duration relationship, anomalies on recovery cycle, abnormal response to polarizing currents, expressed by less threshold changes in response to depolarizing electrotonus and smaller minimum index on the current threshold slope. It is worth noting that the above parameters are related to peripheral nerve excitability and not to muscle excitability (Boerio et al., 2009; Bostock et al., 1998). A

hypothesis to explore the changes in recovery cycle and strength-duration relationship could be the different contribution of sodium channels (transient and persistent) in *mdx* and C57BL/10 animals. Hence, it is likely that longer transient inactivation of voltage-gated sodium channels induces the greater refractory period in saline-treated *mdx* mice. Likewise, threshold electrotonus and current threshold relationship provide an assessment of intermodal properties suggesting an abnormal function of different subtypes of potassium channels. Altogether, these changes could reflect structural alterations of both paranodal and intermodal regions and, may suggest a subtle disorganization of the myelin sheath of the peripheral nerve (Kiernan et al., 2000; Krishnan et al., 2008), which could result in modifications of repartition and density of ion channels in *mdx* mice. This hypothesis is also in line with previous findings suggesting an important role of sarcoglycans, members of the DAPC, in the stability of peripheral nerve myelin (Cai et al., 2007). In AB-treated *mdx* mice, most (tail) if not all (foot) excitability parameters did no longer differ significantly from C57BL/10 animals.

In addition, the CMAP amplitude was reduced and the latency prolonged in the tail muscle recordings of saline-treated *mdx* mice compared with C57BL/10 animals. Unfortunately these modifications remained abnormal despite AB treatment. Although persistent (background) channels may be more abundant in *mdx* mice, allowing thus a decreased threshold and an increased current intensity able to evoke a CMAP, a decreased number of voltage-gated sodium channels could also explain the decrease of the CMAP amplitude. In accordance with this hypothesis, it has been described that the fragmentation of the neuromuscular junction, the excessive nerve sprouting (Marques et al., 2007) and a decrease of the number and depth of synaptic folds that promote the decrease of the density of voltage-gated sodium channels to the synapse (Banks et al., 2009). Moreover, the increased latency of CMAP in saline-treated *mdx* mice may reflect the morphological alterations at the neuromuscular junction that influence action potential propagation.

2. *Per os* administration could be a way of admistration to DMD patients

In the first article published during my PhD project, we have shown that many of the structural, biochemical and functional hallmarks of the principal animal model of DMD were improved by AB treatment after intraperitoneal administration and that L-arginine and butyrate act synergically (Vianello et al., 2013). Different structural and functional parameters have been monitored to

investigate if the oral administration of AB could be envisaged to treat DMD patients, as demonstrated for ABE and ABA. Whatever the mode of administration, (i) the reduction of the percentage of necrotic surface in heart observed after intraperitoneal injection is the same after oral administration and close to the C57BL/10 value, suggesting, in addition, that starting the treatment in young animals temporally protects the heart from structural deterioration processes such as necrosis and fibrosis, (ii) force and fatigue measures displayed similar values in AB-treated *mdx* mice compared with C57BL/10 mice and (iii) finally, the majority of tail and foot excitability parameters that were modified in saline-treated *mdx* mice did not show any significant difference when *mdx* mice were treated with AB.

Taken all together these data indicated that the positive effects observed after the intraperitoneal injection of AB can be obtained after oral administration, suggesting that oral administration could be considered as the mode of treatment in DMD children.

3. Protection against cardiomyopathy

To explore the effect of the molecules on heart structure and function, the animals were treated before the appearance of functional symptoms of cardiomyopathy (6 weeks old mice) and echocardiography was recorded in a follow-up study monthly from the 8^{th} to the 14^{th} month of age. In particular, EF and FS were monitored in order to investigate heart activity. As expected, any changes in C57BL/10 mice were visible during the monitored period but saline-treated *mdx* mice displayed about 20% progressive decrease of EF (23% for FS), over the studied period. On the other hand EF and FS in AB-treated *mdx* mice were maintained all along the 7 months of recording, indicating that the cardiac function is preserved in treated animals. This strongly suggests that AB compensates, at least partially, the lack of dystrophin in heart and could ameliorate some of heart dysfunctions in DMD patients. Cardiac enlargement was also investigated to examine the effect of AB on left ventricular dilatation: as observed for EF and FS, treatment with AB protects heart from the ventricular dilatation that progressively set up in *mdx* mice. In addition, the heart weight in 14 month-old saline-treated *mdx* mice was increased by about 25% compared with C57BL/10 mice while AB treatment maintained a value similar to C57BL/10 mice, supporting the hypothesis that the treatment causes cardiac metabolic adaptations and protects heart from hypertrophy.

Several hypotheses could be advanced to explain the strong benefit of AB treatment on cardiac function. In heart of *mdx* mice, the decrease of NO production is about 75-80%, which is similar to

the loss of NOS activity that occurs in skeletal muscle (Bia et al., 1999; Ramachandran et al., 2012a). While in skeletal muscles nNOS is located at the sarcolemma, in heart tissue the enzyme can be found at the sarcolemma but also in the sarcoplasmic reticulum and mitochondria (Kanai et al., 2001; Wehling-Henricks et al., 2005; Xu et al., 1999). Thus deficiency in nNOS activity in heart may primarily reflect defects in its regulation and/or the loss of binding to the dystrophin complex. In addition a deregulation of L-arginine transporters at the membrane of dystrophic cardiomyocyte in *mdx* mice has been observed. Ramachandran et al. (2012) observed a spontaneous/intrinsic increase of CATs (cationic amino acid transporters) expression in *mdx* mice and *mdx:utro* mice in order to improve the transport inside the cell and produce NO. In particular, they shown that the lower-affinity CAT (CAT-2A) is more expressed and a possible compensatory mechanism could be develop by DMD cardiac muscle cells to oppose the effects of nNOS reduction (Ramachandran et al., 2012a). Moreover it is known that NO pathway is implicated in utrophin expression through cGMP (Chaubourt et al., 1999) and that cGMP, when enhanced, improves contractile function, energy metabolism and sarcolemmal integrity of dystrophin deficient mice heart (Adamo et al., 2010; Khairallah et al., 2008) In our case the fetal homologue of dystrophin, utrophin, is re-expressed and we can suppose that the correct re-organization of the plasmatic membrane stop or reverse dystrophic features. In particular our results indicate that utrophin and β-dystroglycan are properly localized in heart membrane after AB treatment, suggesting that the treatment may be sufficient to restore sarcolemmal integrity. Besides, HDAC inhibitors could regulate the HDAC/acetylase functional balance which is altered in *mdx* mice (Colussi et al., 2010c).

Moreover, similar to DMD patients, who develop structural, functional and metabolic alterations of the heart during the progression of the diseases (Momose et al., 2001; Ogata et al., 2007; Quinlivan et al., 1996), in the *mdx* mice abnormal structure, function and metabolism have been observed (Zhang et al., 2008). In particular Zhang et al. shown that at 8 month of age a decrease in citrate synthase activity, in phosphocreatine level, a higher cytosolic free ADP concentration and a lower free-energy available from ATP hydrolysis are yet present and, like us, any difference on EF between *mdx* and control mice was detected. Moreover, a defect on NO/cGMP pathway has been observed in the cardiomyocytes of *mdx* mice (Khairallah et al., 2007) because of the decrease of NO production (Bia et al., 1999; Ramachandran et al., 2012b) and it has been shown that the enhancement of cGMP pathway in heart protect cardiomyocytes against sarcolemmal damage, preserve mitochondrial metabolic status and prevents the deterioration of cardiac function

(Khairallah et al., 2008). Furthermore, recently it has been described ultrastructural and functional alterations in the heart of *mdx* mice due to the absence of dystrophin (Lorin et al., 2013). So, different hypothesis could explain the beneficial effect of AB on cardiac function. For example we can assume (i) an increase of NO production through L-arginine, (ii) an enhanced utrophin expression through L-arginine *via* cGMP and the re-localization at the membrane of dystrophin/utrophin associated proteins such β-dystroglycan, (iii) the regulation of the HDAC/acetylase balance *via* butyrate and (iv) a role of NO on metabolism regulation enhancing the defects of the NO/cGMP pathway, even if the direct interaction between NO and the pathway has to be verify.

4. Protection against spinal cord deformity

At the end of the long term protocol the effect of the treatment on spinal cord deformity observed in *mdx* mice, was evaluated by measuring the index of kyphosis, calculated by RMI (anesthetized mice) and by radiography (awaked mice). The measures clearly indicated that the deformity described in saline-treated *mdx* mice did not appear in AB-treated mice. The reversion obtained with AB strongly suggests that the treatment could stop the progression of spinal deformity in patients and, indirectly, could reduces respiratory complications (Oda et al., 1993), thus avoiding surgery for spinal fusion and stabilization. Histological analysis performed on the diaphragm revealed that fibrotic tissue in AB-treated *mdx* mice did not differ from saline-treated group. Nevertheless under AB treatment the respiratory muscle function could be ameliorate by the protective effect against lordose.

5. Chronic administration is beneficial for skeletal muscle and safe

The global benefit of AB after long term force-feeding protocol was supported by the decrease of CK level in the serum and by the better resistance to fatigue. The decrease in the level of CK comes from the skeletal muscle enzyme rather than cardiac contribution because the percentage of necrotic tissue in the heart of AB treated mice is 3%, similar to saline-treated *mdx* mice. The safety of the product was confirmed by the fact that any change in body weight was observed during both types of treatments. A sign that in the case of a clinical trial AB administration should be well tolerated by patients.

6. Increase of utrophin level on human dystrophin myotubes

In vitro studied consisted of testing many concentrations of AB on human dystrophic myotubes to verify the increase in the expression of utrophin and, where applicable β-dystroglycan and embryonic myosin. Semi-quantitative western-blot analyses reveal that after AB treatment utrophin, βDG and embryonic myosin protein levels are increased around 1.5-2 fold compared to untreated cells and a clear dose-response effects was observed with a maximal increase at doses over 0.2 mM.

The ABE and ABA compounds

1. Rescue of neuromuscular excitability parameters in a dose dependent manner

Similar to AB, neuromuscular excitability paramenters have been monitored in ABE- and ABA-treated mice. For both compounds and muscles analysed (tail or foot) all abnormal excitability parameters return to C57BL/10 animal values, in a dose-dependent manner, with a maximum of efficiency at doses around 80 mg/kg/d. Higher doses (200-800 mg/kg/d) of both prodrugs were not efficient, compared with C57BL/10 mice, probably resulting from a toxic effect of the two molecules at high dose**.**

The decrease of the CMAP amplitude and the prolongation of the latency in the tail muscle recordings of saline-treated *mdx* mice compared with C57BL/10 animals were rescued after ABE treatment whatever the dose applied, while after ABA treatment, only at dose 100 mg/kg/d both parameters were comparable to C57BL/10 animal values. On the other hand changes on CMAP amplitude and latency on plantar muscle, normally not modified in *mdx* mice, are visible only at ABE 400 mg/kg/d, but we suppose that the same scenario could be observed with the higher dose (800 mg/kg/d).

2. Improvement of muscle strength, tirelessness, muscle structure and sarcolemmal integrity

Strength and tirelessness have been monitored in ABE and ABA treated animals and, once again, the best results were obtained with doses around 80 mg/kg/d, the lower percentage of necrotic surface in the heart was observed at doses 80 mg/kg/d and 100-200 mg/kg/d, after ABE and ABA treatment, respectively. The increase of necrotic surface after the administration of higher doses supports the idea of the toxicity of high doses.

All these results made us confident that the oral administration of both drugs, produce beneficial effects on dystrophic phenotype at doses 10 times lower than AB. I focussed my attention on the effects of doses 50 and 80 mg/kg/d in particular on sarcolemmal integrity of skeletal and cardiac membranes. A reduction of the CK level in the serum was measured (about 63%), a decrease in Evans blue dye incorporation and an increase in utrophin level (about 40%) were detected in ABE 80 mg/kg/d treated animals. Once again the esteric formulation seems to be the best candidate for future clinical trials to limit the quantity of drug to administer.

Furthermore, the incorporation of fatty acids in the membrane of cardiomyocytes of *mdx* mice treated with ABE (80 mg/kg/d), suggested by a previous study performed by mass spectrometry on skeletal muscle (Benabdellah et al., 2009), has been studied in the heart, a non regenerative tissue, and we conclude that ABE modifies the lipid profile composition. In particular, we revealed two different markers of necrotic and structured areas in heart, C16:0 and R3 ions signals. Our data indicate that treatment with *ABE* (80 mg/kg/d) induces a direct modification of lipid composition in heart membrane, independently of the regeneration process. In addition to C16:0 signal and ratio R3 signal, two other new markers were evidenced that could be used, in dystrophic animals (*mdx* mice and presumably canine model), to separate necrotic/structured areas and specifically follow the benefit of a treatment. The results obtained by mass spectrometry are very encouraging at this stage, but limited to preclinical studies, invasive heart biopsies could not be envisaged on children to check the benefit of a treatment.

3. Young patients' administration for a better efficiency

The short-term protocol has been applied to aged *mdx* mice (10 months-old) in order to investigate if ABE improves dystrophic phenotype in animals with established dystrophy, but the treatment failed, even if a global beneficial effect on skeletal muscle was suggested by the strong decrease of CK in the serum. These results support the idea that DMD patients must to be treated as early as possible.

4. Inability of ABE (80 mg/kg/d) to confer long-term significant protection from muscle degradation and spinal cord deformity

We addressed the capacity of ABE to confer significant protection from muscle deterioration in case of long term treatment. The dose 80 mg/kg/d of ABE was chosen for its ability to improve

many dystrophic parameters in a short term treatment (muscle strength, timeliness and sarcolemmal integrity). Unfortunately, the benefits obtained with AB, were not observed after ABE treatment. In particular, the rescue of cardiac function is not obtained with ABE and the progressive functional deterioration was not stopped. Moreover, concerning the structure, ABE-treated heart samples exhibit an increase in LVID, sign of LV dilatation, and an increase in heart weight, sigh of cardiac hypertrophy. The percentage of necrosis in heart was increase by about 52%, compared with saline-treated *mdx* mice and any improvment on muscular strength was observed after the treatment. On the other hand, a nearly significant decrease in CK level in the serum has been detected after ABE treatment.

The discrepancy of the results obtained with the short-term protocol and the long one for ABE at 80 mg/kg/d could be explained by duration of the protocol an extention of the treatment for several months could have induced tolerance to the effects of ABE, thus making the treatment ineffective. In order to further understand how the molecule interacts with the physiological process pharmacokinetic studies could be performed. Further experiments are necessary to determine the optimal dose of ABE for long term treatment

Furthermore, the long term administration of ABE at dose 80 mg/kg/d does not protect from the progressive deterioration of the spinal cord deformity.

5. Increase of utrophin protein level in primary DMD cultures and pure myoblast culture after 48h of treatment.

The abilities to increase utrophin, βDG and embryonic myosin protein levels have been monitored also for ABE and ABA. Semi-quantitative western-blot analyses reveal that after ABE and ABA treatment utrophin, βDG and embryonic myosin protein levels are increased around 1.5-2 fold compared to untreated cells. Dose-response effects were observed for utrophin, β-dystroglycan and embryonic myosin levels, with a maximal increase at dose 0.05 mM for ABE (a lower doses compared with *AB*, 0.2 mM), For *ABA*, a maximal increase was obtained with doses from 0.1 to 0.5 mM, although no clear dose-effect response was observed.

Further analyses on utrophin transcript should be performed to check if the increase of the protein is associated with an increase of the transcript. In this second hypothesis it would be opportune to verify if the drugs induce the stabilization of the transcript as yet observed after activation of p38 signalling (Amirouche et al., 2013). Nevertheless, utrophin-A mRNA was

upregulated in skeletal muscle of AB-treated *mdx* mice after single series of 4 daily injections (Vianello et al., 2013). Because primary muscle cell cultures are a mix of fibroblasts and myoblasts, I also tested the compounds on a pure myoblast cultures and observed that the increase of the protein levels is two fold higher than in a primary culture. This suggests a better response to the treatment of the myotubes from the cell line, than the myotubes from primary cultures. Another hypotheses could be that myoblasts are more responsive than fibroblast or that fibroblasts inhibit ABE/ABA processing.

Two *in vitro* studies have been performed during my PhD: a study on utrophin level after HDAC inhibitor treatment (F. Consolaro, M2 student) and a focus on calcium homeostasis (preliminary experiments were performent by F. Consolaro, M2 student).

1. HDAC inhibitors increase utrophin level.

To investigate the contribution of butyrate on the increase of utrophin protein level, we tested four HDAC inhibitors: butyrate, but also trichostatin A (TSA), valproic acid (VPA), isobutyramide and butyrate and we demonstrated that each of them increase the level of utrophin and related proteins (β-dystroglycan and embryonic myosin) around 2-3 fold. Trichostatin has been tested *in vivo* on *mdx* mice and no utrophin expression was reported (Minetti et al., 2006). However we observed an increase of utrophin and related protein (β-dystroglycan and embryonic myosin) in *mdx* mice treated with trichostatin (unpublished data). A possible explanation for this discrepancy could be the concentrations used or the duration of treatment or the muscle used: 0.5 mg/kg/d for 6 weeks in *tibialis anterior* in our *in vivo* conditions, and 0.6 mg/kg/d for 3 months in *extensor digitorum longus* in Minetti's study.

Similar to trichostatin, valproic acid has been tested *in vivo* on *mdx*/utrn$^{-/-}$ mice and *in vitro* on $\alpha7^{+/-}$ cells and its action has been descrided. VPA activate the PI3K/Akt/mTOR pathway acting on PI3K (Gurpur et al., 2009) and this pathway is implicated in skeletal muscle remodelling, in particular in hypertrophy, allowing protein expression (Bassel-Duby and Olson, 2006). Recently it has been shown that activation of Akt is implicated in utrophin expression (Marshall et al., 2012).

Finally, after isobutyramide, a butyrate analogue, and butyrate treatment an increase in the level of utrophin has also been observed. The increase of expression of utrophin after HDAC inhibitors treatment is reinforced by the evidence of *in vivo* studies in which an increase of the protein has been observed with the 4 HDAC inhibitors (Voisin PhD manuscript and unpublished data). A direct role of these inhibitors on utrophin expression is reinforced by the fact that butyrate acts

preferentially on HDAC 1 and 2, that regulate the transcription factors, Sp1 and Sp3, which in turns are implicated on utrophin expression (Davie, 2003; Miura and Jasmin, 2006). This mechanism could be implicated in the increase of utrophin observed after ABE and ABA treatment.

NO has been described to play a role as an epigenetic molecule able to induce chromatin changes in order to allow genes expression (Colussi et al., 2009), suggesting a direct implication of NO on utrophin expression. Moreover HDAC2 seems to be particularly active in case of dystrophy and be a common target for NO and HDACi (Colussi et al., 2008). Nevertheless, this hypothesis was not verified in our study: the comparison of chromatin acetylation states in human myotubes treated with L-arginine, butyrate and AB was use to confirm that the combined formula of AB acts synergistically, but, in these experiments L-arginine alone did not induce any chromatin change (Vianello et al., 2013).

Taken together these results make us confident of the double role of ABE and ABE molecules I regulating utrophin level, through the NO pathway (Chaubourt et al., 1999) and the direct action of butyrate on histone deacetylase enzyme inhibition. Nevertheless, the level of utrophin mRNA after ABE or ABA treatment has to be investigated.

Finally, the follistatin-myostatin pathway has been shown as a possible way to treat dystrophic patients (Brunelli et al., 2007; Iezzi et al., 2004; Pisconti et al., 2006) and different studies have shown that the inhibition of HDAC allow the expression of follistatin (Colussi et al., 2008; Minetti et al., 2006*)*. It has been described that HDAC2, particularly active in dystrophic *scenario*, target of butyrate (Davie, 2003) and NO (Colussi et al., 2008), is implicated not only in utrophin but also in follistatin expression, so the expression of follistatin has to be verified after the treatment with our drugs

2. AB/ABE/ABA, TSA, Butyrate and L-arginine reduce spontaneous Ca^{2+} spikes in DMD myotubes.

We verify the hypothesis that the spontaneous spikes we observed in untreated DMD myotubes, and absent in healthy myotubes, could be related to the absence of dystophin, with as consequence a deregulation of the Ca^{2+} flows in/out the cell. Each molecule tested decreased calcium spikes in human myotubes after 48 h of treatment, compared with untreated cells, and we have observed that the same molecules allowed the increase of utrophin level (see below) supporting the hypothesis of a direct relation between the localisation of utrophin at the

membrane and the restauration of correct Ca^{2+} homeostasis. Furthermore, the correct concentration of the Ca^{2+} can activate the Ca^{2+}/calmodulin pathway that is implicated in gene expression, and increased utrophin expression (Al-Shanti and Stewart, 2009). Future experiments will have to investigate: Where calcium comes from? Does it come from cellular or extracellular compartments? The Ca^{2+} concentration in treated or untreated dystrophic cells?

Conclusion

The consequences of the absence of dystrophin in DMD patients muscles are: deregulation of calcium homeostasis, tissues necrosis, progressive accumulation of fat and fibrosis, progressive muscle weakness and cardiac and respiratory failures.

All the results obtained during my thesis make us confident of a possible future clinical trial with the molecules studied.

Numerous aspects have been investigated in my PhD project and almost all of them support the hypothesis that the combination of two independent pathways (NO-pathway and inhibition of the histone deacetylase) is a common target to treat DMD patients. Arginine butyrate is already utilized in clinical trials to treat β-hemoglobinopathies but administered only via a catheter, so the observation that the positive effects (reduction of the percentage of necrotic surface in heart, measures of force and fatigue, tail and foot excitability parameters) after intraperitoneal administration are obtained after oral administration is a great goal of the study.

Furthermore, we have demonstrated that the chronic administration of AB is not only safe (this is confirmed by the decrease of CK level in the serum, the better fatigability, no effect on body weight) but protects against cardiomyopathy (EF and FS values are preserved in treated animals, and ventricular dilatation and heart hypertrophy also) and against spinal cord deformity.

On the other hand, the positive effects (restoration of neuromuscular excitability parameters, improvement of muscle strength and fatigability, sarcolemmal integrity and increase of utrophin level) that we have recorded after ABE and ABA treatment have been observed at lower doses than with AB.

Further experiments are necessary to determine the optimal dose of ABE for long term treatment, *in vivo*.

In addition, we have demonstrated that ABE and ABA, *via* L-arg and *via* B, increase utrophin and associated proteins in human myotubes and regulate the spontaneous Ca^{2+} activity implicated in Ca^{2+} homeostatis.

Our results support the possibility AB could be rapidly tested in a pilot study and that ABE and ABA could be developed for future clinical trials on DMD and potentially, hemoglobinopathic patients.

BIBLIOGRAPHY

’t Hoen, P.A.C., de Meijer, E.J., Boer, J.M., Vossen, R.H.A.M., Turk, R., Maatman, R.G.H.J., Davies, K.E., van Ommen, G.-J.B., van Deutekom, J.C.T., and den Dunnen, J.T. (2008). Generation and characterization of transgenic mice with the full-length human DMD gene. J. Biol. Chem. *283*, 5899–5907.

Aartsma-Rus, A. (2012). Overview on DMD Exon Skipping. Methods Mol. Biol. *867*, 97–116.

Abdulrazzak, H., Noro, N., Simons, J.P., Goldspink, G., Barnard, E.A., and Górecki, D.C. (2001). Structural diversity despite strong evolutionary conservation in the 5’-untranslated region of the P-type dystrophin transcript. Mol. Cell. Neurosci. *17*, 500–513.

Abmayr, S., Crawford, R.W., and Chamberlain, J.S. (2004). Characterization of ARC, apoptosis repressor interacting with CARD, in normal and dystrophin-deficient skeletal muscle. Hum. Mol. Genet. *13*, 213–221.

Adamo, C.M., Dai, D.-F., Percival, J.M., Minami, E., Willis, M.S., Patrucco, E., Froehner, S.C., and Beavo, J.A. (2010). Sildenafil reverses cardiac dysfunction in the mdx mouse model of Duchenne muscular dystrophy. Proc. Natl. Acad. Sci. U.S.A. *107*, 19079–19083.

Ahn, A.H., Freener, C.A., Gussoni, E., Yoshida, M., Ozawa, E., and Kunkel, L.M. (1996). The three human syntrophin genes are expressed in diverse tissues, have distinct chromosomal locations, and each bind to dystrophin and its relatives. J. Biol. Chem. *271*, 2724–2730.

Alderton, W.K., Cooper, C.E., and Knowles, R.G. (2001). Nitric oxide synthases: structure, function and inhibition. Biochem. J. *357*, 593–615.

Altamirano, F., López, J.R., Henríquez, C., Molinski, T., Allen, P.D., and Jaimovich, E. (2012). Increased resting intracellular calcium modulates NF-κB-dependent inducible nitric-oxide synthase gene expression in dystrophic mdx skeletal myotubes. J. Biol. Chem. *287*, 20876–20887.

Alter, J., Lou, F., Rabinowitz, A., Yin, H., Rosenfeld, J., Wilton, S.D., Partridge, T.A., and Lu, Q.L. (2006). Systemic delivery of morpholino oligonucleotide restores dystrophin expression bodywide and improves dystrophic pathology. Nat. Med. *12*, 175–177.

Amann, K.J., Renley, B.A., and Ervasti, J.M. (1998). A cluster of basic repeats in the dystrophin rod domain binds F-actin through an electrostatic interaction. J. Biol. Chem. *273*, 28419–28423.

Amenta, A.R., Yilmaz, A., Bogdanovich, S., McKechnie, B.A., Abedi, M., Khurana, T.S., and Fallon, J.R. (2011). Biglycan recruits utrophin to the sarcolemma and counters dystrophic pathology in mdx mice. Proc. Natl. Acad. Sci. U.S.A. *108*, 762–767.

Amirouche, A., Tadesse, H., Lunde, J.A., Bélanger, G., Côté, J., and Jasmin, B.J. (2013). Activation of p38 Signalling Increases Utrophin A Expression in Skeletal Muscle via the RNA-binding Protein KSRP and Inhibition of AU-rich Element-mediated mRNA Decay: Implications for Novel DMD Therapeutics. Hum. Mol. Genet.

Anderson, J.E. (2000). A role for nitric oxide in muscle repair: nitric oxide-mediated activation of muscle satellite cells. Mol. Biol. Cell *11*, 1859–1874.

Anderson, J.E., and Vargas, C. (2003). Correlated NOS-Imu and myf5 expression by satellite cells in mdx mouse muscle regeneration during NOS manipulation and deflazacort treatment. Neuromuscul. Disord. *13*, 388–396.

Angus, L.M., Chakkalakal, J.V., Méjat, A., Eibl, J.K., Bélanger, G., Megeney, L.A., Chin, E.R., Schaeffer, L., Michel, R.N., and Jasmin, B.J. (2005). Calcineurin-NFAT signaling, together with GABP and peroxisome PGC-1{alpha}, drives utrophin gene expression at the neuromuscular junction. Am. J. Physiol., Cell Physiol. *289*, C908–917.

Apel, E.D., and Merlie, J.P. (1995). Assembly of the postsynaptic apparatus. Curr. Opin. Neurobiol. *5*, 62–67.

Archer, J.D., Vargas, C.C., and Anderson, J.E. (2006). Persistent and improved functional gain in mdx dystrophic mice after treatment with L-arginine and deflazacort. FASEB J. *20*, 738–740.

Ascah, A., Khairallah, M., Daussin, F., Bourcier-Lucas, C., Godin, R., Allen, B.G., Petrof, B.J., Des Rosiers, C., and Burelle, Y. (2011). Stress-induced opening of the permeability transition pore in the dystrophin-deficient heart is attenuated by acute treatment with sildenafil. Am. J. Physiol. Heart Circ. Physiol. *300*, H144–153.

Au, C.G., Butler, T.L., Sherwood, M.C., Egan, J.R., North, K.N., and Winlaw, D.S. (2011). Increased connective tissue growth factor associated with cardiac fibrosis in the mdx mouse model of dystrophic cardiomyopathy. Int J Exp Pathol *92*, 57–65.

Baltgalvis, K.A., Call, J.A., Nikas, J.B., and Lowe, D.A. (2009). Effects of prednisolone on skeletal muscle contractility in mdx mice. Muscle Nerve *40*, 443–454.

Banks, G.B., Gregorevic, P., Allen, J.M., Finn, E.E., and Chamberlain, J.S. (2007). Functional capacity of dystrophins carrying deletions in the N-terminal actin-binding domain. Hum. Mol. Genet. *16*, 2105–2113.

Banks, G.B., Chamberlain, J.S., and Froehner, S.C. (2009). Truncated dystrophins can influence neuromuscular synapse structure. Mol. Cell. Neurosci. *40*, 433–441.

Baranano, D.E., and Snyder, S.H. (2001). Neural roles for heme oxygenase: Contrasts to nitric oxide synthase. Proc Natl Acad Sci U S A *98*, 10996–11002.

Barresi, R., Moore, S.A., Stolle, C.A., Mendell, J.R., and Campbell, K.P. (2000). Expression of gamma -sarcoglycan in smooth muscle and its interaction with the smooth muscle sarcoglycan-sarcospan complex. J. Biol. Chem. *275*, 38554–38560.

Barton, E.R., Morris, L., Kawana, M., Bish, L.T., and Toursel, T. (2005). Systemic administration of L-arginine benefits mdx skeletal muscle function. Muscle Nerve *32*, 751–760.

Barton-Davis, E.R., Cordier, L., Shoturma, D.I., Leland, S.E., and Sweeney, H.L. (1999). Aminoglycoside antibiotics restore dystrophin function to skeletal muscles of mdx mice. J. Clin. Invest. *104*, 375–381.

Bassel-Duby, R., and Olson, E.N. (2006). Signaling pathways in skeletal muscle remodeling. Annu. Rev. Biochem. *75*, 19–37.

Basu, U., Gyrd-Hansen, M., Baby, S.M., Lozynska, O., Krag, T.O.B., Jensen, C.J., Frödin, M., and Khurana, T.S. (2007). Heregulin-induced epigenetic regulation of the utrophin-A promoter. FEBS Lett. *581*, 4153–4158.

Basu, U., Lozynska, O., Moorwood, C., Patel, G., Wilton, S.D., and Khurana, T.S. (2011). Translational regulation of utrophin by miRNAs. PLoS ONE *6*, e29376.

Benabdellah, F., Yu, H., Brunelle, A., Laprévote, O., and De La Porte, S. (2009). MALDI reveals membrane lipid profile reversion in MDX mice. Neurobiol. Dis. *36*, 252–258.

Bennett, R.R., den Dunnen, J., O'Brien, K.F., Darras, B.T., and Kunkel, L.M. (2001). Detection of mutations in the dystrophin gene via automated DHPLC screening and direct sequencing. BMC Genet *2*, 17.

Bewick, G.S., Nicholson, L.V., Young, C., O'Donnell, E., and Slater, C.R. (1992). Different distributions of dystrophin and related proteins at nerve-muscle junctions. Neuroreport *3*, 857–860.

Bhagavati, S., and Xu, W. (2004). Isolation and enrichment of skeletal muscle progenitor cells from mouse bone marrow. Biochem. Biophys. Res. Commun. *318*, 119–124.

Bia, B.L., Cassidy, P.J., Young, M.E., Rafael, J.A., Leighton, B., Davies, K.E., Radda, G.K., and Clarke, K. (1999). Decreased myocardial nNOS, increased iNOS and abnormal ECGs in mouse models of Duchenne muscular dystrophy. Journal of Molecular and Cellular Cardiology *31*, 1857–1862.

Blain, A., Greally, E., Laval, S., Blamire, A., Straub, V., and Macgowan, G.A. (2013). Beta-blockers, left and right ventricular function, and in-vivo calcium influx in muscular dystrophy cardiomyopathy. PLoS ONE *8*, e57260.

Blake, D.J., Tinsley, J.M., Davies, K.E., Knight, A.E., Winder, S.J., and Kendrick-Jones, J. (1995). Coiled-coil regions in the carboxy-terminal domains of dystrophin and related proteins: potentials for protein-protein interactions. Trends Biochem. Sci. *20*, 133–135.

Blake, D.J., Nawrotzki, R., Loh, N.Y., Gorecki, D.C., and Davies, K.E. (1998). beta-dystrobrevin, a member of the dystrophin-related protein family. Proceedings of the National Academy of Sciences of the United States of America *95*, 241–246.

Blake, D.J., Weir, A., Newey, S.E., and Davies, K.E. (2002). Function and genetics of dystrophin and dystrophin-related proteins in muscle. Physiological Reviews *82*, 291–329.

Boerio, D., Greensmith, L., and Bostock, H. (2009). Excitability properties of motor axons in the maturing mouse. J Peripher Nerv Syst *14*, 45–53.

Bogdan, C. (2001). Nitric oxide and the regulation of gene expression. Trends Cell Biol. *11*, 66–75.

Bostock, H., Cikurel, K., and Burke, D. (1998). Threshold tracking techniques in the study of human peripheral nerve. Muscle Nerve *21*, 137–158.

Brenman, J.E., Chao, D.S., Xia, H., Aldape, K., and Bredt, D.S. (1995). Nitric oxide synthase complexed with dystrophin and absent from skeletal muscle sarcolemma in Duchenne muscular dystrophy. Cell *82*, 743–752.

Brenman, J.E., Chao, D.S., Gee, S.H., McGee, A.W., Craven, S.E., Santillano, D.R., Wu, Z., Huang, F., Xia, H., Peters, M.F., et al. (1996). Interaction of nitric oxide synthase with the postsynaptic density protein PSD-95 and alpha1-syntrophin mediated by PDZ domains. Cell *84*, 757–767.

Briguet, A., Bleckmann, D., Bettan, M., Mermod, N., and Meier, T. (2003). Transcriptional activation of the utrophin promoter B by a constitutively active Ets-transcription factor. Neuromuscul. Disord. *13*, 143–150.

Brooks, S.V. (1998). Rapid recovery following contraction-induced injury to in situ skeletal muscles in mdx mice. J. Muscle Res. Cell. Motil. *19*, 179–187.

Brunelli, S., Sciorati, C., D'Antona, G., Innocenzi, A., Covarello, D., Galvez, B.G., Perrotta, C., Monopoli, A., Sanvito, F., Bottinelli, R., et al. (2007). Nitric oxide release combined with nonsteroidal antiinflammatory activity prevents muscular dystrophy pathology and enhances stem cell therapy. Proc. Natl. Acad. Sci. U.S.A. *104*, 264–269.

Bulfield, G., Siller, W.G., Wight, P.A., and Moore, K.J. (1984). X chromosome-linked muscular dystrophy (mdx) in the mouse. Proc. Natl. Acad. Sci. U.S.A. *81*, 1189–1192.

Burton, E.A., Tinsley, J.M., Holzfeind, P.J., Rodrigues, N.R., and Davies, K.E. (1999). A second promoter provides an alternative target for therapeutic up-regulation of utrophin in Duchenne muscular dystrophy. Proc. Natl. Acad. Sci. U.S.A. *96*, 14025–14030.

Cai, H., Erdman, R.A., Zweier, L., Chen, J., Shaw, J.H., 4th, Baylor, K.A., Stecker, M.M., Carey, D.J., and Chan, Y.M. (2007). The sarcoglycan complex in Schwann cells and its role in myelin stability. Exp. Neurol. *205*, 257–269.

Campanelli, J.T., Gayer, G.G., and Scheller, R.H. (1996). Alternative RNA splicing that determines agrin activity regulates binding to heparin and alpha-dystroglycan. Development *122*, 1663–1672.

Carpenter, J.L., Hoffman, E.P., Romanul, F.C., Kunkel, L.M., Rosales, R.K., Ma, N.S., Dasbach, J.J., Rae, J.F., Moore, F.M., and McAfee, M.B. (1989). Feline muscular dystrophy with dystrophin deficiency. Am. J. Pathol. *135*, 909–919.

Cartaud, A., Coutant, S., Petrucci, T.C., and Cartaud, J. (1998). Evidence for in situ and in vitro association between beta-dystroglycan and the subsynaptic 43K rapsyn protein. Consequence for acetylcholine receptor clustering at the synapse. J. Biol. Chem. *273*, 11321–11326.

Carter, G.T., Wineinger, M.A., Walsh, S.A., Horasek, S.J., Abresch, R.T., and Fowler, W.M., Jr (1995). Effect of voluntary wheel-running exercise on muscles of the mdx mouse. Neuromuscul. Disord. *5*, 323–332.

Casar, J.C., McKechnie, B.A., Fallon, J.R., Young, M.F., and Brandan, E. (2004). Transient up-regulation of biglycan during skeletal muscle regeneration: delayed fiber growth along with decorin increase in biglycan-deficient mice. Dev. Biol. *268*, 358–371.

Di Certo, M.G., Corbi, N., Strimpakos, G., Onori, A., Luvisetto, S., Severini, C., Guglielmotti, A., Batassa, E.M., Pisani, C., Floridi, A., et al. (2010). The artificial gene Jazz, a transcriptional regulator of utrophin, corrects the dystrophic pathology in mdx mice. Hum. Mol. Genet. *19*, 752–760.

Chakkalakal, J.V., Thompson, J., Parks, R.J., and Jasmin, B.J. (2005). Molecular, cellular, and pharmacological therapies for Duchenne/Becker muscular dystrophies. FASEB J. *19*, 880–891.

Chang, W.J., Iannaccone, S.T., Lau, K.S., Masters, B.S., McCabe, T.J., McMillan, K., Padre, R.C., Spencer, M.J., Tidball, J.G., and Stull, J.T. (1996). Neuronal nitric oxide synthase and dystrophin-deficient muscular dystrophy. Proc. Natl. Acad. Sci. U.S.A. *93*, 9142–9147.

Chao, D.S., Silvagno, F., and Bredt, D.S. (1998). Muscular dystrophy in mdx mice despite lack of neuronal nitric oxide synthase. J. Neurochem. *71*, 784–789.

Chargé, S.B.P., and Rudnicki, M.A. (2004). Cellular and molecular regulation of muscle regeneration. Physiol. Rev. *84*, 209–238.

Chaubourt, E., Fossier, P., Baux, G., Leprince, C., Israël, M., and De La Porte, S. (1999). Nitric oxide and l-arginine cause an accumulation of utrophin at the sarcolemma: a possible compensation for dystrophin loss in Duchenne muscular dystrophy. Neurobiol. Dis. *6*, 499–507.

Chaubourt, E., Voisin, V., Fossier, P., Baux, G., Israël, M., and De La Porte, S. (2002). Muscular nitric oxide synthase (muNOS) and utrophin. J. Physiol. Paris *96*, 43–52.

Chazalette, D., Hnia, K., Rivier, F., Hugon, G., and Mornet, D. (2005). alpha7B integrin changes in mdx mouse muscles after L-arginine administration. FEBS Lett. *579*, 1079–1084.

Chelly, J., Hamard, G., Koulakoff, A., Kaplan, J.C., Kahn, A., and Berwald-Netter, Y. (1990). Dystrophin gene transcribed from different promoters in neuronal and glial cells. Nature *344*, 64–65.

Chung, W., and Campanelli, J.T. (1999). WW and EF hand domains of dystrophin-family proteins mediate dystroglycan binding. Mol. Cell Biol. Res. Commun. *2*, 162–171.

Ciciliot, S., and Schiaffino, S. (2010). Regeneration of mammalian skeletal muscle. Basic mechanisms and clinical implications. Curr. Pharm. Des. *16*, 906–914.

Clerk, A., Morris, G.E., Dubowitz, V., Davies, K.E., and Sewry, C.A. (1993). Dystrophin-related protein, utrophin, in normal and dystrophic human fetal skeletal muscle. Histochem. J. *25*, 554–561.

Colussi, C., Mozzetta, C., Gurtner, A., Illi, B., Rosati, J., Straino, S., Ragone, G., Pescatori, M., Zaccagnini, G., Antonini, A., et al. (2008). HDAC2 blockade by nitric oxide and histone deacetylase inhibitors reveals a common target in Duchenne muscular dystrophy treatment. Proc. Natl. Acad. Sci. U.S.A. *105*, 19183–19187.

Colussi, C., Gurtner, A., Rosati, J., Illi, B., Ragone, G., Piaggio, G., Moggio, M., Lamperti, C., D'Angelo, G., Clementi, E., et al. (2009). Nitric oxide deficiency determines global chromatin changes in Duchenne muscular dystrophy. Faseb J *23*, 2131–2141.

Colussi, C., Banfi, C., Brioschi, M., Tremoli, E., Straino, S., Spallotta, F., Mai, A., Rotili, D., Capogrossi, M.C., and Gaetano, C. (2010a). Proteomic profile of differentially expressed plasma proteins from dystrophic mice and following suberoylanilide hydroxamic acid treatment. Proteomics Clin Appl *4*, 71–83.

Colussi, C., Berni, R., Rosati, J., Straino, S., Vitale, S., Spallotta, F., Baruffi, S., Bocchi, L., Delucchi, F., Rossi, S., et al. (2010b). The histone deacetylase inhibitor suberoylanilide hydroxamic acid reduces cardiac arrhythmias in dystrophic mice. Cardiovasc. Res. *87*, 73–82.

Colussi, C., Illi, B., Rosati, J., Spallotta, F., Farsetti, A., Grasselli, A., Mai, A., Capogrossi, M.C., and Gaetano, C. (2010c). Histone deacetylase inhibitors: keeping momentum for neuromuscular and cardiovascular diseases treatment. Pharmacol. Res. *62*, 3–10.

Consalvi, S., Mozzetta, C., Bettica, P., Germani, M., Fiorentini, F., Del Bene, F., Rocchetti, M., Leoni, F., Mascagni, P., Puri, P.L., et al. (2013). Preclinical studies in the mdx mouse model of Duchenne Muscular Dystrophy with the Histone Deacetylase inhibitor Givinostat. Mol. Med.

Constantin, B., Sebille, S., and Cognard, C. (2006). New insights in the regulation of calcium transfers by muscle dystrophin-based cytoskeleton: implications in DMD. Journal of Muscle Research and Cell Motility *27*, 375–386.

Cooper, B.J., Winand, N.J., Stedman, H., Valentine, B.A., Hoffman, E.P., Kunkel, L.M., Scott, M.O., Fischbeck, K.H., Kornegay, J.N., and Avery, R.J. (1988). The homologue of the Duchenne locus is defective in X-linked muscular dystrophy of dogs. Nature *334*, 154–156.

Corbi, N., Libri, V., Fanciulli, M., Tinsley, J.M., Davies, K.E., and Passananti, C. (2000). The artificial zinc finger coding gene “Jazz” binds the utrophin promoter and activates transcription. Gene Ther. *7*, 1076–1083.

Coulton, G.R., Morgan, J.E., Partridge, T.A., and Sloper, J.C. (1988). The mdx mouse skeletal muscle myopathy: I. A histological, morphometric and biochemical investigation. Neuropathology and Applied Neurobiology *14*, 53–70.

Crisona, N.J., Allen, K.D., and Strohman, R.C. (1998). Muscle satellite cells from dystrophic (mdx) mice have elevated levels of heparan sulphate proteoglycan receptors for fibroblast growth factor. Journal of Muscle Research and Cell Motility *19*, 43–51.

Crosbie, R.H., Straub, V., Yun, H.Y., Lee, J.C., Rafael, J.A., Chamberlain, J.S., Dawson, V.L., Dawson, T.M., and Campbell, K.P. (1998). mdx muscle pathology is independent of nNOS perturbation. Hum. Mol. Genet. *7*, 823–829.

Cross, R.A., Stewart, M., and Kendrick-Jones, J. (1990). Structural predictions for the central domain of dystrophin. FEBS Lett. *262*, 87–92.

Darmani, H., Crossan, J., McLellan, S.D., Meek, D., and Adam, C. (2004). Expression of nitric oxide synthase and transforming growth factor-beta in crush-injured tendon and synovium. Mediators Inflamm. *13*, 299–305.

Davie, J.R. (2003). Inhibition of histone deacetylase activity by butyrate. J. Nutr. *133*, 2485S–2493S.

Decary, S., Mouly, V., and Butler-Browne, G.S. (1996). Telomere length as a tool to monitor satellite cell amplification for cell-mediated gene therapy. Hum. Gene Ther. *7*, 1347–1350.

Decary, S., Mouly, V., Hamida, C.B., Sautet, A., Barbet, J.P., and Butler-Browne, G.S. (1997). Replicative potential and telomere length in human skeletal muscle: implications for satellite cell-mediated gene therapy. Hum. Gene Ther. *8*, 1429–1438.

Decary, S., Hamida, C.B., Mouly, V., Barbet, J.P., Hentati, F., and Butler-Browne, G.S. (2000). Shorter telomeres in dystrophic muscle consistent with extensive regeneration in young children. Neuromuscul. Disord. *10*, 113–120.

Deng, B., Wehling-Henricks, M., Villalta, S.A., Wang, Y., and Tidball, J.G. (2012). IL-10 triggers changes in macrophage phenotype that promote muscle growth and regeneration. J. Immunol. *189*, 3669–3680.

Dennis, C.L., Tinsley, J.M., Deconinck, A.E., and Davies, K.E. (1996). Molecular and functional analysis of the utrophin promoter. Nucleic Acids Res. *24*, 1646–1652.

Dominov, J.A., Kravetz, A.J., Ardelt, M., Kostek, C.A., Beermann, M.L., and Miller, J.B. (2005). Muscle-specific BCL2 expression ameliorates muscle disease in laminin {alpha}2-deficient, but not in dystrophin-deficient, mice. Hum. Mol. Genet. *14*, 1029–1040.

Di Donna, S., Mamchaoui, K., Cooper, R.N., Seigneurin-Venin, S., Tremblay, J., Butler-Browne, G.S., and Mouly, V. (2003). Telomerase can extend the proliferative capacity of human myoblasts, but does not lead to their immortalization. Mol. Cancer Res. *1*, 643–653.

Einbond, A., and Sudol, M. (1996). Towards prediction of cognate complexes between the WW domain and proline-rich ligands. FEBS Lett. *384*, 1–8.

Emery, A.E., and Emery, M.L. (1993). Edward Meryon (1809-1880) and muscular dystrophy. J. Med. Genet. *30*, 506–511.

Ervasti, J.M., and Campbell, K.P. (1993). A role for the dystrophin-glycoprotein complex as a transmembrane linker between laminin and actin. J. Cell Biol. *122*, 809–823.

Ervasti, J.M., Ohlendieck, K., Kahl, S.D., Gaver, M.G., and Campbell, K.P. (1990). Deficiency of a glycoprotein component of the dystrophin complex in dystrophic muscle. Nature *345*, 315–319.

Escolar, D.M., Hache, L.P., Clemens, P.R., Cnaan, A., McDonald, C.M., Viswanathan, V., Kornberg, A.J., Bertorini, T.E., Nevo, Y., Lotze, T., et al. (2011). Randomized, blinded trial of weekend vs daily prednisone in Duchenne muscular dystrophy. Neurology *77*, 444–452.

Ettinger, A.J., Feng, G., and Sanes, J.R. (1997). epsilon-Sarcoglycan, a broadly expressed homologue of the gene mutated in limb-girdle muscular dystrophy 2D. J. Biol. Chem. *272*, 32534–32538.

Fairclough, R.J., Bareja, A., and Davies, K.E. (2011). Progress in therapy for Duchenne muscular dystrophy. Exp. Physiol. *96*, 1101–1113.

Fairclough, R.J., Perkins, K.J., and Davies, K.E. (2012). Pharmacologically targeting the primary defect and downstream pathology in Duchenne muscular dystrophy. Curr Gene Ther *12*, 206–244.

Fakhfakh, R., Lamarre, Y., Skuk, D., and Tremblay, J.P. (2012). Losartan enhances the success of myoblast transplantation. Cell Transplant *21*, 139–152.

Faller, D.V., and Perrine, S.P. (1995). Butyrate in the treatment of sickle cell disease and beta-thalassemia. Curr. Opin. Hematol. *2*, 109–117.

Fardeau, M., Tomé, F.M., Collin, H., Augier, N., Pons, F., Léger, J., and Léger, J. (1990). [Presence of dystrophine-like protein at the neuromuscular junction in Duchenne muscular dystrophy and in "mdx" mutant mice]. C. R. Acad. Sci. III, Sci. Vie *311*, 197–204.

Feener, C.A., Koenig, M., and Kunkel, L.M. (1989). Alternative splicing of human dystrophin mRNA generates isoforms at the carboxy terminus. Nature *338*, 509–511.

Ferlini, A., Sewry, C., Melis, M.A., Mateddu, A., and Muntoni, F. (1999). X-linked dilated cardiomyopathy and the dystrophin gene. Neuromuscul. Disord. *9*, 339–346.

Ferrari, G., Cusella-De Angelis, G., Coletta, M., Paolucci, E., Stornaiuolo, A., Cossu, G., and Mavilio, F. (1998). Muscle regeneration by bone marrow-derived myogenic progenitors. Science (New York, N.Y *279*, 1528–1530.

Filippin, L.I., Moreira, A.J., Marroni, N.P., and Xavier, R.M. (2009). Nitric oxide and repair of skeletal muscle injury. Nitric Oxide *21*, 157–163.

Finkel, R.S. (2010). Read-through strategies for suppression of nonsense mutations in Duchenne/ Becker muscular dystrophy: aminoglycosides and ataluren (PTC124). J. Child Neurol. *25*, 1158–1164.

Fisher, R., Tinsley, J.M., Phelps, S.R., Squire, S.E., Townsend, E.R., Martin, J.E., and Davies, K.E. (2001). Non-toxic ubiquitous over-expression of utrophin in the mdx mouse. Neuromuscul. Disord. *11*, 713–721.

Friedrich, O., Both, M., Gillis, J.M., Chamberlain, J.S., and Fink, R.H.A. (2004). Mini-dystrophin restores L-type calcium currents in skeletal muscle of transgenic mdx mice. J. Physiol. (Lond.) *555*, 251–265.

Le Gallic, L., Virgilio, L., Cohen, P., Biteau, B., and Mavrothalassitis, G. (2004). ERF nuclear shuttling, a continuous monitor of Erk activity that links it to cell cycle progression. Mol. Cell. Biol. *24*, 1206–1218.

Galvagni, F., Cartocci, E., and Oliviero, S. (1998). The dystrophin promoter is negatively regulated by YY1 in undifferentiated muscle cells. J. Biol. Chem. *273*, 33708–33713.

Galvagni, F., Cantini, M., and Oliviero, S. (2002). The utrophin gene is transcriptionally up-regulated in regenerating muscle. J. Biol. Chem. *277*, 19106–19113.

Gaschen, F.P., Hoffman, E.P., Gorospe, J.R., Uhl, E.W., Senior, D.F., Cardinet, G.H., 3rd, and Pearce, L.K. (1992). Dystrophin deficiency causes lethal muscle hypertrophy in cats. J. Neurol. Sci. *110*, 149–159.

Gilgenkrantz, H., Hugnot, J.P., Lambert, M., Chafey, P., Kaplan, J.C., and Kahn, A. (1992). Positive and negative regulatory DNA elements including a CCArGG box are involved in the cell type-specific expression of the human muscle dystrophin gene. J. Biol. Chem. *267*, 10823–10830.

Goldspink, G., Fernandes, K., Williams, P.E., and Wells, D.J. (1994). Age-related changes in collagen gene expression in the muscles of mdx dystrophic and normal mice. Neuromuscul Disord *4*, 183–191.

Gordon, B.S., Delgado Díaz, D.C., and Kostek, M.C. (2013). Resveratrol decreases inflammation and increases utrophin gene expression in the mdx mouse model of duchenne muscular dystrophy. Clin Nutr *32*, 104–111.

Górecki, D.C., Monaco, A.P., Derry, J.M., Walker, A.P., Barnard, E.A., and Barnard, P.J. (1992). Expression of four alternative dystrophin transcripts in brain regions regulated by different promoters. Hum. Mol. Genet. *1*, 505–510.

Gosselin, L.E., Williams, J.E., Deering, M., Brazeau, D., Koury, S., and Martinez, D.A. (2004). Localization and early time course of TGF-beta 1 mRNA expression in dystrophic muscle. Muscle Nerve *30*, 645–653.

Goyenvalle, A., and Davies, K.E. (2011). Challenges to oligonucleotides-based therapeutics for Duchenne muscular dystrophy. Skelet Muscle *1*, 8.

Goyenvalle, A., Seto, J.T., Davies, K.E., and Chamberlain, J. (2011). Therapeutic approaches to muscular dystrophy. Hum. Mol. Genet. *20*, R69–78.

Gramolini, A.O., and Jasmin, B.J. (1999). Expression of the utrophin gene during myogenic differentiation. Nucleic Acids Res. *27*, 3603–3609.

Gramolini, A.O., Angus, L.M., Schaeffer, L., Burton, E.A., Tinsley, J.M., Davies, K.E., Changeux, J.P., and Jasmin, B.J. (1999a). Induction of utrophin gene expression by heregulin in skeletal muscle cells: role of the N-box motif and GA binding protein. Proc. Natl. Acad. Sci. U.S.A. *96*, 3223–3227.

Gramolini, A.O., Karpati, G., and Jasmin, B.J. (1999b). Discordant expression of utrophin and its transcript in human and mouse skeletal muscles. J. Neuropathol. Exp. Neurol. *58*, 235–244.

Gramolini, A.O., Bélanger, G., and Jasmin, B.J. (2001a). Distinct regions in the 3' untranslated region are responsible for targeting and stabilizing utrophin transcripts in skeletal muscle cells. J. Cell Biol. *154*, 1173–1183.

Gramolini, A.O., Bélanger, G., Thompson, J.M., Chakkalakal, J.V., and Jasmin, B.J. (2001b). Increased expression of utrophin in a slow vs. a fast muscle involves posttranscriptional events. Am. J. Physiol., Cell Physiol. *281*, C1300–1309.

Gregorevic, P., Blankinship, M.J., Allen, J.M., Crawford, R.W., Meuse, L., Miller, D.G., Russell, D.W., and Chamberlain, J.S. (2004). Systemic delivery of genes to striated muscles using adeno-associated viral vectors. Nat. Med. *10*, 828–834.

Grozdanovic, Z., and Gossrau, R. (1998). Co-localization of nitric oxide synthase I (NOS I) and NMDA receptor subunit 1 (NMDAR-1) at the neuromuscular junction in rat and mouse skeletal muscle. Cell Tissue Res. *291*, 57–63.

Guerron, A.D., Rawat, R., Sali, A., Spurney, C.F., Pistilli, E., Cha, H.-J., Pandey, G.S., Gernapudi, R., Francia, D., Farajian, V., et al. (2010). Functional and molecular effects of arginine butyrate and prednisone on muscle and heart in the mdx mouse model of Duchenne Muscular Dystrophy. PLoS ONE *5*, e11220.

Gurpur, P.B., Liu, J., Burkin, D.J., and Kaufman, S.J. (2009). Valproic acid activates the PI3K/Akt/mTOR pathway in muscle and ameliorates pathology in a mouse model of Duchenne muscular dystrophy. Am. J. Pathol. *174*, 999–1008.

Hall, J.K., Banks, G.B., Chamberlain, J.S., and Olwin, B.B. (2010). Prevention of muscle aging by myofiber-associated satellite cell transplantation. Sci Transl Med *2*, 57ra83.

Heemskerk, H.A., de Winter, C.L., de Kimpe, S.J., van Kuik-Romeijn, P., Heuvelmans, N., Platenburg, G.J., van Ommen, G.-J.B., van Deutekom, J.C.T., and Aartsma-Rus, A. (2009). In vivo comparison of 2'-O-methyl phosphorothioate and morpholino antisense oligonucleotides for Duchenne muscular dystrophy exon skipping. J Gene Med *11*, 257–266.

Hemmings, L., Kuhlman, P.A., and Critchley, D.R. (1992). Analysis of the actin-binding domain of alpha-actinin by mutagenesis and demonstration that dystrophin contains a functionally homologous domain. J. Cell Biol. *116*, 1369–1380.

Henderson, D.M., Lin, A.Y., Thomas, D.D., and Ervasti, J.M. (2012). The carboxy-terminal third of dystrophin enhances actin binding activity. J. Mol. Biol. *416*, 414–424.

Hnia, K., Gayraud, J., Hugon, G., Ramonatxo, M., De La Porte, S., Matecki, S., and Mornet, D. (2008). L-arginine decreases inflammation and modulates the nuclear factor-kappaB/matrix metalloproteinase cascade in mdx muscle fibers. The American Journal of Pathology *172*, 1509–1519.

Hoffman, E.P., Brown, R.H., and Kunkel, L.M. (1987). Dystrophin: the protein product of the Duchenne muscular dystrophy locus. Cell *51*, 919–928.

Holder, E., Maeda, M., and Bies, R.D. (1996). Expression and regulation of the dystrophin Purkinje promoter in human skeletal muscle, heart, and brain. Hum. Genet. *97*, 232–239.

Hong, F., Lee, J., Song, J.-W., Lee, S.J., Ahn, H., Cho, J.J., Ha, J., and Kim, S.S. (2002). Cyclosporin A blocks muscle differentiation by inducing oxidative stress and inhibiting the peptidyl-prolyl-cis-trans isomerase activity of cyclophilin A: cyclophilin A protects myoblasts from cyclosporin A-induced cytotoxicity. FASEB J. *16*, 1633–1635.

Hudziak, R.M., Barofsky, E., Barofsky, D.F., Weller, D.L., Huang, S.B., and Weller, D.D. (1996). Resistance of morpholino phosphorodiamidate oligomers to enzymatic degradation. Antisense Nucleic Acid Drug Dev. *6*, 267–272.

Ibraghimov-Beskrovnaya, O., Ervasti, J.M., Leveille, C.J., Slaughter, C.A., Sernett, S.W., and Campbell, K.P. (1992). Primary structure of dystrophin-associated glycoproteins linking dystrophin to the extracellular matrix. Nature *355*, 696–702.

Ichim, T.E., Alexandrescu, D.T., Solano, F., Lara, F., Campion, R.D.N., Paris, E., Woods, E.J., Murphy, M.P., Dasanu, C.A., Patel, A.N., et al. (2010). Mesenchymal stem cells as anti-inflammatories: implications for treatment of Duchenne muscular dystrophy. Cell. Immunol. *260*, 75–82.

Iezzi, S., Di Padova, M., Serra, C., Caretti, G., Simone, C., Maklan, E., Minetti, G., Zhao, P., Hoffman, E.P., Puri, P.L., et al. (2004). Deacetylase inhibitors increase muscle cell size by promoting myoblast recruitment and fusion through induction of follistatin. Dev. Cell *6*, 673–684.

Igarashi, A., Okochi, H., Bradham, D.M., and Grotendorst, G.R. (1993). Regulation of connective tissue growth factor gene expression in human skin fibroblasts and during wound repair. Mol. Biol. Cell *4*, 637–645.

Imbert, N., Vandebrouck, C., Duport, G., Raymond, G., Hassoni, A.A., Constantin, B., Cullen, M.J., and Cognard, C. (2001). Calcium currents and transients in co-cultured contracting normal and Duchenne muscular dystrophy human myotubes. J. Physiol. (Lond.) *534*, 343–355.

Ingram V.M. (1956). A specific chemical difference between the globins of normal human and sikle-cell anaemia haemoglobin. 792–794.

Israel, M. (2003). Genetic adaptation controlled by methylations and acetylations at the nuclear and cytosolic levels: a hypothetical model. Neurochemical Research *28*, 631–635.

Itagaki, Y., Saida, K., and Iwamura, K. (1995). Regenerative capacity of mdx mouse muscles after repeated applications of myo-necrotic bupivacaine. Acta Neuropathol. *89*, 380–384.

Jarrett, H.W., and Foster, J.L. (1995). Alternate binding of actin and calmodulin to multiple sites on dystrophin. J. Biol. Chem. *270*, 5578–5586.

Jasmin, B.J., Angus, L.M., Bélanger, G., Chakkalakal, J.V., Gramolini, A.O., Lunde, J.A., Stocksley, M.A., and Thompson, J. (2002). Multiple regulatory events controlling the expression and localization of utrophin in skeletal muscle fibers: insights into a therapeutic strategy for Duchenne muscular dystrophy. J. Physiol. Paris *96*, 31–42.

Jefferies, J.L., Eidem, B.W., Belmont, J.W., Craigen, W.J., Ware, S.M., Fernbach, S.D., Neish, S.R., Smith, E.O., and Towbin, J.A. (2005). Genetic predictors and remodeling of dilated cardiomyopathy in muscular dystrophy. Circulation *112*, 2799–2804.

Jockusch, H., Friedrich, G., and Zippel, M. (1990). Serum parvalbumin, an indicator of muscle disease in murine dystrophy and myotonia. Muscle Nerve *13*, 551–555.

Jung, D., Yang, B., Meyer, J., Chamberlain, J.S., and Campbell, K.P. (1995). Identification and characterization of the dystrophin anchoring site on beta-dystroglycan. J. Biol. Chem. *270*, 27305–27310.

Kagen, L.J., Moussavi, S., Miller, S.L., and Tsairis, P. (1980). Serum myoglobin in muscular dystrophy. Muscle Nerve *3*, 221–226.

Kalman, L., Leonard, J., Gerry, N., Tarleton, J., Bridges, C., Gastier-Foster, J.M., Pyatt, R.E., Stonerock, E., Johnson, M.A., Richards, C.S., et al. (2011). Quality assurance for Duchenne and Becker muscular dystrophy genetic testing: development of a genomic DNA reference material panel. J Mol Diagn *13*, 167–174.

Kanai, A.J., Pearce, L.L., Clemens, P.R., Birder, L.A., VanBibber, M.M., Choi, S.Y., de Groat, W.C., and Peterson, J. (2001). Identification of a neuronal nitric oxide synthase in isolated cardiac mitochondria using electrochemical detection. Proc. Natl. Acad. Sci. U.S.A. *98*, 14126–14131.

Karlsson, S., and Nienhuis, A.W. (1985). Developmental regulation of human globin genes. Annu. Rev. Biochem. *54*, 1071–1108.

Karpati, G., Carpenter, S., Morris, G.E., Davies, K.E., Guerin, C., and Holland, P. (1993). Localization and quantitation of the chromosome 6-encoded dystrophin-related protein in normal and pathological human muscle. J. Neuropathol. Exp. Neurol. *52*, 119–128.

Kayali, R., Ku, J.-M., Khitrov, G., Jung, M.E., Prikhodko, O., and Bertoni, C. (2012). Read-through compound 13 restores dystrophin expression and improves muscle function in the mdx mouse model for Duchenne muscular dystrophy. Hum. Mol. Genet. *21*, 4007–4020.

Keep, N.H., Norwood, F.L., Moores, C.A., Winder, S.J., and Kendrick-Jones, J. (1999). The 2.0 A structure of the second calponin homology domain from the actin-binding region of the dystrophin homologue utrophin. J. Mol. Biol. *285*, 1257–1264.

Khairallah, M., Khairallah, R., Young, M.E., Dyck, J.R.B., Petrof, B.J., and Des Rosiers, C. (2007). Metabolic and signaling alterations in dystrophin-deficient hearts precede overt cardiomyopathy. J. Mol. Cell. Cardiol. *43*, 119–129.

Khairallah, M., Khairallah, R.J., Young, M.E., Allen, B.G., Gillis, M.A., Danialou, G., Deschepper, C.F., Petrof, B.J., and Des Rosiers, C. (2008). Sildenafil and cardiomyocyte-specific cGMP signaling prevent cardiomyopathic changes associated with dystrophin deficiency. Proc. Natl. Acad. Sci. U.S.A. *105*, 7028–7033.

Khairallah, R.J., Shi, G., Sbrana, F., Prosser, B.L., Borroto, C., Mazaitis, M.J., Hoffman, E.P., Mahurkar, A., Sachs, F., Sun, Y., et al. (2012). Microtubules underlie dysfunction in duchenne muscular dystrophy. Sci Signal *5*, ra56.

Khurana, T.S., Hoffman, E.P., and Kunkel, L.M. (1990). Identification of a chromosome 6-encoded dystrophin-related protein. J. Biol. Chem. *265*, 16717–16720.

Khurana, T.S., Rosmarin, A.G., Shang, J., Krag, T.O., Das, S., and Gammeltoft, S. (1999). Activation of utrophin promoter by heregulin via the ets-related transcription factor complex GA-binding protein alpha/beta. Mol. Biol. Cell *10*, 2075–2086.

Kiernan, M.C., Burke, D., Andersen, K.V., and Bostock, H. (2000). Multiple measures of axonal excitability: a new approach in clinical testing. Muscle Nerve *23*, 399–409.

Kimura, E., Li, S., Gregorevic, P., Fall, B.M., and Chamberlain, J.S. (2010). Dystrophin delivery to muscles of mdx mice using lentiviral vectors leads to myogenic progenitor targeting and stable gene expression. Mol. Ther. *18*, 206–213.

Klamut, H.J., Bosnoyan-Collins, L.O., Worton, R.G., Ray, P.N., and Davis, H.L. (1996). Identification of a transcriptional enhancer within muscle intron 1 of the human dystrophin gene. Hum. Mol. Genet. *5*, 1599–1606.

Koenig, M., Beggs, A.H., Moyer, M., Scherpf, S., Heindrich, K., Bettecken, T., Meng, G., Müller, C.R., Lindlöf, M., and Kaariainen, H. (1989). The molecular basis for Duchenne versus Becker muscular dystrophy: correlation of severity with type of deletion. Am. J. Hum. Genet. *45*, 498–506.

Koenig, X., Dysek, S., Kimbacher, S., Mike, A.K., Cervenka, R., Lukacs, P., Nagl, K., Dang, X.B., Todt, H., Bittner, R.E., et al. (2011). Voltage-gated ion channel dysfunction precedes cardiomyopathy development in the dystrophic heart. PLoS ONE *6*, e20300.

Krishnan, A.V., Lin, C.S.-Y., Park, S.B., and Kiernan, M.C. (2008). Assessment of nerve excitability in toxic and metabolic neuropathies. J. Peripher. Nerv. Syst. *13*, 7–26.

Kurebayashi, N., and Ogawa, Y. (2001). [Calcium dynamics in skeletal muscle]. Clinical Calcium *11*, 1417–1423.

Lau, K.S., Grange, R.W., Chang, W.J., Kamm, K.E., Sarelius, I., and Stull, J.T. (1998). Skeletal muscle contractions stimulate cGMP formation and attenuate vascular smooth muscle myosin phosphorylation via nitric oxide. FEBS Lett. *431*, 71–74.

Laws, N., and Hoey, A. (2004). Progression of kyphosis in mdx mice. J. Appl. Physiol. *97*, 1970–1977.

Lee, K.H., Baek, M.Y., Moon, K.Y., Song, W.K., Chung, C.H., Ha, D.B., and Kang, M.S. (1994). Nitric oxide as a messenger molecule for myoblast fusion. J. Biol. Chem. *269*, 14371–14374.

Lefaucheur, J.P., and Sebille, A. (1994). Basic fibroblast growth factor and muscular dystrophy. Annals of Neurology *36*, 800.

Lefaucheur, J.P., Pastoret, C., and Sebille, A. (1995). Phenotype of dystrophinopathy in old mdx mice. The Anatomical Record *242*, 70–76.

Levine, B.A., Moir, A.J., Patchell, V.B., and Perry, S.V. (1992). Binding sites involved in the interaction of actin with the N-terminal region of dystrophin. FEBS Lett. *298*, 44–48.

Li, D., Bareja, A., Judge, L., Yue, Y., Lai, Y., Fairclough, R., Davies, K.E., Chamberlain, J.S., and Duan, D. (2010). Sarcolemmal nNOS anchoring reveals a qualitative difference between dystrophin and utrophin. J. Cell. Sci. *123*, 2008–2013.

Lorin, C., Gueffier, M., Bois, P., Faivre, J.-F., Cognard, C., and Sebille, S. (2013). Ultrastructural and Functional Alterations of EC Coupling Elements in mdx Cardiomyocytes: An Analysis from Membrane Surface to Depth. Cell Biochem. Biophys.

Loufrani, L., Levy, B.I., and Henrion, D. (2002). Defect in microvascular adaptation to chronic changes in blood flow in mice lacking the gene encoding for dystrophin. Circ. Res. *91*, 1183–1189.

Love, D.R., Hill, D.F., Dickson, G., Spurr, N.K., Byth, B.C., Marsden, R.F., Walsh, F.S., Edwards, Y.H., and Davies, K.E. (1989). An autosomal transcript in skeletal muscle with homology to dystrophin. Nature *339*, 55–58.

Lu, Q.L., Mann, C.J., Lou, F., Bou-Gharios, G., Morris, G.E., Xue, S., Fletcher, S., Partridge, T.A., and Wilton, S.D. (2003). Functional amounts of dystrophin produced by skipping the mutated exon in the mdx dystrophic mouse. Nat. Med. *9*, 1009–1014.

Lynch, G.S., Rafael, J.A., Hinkle, R.T., Cole, N.M., Chamberlain, J.S., and Faulkner, J.A. (1997). Contractile properties of diaphragm muscle segments from old mdx and old transgenic mdx mice. Am. J. Physiol. *272*, C2063–2068.

Lynch, G.S., Hinkle, R.T., Chamberlain, J.S., Brooks, S.V., and Faulkner, J.A. (2001). Force and power output of fast and slow skeletal muscles from mdx mice 6-28 months old. The Journal of Physiology *535*, 591–600.

Makover, A., Zuk, D., Breakstone, J., Yaffe, D., and Nudel, U. (1991). Brain-type and muscle-type promoters of the dystrophin gene differ greatly in structure. Neuromuscul. Disord. *1*, 39–45.

Malhotra, S.B., Hart, K.A., Klamut, H.J., Thomas, N.S., Bodrug, S.E., Burghes, A.H., Bobrow, M., Harper, P.S., Thompson, M.W., and Ray, P.N. (1988). Frame-shift deletions in patients with Duchenne and Becker muscular dystrophy. Science *242*, 755–759.

Malik, V., Rodino-Klapac, L.R., and Mendell, J.R. (2012). Emerging drugs for Duchenne muscular dystrophy. Expert Opin Emerg Drugs *17*, 261–277.

Manzur, A.Y., Kuntzer, T., Pike, M., and Swan, A. (2008). Glucocorticoid corticosteroids for Duchenne muscular dystrophy. Cochrane Database Syst Rev CD003725.

Marques, M.J., Luz, M.A.M., Minatel, E., and Neto, H.S. (2005). Muscle regeneration in dystrophic mdx mice is enhanced by isosorbide dinitrate. Neurosci. Lett. *382*, 342–345.

Marques, M.J., Taniguti, A.P.T., Minatel, E., and Neto, H.S. (2007). Nerve terminal contributes to acetylcholine receptor organization at the dystrophic neuromuscular junction of mdx mice. Anat Rec (Hoboken) *290*, 181–187.

Marshall, J.L., Holmberg, J., Chou, E., Ocampo, A.C., Oh, J., Lee, J., Peter, A.K., Martin, P.T., and Crosbie-Watson, R.H. (2012). Sarcospan-dependent Akt activation is required for utrophin expression and muscle regeneration. J. Cell Biol. *197*, 1009–1027.

Martin, P.T. (2003). Dystroglycan glycosylation and its role in matrix binding in skeletal muscle. Glycobiology *13*, 55R–66R.

Martin, E.A., Barresi, R., Byrne, B.J., Tsimerinov, E.I., Scott, B.L., Walker, A.E., Gurudevan, S.V., Anene, F., Elashoff, R.M., Thomas, G.D., et al. (2012). Tadalafil alleviates muscle ischemia in patients with becker muscular dystrophy. Sci Transl Med *4*, 162ra155.

Matsuda, R., Nishikawa, A., and Tanaka, H. (1995). Visualization of dystrophic muscle fibers in mdx mouse by vital staining with Evans blue: evidence of apoptosis in dystrophin-deficient muscle. J. Biochem. *118*, 959–964.

Matsumura, C.Y., Taniguti, A.P.T., Pertille, A., Santo Neto, H., and Marques, M.J. (2011). Stretch-activated calcium channel protein TRPC1 is correlated with the different degrees of the dystrophic phenotype in mdx mice. Am. J. Physiol., Cell Physiol. *301*, C1344–1350.

Matsumura, K., Ervasti, J.M., Ohlendieck, K., Kahl, S.D., and Campbell, K.P. (1992). Association of dystrophin-related protein with dystrophin-associated proteins in mdx mouse muscle. Nature *360*, 588–591.

Matsumura, K., Tomé, F.M., Ionasescu, V., Ervasti, J.M., Anderson, R.D., Romero, N.B., Simon, D., Récan, D., Kaplan, J.C., and Fardeau, M. (1993). Deficiency of dystrophin-associated proteins in Duchenne muscular dystrophy patients lacking COOH-terminal domains of dystrophin. J. Clin. Invest. *92*, 866–871.

Matsumura, K., Burghes, A.H., Mora, M., Tomé, F.M., Morandi, L., Cornello, F., Leturcq, F., Jeanpierre, M., Kaplan, J.C., and Reinert, P. (1994). Immunohistochemical analysis of dystrophin-

associated proteins in Becker/Duchenne muscular dystrophy with huge in-frame deletions in the NH2-terminal and rod domains of dystrophin. J. Clin. Invest. *93*, 99–105.

McArdle, A., Edwards, R.H., and Jackson, M.J. (1995). How does dystrophin deficiency lead to muscle degeneration?--evidence from the mdx mouse. Neuromuscul. Disord. *5*, 445–456.

McCully, K., Giger, U., Argov, Z., Valentine, B., Cooper, B., Chance, B., and Bank, W. (1991). Canine X-linked muscular dystrophy studied with in vivo phosphorus magnetic resonance spectroscopy. Muscle Nerve *14*, 1091–1098.

McNally, E.M. (2007). New approaches in the therapy of cardiomyopathy in muscular dystrophy. Annu. Rev. Med. *58*, 75–88.

Mendell, J.R., Campbell, K., Rodino-Klapac, L., Sahenk, Z., Shilling, C., Lewis, S., Bowles, D., Gray, S., Li, C., Galloway, G., et al. (2010). Dystrophin immunity in Duchenne's muscular dystrophy. N. Engl. J. Med. *363*, 1429–1437.

Mercado, M.L., Amenta, A.R., Hagiwara, H., Rafii, M.S., Lechner, B.E., Owens, R.T., McQuillan, D.J., Froehner, S.C., and Fallon, J.R. (2006). Biglycan regulates the expression and sarcolemmal localization of dystrobrevin, syntrophin, and nNOS. FASEB J. *20*, 1724–1726.

Merlini, L., Gennari, M., Malaspina, E., Cecconi, I., Armaroli, A., Gnudi, S., Talim, B., Ferlini, A., Cicognani, A., and Franzoni, E. (2012). Early corticosteroid treatment in 4 duchenne muscular dystrophy patients: 14-year follow-up. Muscle Nerve *45*, 796–802.

Metzinger, L., Passaquin, A.C., Leijendekker, W.J., Poindron, P., and Rüegg, U.T. (1995). Modulation by prednisolone of calcium handling in skeletal muscle cells. Br. J. Pharmacol. *116*, 2811–2816.

Mezzano, V., Cabrera, D., Vial, C., and Brandan, E. (2007). Constitutively activated dystrophic muscle fibroblasts show a paradoxical response to TGF-beta and CTGF/CCN2. J Cell Commun Signal *1*, 205–217.

Michalak, M., Fu, S.Y., Milner, R.E., Busaan, J.L., and Hance, J.E. (1996). Phosphorylation of the carboxyl-terminal region of dystrophin. Biochem. Cell Biol. *74*, 431–437.

Miller, J.B., and Girgenrath, M. (2006). The role of apoptosis in neuromuscular diseases and prospects for anti-apoptosis therapy. Trends Mol Med *12*, 279–286.

Milner, R.E., Busaan, J.L., Holmes, C.F., Wang, J.H., and Michalak, M. (1993). Phosphorylation of dystrophin. The carboxyl-terminal region of dystrophin is a substrate for in vitro phosphorylation by p34cdc2 protein kinase. J. Biol. Chem. *268*, 21901–21905.

Minetti, G.C., Colussi, C., Adami, R., Serra, C., Mozzetta, C., Parente, V., Fortuni, S., Straino, S., Sampaolesi, M., Di Padova, M., et al. (2006). Functional and morphological recovery of dystrophic muscles in mice treated with deacetylase inhibitors. Nat. Med. *12*, 1147–1150.

Miura, P., and Jasmin, B.J. (2006). Utrophin upregulation for treating Duchenne or Becker muscular dystrophy: how close are we? Trends Mol Med *12*, 122–129.

Miura, P., Andrews, M., Holcik, M., and Jasmin, B.J. (2008). IRES-mediated translation of utrophin A is enhanced by glucocorticoid treatment in skeletal muscle cells. PLoS ONE *3*, e2309.

Miura, P., Chakkalakal, J.V., Boudreault, L., Bélanger, G., Hébert, R.L., Renaud, J.-M., and Jasmin, B.J. (2009). Pharmacological activation of PPARbeta/delta stimulates utrophin A expression in skeletal muscle fibers and restores sarcolemmal integrity in mature mdx mice. Hum. Mol. Genet. *18*, 4640–4649.

Mizuno, Y., Yoshida, M., Nonaka, I., Hirai, S., and Ozawa, E. (1994). Expression of utrophin (dystrophin-related protein) and dystrophin-associated glycoproteins in muscles from patients with Duchenne muscular dystrophy. Muscle Nerve *17*, 206–216.

Mizunoya, W., Upadhaya, R., Burczynski, F.J., Wang, G., and Anderson, J.E. (2011). Nitric oxide donors improve prednisone effects on muscular dystrophy in the mdx mouse diaphragm. Am. J. Physiol., Cell Physiol. *300*, C1065–1077.

Moens, P., Baatsen, P.H., and Maréchal, G. (1993). Increased susceptibility of EDL muscles from mdx mice to damage induced by contractions with stretch. J. Muscle Res. Cell. Motil. *14*, 446–451.

Momose, M., Iguchi, N., Imamura, K., Usui, H., Ueda, T., Miyamoto, K., and Inaba, S. (2001). Depressed myocardial fatty acid metabolism in patients with muscular dystrophy. Neuromuscul. Disord. *11*, 464–469.

Monaco, A.P., Bertelson, C.J., Liechti-Gallati, S., Moser, H., and Kunkel, L.M. (1988). An explanation for the phenotypic differences between patients bearing partial deletions of the DMD locus. Genomics *2*, 90–95.

Moncada, S. (1999). Nitric oxide: discovery and impact on clinical medicine. J R Soc Med *92*, 164–169.

Moores, C.A., Keep, N.H., and Kendrick-Jones, J. (2000). Structure of the utrophin actin-binding domain bound to F-actin reveals binding by an induced fit mechanism. J. Mol. Biol. *297*, 465–480.

Morandi, L., Bernasconi, P., Gebbia, M., Mora, M., Crosti, F., Mantegazza, R., and Cornelio, F. (1995). Lack of mRNA and dystrophin expression in DMD patients three months after myoblast transfer. Neuromuscul. Disord. *5*, 291–295.

Moriuchi, T., Kagawa, N., Mukoyama, M., and Hizawa, K. (1993). Autopsy analyses of the muscular dystrophies. Tokushima J. Exp. Med. *40*, 83–93.

Mozzetta, C., Minetti, G., and Puri, P.L. (2009). Regenerative pharmacology in the treatment of genetic diseases: the paradigm of muscular dystrophy. Int. J. Biochem. Cell Biol. *41*, 701–710.

Muntoni, F., Torelli, S., and Ferlini, A. (2003). Dystrophin and mutations: one gene, several proteins, multiple phenotypes. Lancet Neurol *2*, 731–740.

Newey, S.E., Benson, M.A., Ponting, C.P., Davies, K.E., and Blake, D.J. (2000). Alternative splicing of dystrobrevin regulates the stoichiometry of syntrophin binding to the dystrophin protein complex. Curr. Biol. *10*, 1295–1298.

Newey, S.E., Gramolini, A.O., Wu, J., Holzfeind, P., Jasmin, B.J., Davies, K.E., and Blake, D.J. (2001). A novel mechanism for modulating synaptic gene expression: differential localization of alpha-dystrobrevin transcripts in skeletal muscle. Mol. Cell. Neurosci. *17*, 127–140.

Oda, T., Shimizu, N., Yonenobu, K., Ono, K., Nabeshima, T., and Kyoh, S. (1993). Longitudinal study of spinal deformity in Duchenne muscular dystrophy. J Pediatr Orthop *13*, 478–488.

Ogata, H., Nakatani, S., Ishikawa, Y., Negishi, A., Kobayashi, M., Ishikawa, Y., and Minami, R. (2007). Myocardial strain changes in Duchenne muscular dystrophy without overt cardiomyopathy. Int. J. Cardiol. *115*, 190–195.

Ohlendieck, K., Matsumura, K., Ionasescu, V.V., Towbin, J.A., Bosch, E.P., Weinstein, S.L., Sernett, S.W., and Campbell, K.P. (1993). Duchenne muscular dystrophy: deficiency of dystrophin-associated proteins in the sarcolemma. Neurology *43*, 795–800.

OKINAKA, S., KUMAGAI, H., EBASHI, S., SUGITA, H., MOMOI, H., TOYOKURA, Y., and FUJIE, Y. (1961). Serum creatine phosphokinase. Activity in progressive muscular dystrophy and neuromuscular diseases. Arch. Neurol. *4*, 520–525.

Olivé, M., Martinez-Matos, J.A., Montero, J., and Ferrer, I. (1997). Apoptosis is not the mechanism of cell death of muscle fibers in human muscular dystrophies and inflammatory myopathies. Muscle Nerve *20*, 1328–1330.

Onori, A., Desantis, A., Buontempo, S., Di Certo, M.G., Fanciulli, M., Salvatori, L., Passananti, C., and Corbi, N. (2007). The artificial 4-zinc-finger protein Bagly binds human utrophin promoter A at the endogenous chromosomal site and activates transcription. Biochem. Cell Biol. *85*, 358–365.

Ort, T., Maksimova, E., Dirkx, R., Kachinsky, A.M., Berghs, S., Froehner, S.C., and Solimena, M. (2000). The receptor tyrosine phosphatase-like protein ICA512 binds the PDZ domains of beta2-syntrophin and nNOS in pancreatic beta-cells. Eur. J. Cell Biol. *79*, 621–630.

Ozawa, E., Hagiwara, Y., and Yoshida, M. (1999). Creatine kinase, cell membrane and Duchenne muscular dystrophy. Mol. Cell. Biochem. *190*, 143–151.

Palmer, E., Wilhelm, J.M., and Sherman, F. (1979). Phenotypic suppression of nonsense mutants in yeast by aminoglycoside antibiotics. Nature *277*, 148–150.

Pan, Z., Yang, D., Nagaraj, R.Y., Nosek, T.A., Nishi, M., Takeshima, H., Cheng, H., and Ma, J. (2002). Dysfunction of store-operated calcium channel in muscle cells lacking mg29. Nat. Cell Biol. *4*, 379–383.

Partridge, M., Vincent, A., Matthews, P., Puma, J., Stein, D., and Summerton, J. (1996). A simple method for delivering morpholino antisense oligos into the cytoplasm of cells. Antisense Nucleic Acid Drug Dev. *6*, 169–175.

Pastoret, C., and Sebille, A. (1993). Further aspects of muscular dystrophy in mdx mice. Neuromuscul Disord *3*, 471–475.

Pastoret, C., and Sebille, A. (1995). Age-related differences in regeneration of dystrophic (mdx) and normal muscle in the mouse. Muscle & Nerve *18*, 1147–1154.

Pauling C., Italo H.A., Singer S.J., and Wells I.C. (1949). Sikle cell anamia, a molecular disease. 543–548.

Pearce, M., Blake, D.J., Tinsley, J.M., Byth, B.C., Campbell, L., Monaco, A.P., and Davies, K.E. (1993). The utrophin and dystrophin genes share similarities in genomic structure. Hum. Mol. Genet. *2*, 1765–1772.

Pellegrini, K.L., and Beilharz, M.W. (2011). The survival of myoblasts after intramuscular transplantation is improved when fewer cells are injected. Transplantation *91*, 522–526.

Perkins, K.J., and Davies, K.E. (2003). Ets, Ap-1 and GATA factor families regulate the utrophin B promoter: potential regulatory mechanisms for endothelial-specific expression. FEBS Lett. *538*, 168–172.

Perkins, K.J., Basu, U., Budak, M.T., Ketterer, C., Baby, S.M., Lozynska, O., Lunde, J.A., Jasmin, B.J., Rubinstein, N.A., and Khurana, T.S. (2007). Ets-2 repressor factor silences extrasynaptic utrophin by N-box mediated repression in skeletal muscle. Mol. Biol. Cell *18*, 2864–2872.

Perrine, S.P. (2008). Fetal globin stimulant therapies in the beta-hemoglobinopathies: principles and current potential. Pediatr Ann *37*, 339–346.

Perrine, S.P., and Faller, D.V. (1993). Butyrate-induced reactivation of the fetal globin genes: a molecular treatment for the beta-hemoglobinopathies. Experientia *49*, 133–137.

Perrine, S.P., Ginder, G.D., Faller, D.V., Dover, G.H., Ikuta, T., Witkowska, H.E., Cai, S.P., Vichinsky, E.P., and Olivieri, N.F. (1993). A short-term trial of butyrate to stimulate fetal-globin-gene expression in the beta-globin disorders. N. Engl. J. Med. *328*, 81–86.

Perrine, S.P., Olivieri, N.F., Faller, D.V., Vichinsky, E.P., Dover, G.J., and Ginder, G.D. (1994). Butyrate derivatives. New agents for stimulating fetal globin production in the beta-globin disorders. Am J Pediatr Hematol Oncol *16*, 67–71.

Perronnet, C., Chagneau, C., Le Blanc, P., Samson-Desvignes, N., Mornet, D., Laroche, S., De La Porte, S., and Vaillend, C. (2012). Upregulation of brain utrophin does not rescue behavioral alterations in dystrophin-deficient mice. Hum. Mol. Genet. *21*, 2263–2276.

Peters, M.F., Kramarcy, N.R., Sealock, R., and Froehner, S.C. (1994). beta 2-Syntrophin: localization at the neuromuscular junction in skeletal muscle. Neuroreport *5*, 1577–1580.

Peters, M.F., Adams, M.E., and Froehner, S.C. (1997). Differential association of syntrophin pairs with the dystrophin complex. J. Cell Biol. *138*, 81–93.

Petrof, B.J., Stedman, H.H., Shrager, J.B., Eby, J., Sweeney, H.L., and Kelly, A.M. (1993). Adaptations in myosin heavy chain expression and contractile function in dystrophic mouse diaphragm. Am. J. Physiol. *265*, C834–841.

Pichavant, C., Aartsma-Rus, A., Clemens, P.R., Davies, K.E., Dickson, G., Takeda, S., Wilton, S.D., Wolff, J.A., Wooddell, C.I., Xiao, X., et al. (2011). Current status of pharmaceutical and genetic therapeutic approaches to treat DMD. Mol. Ther. *19*, 830–840.

Piluso, G., Mirabella, M., Ricci, E., Belsito, A., Abbondanza, C., Servidei, S., Puca, A.A., Tonali, P., Puca, G.A., and Nigro, V. (2000). Gamma1- and gamma2-syntrophins, two novel dystrophin-binding proteins localized in neuronal cells. J. Biol. Chem. *275*, 15851–15860.

Pisconti, A., Brunelli, S., Di Padova, M., De Palma, C., Deponti, D., Baesso, S., Sartorelli, V., Cossu, G., and Clementi, E. (2006). Follistatin induction by nitric oxide through cyclic GMP: a tightly regulated signaling pathway that controls myoblast fusion. J. Cell Biol. *172*, 233–244.

Podhorska-Okolow, M., Sandri, M., Zampieri, S., Brun, B., Rossini, K., and Carraro, U. (1998). Apoptosis of myofibres and satellite cells: exercise-induced damage in skeletal muscle of the mouse. Neuropathol. Appl. Neurobiol. *24*, 518–531.

Prior, T.W., Papp, A.C., Snyder, P.J., Burghes, A.H., Bartolo, C., Sedra, M.S., Western, L.M., and Mendell, J.R. (1993). A missense mutation in the dystrophin gene in a Duchenne muscular dystrophy patient. Nat. Genet. *4*, 357–360.

Prosser, B.L., Ward, C.W., and Lederer, W.J. (2011). X-ROS signaling: rapid mechano-chemo transduction in heart. Science *333*, 1440–1445.

Quinlan, J.G., Hahn, H.S., Wong, B.L., Lorenz, J.N., Wenisch, A.S., and Levin, L.S. (2004). Evolution of the mdx mouse cardiomyopathy: physiological and morphological findings. Neuromuscul. Disord. *14*, 491–496.

Quinlivan, R.M., Lewis, P., Marsden, P., Dundas, R., Robb, S.A., Baker, E., and Maisey, M. (1996). Cardiac function, metabolism and perfusion in Duchenne and Becker muscular dystrophy. Neuromuscul. Disord. *6*, 237–246.

Ramachandran, J., Schneider, J.S., Crassous, P.-A., Zheng, R., Gonzalez, J.P., Xie, L.-H., Beuve, A., Fraidenraich, D., and Peluffo, R.D. (2012a). Nitric Oxide Signaling Pathway in Duchenne Muscular Dystrophy Mice: Upregulation of L-arginine Transporters. Biochem. J.

Ramachandran, J., Schneider, J.S., Crassous, P.-A., Zheng, R., Gonzalez, J.P., Xie, L.-H., Beuve, A., Fraidenraich, D., and Peluffo, R.D. (2012b). Nitric Oxide Signaling Pathway in Duchenne Muscular Dystrophy Mice: Upregulation of L-arginine Transporters. Biochem. J.

Rentschler, S., Linn, H., Deininger, K., Bedford, M.T., Espanel, X., and Sudol, M. (1999). The WW domain of dystrophin requires EF-hands region to interact with beta-dystroglycan. Biol. Chem. *380*, 431–442.

Roberds, S.L., Anderson, R.D., Ibraghimov-Beskrovnaya, O., and Campbell, K.P. (1993). Primary structure and muscle-specific expression of the 50-kDa dystrophin-associated glycoprotein (adhalin). J. Biol. Chem. *268*, 23739–23742.

Roberts, R.G., Bobrow, M., and Bentley, D.R. (1992). Point mutations in the dystrophin gene. Proc. Natl. Acad. Sci. U.S.A. *89*, 2331–2335.

Roberts, R.G., Gardner, R.J., and Bobrow, M. (1994). Searching for the 1 in 2,400,000: a review of dystrophin gene point mutations. Hum. Mutat. *4*, 1–11.

Russo, K., Di Stasio, E., Macchia, G., Rosa, G., Brancaccio, A., and Petrucci, T.C. (2000). Characterization of the beta-dystroglycan-growth factor receptor 2 (Grb2) interaction. Biochem. Biophys. Res. Commun. *274*, 93–98.

Sabourin, J., Cognard, C., and Constantin, B. (2009). Regulation by scaffolding proteins of canonical transient receptor potential channels in striated muscle. Journal of Muscle Research and Cell Motility *30*, 289–297.

Sadoulet-Puccio, H.M., Khurana, T.S., Cohen, J.B., and Kunkel, L.M. (1996). Cloning and characterization of the human homologue of a dystrophin related phosphoprotein found at the Torpedo electric organ post-synaptic membrane. Human Molecular Genetics *5*, 489–496.

Sadoulet-Puccio, H.M., Rajala, M., and Kunkel, L.M. (1997). Dystrobrevin and dystrophin: an interaction through coiled-coil motifs. Proc. Natl. Acad. Sci. U.S.A. *94*, 12413–12418.

Sali, A., Guerron, A.D., Gordish-Dressman, H., Spurney, C.F., Iantorno, M., Hoffman, E.P., and Nagaraju, K. (2012). Glucocorticoid-Treated Mice Are an Inappropriate Positive Control for Long-Term Preclinical Studies in the mdx Mouse. PLoS ONE *7*, e34204.

Sampaolesi, M., Blot, S., D'Antona, G., Granger, N., Tonlorenzi, R., Innocenzi, A., Mognol, P., Thibaud, J.-L., Galvez, B.G., Barthélémy, I., et al. (2006). Mesoangioblast stem cells ameliorate muscle function in dystrophic dogs. Nature *444*, 574–579.

Sander, M., Chavoshan, B., Harris, S.A., Iannaccone, S.T., Stull, J.T., Thomas, G.D., and Victor, R.G. (2000). Functional muscle ischemia in neuronal nitric oxide synthase-deficient skeletal muscle of children with Duchenne muscular dystrophy. Proc. Natl. Acad. Sci. U.S.A. *97*, 13818–13823.

Sandri, M., Carraro, U., Podhorska-Okolov, M., Rizzi, C., Arslan, P., Monti, D., and Franceschi, C. (1995). Apoptosis, DNA damage and ubiquitin expression in normal and mdx muscle fibers after exercise. FEBS Lett. *373*, 291–295.

Sandri, M., Podhorska-Okolow, M., Geromel, V., Rizzi, C., Arslan, P., Franceschi, C., and Carraro, U. (1997). Exercise induces myonuclear ubiquitination and apoptosis in dystrophin-deficient muscle of mice. J. Neuropathol. Exp. Neurol. *56*, 45–57.

Sandri, M., El Meslemani, A.H., Sandri, C., Schjerling, P., Vissing, K., Andersen, J.L., Rossini, K., Carraro, U., and Angelini, C. (2001). Caspase 3 expression correlates with skeletal muscle apoptosis in Duchenne and facioscapulo human muscular dystrophy. A potential target for pharmacological treatment? J. Neuropathol. Exp. Neurol. *60*, 302–312.

Sarma, S., Li, N., van Oort, R.J., Reynolds, C., Skapura, D.G., and Wehrens, X.H.T. (2010). Genetic inhibition of PKA phosphorylation of RyR2 prevents dystrophic cardiomyopathy. Proc. Natl. Acad. Sci. U.S.A. *107*, 13165–13170.

Schmalbruch, H. (1986). Muscle regeneration: fetal myogenesis in a new setting. Bibliotheca Anatomica 126–153.

Schofield, J.N., Górecki, D.C., Blake, D.J., Davies, K., and Edwards, Y.H. (1995). Dystroglycan mRNA expression during normal and mdx mouse embryogenesis: a comparison with utrophin and the apo-dystrophins. Dev. Dyn. *204*, 178–185.

Schultz, J., Hoffmüller, U., Krause, G., Ashurst, J., Macias, M.J., Schmieder, P., Schneider-Mergener, J., and Oschkinat, H. (1998). Specific interactions between the syntrophin PDZ domain and voltage-gated sodium channels. Nat. Struct. Biol. *5*, 19–24.

Sciorati, C., Miglietta, D., Buono, R., Pisa, V., Cattaneo, D., Azzoni, E., Brunelli, S., and Clementi, E. (2011). A dual acting compound releasing nitric oxide (NO) and ibuprofen, NCX 320, shows significant therapeutic effects in a mouse model of muscular dystrophy. Pharmacol. Res. *64*, 210–217.

Ségalat, L., Grisoni, K., Archer, J., Vargas, C., Bertrand, A., and Anderson, J.E. (2005). CAPON expression in skeletal muscle is regulated by position, repair, NOS activity, and dystrophy. Exp. Cell Res. *302*, 170–179.

Senter, L., Ceoldo, S., Petrusa, M.M., and Salviati, G. (1995). Phosphorylation of dystrophin:effects on actin binding. Biochem. Biophys. Res. Commun. *206*, 57–63.

Al-Shanti, N., and Stewart, C.E. (2009). Ca2+/calmodulin-dependent transcriptional pathways: potential mediators of skeletal muscle growth and development. Biol Rev Camb Philos Soc *84*, 637–652.

Sharp, N.J., Kornegay, J.N., Van Camp, S.D., Herbstreith, M.H., Secore, S.L., Kettle, S., Hung, W.Y., Constantinou, C.D., Dykstra, M.J., and Roses, A.D. (1992). An error in dystrophin mRNA processing in golden retriever muscular dystrophy, an animal homologue of Duchenne muscular dystrophy. Genomics *13*, 115–121.

Sher, G.D., Ginder, G.D., Little, J., Yang, S., Dover, G.J., and Olivieri, N.F. (1995). Extended therapy with intravenous arginine butyrate in patients with beta-hemoglobinopathies. N. Engl. J. Med. *332*, 1606–1610.

Sicinski, P., Geng, Y., Ryder-Cook, A.S., Barnard, E.A., Darlison, M.G., and Barnard, P.J. (1989). The molecular basis of muscular dystrophy in the mdx mouse: a point mutation. Science (New York, N.Y *244*, 1578–1580.

Silvagno, F., Xia, H., and Bredt, D.S. (1996). Neuronal nitric-oxide synthase-mu, an alternatively spliced isoform expressed in differentiated skeletal muscle. J. Biol. Chem. *271*, 11204–11208.

Sitnik, R., Campiotto, S., Vainzof, M., Pavanello, R.C., Takata, R.I., Zatz, M., and Passos-Bueno, M.R. (1997). Novel point mutations in the dystrophin gene. Hum. Mutat. *10*, 217–222.

Sklar, R.M., Hudson, A., and Brown, R.H., Jr (1991). Glucocorticoids increase myoblast proliferation rates by inhibiting death of cycling cells. In Vitro Cell. Dev. Biol. *27A*, 433–434.

Sonnemann, K.J., Heun-Johnson, H., Turner, A.J., Baltgalvis, K.A., Lowe, D.A., and Ervasti, J.M. (2009). Functional substitution by TAT-utrophin in dystrophin-deficient mice. PLoS Med. *6*, e1000083.

Sotgia, F., Lee, J.K., Das, K., Bedford, M., Petrucci, T.C., Macioce, P., Sargiacomo, M., Bricarelli, F.D., Minetti, C., Sudol, M., et al. (2000). Caveolin-3 directly interacts with the C-terminal tail of beta -dystroglycan. Identification of a central WW-like domain within caveolin family members. J. Biol. Chem. *275*, 38048–38058.

Spurney, C.F., Knoblach, S., Pistilli, E.E., Nagaraju, K., Martin, G.R., and Hoffman, E.P. (2008). Dystrophin-deficient cardiomyopathy in mouse: expression of Nox4 and Lox are associated with fibrosis and altered functional parameters in the heart. Neuromuscul. Disord. *18*, 371–381.

Squire, S., Raymackers, J.M., Vandebrouck, C., Potter, A., Tinsley, J., Fisher, R., Gillis, J.M., and Davies, K.E. (2002). Prevention of pathology in mdx mice by expression of utrophin: analysis using an inducible transgenic expression system. Hum. Mol. Genet. *11*, 3333–3344.

Stedman, H.H., Sweeney, H.L., Shrager, J.B., Maguire, H.C., Panettieri, R.A., Petrof, B., Narusawa, M., Leferovich, J.M., Sladky, J.T., and Kelly, A.M. (1991). The mdx mouse diaphragm reproduces the degenerative changes of Duchenne muscular dystrophy. Nature *352*, 536–539.

Stevens, E.D., and Faulkner, J.A. (2000). The capacity of mdx mouse diaphragm muscle to do oscillatory work. J. Physiol. (Lond.) *522 Pt 3*, 457–466.

Straub, V., Rafael, J.A., Chamberlain, J.S., and Campbell, K.P. (1997). Animal models for muscular dystrophy show different patterns of sarcolemmal disruption. J. Cell Biol. *139*, 375–385.

Straub, V., Ettinger, A.J., Durbeej, M., Venzke, D.P., Cutshall, S., Sanes, J.R., and Campbell, K.P. (1999). epsilon-sarcoglycan replaces alpha-sarcoglycan in smooth muscle to form a unique dystrophin-glycoprotein complex. J. Biol. Chem. *274*, 27989–27996.

Strutz, F., and Neilson, E.G. (2003). New insights into mechanisms of fibrosis in immune renal injury. Springer Seminars in Immunopathology *24*, 459–476.

Stuckey, D.J., Carr, C.A., Camelliti, P., Tyler, D.J., Davies, K.E., and Clarke, K. (2012). In vivo MRI characterization of progressive cardiac dysfunction in the mdx mouse model of muscular dystrophy. PLoS ONE *7*, e28569.

Stuehr, D.J., Tejero, J., and Haque, M.M. (2009). Structural and mechanistic aspects of flavoproteins: electron transfer through the nitric oxide synthase flavoprotein domain. The FEBS Journal *276*, 3959–3974.

Sun, G., Haginoya, K., Wu, Y., Chiba, Y., Nakanishi, T., Onuma, A., Sato, Y., Takigawa, M., Iinuma, K., and Tsuchiya, S. (2008). Connective tissue growth factor is overexpressed in muscles of human muscular dystrophy. Journal of the Neurological Sciences *267*, 48–56.

Suzuki, A., Yoshida, M., Yamamoto, H., and Ozawa, E. (1992). Glycoprotein-binding site of dystrophin is confined to the cysteine-rich domain and the first half of the carboxy-terminal domain. FEBS Lett. *308*, 154–160.

Suzuki, A., Yoshida, M., Hayashi, K., Mizuno, Y., Hagiwara, Y., and Ozawa, E. (1994). Molecular organization at the glycoprotein-complex-binding site of dystrophin. Three dystrophin-associated proteins bind directly to the carboxy-terminal portion of dystrophin. Eur. J. Biochem. *220*, 283–292.

Tahallah, N., Brunelle, A., De La Porte, S., and Laprevote, O. (2008). Lipid mapping in human dystrophic muscle by cluster-time-of-flight secondary ion mass spectrometry imaging. Journal of Lipid Research *49*, 438–454.

Tanabe, Y., Esaki, K., and Nomura, T. (1986). Skeletal muscle pathology in X chromosome-linked muscular dystrophy (mdx) mouse. Acta Neuropathologica *69*, 91–95.

Tatsumi, R., Hattori, A., Ikeuchi, Y., Anderson, J.E., and Allen, R.E. (2002). Release of Hepatocyte Growth Factor from Mechanically Stretched Skeletal Muscle Satellite Cells and Role of pH and Nitric Oxide. Mol Biol Cell *13*, 2909–2918.

Thomas, G.D., Sander, M., Lau, K.S., Huang, P.L., Stull, J.T., and Victor, R.G. (1998). Impaired metabolic modulation of alpha-adrenergic vasoconstriction in dystrophin-deficient skeletal muscle. Proc. Natl. Acad. Sci. U.S.A. *95*, 15090–15095.

Thomas, G.D., Ye, J., De Nardi, C., Monopoli, A., Ongini, E., and Victor, R.G. (2012). Treatment with a nitric oxide-donating NSAID alleviates functional muscle ischemia in the mouse model of Duchenne muscular dystrophy. PLoS ONE *7*, e49350.

Tidball, J.G., and Wehling-Henricks, M. (2007). Macrophages promote muscle membrane repair and muscle fibre growth and regeneration during modified muscle loading in mice in vivo. J. Physiol. (Lond.) *578*, 327–336.

Tidball, J.G., Albrecht, D.E., Lokensgard, B.E., and Spencer, M.J. (1995). Apoptosis precedes necrosis of dystrophin-deficient muscle. J. Cell. Sci. *108 (Pt 6)*, 2197–2204.

Tinsley, J., Deconinck, N., Fisher, R., Kahn, D., Phelps, S., Gillis, J.M., and Davies, K. (1998). Expression of full-length utrophin prevents muscular dystrophy in mdx mice. Nat. Med. *4*, 1441–1444.

Tinsley, J.M., Blake, D.J., Roche, A., Fairbrother, U., Riss, J., Byth, B.C., Knight, A.E., Kendrick-Jones, J., Suthers, G.K., and Love, D.R. (1992). Primary structure of dystrophin-related protein. Nature *360*, 591–593.

Tinsley, J.M., Potter, A.C., Phelps, S.R., Fisher, R., Trickett, J.I., and Davies, K.E. (1996). Amelioration of the dystrophic phenotype of mdx mice using a truncated utrophin transgene. Nature *384*, 349–353.

Tinsley, J.M., Fairclough, R.J., Storer, R., Wilkes, F.J., Potter, A.C., Squire, S.E., Powell, D.S., Cozzoli, A., Capogrosso, R.F., Lambert, A., et al. (2011). Daily treatment with SMTC1100, a novel small molecule utrophin upregulator, dramatically reduces the dystrophic symptoms in the mdx mouse. PLoS ONE *6*, e19189.

Tommasi di Vignano, A., Di Zenzo, G., Sudol, M., Cesareni, G., and Dente, L. (2000). Contribution of the different modules in the utrophin carboxy-terminal region to the formation and regulation of the DAP complex. FEBS Lett. *471*, 229–234.

Touboul, D., Piednoel, H., Voisin, V., De La Porte, S., Brunelle, A., Halgand, F., and Laprevote, O. (2004). Changes of phospholipid composition within the dystrophic muscle by matrix-assisted laser desorption/ionization mass spectrometry and mass spectrometry imaging. European Journal of Mass Spectrometry (Chichester, England) *10*, 657–664.

Valentine, B.A., Cooper, B.J., de Lahunta, A., O'Quinn, R., and Blue, J.T. (1988). Canine X-linked muscular dystrophy. An animal model of Duchenne muscular dystrophy: clinical studies. J. Neurol. Sci. *88*, 69–81.

Vandebrouck, C., Duport, G., Cognard, C., and Raymond, G. (2001). Cationic channels in normal and dystrophic human myotubes. Neuromuscul. Disord. *11*, 72–79.

Vater, R., Young, C., Anderson, L.V., Lindsay, S., Blake, D.J., Davies, K.E., Zuellig, R., and Slater, C.R. (1998). Utrophin mRNA expression in muscle is not restricted to the neuromuscular junction. Mol. Cell. Neurosci. *10*, 229–242.

Vianello, S., Yu, H., Voisin, V., Haddad, H., He, X., Foutz, A.S., Sebrié, C., Gillet, B., Roulot, M., Fougerousse, F., et al. (2013). Arginine butyrate: a therapeutic candidate for Duchenne muscular dystrophy. FASEB J.

Villalta, S.A., Rinaldi, C., Deng, B., Liu, G., Fedor, B., and Tidball, J.G. (2011a). Interleukin-10 reduces the pathology of mdx muscular dystrophy by deactivating M1 macrophages and modulating macrophage phenotype. Hum. Mol. Genet. *20*, 790–805.

Villalta, S.A., Deng, B., Rinaldi, C., Wehling-Henricks, M., and Tidball, J.G. (2011b). IFN-γ promotes muscle damage in the mdx mouse model of Duchenne muscular dystrophy by suppressing M2 macrophage activation and inhibiting muscle cell proliferation. J. Immunol. *187*, 5419–5428.

Voisin, V., and de la Porte, S. (2004). Therapeutic strategies for Duchenne and Becker dystrophies. Int. Rev. Cytol. *240*, 1–30.

Voisin, V., Sébrié, C., Matecki, S., Yu, H., Gillet, B., Ramonatxo, M., Israël, M., and De la Porte, S. (2005). L-arginine improves dystrophic phenotype in mdx mice. Neurobiol. Dis. *20*, 123–130.

Wagner, K.R., Cohen, J.B., and Huganir, R.L. (1993). The 87K postsynaptic membrane protein from Torpedo is a protein-tyrosine kinase substrate homologous to dystrophin. Neuron *10*, 511–522.

Wallace, G.Q., and McNally, E.M. (2009). Mechanisms of muscle degeneration, regeneration, and repair in the muscular dystrophies. Annu. Rev. Physiol. *71*, 37–57.

Wang, B., Li, J., and Xiao, X. (2000). Adeno-associated virus vector carrying human minidystrophin genes effectively ameliorates muscular dystrophy in mdx mouse model. Proc. Natl. Acad. Sci. U.S.A. *97*, 13714–13719.

Webster, C., Silberstein, L., Hays, A.P., and Blau, H.M. (1988). Fast muscle fibers are preferentially affected in Duchenne muscular dystrophy. Cell *52*, 503–513.

Wehling, M., Spencer, M.J., and Tidball, J.G. (2001). A nitric oxide synthase transgene ameliorates muscular dystrophy in mdx mice. The Journal of Cell Biology *155*, 123–131.

Wehling-Henricks, M., Jordan, M.C., Roos, K.P., Deng, B., and Tidball, J.G. (2005). Cardiomyopathy in dystrophin-deficient hearts is prevented by expression of a neuronal nitric oxide synthase transgene in the myocardium. Hum. Mol. Genet. *14*, 1921–1933.

Weir, A.P., Burton, E.A., Harrod, G., and Davies, K.E. (2002). A- and B-utrophin have different expression patterns and are differentially up-regulated in mdx muscle. J. Biol. Chem. *277*, 45285–45290.

Welch, E.M., Barton, E.R., Zhuo, J., Tomizawa, Y., Friesen, W.J., Trifillis, P., Paushkin, S., Patel, M., Trotta, C.R., Hwang, S., et al. (2007). PTC124 targets genetic disorders caused by nonsense mutations. Nature *447*, 87–91.

Whitehead, N.P., Yeung, E.W., and Allen, D.G. (2006). Muscle damage in mdx (dystrophic) mice: role of calcium and reactive oxygen species. Clin. Exp. Pharmacol. Physiol. *33*, 657–662.

Williams, I.A., and Allen, D.G. (2007a). The role of reactive oxygen species in the hearts of dystrophin-deficient mdx mice. Am. J. Physiol. Heart Circ. Physiol. *293*, H1969–1977.

Williams, I.A., and Allen, D.G. (2007b). Intracellular calcium handling in ventricular myocytes from mdx mice. Am. J. Physiol. Heart Circ. Physiol. *292*, H846–855.

Wilson, L.A., Cooper, B.J., Dux, L., Dubowitz, V., and Sewry, C.A. (1994). Expression of utrophin (dystrophin-related protein) during regeneration and maturation of skeletal muscle in canine X-linked muscular dystrophy. Neuropathol. Appl. Neurobiol. *20*, 359–367.

Winder, S.J., and Kendrick-Jones, J. (1995). Calcium/calmodulin-dependent regulation of the NH2-terminal F-actin binding domain of utrophin. FEBS Lett. *357*, 125–128.

Winder, S.J., Hemmings, L., Maciver, S.K., Bolton, S.J., Tinsley, J.M., Davies, K.E., Critchley, D.R., and Kendrick-Jones, J. (1995). Utrophin actin binding domain: analysis of actin binding and cellular targeting. J. Cell. Sci. *108 (Pt 1)*, 63–71.

Winnard, A.V., Klein, C.J., Coovert, D.D., Prior, T., Papp, A., Snyder, P., Bulman, D.E., Ray, P.N., McAndrew, P., and King, W. (1993). Characterization of translational frame exception patients in Duchenne/Becker muscular dystrophy. Hum. Mol. Genet. *2*, 737–744.

Wu, B., Moulton, H.M., Iversen, P.L., Jiang, J., Li, J., Li, J., Spurney, C.F., Sali, A., Guerron, A.D., Nagaraju, K., et al. (2008). Effective rescue of dystrophin improves cardiac function in dystrophin-deficient mice by a modified morpholino oligomer. Proc. Natl. Acad. Sci. U.S.A. *105*, 14814–14819.

Xu, K.Y., Huso, D.L., Dawson, T.M., Bredt, D.S., and Becker, L.C. (1999). Nitric oxide synthase in cardiac sarcoplasmic reticulum. Proc. Natl. Acad. Sci. U.S.A. *96*, 657–662.

Yamada, H., Shimizu, T., Tanaka, T., Campbell, K.P., and Matsumura, K. (1994). Dystroglycan is a binding protein of laminin and merosin in peripheral nerve. FEBS Lett. *352*, 49–53.

Yiu, E.M., and Kornberg, A.J. (2008). Duchenne muscular dystrophy. Neurol India *56*, 236–247.

Yoshida, M., Suzuki, A., Yamamoto, H., Noguchi, S., Mizuno, Y., and Ozawa, E. (1994). Dissociation of the complex of dystrophin and its associated proteins into several unique groups by n-octyl beta-D-glucoside. European Journal of Biochemistry / FEBS *222*, 1055–1061.

Zatz, M., Shapiro, L.J., Campion, D.S., Oda, E., and Kaback, M.M. (1978). Serum pyruvate-kinase (PK) and creatine-phosphokinase (CPK) in progressive muscular dystrophies. J. Neurol. Sci. *36*, 349–362.

Zatz, M., Rapaport, D., Vainzof, M., Passos-Bueno, M.R., Bortolini, E.R., Pavanello, R. de C., and Peres, C.A. (1991). Serum creatine-kinase (CK) and pyruvate-kinase (PK) activities in Duchenne (DMD) as compared with Becker (BMD) muscular dystrophy. J. Neurol. Sci. *102*, 190–196.

Zhang, W., ten Hove, M., Schneider, J.E., Stuckey, D.J., Sebag-Montefiore, L., Bia, B.L., Radda, G.K., Davies, K.E., Neubauer, S., and Clarke, K. (2008). Abnormal cardiac morphology, function and energy metabolism in the dystrophic mdx mouse: an MRI and MRS study. J. Mol. Cell. Cardiol. *45*, 754–760.

Ziche, M., and Morbidelli, L. (2000). Nitric oxide and angiogenesis. J. Neurooncol. *50*, 139–148.

Zoratti, M., and Szabò, I. (1995). The mitochondrial permeability transition. Biochim. Biophys. Acta *1241*, 139–176.

Appendix

SIMS proceedings paper

SURFACE and INTERFACE ANALYSIS

Received: 11 September 2011 Accepted: 20 December 2011 Published online in Wiley Online Library

(wileyonlinelibrary.com) DOI 10.1002/sia.4846

Compatibility between TOF-SIMS lipid imaging and histological staining on a rat brain section

C. Bich,[a] S. Vianello,[b] V. Guérineau,[a] D. Touboul,[a] S. De La Porte[b] and A. Brunelle[a]*

ABSTRACT: While ToF-SIMS is typically used to localize elemental ions in inorganic materials, it is also successfully utilized since several years to get images of a large variety of organic compounds, such as lipids (up to *m/z* 1500) at the surface of biological tissue sections. This technique can be associated with histology for medical diagnosis in order to correlate structural features with ion images. The possibility to use the same tissue section for both histology and mass spectrometry imaging would be a major advantage in terms of sample preparation and precision on the histological structure localization. In this study, on the one hand, rat brain sections were stained with Hematoxylin-Eosin (HE) after a ToF-SIMS surface analysis, and on the other hand, the lipid mapping with ToF-SIMS was performed after the HE staining procedure. In the first case, we evidenced that the high vacuum conditions applied in ToF-SIMS imaging did not disturb the staining neither the recognition of the brain structures. In the second case, a cholesterol fragment ion, chosen for imaging, was still detected in the brain structure after HE staining. However, it has not been possible to totally overlay the optical image before the staining with the ionic images after the staining, likely because of a distention of the tissue. Copyright © 2012 John Wiley & Sons, Ltd.

Keywords: histology; mass spectrometry imaging; ToF-SIMS; lipids

Introduction

Mass spectrometry imaging (MSI) [1,2] is a surface analysis method which was widely investigated with biological samples since ten years. Mapping small compounds of medical interest such as drugs or biomarkers at the surface of a tissue section is becoming a gold standard in health research. For the interpretation of MSI results, it is necessary to correlate the ion images to the histological information obtained from stained tissue sections. The combination of both techniques usually implies the use of adjacent tissue sections. Nevertheless, some small structures can vary from one section to the next depending on their size, relative to the thickness of the sections.

Working on a single tissue section with both techniques has already been investigated in the case of MALDI-MSI (matrix-assisted laser desorption/ionization) associated with HE staining.[3] HE, which uses two separate dyes, the first one to stain the nucleus (in brown) and the other one to stain the cytoplasm and connective tissue (in a various shade of red/pink color), is the most commonly and routinely used staining procedure. However, using HE prior to the MALDI imaging experiment compromises the overall MALDI spectra quality. The best approach to obtain optimum results from both methods is thus to stain the sample after the MSI analysis.[4,5] Since MALDI imaging needs to coat the sample surface with a matrix, this latter has to be removed before the HE staining as shown by Schwamborn *et al*. They also demonstrated the possibility to unambiguously correlate histological information with MALDI-MSI.[6] Since a few years, time-of-flight secondary ion mass spectrometry (ToF-SIMS) is more and more utilized to identify a large variety of organic compounds below *m/z* 1500 and to acquire ion density maps on biological tissue sections.[7,8] ToF-SIMS MSI permits to obtain the spatial distribution of a wide range of molecules, especially lipid compounds, without any sample preparation and with a high lateral resolution of 1 μm or less.[9,10]

In this paper, the compatibility between staining and ToF-SIMS imaging on rat brain sections has been investigated. Microscopic structures, lipid localization and signal intensities will be discussed.

Experimental

Rat brains were stored at −80 °C before analysis. Sections were cut at −20 °C with a CM3050-S cryostat (Leica Microsystèmes SA, Nanterre, France), deposited on a glass slide and dried under vacuum during 10 min. Staining and ToF-SIMS analyses were performed on the same sections (16-μm thickness) one after another. The HE protocol is the following: rinse with phosphate buffered solution, stain with hematoxylin, wash to remove the excess of stain with tap water and acidic alcohol solution and wash again with tap water; counterstain with eosin then wash with tap water and pure water before the successive alcohol baths for dehydration and the mounting

* *Correspondence to: Alain Brunelle, Centre de Recherche de Gif, Institut de Chimie des Substances Naturelles, CNRS, Avenue de la Terrasse, 91198 Gif-sur-Yvette Cedex, France.*
E-mail: Alain.Brunelle@icsn.cnrs-gif.fr

a *Centre de Recherche de Gif, Institut de Chimie des Substances Naturelles, CNRS, Avenue de la Terrasse, 91198 Gif-sur-Yvette Cedex, France*

b *Centre de Recherche de Gif, Institut de Neurobiologie Alfred Fessard, Laboratoire de Neurobiologie et Développement, CNRS, Avenue de la Terrasse, 91198 Gif-sur-Yvette Cedex, France*

with a resin. In the case where the plate is analyzed by ToF-SIMS after staining procedure, the dehydration baths were not done, the plates were simply dried under vacuum.

The ToF-SIMS imaging experiments were performed on a ToF-SIMS IV mass spectrometer (ION-TOF GmbH, Münster, Germany) located at the Institut de Chimie des Substances Naturelles in Gif-sur-Yvette (France). The primary ion source was a liquid metal ion gun, which delivers bismuth cluster ions (Bi_3^+ were selected). Positive ion images were always recorded with the same parameters, i.e. 500 µm x 500 µm (256 x 256 pixels) with a primary ion dose density of 3 x 10^{11} ions/cm^2. The name of the compound or the *m/z* value, the maximum of counts in a pixel (mc) and the total counts (tc) are shown below each image. The color scales correspond to the interval [0,mc].

Results and discussion

Some global structures of the rat brain such as the *corpus callosum* (*cc*) can be easily identified, and an optical image of a brain section is presented in Fig. 1. ToF-SIMS analyses were performed at one extremity of the *corpus callosum*, on the area corresponding to the red square shown in Fig.1. The two types of protocols used for this study are also described in Fig. 1. In protocol 1, the surface analysis is performed prior the staining, and in protocol 2, the slice was analyzed by ToF-SIMS imaging after HE staining. An ion image obtained from the ToF-SIMS analysis performed prior to the HE staining (protocol 1) is shown in Fig. 2. The optical image of the *corpus callosum* (red lines, Fig. 2A)

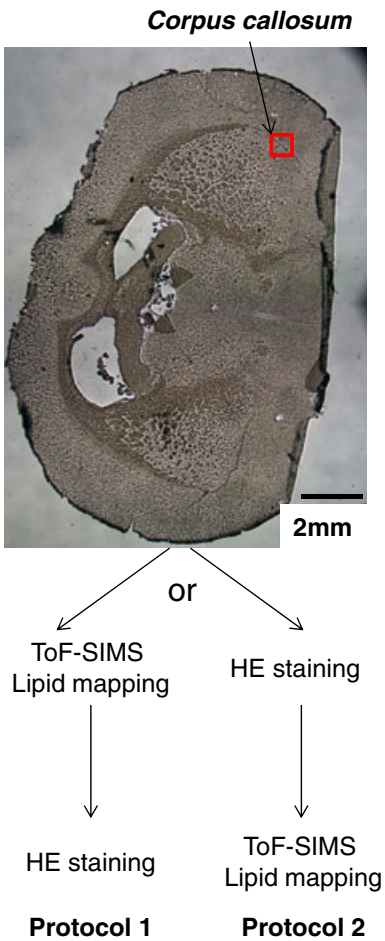

Figure 1. Optical image (x 1.25) of rat brain section and schemes of the experimental protocols.

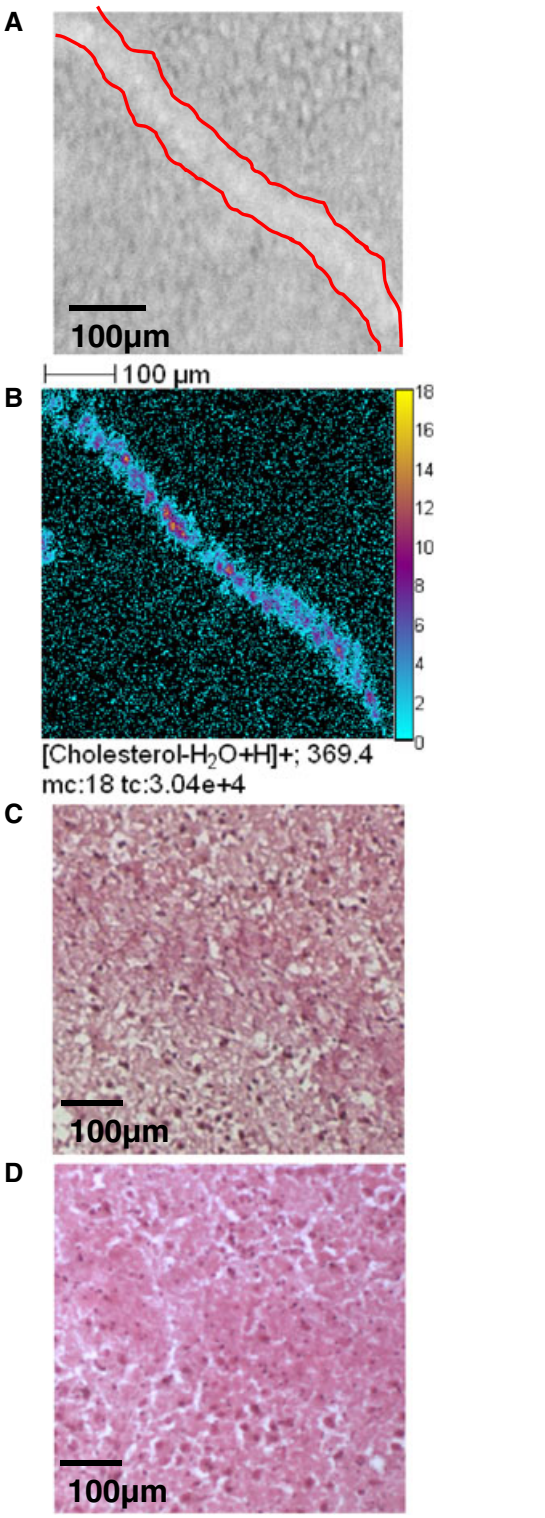

Figure 2. ToF-SIMS analysis prior Hematoxylin-Eosin (HE) stain. (A) Optical image of the extremity of the *corpus callosum* recorded with the video camera of the ToF-SIMS spectrometer. (B) Ionic image of the same area, *m/z* 369.4 $[M\text{-}H_2O + H]^+$, mc corresponds to the maximal counts in one pixel and tc to the total counts on the image. (C) Optical image of the rat brain section after the ToF-SIMS analysis and HE staining. (D) Optical image of the rat brain section after having been stained with HE.

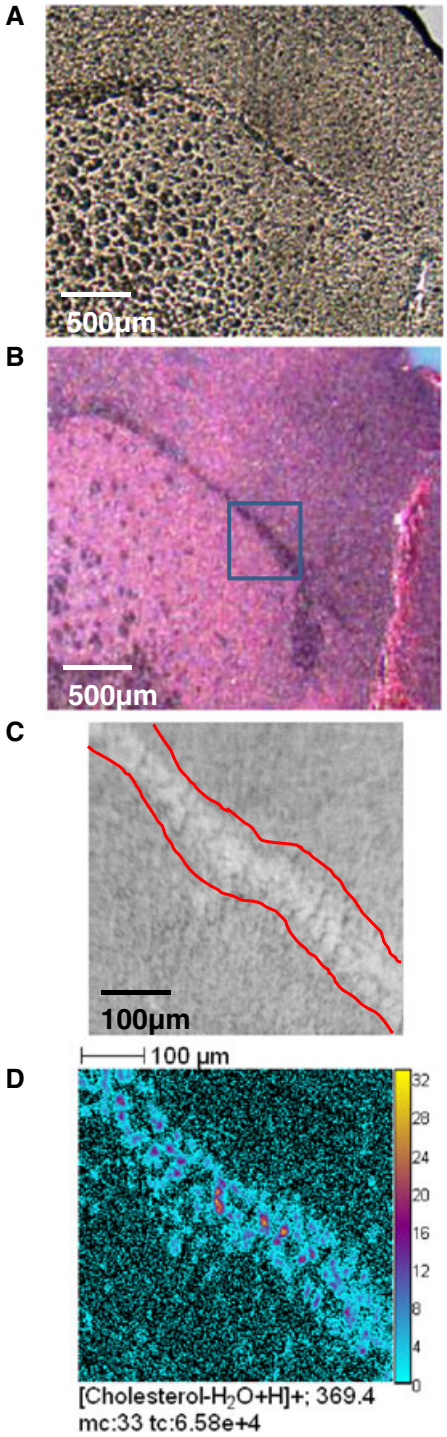

Figure 3. ToF-SIMS analysis after Hematoxylin-Eosin (HE) stain. (A and B) Optical images of the *corpus callosum* stained with HE, (A) recorded with an optic microscope and (B) recorded with the video camera of the ToF-SIMS spectrometer. (C) Optical image of the region of interest, extremity of the cc with no sample pre-treatment. (D) Image of the *m/z* 369.4 ion $[M\text{-}H_2O + H]^+$ in the same region.

looks similar to the image of a fragment ion from cholesterol, $[M\text{-}H_2O + H]^+$ at *m/z* 369.4 (Fig. 2B). Optical pictures obtained when HE staining was applied after the TOF-SIMS analysis (Fig. 2C) were compared with a reference slide (without ToF-SIMS analysis) (Fig. 2D). These two images are similar, with nuclei (in brown) and the aspect and thickness of the *corpus callosum* easily identified. The pale pink color of the tissue in Fig. 2C, compared to Fig. 2D, could be due to the dehydration of the section by the high vacuum ($\sim 10^{-8}$ hPa) in which the sample is maintained during the ToF-SIMS data acquisition. Nevertheless, the tissue remains intact, and no particular damage can be observed. This is more likely due to different microscope image acquisition conditions, like light reflection, since this slide was mounted with glass after staining in Fig. 2D, contrary to Fig. 2C for which the slide after ToF-SIMS analysis plus staining is not covered. Finally, we concluded that lipid imaging by ToF-SIMS and HE staining are compatible when mapping lipid ions before staining.

In the protocol 2, the analysis by ToF-SIMS was done on HE stained tissue. The staining procedure was in this case modified: neither fixation nor alcohol baths were applied on the tissue, and only the staining and washing steps were performed. Indeed, no signal could be recorded if a fixation is applied to the tissue before ToF-SIMS analysis (data not shown). Fig. 3A shows a reference slide (without staining). ToF-SIMS analyses were performed at the extremity of the *corpus callosum*, on the area corresponding to the blue square on the stained slice (Fig. 3B). Fig. 3C shows the optical images of the stained tissue (*corpus callosum* (*cc*): red lines), and Fig. 3D shows the ionic image of the *m/z* 369.4 ion. It is noticeable that the image of the cholesterol fragment ion is similar to the structure of the *cc* in the optical image (Fig. 3C). However, a difference appears between the picture of the tissue reference (Fig. 3A) and the picture of the tissue after HE staining (Fig. 3B): the *corpus callosum* looks wider than in the reference suggesting a distention of the tissue. This modification of the tissue can be explained by the absence of fixation in the protocol of HE staining prior to the surface analysis by ToF-SIMS. This modification of the tissue is also observed when comparing the optical images in Fig. 2A and Fig. 3C, for which the red lines drawn are not identical: after staining: in Fig. 3C, the distance between the two lines looks larger. In spite of this distention of the tissue, the cholesterol remains detected in the same region, with no significant delocalization encountered. Nevertheless, the tc value measured for the ion at *m/z* 369.4 (Fig. 3D) is higher after HE staining than in Fig. 2B. This could indicate better ionization efficiency from the studied area. The mc value is also higher in the Fig. 3D (33) than in Fig. 2B (18) so in one pixel, the maximum count detected after HE staining is almost twice than in the sample without staining. These differences can be explained by the stain itself, which probably increases the ionization efficiency (matrix effect) but also by the modification of the distribution due to the staining and washing steps: evaporation of solvents and/or washing steps with water may induce droplets fusion thus locally increasing the amount of lipids.

Conclusion

While the useful complementarity between histology and MSI using ToF-SIMS on two adjacent tissue sections is known, their reciprocal compatibility on a single tissue section was never investigated. Optical pictures show that the staining procedure still allows the recognition of the global brain structures. When applying a HE stain protocol after the ToF-SIMS analysis, histological structures are enlightened in the same way as in a brain section without any treatment prior to the staining.

When acquiring ToF-SIMS images after having stained the tissue, optical pictures and ionic images are correlated. Nevertheless, the ion images recorded before or after HE stains are slightly different although the cholesterol fragment ion remains in the same region with no strong delocalization. Thus, it is possible to work on the same tissue section with both analysis methods, preferably by acquiring the ToF-SIMS images prior to the HE staining. Different types of staining procedures, such as luxol blue for myelin and sulfatides, will be tested with ToF-SIMS imaging, as well as the influence of these staining on the imaging of other lipid classes.

Acknowledgements

This work was supported by the Agence Nationale de la Recherche (grant ANR-2010-BLAN-0805-01-MASS-IMAGE).

References

[1] J. Pól, M. Strohalm, V. Havlíček, M. Volný, *Histochem Cell Biol* **2010**, *134*, 423.
[2] D. Touboul, A. Brunelle, O. Laprévote, *Biochimie* **2011**, *93*, 113.
[3] P. Chaurand, S. A. Schwartz, D. Billheimer, B. J. Xu, A. Crecelius, R. M. Caprioli, *Anal. Chem.* **2004**, *76*, 1145.
[4] A. Walch, S. Rauser, S. O. Deininger, H. Hofler, *Histochem Cell Biol* **2008**, *130*, 421.
[5] A. C. Crecelius, D. S. Cornett, R. M. Caprioli, B. Williams, B. M. Dawant, B. Bodenheimer, *J Am Soc Mass Spectrom* **2005**, *16*, 1093.
[6] K. Schwamborn, R. C. Krieg, M. Reska, G. Jakse, R. Knuechel, A. Wellmann, *Int J Mol Med* **2007**, *20*, 155.
[7] D. Touboul, F. Halgand, A. Brunelle, R. Kersting, E. Tallarek, B. Hagenhoff, O. Laprévote, *Anal. Chem.* **2004**, *76*, 1550.
[8] B. Johansson, *Surf Interface Anal* **2010**, *38*, 1401.
[9] A. Brunelle, O. Laprévote, *Anal. Bioanal. Chem.* **2009**, *393*, 31.
[10] D. Touboul, O. Laprévote, A. Brunelle, *Curr. Opin. Chem. Biol.* **2011**, *15*, 725.

Résumé

La dystrophie musculaire de Duchenne est une maladie neuromusculaire progressive qui touche 1 enfant sur 3500. Elle est liée au chromosome X et caractérisée par l'absence de dystrophine, une protéine du cytosquelette située sous le sarcolemme qui confère de la stabilité à la membrane cellulaire en connectant l'actine du cytosquelette avec la matrice extracellulaire. Elle fait partie d'un complexe multi protéique, nommé « dystrophin associated protein complex (DAPC)», qui contient, parmi d'autres composants, le β-dystroglycane et l'oxyde nitrique synthase (NOS).
L'absence de la dystrophine entraine la dérégulation de l'homéostasie calcique, la nécrose tissulaire, l'accumulation progressive de tissu graisseux et fibreux, l'incapacité de mouvement et des déficits cardiaques et respiratoires qui aboutissent au décès des patients.
Mon travail de thèse avait comme objectif l'amélioration de différents aspects du phénotype dystrophique. J'ai utilisé, en association, des molécules capables d'agir par activation deux voies de signalisations (la voie du NO et l'inhibition des histones deacetylase (HDAC)). Chacune de ces voies est connue pour induire l'amélioration du phénotype dystrophique chez la souris *mdx*, modèle de la maladie.
Plus particulièrement, j'ai testé chez la souris, deux mode d'administration du butyrate d'arginine (AB), la drogue de référence car déjà utilisée en clinique sur des jeunes patients pour une autre indication, par gavage et par injection intrapéritonéale. En parallèle, j'ai étudié deux nouvelles molécules dérivées du AB, qui pourraient être administrées par voie orale aux patients et être efficace à faible dose. Il s'agit du 3-Hydroxybutyrate arginate (ABE) et du N-butyril arginine (ABA).
AB, ABE et ABA ont été testés *in vitro* sur les myotubes de patients dystrophiques et *in vivo* sur des souris *mdx*.
L'administration orale du AB a les mêmes effets positifs que l'injection intrapéritonéale chez les souris *mdx*. Ces résultats démontrent que l'administration par voie orale doit être prise en considération lors des futurs essais cliniques.
Dans un deuxième temps, je me suis focalisée sur les défauts cardiaques. Un suivi par échocardiographie mensuelle a été réalisé sur des souris de 8 mois (au début de l'expérience) traitées avec du AB. En parallèle nous avons analysé les effets de l'administration par voie orale du AB sur les déformations de la colonne vertébrale. Enfin, les altérations des signaux de l'électromyogramme (réalisé avec une méthode non invasive développée en clinique et appliquée pour les animaux) ont été également analysées. L'ensemble des résultats obtenus montre que le AB est capable de préserver l'activité cardiaque, d'empêcher la déformation de la colonne vertébrale et de rétablir les paramètres d'excitabilité axonale mesurés chez les souris *mdx* traitées.
J'ai aussi testé différentes concentrations des molécules ABE et ABA *in vivo* et observé à des faibles doses les mêmes résultats bénéfiques sur de nombreux paramètres structuraux et fonctionnels, que ceux obtenu avec une dose importante de AB (800mg/kg/j). En effet, les deux nouvelles drogues peuvent être administrées à une dose 10 fois plus basse que la dose de AB pour obtenir les mêmes effets. En parallèle, j'ai testé *in vitro*, sur des cellules musculaires humaines, la capacité des deux produits à induire une augmentation des niveaux intracellulaires d'utrophine et des protéines associées (β-dystroglycan et la myosine embryonnaire). J'ai aussi démontré qu'une augmentation de l'expression de l'utrophine et des protéines associées pouvait être induite par les inhibiteurs d'HDAC (le butyrate, la trichostatine A, l'acide valproique et l'isobutyramide).
Enfin, une étude portant sur l'homéostasie calcique a été réalisé car des altérations de cet équilibre sont en partie responsables de la nécrose/dégénérescence du tissue musculaire. En particulier, l'activité spontanée du Ca^{2+}, enregistrée sur le myotubes de patients (donc avec perte de l'intégrité du sarcolemme), été fortement réduite après un traitement agissant sur la voie d'activation du NO et/ou par des inhibiteurs des HDAC.
L'ensemble des résultats obtenus apportent la preuve de principe des effets bénéfiques du AB et de ses dérivés sur la dystrophie musculaire, en activant la voie du NO et en inhibant les HDAC.